
THE UNIVERSITY *of* EDINBURGH

THE UNIVERSITY *of* EDINBURGH

# Synthetic biology enabled wearable biosensors for non-invasive biomarker monitoring using sweat

**Margaret Hicks**

Thesis submitted for the degree of Doctor of Philosophy

University of Edinburgh

School of Biological Sciences

Year of submission 2022

# Declaration

I declare that this thesis was composed by myself, that the work contained herein is my own except where explicitly stated otherwise in the text, and that this work has not been submitted for any other degree or processional qualification except as specified.

Margaret Hicks

21/12/2022

# Acknowledgements

Firstly I would like to thank my supervisors Professor Baojun Wang, Professor Chris French and Professor Till Bachmann for all their support and advice during my PhD as well as giving me the freedom to explore the research which sparked my interest. Beyond this I also wanted to thank everyone in the department who has also supported me during my PhD including Dr Nadanai Laohakunakorn for teaching me the techniques to work on cell-free systems.

A special thank you to my friends and family who have been a huge support during the whole course of my PhD. I would like to give a special mention to my mum Carole Hicks for all her help in proof reading and encouragement whilst writing my thesis. I would also like to mention all of the great friends I have met in Edinburgh during my PhD, espcially Holly, Kiani and Pop, for understanding my stresses and supporting me through all of them.

I also would not have been able to complete this PhD without the support of both the Wang and French labs in particular Xinyi, Filipe and Behide for all their advice and Flo, Maxine, Julija and Marcos for their encouragement.

Finally I would like to thank EastBio DTP for funding me during my PhD and giving me access to a wonderful cohort of fellow PhD students throughout Scotland. Additionally I would also like to thank the Office of Naval Research Global and Patrick Rose for believing in this project and providing us with extra funding to really push the project forward.

# Contents

# Lay summary

Monitoring markers of human health, known as biomarkers, is highly important in a range of different areas, for example the monitoring and diagnosing of health conditions, studying physical fitness in elite sports and stress levels in safety critical roles such as flying crew. Up to now blood samples have been considered the gold standard for monitoring these markers. The ongoing challenge is that to obtain a blood sample specialist training and equipment is required for sampling and analysis and this limits how often and where testing of health markers can be carried out. To obtain a better understanding of biomarkers and how they change for different situations and over time their monitoring would need to be carried out far more regularly than is possible with blood sampling. Sweat is another body fluid which contains a large number of biomarkers and has not been previously used for this kind of monitoring. Sweat is easily available and can potentially be sampled without specialist training or equipment and would therefore allow biomarker monitoring more frequently and without requiring a medical facility. Due to these advantages developing methods to monitor health using sweat has become a large area of research particularly into developing devices that can be worn which allow continuous monitoring without any users' input, so called passive monitoring.

Biosensors which use biological parts to detect biomarkers are a common method used to detect biomarkers. The majority of the work to date has focused on combining these biological parts with electronics to generate devices capable of sensing biomarkers in sweat. However, this approach has its own challenges because the electronics can be affected by many environmental factors including movement, temperature, humidity and pH. An alternative approach is to develop biosensors which do not require any electronics but can generate the response entirely on their own. These could help in overcoming the challenges posed by environmental factors. This project aimed to develop a wearable patch that incorporates biosensors to

detect health markers. Biosensors for lactate, tryptophan and potassium were developed and optimised to detect these three markers at the concentration ranges found in human sweat. Further biosensors for histamine, cortisol and testosterone were also constructed and studied. But further work to optimise these biosensors is needed for them to be able to detect these markers at the concentration levels found in human sweat. The three optimised biosensors were then used to study how these biosensors could be combined with materials to generate a wearable patch. For these three biosensors a method was developed that generated a material containing the biosensors and that could act as a wearable patch, although there was a reduction in the ability of the biosensor to function. More optimisation would be needed to make the sensors in the patch sufficiently sensitive to the concentration ranges found in human sweat. In addition work into generating a phone App which would automate the analysis of the monitoring was carried out to demonstrate proof of principle for an automated method of monitoring health markers which would be suitable for use by anyone without training,

# Abstract

Monitoring biomarkers is key to understanding human health and diagnosing disease. Frequently this requires blood samples to be taken for subsequent testing. It has disadvantages including pain and infection risk to the individual being sampled and a significant time lag before the results are known. Most blood-based monitoring tests require samples to be taken in a healthcare setting by trained personnel and the sample sent to a laboratory for analysis. This limits access to biomarker monitoring. Using alternative biofluids such as saliva and urine still requires active sample production so sampling can be inconvenient for individuals. Sweat has many potential advantages for monitoring biomarkers as it allows for non-invasive sampling, which can be carried out passively, and sweat contains a number of different potential markers of health and physiological status. As a result sweat has become a key area of focus in developing new monitoring devices, particularly in the use of wearable devices that allow passive monitoring. Research in this area has used electrochemical sensors for detection of biomarkers, but electrochemical sensors have potential disadvantages in terms of cost and how the sensing is impacted by temperature, humidity, movement and other variables. Synthetic biology has developed a wide range of tools capable of generating biosensors with highly tailorable characteristics, which are potentially suitable for monitoring biomarkers whilst being more capable of withstanding changes to their environment. In this project multiple biosensors using different approaches of whole cell biosensors, aptamer-based sensors and fluorescent protein-binding based sensors have been developed and shown to be capable of detecting biomarkers for lactate, potassium, tryptophan, histamine, testosterone and cortisol, all of which are thought to show information on physiological state. To test the suitability of whole cell sense and respond genetic circuits, a novel tryptophan biosensor was developed as part of the project. Engineered proteins containing circularly permuted GFP were also developed to generate biosensors for cortisol, testosterone and histamine. These sensors have been shown to respond to

target analytes in sweat at the required range. These sensors have also been encapsulated into a hydrogel material to show it is possible to combine these sensors into a wearable device which would be suitable for passive monitoring, thus demonstrating the suitability of biosensors to generate a new approach to biomarker monitoring.

# List of abbreviations

| | |
|---|---|
| 3-PGA | 3-Phosphoglyceric acid |
| ATP | adenosine triphosphate |
| C | cytosine |
| $CaCl_2$ | calcium chloride |
| cpGFP | circularly permuted green fluorescent protein |
| CTP | cytosine triphosphate |
| DMSO | dimethyl sulfoxide |
| dNTP | deoxynucleotide triphosphate |
| DNA | deoxyribonucleic acid |
| DTT | dithiothreitol |
| EDTA | ethylenediaminetetraacetic acid |
| FRET | Förster resonance energy transfer |
| G | guanidine |
| GFP | green fluorescent protein |
| GTP | guanine triphosphate |
| $K^+$ | potassium ion |
| KCl | potassium chloride |
| LanYFP | *Branchiostoma lanceolatum* yellow fluorescent protein |
| LB | Luria-Bertani broth |
| LED | light emitting diode |
| LOD | limit of detection |
| $MgCl_2$ | magnesium chloride |

| | |
|---|---|
| mRFP | monomeric red fluorescent protein |
| NaCl | sodium chloride |
| OD | optical density |
| PAGE | Polyacrylamide gel electrophoresis |
| PCR | polymerase chain reaction |
| PEG | polyethylene glycol |
| PEGDMA | polyethylene glycol dimethacrylate |
| RBS | ribosome binding site |
| RGB | red green blue |
| RNA | ribonucleic acid |
| sfGFP | super folder green fluorescent protein |
| ssDNA | single stranded DNA |
| TBE | tris borate EDTA |
| TCS | two component system |
| tRNA | transfer ribonucleic acid |
| UTP | uracil triphosphate |
| UV | ultraviolet |
| XNA | xeno nucleic acid |

# List of figures

# List of tables

# 1 Introduction

The accurate detection and quantification of a molecule of interest is highly important in many fields. Many analytical methods have been developed for this purpose, each with their own advantages and disadvantages. In biology being able to detect molecules of interest is also highly important for survival, so organisms have developed their own systems for sensing and responding to a wide range of molecules. These biological systems can be reengineered and used as an analytical method to detect and quantify molecules of interest and are known as biosensors. They have many potential advantages in cost, ease of use, portability and sustainability. As a result, a large amount of research work has been carried out into the development of biosensors. However despite this there are very few successful commercial biosensors. One is Modern Water's MicroTox which determines the presence of toxic compounds based on the luminescence of bacteria contained within the device (Bulich and Isenberg, 1981). However it is not specific to a compound which could be an issue in certain situations (Ames et al., 1973, Bulich and Isenberg, 1981). Enzymatic sensors were already commonly used that were far more selective which was a challenge in commercialisation even though the advantage of whole cell biosensors in terms of cost was already understood (Bousse, 1996, Moraskie et al., 2021). The earliest biosensors were developed before recombinant DNA technology which limited the range of analytes which could be detected because they relied on the use of native pathways (Moraskie et al., 2021). Some of the sensors which were developed often had high basal expression and low maximal output with poor sensitivity, so they could not detect the concentrations of the molecule of interest that were required (Tauriainen et al., 1997, Wackwitz et al., 2008). Recombinant DNA technology and the increased understanding of genomes resulted in the increase of the number of available parts and the ability to generate new parts (Utsumi et al., 1989). More recently, synthetic biology has focused on rational design, resulting in the development of tools and better understanding which allows for targeted optimisation of biosensors to

ensure a good response to the molecule of interest, and this has also helped to renew interest as optimisation has become easier.

Now many biosensors have been developed for a wide range of applications including environmental monitoring (Wan et al., 2019a, Shemer et al., 2015), process monitoring (Goers et al., 2017) and food safety (Dwidar and Yokobayashi, 2019, Yousefi et al., 2018). Health and medical applications are a large focus in the development of biosensors due to their advantages in cost, ease of use and portability, with biosensors being developed for diagnostics (Magro et al., 2017, Kylilis et al., 2019) and biomarker monitoring (Watstein and Styczynski, 2018, Kim et al., 2019). They not only have the potential to reduce the cost of testing but also to increase access to diagnostics. Recently research has looked into the development of wearable devices which would allow continuous monitoring of human biomarkers outside of a medical setting and which would allow a better understanding of the natural variations in biomarkers and early detection of biomarkers outside of the normal range providing early warning signs for interventions.

Biological parts have also been used with materials to generate new materials with functionalities that previously have not been possible. This allows new functionality to be added, including biosensing. Generating biomaterials with sensing capabilities is one method that could be used to generate wearable devices for health monitoring (Liu et al., 2018b).

The aim of my PhD is to use synthetic biology approaches to develop a panel of biosensors for biomarkers of human health found in sweat which could then be used to generate a smart biomaterial to develop a wearable device for health monitoring using sweat on the skin. In this chapter I will outline the current state of biosensor development and optimisation with a focus on the tools for optimisation but also commenting on the other challenges which exist. The interest in wearable devices, the development of biomaterials and the objectives of my PhD will also be discussed.

## 1.1. Biosensors

Biosensors use biological parts to generate systems able to detect and respond to a molecule of interest. Biosensors gained interest as a method of detecting and quantifying molecules over other traditional analytical methods because of the low cost to produce biosensors, their ease of use, portability and the sustainability of the sensors (Wen et al., 2019). Historically cell-based biosensors have been a common format used to develop biosensors, either in an on and off response or an analogue response for quantification (Moraskie et al., 2021). **Figure 1.1a** shows a generic analogue response curve for a biosensor. To generate this response, most frequently natural sensing pathways in the cell are rewired to link them to a desired output. Transcription factor based genetic circuits are one of the most common architectures used (Chen et al., 2018), a schematic of their design is shown in **Figure 1.1b,** and many of the tools developed to improve biosensor response have developed from this architecture. Cell-based biosensors have been developed using a range of different cellular hosts, from both eukaryotic (Shetty et al., 2004) and prokaryotic cells (Goers et al., 2017). Prokaryotic cells are most commonly used due to their ease of engineering and fast growth.

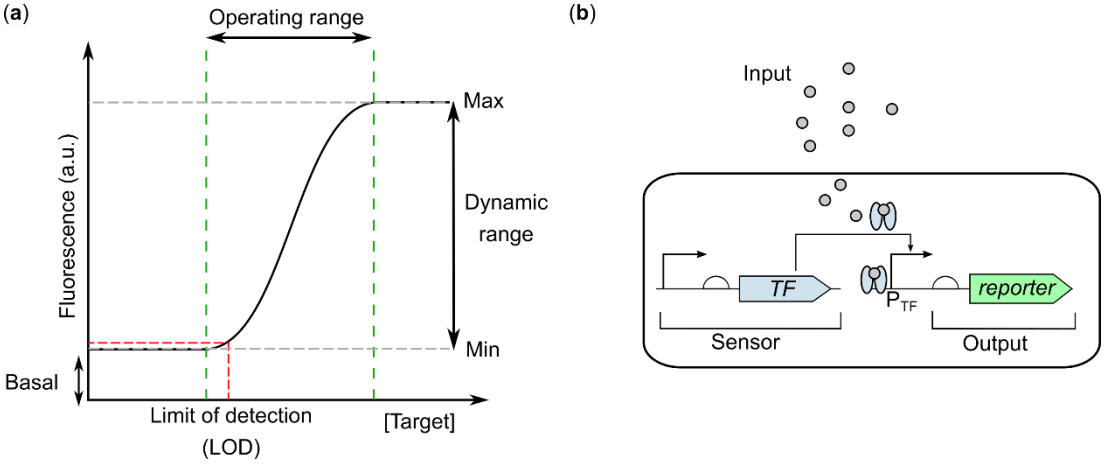


**Figure 1.1 Generic biosensor response curve and architecture.** (**a**) Shows a standard response curve highlighting the characteristics that are of interest for determining biosensor performance. The operating range gives the range of concentrations of the target which produce a change in the output. The basal expression shows the level of output produced without the target present. The limit of

detection gives the lowest concentration of the target which gives a response that can be distinguished from the basal expression. The dynamic range is the range of the output produced by the sensor, shown by the maximum expression over basal expression ($\boldsymbol{max/min}$). (**b**) Shows the basic architecture of a biosensor containing a sensing module, frequently a transcription factor (TF), which detects signal of interest (input) and then converts this into a detectable output, frequently through the expression of a gene (reporter) (Wen et al., 2019).

The dynamic range, the operating range and limit of detection are particularly important when developing biosensors which are capable of detecting a molecule of interest at relevant concentrations. The dynamic range is the change between the uninduced basal expression and the maximal expression when activated, usually calculated as $max/min$. The operating range is the range of concentrations of the molecule of interest which result in a change in the response (Rogers et al., 2016). The limit of detection is the lowest concentration which generates an output which is detectable over the basal expression. In general terms for a biosensor to have good performance a large dynamic range is needed, the operating range needs to cover the concentrations range that will be found when measuring real samples and have the limit of detection below the minimum concentration which needs to be sensed (Wen et al., 2019). Many early biosensors could not reach the required sensing characteristics which caused challenges (Tauriainen et al., 1997, Wackwitz et al., 2008).

Other concerns in the output detection, the stability and reliability of the sensor also impacted the development of cell-based biosensors as these properties are highly important for the development of viable commercial devices. Fears concerning the release of genetically modified organisms into the environment have also hindered the commercialisation of cell-based biosensors that do meet the requirements in terms of performance (Dana et al., 2012). The tools to overcome these challenges and ongoing research to develop cell-based biosensors which can meet commercial requirements are discussed in the following sections.

### 1.1.1 Synthetic biology tools to optimise biosensor dynamic range

Initially optimisation was done in an ad hoc manner meaning that changes made to the sensor were specific to that sensor and so did not help more generally in the development of new biosensors (King et al., 1990). Synthetic biology aims to develop rational approaches which are broadly applicable to speed up the development of new sensors and to allow optimisation to be carried out in a targeted manner.

Tools built for optimisation of biosensors using whole cell systems will also apply to sensors working in cell-free transcription-translation systems that similarly rely on genetic circuits.

Mathematical modelling has been applied to identify how the parts of biological systems interact and how altering one part of the system will affect the whole system. This modelling has been applied to the genetic circuits of cell-based biosensors and the response curve of the sensors to determine how the response curve can be specifically altered. This can identify which parts of the circuit can be used to generate these changes (Mannan et al., 2017, Ang et al., 2013, Berepiki et al., 2020). This increased understanding of how each part alters the response curve has also allowed the development of programs to help the design of biosensor circuits allowing more suitable parts to be selected from the beginning (Nielsen et al., 2016). Tools for each part of the sensing circuit have been developed allowing quicker optimisation and improved performance.

#### 1.1.1.1 Transcriptional tools to optimise cell-based biosensors

The transcription of the reporter gene which converts the sensing by the transcription factor into the output is important in determining the basal and maximal expression and the dynamic range that can be achieved. The promoter which controls expression of the reporter will determine the level of transcription and can be altered to optimise this.

The strength of the promoter responsible for controlling the expression of the reporter gene is one method of transcriptional optimisation. The -10 and -35 sites are responsible for the binding of RNA polymerase to the promoter to initiate transcription of the gene. The closer these sequences are to the consensus sequence the better the polymerase binds and this results in more transcription. Larger differences between the -10 and -35 sequences and the consensus will weaken polymerase binding, the dissociation constant will be larger and less transcription will occur (Chen et al., 2018). By altering the strength of these two sites the level of transcription of the gene can be altered. But their strength needs to be balanced to optimise activation and minimise leakiness. For activators these two sites are often fairly weak and can be compensated by the transcription factor which helps to recruit the polymerase. Conversely, for repressors the -10 and -35 are stronger then the transcription factor acts as a block to the polymerase to prevent transcription. But if the -10 and -35 are too strong then transcription will still occur because the polymerase rapidly binds to initiate transcription. And if the -10 and -35 sites are too weak then polymerase will bind poorly and there will be very little transcription. This is shown in **Figure 1.2a**.

For responsive promoters the operator sequence is also important in the detection of the molecule of interest and it being converted to an output. If the operator sequence is well known then the operator sequence can be combined with a well characterised constitutive promoter to create a synthetic promoter with the desired strength (Goers et al., 2017). For repressors the position of the operator site can also be changed to improve repression. There are three possible sites for the operator in a promoter that is negatively regulated. First is the core site between the -10 and -35 sequences which gives the strongest repression because it blocks the polymerase binding site and this repression is enhanced if the operator overlaps with either the -10 or -35 (Chen et al., 2018). Second there is the proximal site which is downstream of the promoter and acts as a physical roadblock. Third there is also the distal site upstream of the promoter which gives the weakest repression (Cox et al., 2007). To further improve

repression an additional operator site can be added downstream of the promoter, which acts as a roadblock to the polymerase to increase repression (Hao et al., 2014), shown in **Figure 1.2b**.

The addition of extra operator sites away from the promoter has also been used to improve to response of biosensors. These decoy sites titrate the binding of the transcription factor away from the promoter, shown in **Figure 1.2d**. If the transcription factor is able to bind to the promoter even without the presence of the molecule of interest this can reduce the leakiness of the biosensor. These decoy sites can also reduce the sensitivity of the biosensors, depending on their number (Lee and Maheshri, 2012).

The final method that can be used to alter the transcription of the reporter and consequently to change the biosensor response is antisense transcription (Brophy and Voigt, 2016). A promoter is placed downstream of the reporter gene on the opposite strand so that a complementary piece of RNA to the reporter gene mRNA is also transcribed. This complementary RNA will bind to the mRNA to form a duplex which can trigger degradation of the RNA or prevent translation by preventing the binding of the ribosome to initiate translation (Brophy and Voigt, 2016, Thomason and Storz, 2010), shown in **Figure 1.2c**.

#### 1.1.1.2 Translational tools to optimise cell-based biosensors

The response generated by the biosensor can also be adjusted by altering translation of the mRNA of the reporter produced. The RBS (Ribosome binding site) is mostly responsible for the translation rate. The closer the RBS sequence is to the consensus the better ribosomes are recruited so more translation will occur. A very strong RBS will result in high translation even when there is very little mRNA and this can increase leakiness, whilst a very weak RBS will result in very little translation even when there is lots of mRNA resulting in low maximal expression giving low leakiness. There is a group of well characterised RBS which can be used to pick an RBS of a desired

strength (http://parts.igem.org). The factors which affect the strength of an RBS are well understood. Programs which can look at the surrounding sequence and design an RBS of a particular strength have also been developed (Salis et al., 2009, Espah Borujeni et al., 2014). **Figure 1.2e** shows how RBS strength can alter the response curve.

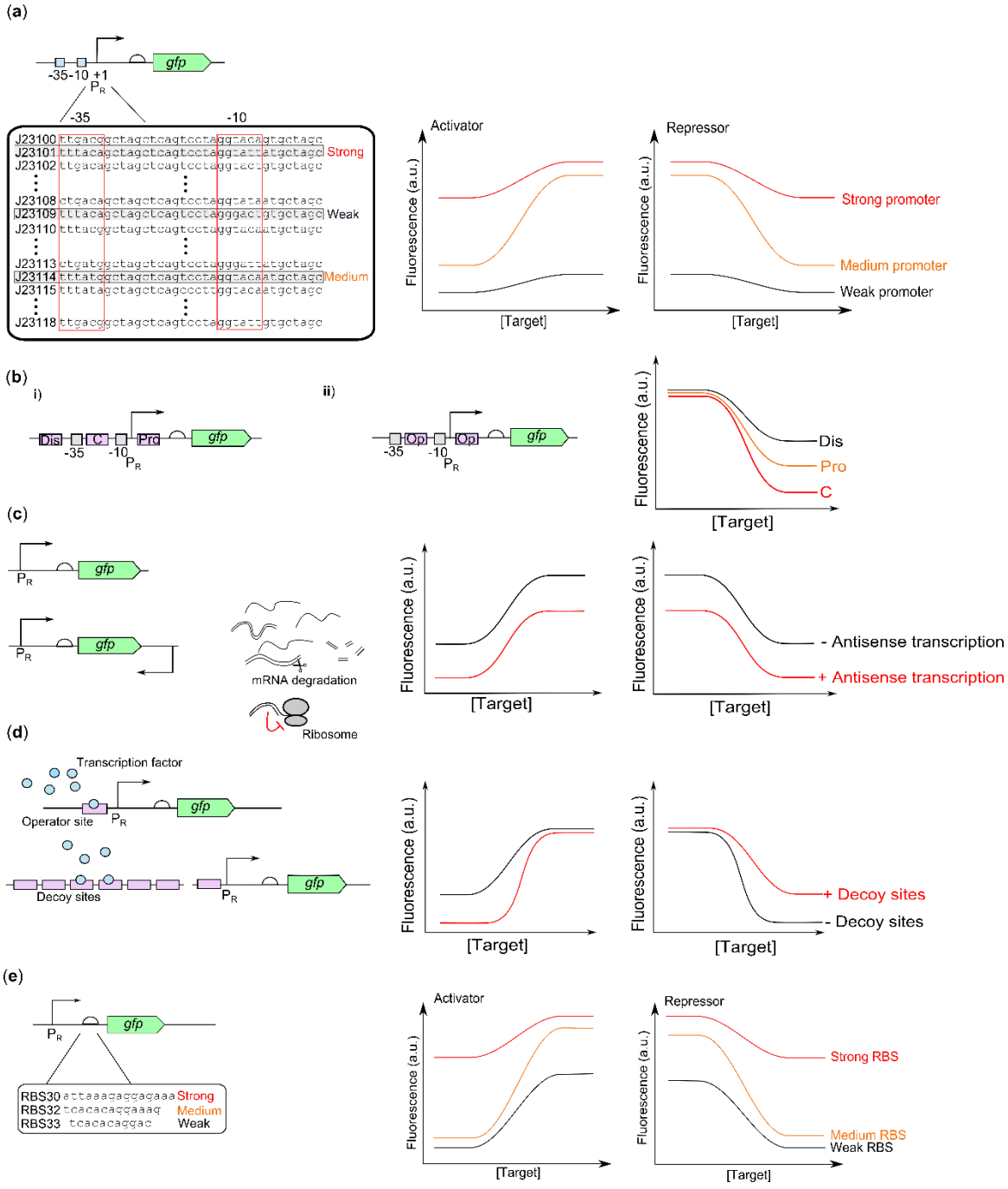


**Figure 1.2 Transcriptional and translational tools for biosensor optimisation.** The figure shows the different transcriptional and translational tools that can be used to alter the response of a biosensor

and the effect these can generate on the response curve. (**a**) Shows how altering the strength of the responsive promoter ($P_R$) alters the dynamic range, with examples of different strength promoters from the Anderson collection (http://parts.igem.org/Promoters/Catalog/Anderson).The effect on the dynamic range for activators and repressors is shown (Chen et al., 2018). (**b**) (**i**)The possible positions where the operator site in the responsive promoter ($P_R$) for a repressor can be found is shown and how the strength of the repression is affected by the position, the core (C) site gives the strongest repression followed by the proximal site (Pro) then the distal site (Dis) (Cox et al., 2007). (**ii**) A second operator site can be added downstream of the responsive promoter ($P_R$) to improve repression (Hao et al., 2014). Response curves for the different operator positions are shown. (**c**) Shows the use of antisense transcription to alter biosensor response. A promoter is place downstream of the reporter gene (*gfp*) on the opposite strand to the responsive promoter ($P_R$) to generate a complementary RNA. The duplex RNA is then either degraded or prevents translation of the reporter mRNA by blocking ribosome binding (Brophy and Voigt, 2016). (**d**) Decoy sites can be used to titrate the binding of the transcription factor away from the responsive promoter ($P_R$) to reduce leakiness from the transcription factor without affecting the output, and the effect on the response curve of both activators and repressors is shown (Lee and Maheshri, 2012). (**e**) Shows the effect of changing the RBS on the response curves for both activators and repressors, different strength RBS are shown from the iGEM collection (http://parts.igem.org).

#### 1.1.1.3 Post-translational tools to optimise cell-based biosensors

If the dynamic range is not optimal after altering the transcription and translation of the reporter then the level of the reporter can be altered post-translationally. A simple method to reduce the leakiness of a biosensor is to add a degradation tag to the reporter protein to reduce the amount in the cell. Tags for both N- and C-terminal degradation have been developed which can give a range of degradation rates (Sekar et al., 2016, Cameron and Collins, 2014). But this will also reduce the maximal activation which is not desired, shown in **Figure 1.3a**. The addition of a cleavage tag between the reporter and the degradation tag and controlling the expression of the protease for the cleavage tag by the inducible promoter means that when the molecule of interest is present the degradation tag is lost and the reporter is not degraded (Wan et al., 2019a). This ensures leaky expression is minimised by the degradation tag whilst at the same time reducing the effect on the maximal expression when activated.

For some biosensors the maximal expression is very low and hard to increase. Positive feedback loops can ensure that when the sensor is activated further production of the transcription factor is generated to increase the response (Dacquay and McMillen, 2021), shown in **Figure 1.3a**. Alternatively transcription factors which have no ligand and activate their cognate promoters very strongly have been identified and can be used as amplifiers to increase the maximal activation. These transcription factors are placed downstream of the inducible promoter and the small level of the amplifier transcription factor expressed by the sensor can initiate strong expression of the reporter from the amplifier promoter, shown in **Figure 1.3b**. The level of amplification can be adjusted to the specific requirement of the sensor using an additional protein which represses the amplifier promoter. Altering the strength of expression of this repressor can alter how much the signal is amplified (Wang et al., 2014). Amplification has been combined with other approaches. Combining amplification and using positive feedback where the amplifier transcription factors are also expressed by the amplifier promoter means that when activated the level increases even further thus increasing the amplification (Nistala et al., 2010). Different amplifiers can also be used in series to further boost the amplification (Wan et al., 2019a). Strong repressors can also be used as amplifiers as well as strong activators (Hooshangi et al., 2005). However, amplifiers will also amplify basal expression, as only a small amount of the amplifier transcription factor is required to activate the promoter, and this can be an issue.

Combinations of these techniques have been used to ensure that the maximal expression can be increased whilst minimising the basal expression, shown in **Figure 1.3c** (Wan et al., 2019a).

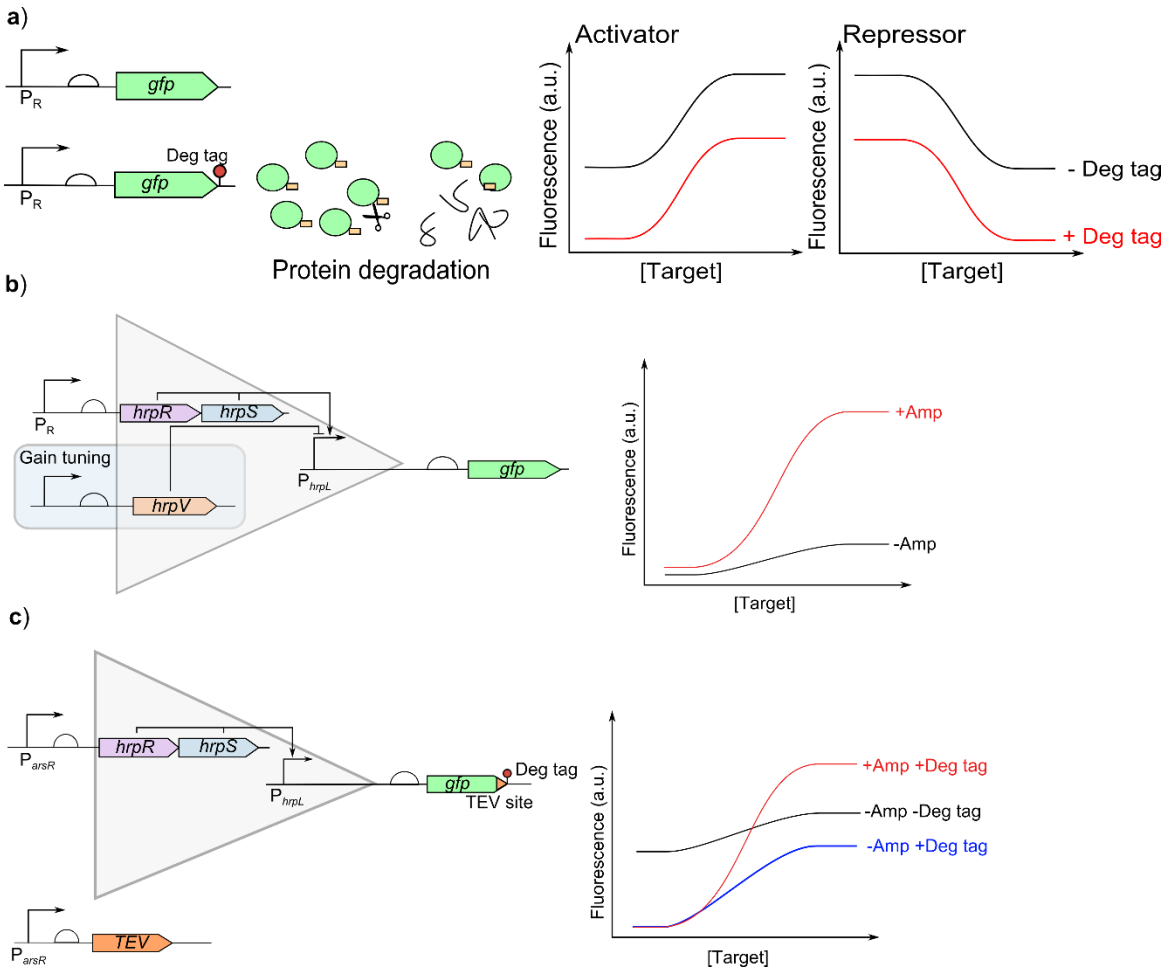


**Figure 1.3 Post-translational tools to optimise biosensors.** (**a**) The addition of a degradation tag to the reporter gene (*gfp*) can be used to reduce the level of reporter produced, the effect this has on the response curve is shown for both an activator and repressor. (**b**) Amplifiers can be used to increase the maximum expression. A stronger ligand free transcription factor (hrpRS) is expressed by the responsive promoter ($P_R$) to activate the amplifier promoter ($P_{hrpL}$) to generate strong expression of the output (*gfp*). The level of amplification can be tuned by the addition of another regulator (*hrpV*). (**c**) Shows how combinations of these optimisation methods can be used. An amplifier can be used to increase the maximal expression whilst a degradation tag which can be cleaved by a protease also under the control of the responsive promoter ($P_{arsR}$) will reduce the basal expression with little effect on the maximal expression (Wan et al., 2019a).

### 1.1.2 Methods to optimise sensor sensitivity

Tools outlined previously such as the use of an amplifier and the presence of decoy sites can also impact the sensitivity, but this is not the main use of the tool, however the sensitivity of the biosensor is highly important to it being

suitable for the desired application. The ability of the sensing element of the genetic circuit to detect the molecule of interest and activate the response is highly important in determining the sensitivity of the biosensor. The number of transcription factor molecules present inside the cell has a large impact on whether the cell is able to respond to the molecule of interest once it has entered the cell. In the case of activators increasing the level of transcription factor in the cell will increase the sensitivity of the biosensor whilst in repressors reducing the level of transcription factor will improve sensitivity (Georgi et al., 2012), shown in **Figure 1.4a**. However this can also affect the basal expression, as too high levels of the activator or too low levels of repressor will increase basal expression (Wang et al., 2015a). The strength of the constitutive promoter used to express the transcription factor can be varied to alter the intracellular levels, and a library of constitutive promoters of different strengths is available (http://parts.igem.org/Promoters/Catalog/Anderson).

In the case of cell-based sensors the degree of entry into the cell is also important. Depending on the molecule of interest some are easily able to enter the cell through diffusion or transport channels, whilst for other molecules the rate of uptake into the cell is much slower and the cell has a lower intracellular concentration than the environment. This reduces the sensitivity of the biosensor. Improving the transport of the molecule into the cell can improve the sensitivity by making more of the molecule of interest available within the cell, shown in **Figure 1.4b** (Cayron et al., 2017). This can be achieved by overexpressing transport channels in the cell. Changing the level of export of the analyte by altering exporter expression can also be used to alter the concentration of the ligand within the cell and thus alter the sensitivity of the sensor (Raman et al., 2014).

If improving the availability of the molecule of interest and optimisation of the transcription factor levels are not enough further steps can be taken to improve the sensitivity. Altering the responsive promoter can be a key approach to optimise the sensitivity of the biosensor. This has been used in

the case of generating arsenic responsive promoters where reducing the leakiness of the sensor by the addition of an extra ArsR binding site down stream of the promoter to near the transcription initiation site resulted in a large increase in the sensitivity (Chen et al., 2019), shown in **Figure 1.4c**.

Alternatively, feedback loops can also be used to optimise the sensitivity. In the case of a cadmium whole cell biosensor, by placing the expression of the transcription factor under a promoter that is repressed by its own products by co-expressing TetR this feedback loop was shown to improve the sensitivity of the biosensor by amplifying the response at the lower concentrations (Zhang et al., 2021a), shown in **Figure 1.4d**.

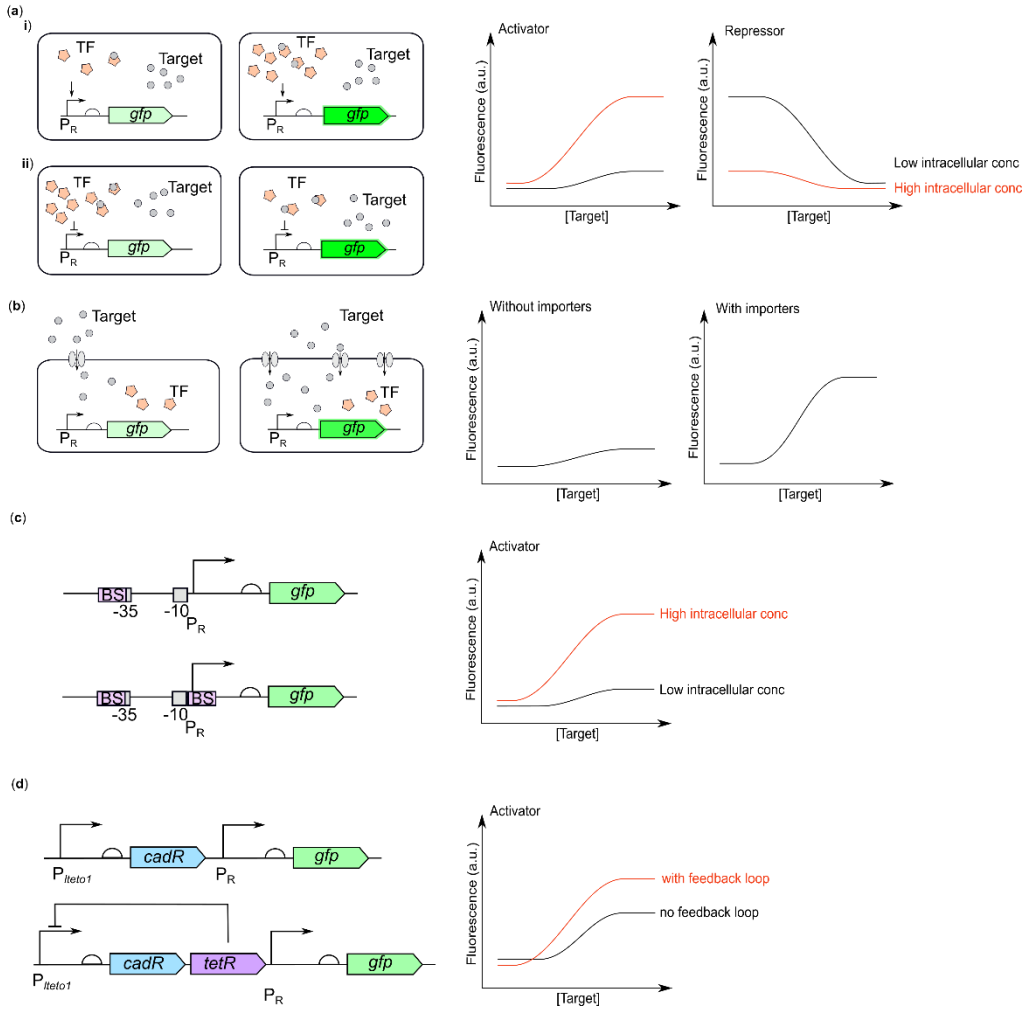


**Figure 1.4 Tools to improve sensitivity of cell-based biosensors.** (**a**) Altering the intracellular level of the transcription factor (TF) can improve the sensitivity of a genetic circuit. (**i**) For activators increasing the level of the transcription factor improves the sensitivity and increases output (**ii**) for repressors reducing the level of the transcription factor improves the sensitivity and increases output (Wang et al., 2015a). The graphs on the right show the impact on these changes on the response curve for both activators and repressors. (**b**) The addition of import machinery can improve the intracellular concentration of the molecule of interest to improve the biosensor sensitivity (Cayron et al., 2017). (**c**) shows how optimisation of the responsive promoter ($P_R$) can be used to increase the sensitivity of the whole cell biosensor through optimisation of the transcription binding sites (BS), figure adapted from (Chen et al., 2019). (**d**) shows how a negative feedback loop can be used to remove leakiness and improve the sensitivity of a biosensor

### 1.1.3 Alternative sensing approaches

More recently with the continued concerns about genetically modified organisms, other approaches to utilise the sense and respond genetic circuits without the issues that whole cell biosensor approaches have faced are being considered for commercial use.

#### 1.1.3.1 Cell-free transcription-translation systems

The first step towards overcoming the fear surrounding genetically modified organisms was to remove the replicative ability to ensure escape was not possible whilst retaining the cellular machinery to respond to external signals.

Cell-free transcription-translation systems have been used to test sense and respond genetic circuits that were previously used in whole cells (Wan et al., 2019a). Beyond the advantages of the lack of replicative ability which reduces the fear of accidental release it also allows for products that have otherwise toxic parts to be utilised and sensors to be developed for molecules of interest so expands the range of sensing beyond what can be achieved by whole cell sensors. The removal of the cell wall and membrane also circumvents the issue surrounding how to ensure that the molecules of interest are present in high enough levels within the cell to result in a response, as outlined in section 1.1.1.3. Cell free systems can also allow for a faster response because the time for the molecule of interest to be transported into the cell is no longer an issue.

The same format of using a transcription factor and responsive promoter being used in many of the tools highlighted in sections 1.1.1 and 1.1.2 are also applicable to the optimisation of biosensors using cell-free transcription translation systems. In addition, further tools and approaches to optimise the sensors have been developed to take into account the challenges and characteristics that are specific to cell-free systems.

Firstly, the exact concentration of the plasmid being used to express the biosensor construct can be accurately controlled allowing this to be used to adjust the ratio between the transcription factor and responsive promoter, which is known to be highly important for the sensitivity of the biosensor and the leakiness. Often in the case of cell-free transcription translation systems the transcription factor will be expressed on a separate plasmid to the responsive promoter to allow a wider combination of levels of the transcription factor and responsive promoter to be tested (Voyvodic et al., 2019).

Another advantage of having the transcription factor expressed from a separate plasmid is that, which can further reduce the time for the response because the transcription factor is already available (Silverman et al., 2020, Pandi et al., 2019).

The response of biosensors using cell-free transcription-translation systems have been shown to have issues with high variability between different experiments. This is frequently thought to be due to variability within the cell free lysate, and methods to reduce the variability have been developed to improve the use of cell free transcription translation systems for biosensors (Dopp et al., 2019a, Rhea et al., 2022). Further work into developing cell-free transcription-translation systems has shown that the buffer used in conjunction with the lysate is highly important for the functionality and can be adjusted to improve a specific characteristic as desired, such as the response time or the protein output (Banks et al., 2022b).

However, removing the replicative ability and the cell wall also means that the transcription translation machinery within the cell free lysate is more affected by changes in the environmental conditions such as the pH of the system which can have a large impact on the ability of the lysate to function. Retaining separation of the transcription-translation machinery from the wider environment can help to mitigate this issue. One way to do this is to encapsulate the cell free transcription translation system within a lipid membrane to generate a more cell like environment. This approach requires

the molecule of interest to be able to diffuse across the lipid membrane for the response to be generated which would not be suitable for all molecules of interest or functionalisation to allow transport (Boyd and Kamat, 2021, Boyd et al., 2023).

An alternative approach to cell-free is the use of synthetic cells which do not possess the ability to reproduce in common with cell-free systems but retain a more cell like environment for the biosensor. These cells are produced through the removal of the host genome (Fan et al., 2020). In the case of biosensors this removes the interaction of the biosensor circuit and the host genome which can also help to improve the response of a biosensor and increase the sensitivity to the analyte (Chen et al., 2021). Since this method also retains more cell-like features compared to cell-free transcription translation systems it has potential advantages for transcription factor based biosensors which do not function well in cell-free systems (Wan, 2019).

#### 1.1.3.2 Cell-free transcription only

More recently the length of time that biosensors which require both transcription and translation has been an area of focus for biosensor optimisation because the time for the response to be detectable is considered too long for many applications. The process of transcription occurs on a much faster timescale than translation and protein maturation, therefore if the response could be generated from transcription only this could provide a much faster response time.

The development of fluorescent RNA aptamers means that the output from transcription could be detected using optical approaches, as is frequently used for biosensors. This has been used when developing biosensors for heavy metal detection (Millacura et al., 2019) and other water contaminants (Jung et al., 2020). In this case tools previously outlined for whole cell biosensors and transcription-translation systems were adapted for use in transcription only sensors, such as using feedback loops. A range of different

colour RNA aptamers also exist which could be used for the detection of multiple molecules of interest at once.

An alternative approach is to use strand displacement reactions which also occur over very fast time frames. in this case the response can be detected through the release of a fluorescently labelled RNA from a quenching strand which prevents the detection of the fluorescence without the presence of the molecules of interest. An advantage of this system is the ability to generate complex logic gates in the systems which allows more complex signals to be detected and integrated which has advantages in some situations where biosensing could be used (Jung et al., 2022).

Although these systems expanded the number of biosensors that could be engineered because it allows proteins that have been shown to be toxic to cells when generating whole cell biosensors it still relies on the knowledge of a transcription factor and responsive promoter pair. So the work on expanding the range known is also important. The increasing ease and the reduction in cost of sequencing has resulted in a large increase both in the number of bacterial genomes available and new potential transcription factors. Genome mining has been important in identifying the sequences of potential transcription factors which could be used in the construction of biosensors for a wider number of molecules of interest. Genome mining can be carried out by either looking at DNA sequences which show homology to known transcription factors so are likely to also have similar functionality (Johns et al., 2018), or through searching part labels in protein and genome databases to find new parts (Xue et al., 2014).

Directed evolution has also been used with some success to alter the specificity of a transcription factor to generate a new version of the protein that detects a different molecule of interest (Beggah et al., 2008). However these approaches are specific to each protein used and will not always work when attempting to expand the range of molecules that can be detected. These techniques have increased the available potential parts for biosensors. These limitations mean there is a lot of interest in developing a universal

approach to generate biosensors that could be used to detect any chosen molecule of interest. Since a universal approach could potentially speed up biosensor development and improve performance.

#### 1.1.3.3 Binding protein biosensors

One potential approach is the use of a protein capable of binding the molecule of interest but that is not related to a downstream process which generates an output, and to then link this to an output. One method to generate an output is to use a split protein where the binding of the two parts of the protein generates the active form which generates the output. The reconstitution of the split protein can be controlled by another protein fused to split protein parts which responds to a molecule of interest, shown in **Figure 1.5**. Split T7 polymerase is one protein which has been studied for this purpose (Pu et al., 2017, Koh et al., 2016). Other split proteins have also been considered such as split enzymes (Guo et al., 2016) or through splitting fluorescent proteins which regain fluorescence when brought close together such as in protein dimerization on binding with a molecule of interest (Fan et al., 2008).

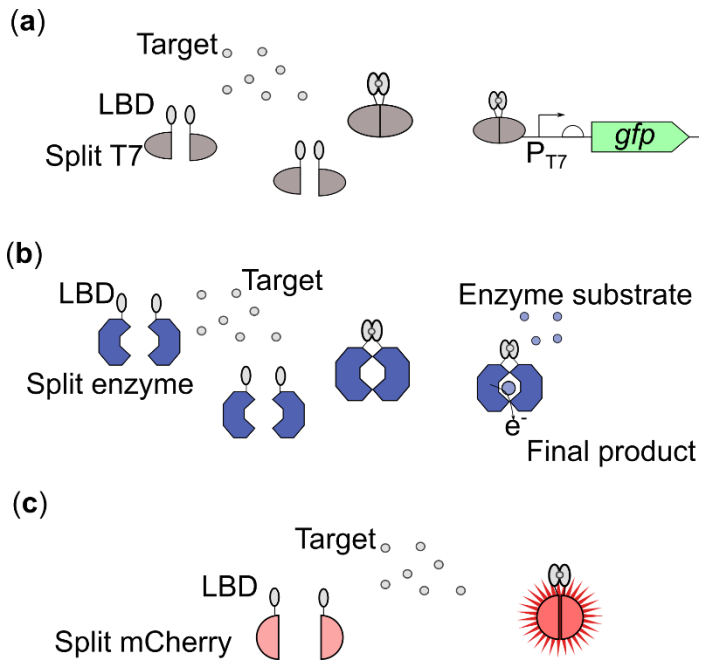


**Figure 1.5 Universal biosensor using split proteins.** The figure shows the use of split proteins to generate universal biosensors. A ligand binding domain (LBD) which binds to the target is fused to each half of the split protein. On binding with the target, the LBDs dimerise to bring the split protein together to allow it to regain function and generate the output. (**a**) The T7 polymerase is split, and on reconstitution the T7 polymerase binds to its promoter ($P_{T7}$) to express a reporter (*gfp*) (Pu et al., 2017). (**b**) An enzyme is split, and when the LBDs bind the target the enzyme is reconstituted to generate the active enzyme which will bind its substrate to carry out a reaction which will generate an output (Final product) (Guo et al., 2016). (**c**) A fluorescent protein can be split removing its ability to fluoresce; on proximity to the target the protein parts combine and the fluorescence can be regained to generate an output which could be detected (Fan et al., 2008).

Alternatively, rather than combining the protein used to sense the analytes with a split protein the output could be directly engineered into the protein (Marvin et al., 2011, Zhang et al., 2021b). When the binding protein interacts with the molecule of interest a conformational change occurs which is dose dependent, based on the number of protein molecules and the concentration of the molecule of interest. This conformational change needs to be linked to an output to generate sensors.

Fluorescence is an output that is often used in developing biosensors because of its easy detection. Circularly permuted fluorescent proteins have been engineered so that the N and C termini of the proteins are now within the protein sequence rather than at the natural end of the proteins (Kostyuk

et al., 2019). When this is inserted into a region of the binding protein that undergoes a large conformational change the new structure of the fluorescent proteins means that when the binding protein is in the unbound structure the fluorescent protein is out of its mature structure so it is not capable of fluorescing. When the molecule of interest binds the conformational change that occurs is transferred resulting in the fluorescent protein reaching its final folded structure to fluoresce which can then be detected, shown in **Figure 1.6**. This method has garnered interest because of its potential to be fast, sensitive and generally applicable to a wide range of molecules.

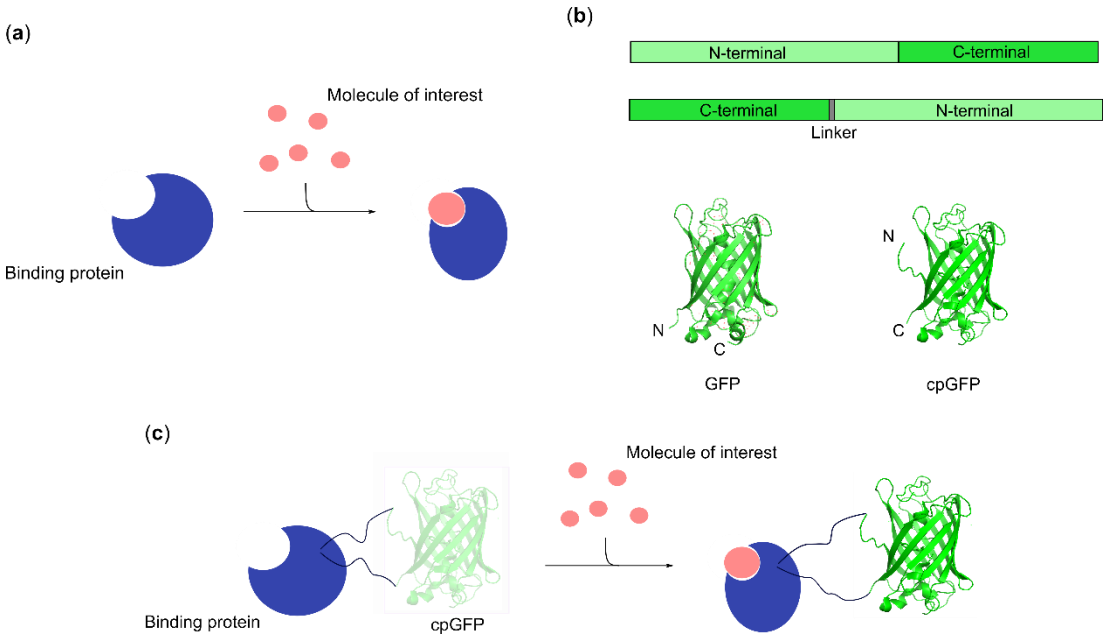


**Figure 1.6 Generating a fluorescent biosensor using a binding protein.** (**a**) shows the overview of how the binding of a molecule of interest generates a conformational change in a binding protein. (**b**) shows the difference between GFP and circularly permuted GFP (cpGFP). The N and C-termini are swapped in orientation between the two proteins so that the original N and C-termini are now in the middle of the amino acid sequence with a short linker added between. The crystal structures highlighting the change in the position of the N and C-termini (Kostyuk et al., 2019). (**c**) shows how a cpGFP protein could be inserted into a binding protein so that the conformational change of a binding protein can be used to generate a fluorescent output (Marvin et al., 2011).

When determining the best site for insertion rational approaches can be used when crystal structures of bound and unbound states are available. Programs to analyse the changes between the two structures in order to

determine where large conformational changes occur have been used (Grant et al., 2006). This program analyses the pseudo-torsion angle of four consecutive amino acids, shown in **Figure 1.7**. The pseudo-torsion angle is considered to be better for looking at the secondary structure and the changes in different states than per amino acid (DeWitte and Shakhnovich, 1994a). The angles are calculated for each structure and the differences between the angles of the two crystal structures are determined, this is then plotted to show regions that have high conformational changes. However, the two crystals structures will not always be available so this could limit the range of molecules that this approach could be applied to. Random insertion to find an insertion point could be used as an alternative and would allow many different sites to be studied, meaning proteins without detailed crystal structures for bound and unbound states could be used (Nadler et al., 2016).

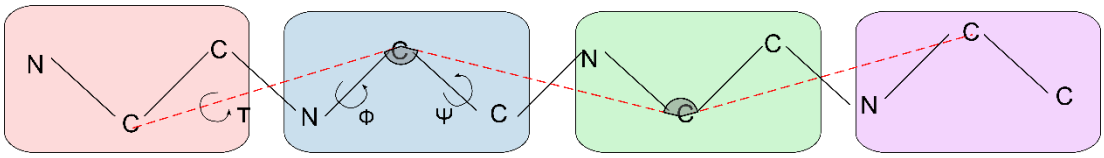


**Figure 1.7 Diagram showing pseudo-torsion angles compared to dihedral angles.** The figure shows a sequence of four consecutive amino acids (each individual amino acid is shown by a coloured box with only the backbone given). Dihedral angles are shown by the phi (Φ) and psi (Ψ) angles around the central carbon of an amino acid and give the amount of rotation in the bond between the central carbon and the neighbouring atom. The pseudo-torsion angles shown by tau (τ) are calculated along the red dashed line in the figure and show the amount of rotation possible between the central carbon of neighbouring amino acids. Figure adapted from (DeWitte and Shakhnovich, 1994a, Chandra et al., 2018).

A large challenge for these sensors is the ability of the conformational change to be transferred from the binding protein to the fluorescent protein. Also, it needs to be ensured that the insertion of the fluorescent protein does not alter the structure of the protein and impact its ability to bind to the molecule of interest as this might reduce the sensitivity to the molecule of interest. The linker region has been shown to be important to this and is often the focus of optimisation. However, the rules to generate a linker which has the required characteristics are unknown so non-rational approaches must be used, such as random mutagenesis. This is because the understanding

between amino acid sequence and the final protein structure are not fully understood. Further optimisation can also be made to the protein itself but again this would focus on non-rational approaches using random mutagenesis to try and increase sensitivity.

Antibodies and related proteins such as nanobodies can be generated in response to almost any molecule and so can work as a method of generating a protein which will respond to a molecule of interest, although large variability in antibody batches has been identified and cross reactivity can also be a challenge (Baker, 2015). This interaction then needs to be linked to a detectable output which could be split proteins. Another method is to display the nanobodies on the surface of the cell. The interaction with the molecule of interest will then result in agglutination which can be detected (Kylilis et al., 2019). The use of protein displayed on the surface of cells also allows the detection of proteins which do not effectively cross the cell membrane.

Two component systems (TCS) are a huge class of proteins found in all cells for signal detection and response. TCS work by a sensor kinase detecting the molecule of interest triggering autophosphorylation of the kinase domain. The kinase domain then interacts with the response regulator phosphorylating it to activate the response regulator which will then bind to the promoter and trigger the response, as shown in **Figure 1.8a** (Gao and Stock, 2009). However these sensing systems have rarely been used in the construction of biosensors mainly due to their poor performance outside of their natural context (Daeffler et al., 2017). TCS are highly specific and have complex regulation resulting in unexpected responses when reengineered (Gao and Stock, 2009). Work to improve the activity of TCS for use in biosensor development sought to change the sensing domain on the sensing protein to allow the sensing domains to be combined with TCS that showed better activity (Wang et al., 2013b, Mao et al., 2018, Levskaya et al., 2005, Baumgartner et al., 1994). However, there is a high level of variation in the sensor kinase domains and how the sensing of the target results in

autophosphorylation. The response regulator is far more modular with more overlap between different TCS. This allows the DNA binding domain to be swapped to one which interacts with a known promoter sequence that has good performance (Schmidl et al., 2019), as shown in **Figure 1.8b**.

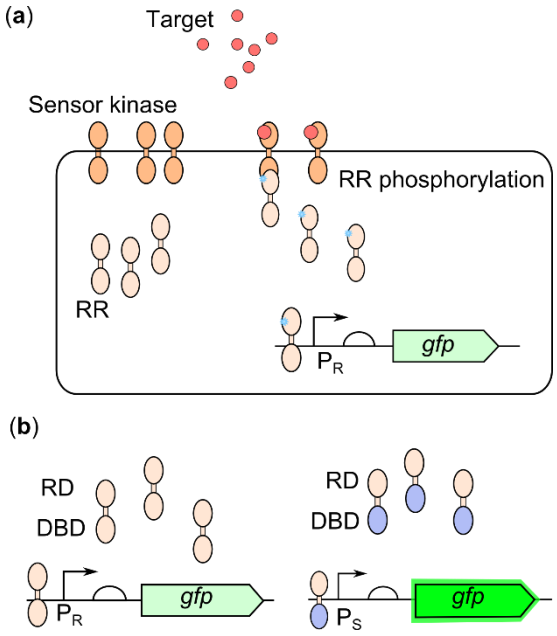


**Figure 1.8 Two component system architecture and optimisation.** (**a**) TCS are composed of a sensor kinase which detects the target, the signal is then transferred to the response regulator (RR) through phosphorylation, the response regulator then binds to the responsive promoter ($P_R$) to activate expression of the output (*gfp*). (**b**) The response regulator binding the responsive promoter ($P_R$) to generate the output (*gfp*) can result in a weak output. The DNA binding domain (DBD) of the response regulator can be swapped with one which binds an alternative promoter ($P_S$) to generate a stronger output (Schmidl et al., 2019).

### 1.1.3.4 Downstream detection

Another approach to generate universal biosensors is to develop a sensor for a metabolic product which the molecule of interest could be used to generate (Voyvodic et al., 2019), shown in **Figure 1.9**. This means that transcription factors capable of detecting the molecule of interest do not need to be identified. The optimisation of each sensor therefore becomes quicker as the sensing is already optimised because only the metabolic pathway to generate the metabolic product needs to be engineered into the cell.

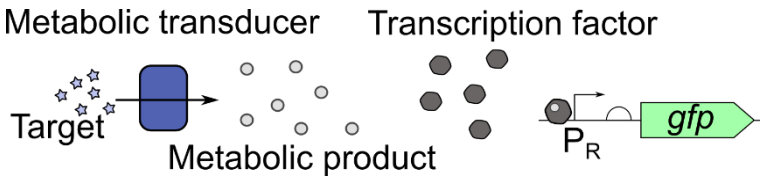


**Figure 1.9 Universal biosensor using metabolic by-products.** The target is converted into a specific metabolic production through a metabolic pathway (metabolic transducer) the metabolic product will then interact with a transcription factor which binds to a responsive promoter ($P_R$) to express a reporter (*gfp*) (Voyvodic et al., 2019).

#### 1.1.3.5 Nucleic acid biosensing

Nucleic acids can also be used for specific detection of a molecule of interest providing an alternative where proteins are not successful (Ueyama et al., 2002, Dwidar and Yokobayashi, 2019).

Aptamers which are short sequences of deoxyribonucleic acid (DNA) or ribonucleic acid (RNA) that fold into specific 3D conformations on binding to the molecule of interest can also be used in the construction of biosensors, shown in **Figure 1.10a**. Aptamers are particularly suited for detecting small molecules where there are only small difference between the molecule and other related molecules because even these small differences can affect the folding of the aptamer into its 3D conformation and alter the aptamer's response to non-target molecules (Dwidar and Yokobayashi, 2019, Ueyama et al., 2002, Mehennaoui et al., 2019, Fetter et al., 2015).

There is a large understanding about how DNA sequences interact with each other and the resulting structure can be predicted therefore allowing approaches to optimise aptamers to be developed. Targeted changes in the DNA sequences will alter the aptamers' ability to fold into the required shape. Commonly these mutations within the aptamer are away from the specific sensing sequence (Porchetta et al., 2012). For some aptamers the specific sensing sequences can be altered to adjust the concentration of the molecule of interest that can be detected. For example, potassium aptamers detect the potassium ion using a G quadruplex. Increasing the number or size of the

bases between the guanidine bases (Gs) alters the size of the loop formed by the G quadruplex which increases the concentration of potassium required to cause the conformational change and therefore the operating range of the aptamer (Wu et al., 2016). For aptamers that already have a 3D conformation or interaction with another nucleic acid before binding to the molecule of interest, increasing the energy required to allow the conformational change to occur through the length of complementary sequence or GC content can increase the concentration of the molecule of interest required for the conformational change to occur, as shown in **Figure 1.10b** (Catherine et al., 2014, Dwidar and Yokobayashi, 2019).

The specific conformational changes of nucleic acids can also be used to control the expression of a reporter through riboswitches. The conformational change reveals an RBS that allows translation (Dwidar et al., 2019). Nucleic acids can also be used to specifically sense the presence of a nucleic acid sequence of interest, thus expanding biosensing by using nucleic acids. Toehold switches are one method of achieving this. The nucleic acid sequence of interest will bind to change the conformation of the toehold switch making a RBS accessible (Pardee et al., 2016, Ma et al., 2018a), as shown in **Figure 1.10c**. DNAzymes are also pieces of DNA which recognise a specific molecule of interest and their conformational change triggers the cleavage of another nucleic acid, frequently RNA. The addition of fluorescent molecules onto these pieces allows the cleavage to be followed and the level of cleavage is dependent on the concentration of the molecule of interest allowing this to be used to detect a molecule of interest (Torabi et al., 2015). This also allows amplification because DNAzymes can cleave more than one molecule. This is an important characteristic for sensors because it strengthens the response. The literature shows that DNAzymes can be converted into aptamers. One method is to use a fluorescent base homologue which mimics the behaviour of the cleaved base (Zhou et al., 2016). A secondary analyte is often needed to allow the cleavage to occur so by prebinding the second nucleic acid with an altered base so that it is uncleavable this can be used to detect the secondary analyte, commonly an

ion. The 3D conformational change which occurs generates a change in the base's fluorescence. Splitting the substrate of the DNAzyme has also been studied to prevent cleavage and again the secondary analyte that is required could be detected through the addition of Förster resonance energy transfer (FRET) pairs which are brought together when the secondary analyte binds (Zhou et al., 2017).

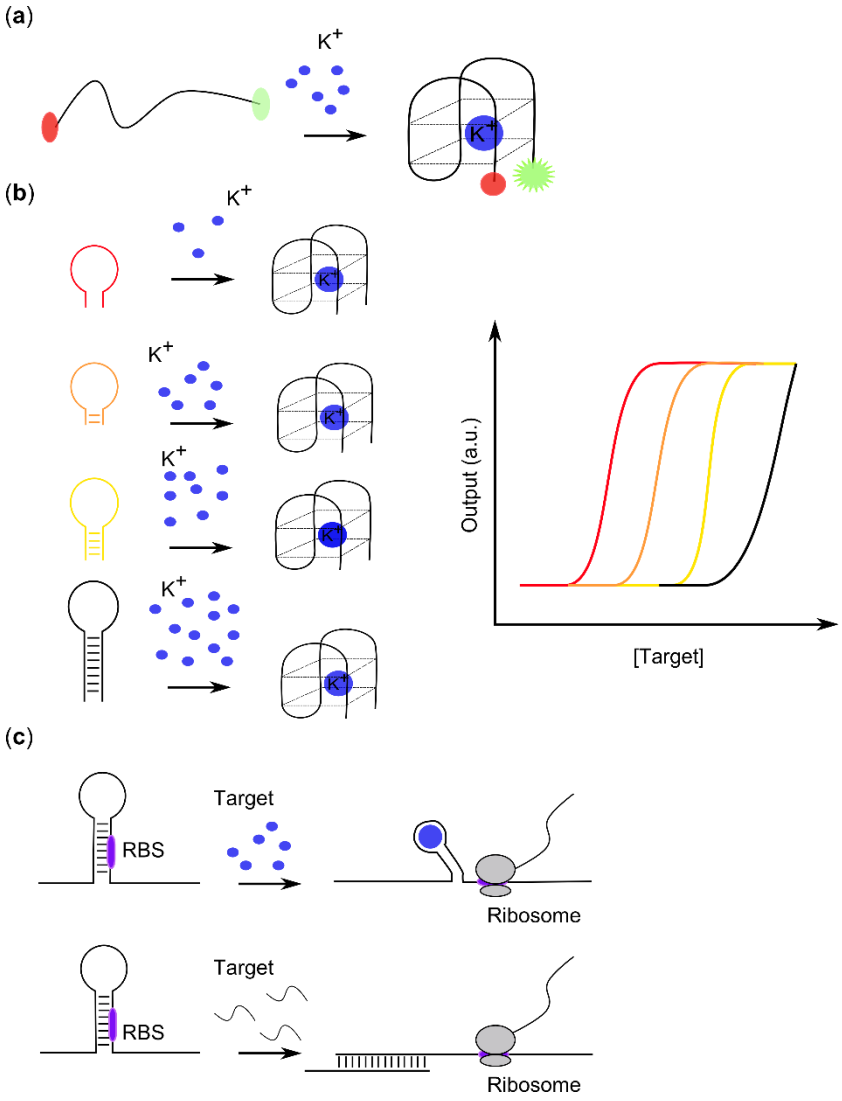


**Figure 1.10 Nucleic acid biosensing methods and optimisation.** (**a**) Shows the general mechanism of aptamers. Often fluorescent dyes are added to the nucleic acid to allow detection, the figure shows a FRET pair which are brought together by the molecule of interest ($K^+$) binding to allow fluorescent monitoring. (**b**) Shows an example of how aptamers can be tuned. By adding sequences for a hairpin the sensitivity of the aptamer can be altered, increasing the length of the hairpin increases the concentration of the target required to generate an output (Catherine et al., 2014). (**c**) Shows the mechanism of riboswitches and toehold switches. An RBS is hidden from ribosomes through the

secondary structure of the mRNA. On the binding of the target molecule or nucleic acid this structure changes to reveal the RBS allowing translation (Dwidar et al., 2019, Pardee et al., 2016).

CRISPR-Cas systems also recognise specific DNA sequences and can be adapted for use in genetic circuits and biosensing to expand the range of targets which can be detected (Bradley et al., 2016). The sensitivity of CRISPR-Cas to the exact sequence allows even single base changes to be detected when sensing, which is important for diagnostics (Pardee et al., 2016). CRISPR-Cas binding to the target DNA can be used to trigger cleavage of the specific nucleic acid (Pardee et al., 2016) and non-specific cleavage of other nucleic acids to generate output. Non-specific cleavage can be used to generate amplification as the activation of one Cas enzyme will cleave lots of nucleic acids to give very high sensitivity (Gootenberg et al., 2017). Detecting specific DNA sequences can be highly useful in diagnostics where the presence or absence of a pathogen's nucleic acids can be used to diagnose disease (Pardee et al., 2016). The cleavage of the CRISPR-Cas system can be removed by introducing mutations to the Cas protein. These deactivated systems can be linked to other proteins which generate the output either directly (Zhang et al., 2017b) or by activating or repressing reporter genes (Bradley et al., 2016). CRISPR-Cas systems have also been combined with other sensing components to allow the sensing of molecules as well as DNA (Xiong et al., 2020).

### 1.1.4 Improving biosensor specificity

Another issue that frequently affects biosensor performance is the specificity towards the sensing molecule. In transcription factor systems, the responsive promoter can have multiple layers of regulation. Cells need to be able to respond to a wide range of different signals and it is not possible to have a separate transcription factor for each signal. But the cell also needs to ensure that the response only occurs under the required conditions, such as in the case of metabolism where the pathway needs to be activated when the metabolite is present but only if the alternative preferred metabolite is not

present. So a single promoter or transcription factor will have interactions with multiple metabolites. When sensing and quantifying a molecule of interest using a biosensor it is important that any response is detected only from the molecule of interest to ensure accurate quantification.

Directed evolution has been used to improve the specificity and response of transcription factors to the molecule of interest (Lönneborg et al., 2012). This approach to remove extra regulation has also been applied to other parts, not just for transcription factors but also for promoters, for example (Yagur-Kroll et al., 2015a). However, this approach has not been a focus in synthetic biology because the aim is to develop approaches which are broadly applicable. The increase in number of available parts means that better suited parts can be picked that improve the specificity.

Where multiple different transcription factors capable of detecting the molecule of interest but that also have non-specific interactions exist, these can be combined in logic gates to ensure only specific interactions generate a response. An AND gate works so that the output response is only detected when both transcription factors are activated. They can be constructed as shown in **Figure 1.11**. This has been used for example in the case of zinc (Wang et al., 2013a). These logic gates can also allow multiple different related molecules of interest to be detected at once, which could be used to sense in more complex situations such as in diagnostics (Wang and Buck, 2012).

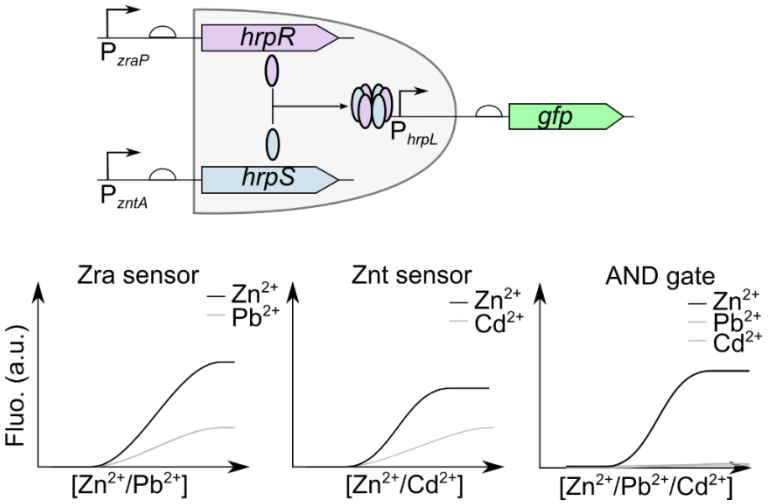


**Figure 1.11 Genetic logic gates to improve biosensor specificity.** Two different responsive promoters which respond to the same molecule of interest can be used to improve the specificity of a sensor through the construction of an AND gate. The two subunits of a transcription factor (*hrpR* and *hrpS*) can be expressed by the different responsive promoters ($P_{zraP}$ and $P_{zntA}$) so that the output (*gfp*) is only expressed from the downstream promoter ($P_{hrpL}$) when both are activated by the molecule of interest. In this case zinc, $P_{zraP}$ responds to both zinc and lead whilst $P_{zntA}$ responds to zinc and cadmium. By using both promoters the response is only generated when zinc is present but not the other ions (Wang et al., 2013a).

Another reason for poor specificity and performance of sensors is that the genetic parts used are derived from parts naturally found in the cell leading to unwanted interaction with the host cell. Genetic logic gates can be used to isolate the circuit from the host cell to improve performance (Wang and Buck, 2014). The genome of the host organism can also be edited to remove native copies of the parts to limit these interactions.

### 1.1.5 Output of sensor

Currently many biosensors are developed using fluorescence as the initial output because it allows quick easy detection which is useful when trying to optimise the sensor. Outside of the laboratory in a commercial setting this requires a light source and detector. Work into common optical outputs has shown that different outputs can change the response time and sensitivity of biosensors (Lopreside et al., 2019). Luminescence is one alternative optical reporter that is often used. It has some advantages because it does not need

a light source to excite the molecule making detection simpler for a commercial device. Luminescence also has very low background output which is good for sensitivity but usually requires additional chemicals for the response and a dark box to allow detection. Colorimetric outputs are another optical reporter that can be used and they do not require specific equipment to detect the output, making this a common output for sensing devices due to the suitability for commercial devices. There is no requirement for a light source or darkness to detect but it is harder to quantify. Semi-quantitative methods have been developed based on using a panel of sensors with different sensitivities where the optical outputs indicate different quantity thresholds. This method can reduce the need for equipment whilst still allowing some level of quantification which can be important for determining the next steps in some applications (Wan et al., 2019b).

For any sensor that is to be used outside of the laboratory setting the output and how this can be detected is an important consideration. The extra equipment required needs to be minimised as far as possible. Advances in mobile phones and miniaturisation of cameras have helped to facilitate the use of biosensors outside of the laboratory because now many small pieces of equipment that can be connected to a phone have been developed and can be used to detect sensor outputs (Zhu et al., 2011, Schulz-Schönhagen et al., 2019). This allows quantification of the sensor output which is highly important for sensing applications. The detection by a mobile phone will be far less sensitive than laboratory equipment meaning the optimisation of the sensor is even more important.

### 1.1.6 Other considerations for commercialisation

Ensuring that a biosensor has a strong, sensitive and easily detectable output is important in biosensor commercialisation but also needs to be done to fit the specific requirements of the application, so the most appropriate biosensor format will vary. The different characteristics and advantages and

disadvantages of each sensor format is highlighted in **Table 1.1**. The table lists the characteristics that need to be considered.

**Table 1.1 Summary of characteristics to consider for biosensor development.** The table outlines key characteristics of the biosensor that are important when developing and optimising a sensor as well as when deciding which sensing approach to use.

| Characteristic | Whole cell biosensor | Cell-free transcription translation biosensor | Protein biosensors | DNA aptamers |
|---|---|---|---|---|
| Response time | Slow - takes hours to be detected | Slow- takes hours but often faster than whole cell | Fast - response within minutes as only relies on binding interaction | Fast - response within minutes as only relies on binding interaction |
| Sensitivity | Will depend on the interaction between the transcription factor and the ligand | Same as for whole cell biosensors | Depends on the interaction between the protein and its ligand | Usually very sensitive |
| Specificity | Depends on the transcription factor and promoter pair used, can be selected for high specificity | Also depends on transcription factor and promoter pair | Will depend on the protein but can be selected for | Usually highly specific |

| Characteristic | Whole cell biosensor | Cell-free transcription translation biosensor | Protein biosensors | DNA aptamers |
|---|---|---|---|---|
| Range of tools | Large number of tools to alter the response curve leakiness and maximal output | Whole cell biosensor optimisation tools also apply | Few optimisation tools, linker region known to be important but optimisation is ad hoc | Some tools available, the rules governing DNA base interactions well understood |
| Cost | Low cost to generate | Commercial cell free lysates expensive Homemade lysates much lower cost | Purification of protein can be expensive depending on the method | Synthesised DNA relatively inexpensive, if fluorescent dyes or special bases the cost increases significantly |
| Output | Can be altered to fit specific requirement including optical, chemical, electrical | Same outputs as for whole cell biosensors can be used | Limited to fluorescence based outputs | Often linked to electrochemical outputs but can be used with fluorescent outputs |

| Characteristic | Whole cell biosensor | Cell-free transcription translation biosensor | Protein biosensors | DNA aptamers |
|---|---|---|---|---|
| More complex sensing | Yes - logic gates can be used to combine different biosensors so that responses are only generated for the correct combination | Yes - same combination of different sensors as in whole cell biosensors can be achieved | No - different proteins required to detect different markers and no way to combine | |
| Multiple reads | No - stability of the output means once produced it remains and cells usually required to be actively dividing for a new response to be possible | No - has similar output issue as whole cell biosensor and the cell free lysate will only have activity for a limited amount of time | Yes - the ligand can unbind to end the response which is regained when the ligand rebinds | Yes - also dependant on a binding reaction so can be reversed |

The characteristics of the biosensor response are highly important for achieving the desired sensing characteristics and the different biosensing approaches are important for selecting abiosensor that can generate the type of response desired. However, there are also other hurdles to commercialisation.

#### 1.1.6.1 Biosafety and containment

The fear over genetically modified organisms and their release into the environment has been a key challenge which has led to a large amount of work into developing methods to ensure that modified organisms are not able to survive in the environment.

Programmable cell death is one method that has been explored. This can be achieved by placing the expression of the toxic gene under the control of an inducible promoter. An anti-toxin is expressed at a level that ensures no accumulation of the toxin occurs in the presence of the inducer contained in the sensing device so the cells are able to survive. If the cells escape into the environment the lack of the specific inducer would result in increased expression of the toxic protein which would cause cell death (Chan et al., 2015, Stirling et al., 2017). However this approach also generates a strong selection pressure. To help speed up the death of the cells the signal to trigger cell death can also trigger degradation of essential genes which would reduce the chance of escape (Chan et al., 2015). Memory elements have also been added to ensure that loss of the cell death system also results in the death of the cell to ensure the biocontainment system is not lost (Stirling et al., 2017). Multiple cell death signals can also be included to restrict cells to one environment. This is useful for sensors that could reach multiple environments such as ingestible sensors for health monitoring to ensure the sensor only works in the right body part (Mimee et al., 2018, Chien et al., 2022).

Generating auxotrophic cells is another method of preventing the cell from escaping into the environment. Essential genes are deleted from the cell's genome so the cells are not able to make all the chemicals needed for them to be able to grow and survive without intervention. Multiple essential genes are usually deleted because this makes it harder for escape mutants to be formed (Lopez and Anderson, 2015).

Unnatural amino acids not found in nature can also be used to prevent cell survival in the environment as well as stop any plasmid transfer to other cells through bacterial conjugation which is an alternative way that genetic modification could escape into the environment. The redundancy of codons for protein translation has meant that stop codons can be reengineered to insert an amino acid rather than terminate translation (Lajoie et al., 2013). By using non-natural amino acids within essential genes cells cannot survive in the environment because without the addition of the non-natural amino acid the cells are not able to express the essential proteins which have been modified, resulting in death (Rovner et al., 2015). The use of recoded codons within the plasmid can also prevent the transfer of the plasmid to cells in the environment because without altering the transfer RNA (tRNA) in the cell the codons will still be recognised as stop codons resulting in truncated proteins (Mandell et al., 2015).

Splitting toxin / anti-toxin systems across the plasmid and the genome is used as a method to prevent plasmid transfer as well as cell escape. The toxin is expressed on the plasmid whilst the anti-toxin is expressed from the genome, so that if the plasmid is taken up by other cells it is toxic (Wright et al., 2015). Placing the initiator protein for the origin of replication of the plasmid on the genome has also been used to prevent the plasmid from being able to replicate in other cells (Wright et al., 2015).

Frequently multiple different control mechanisms are incorporated because it is much less likely that all of the control mechanisms are mutated (Wright et al., 2015, Gallagher et al., 2015).

Xeno nucleic acids (XNA) are nucleic acids that are synthetic using a different backbone to DNA and RNA and not found in nature. Using this would ensure the cells would not survive in the environment because the individual bases of the XNA would need to be supplied to the cells. The genetic information is entirely non-natural and would not be able to be produced through the cell’s metabolism. This would also prevent the modified

parts being taken up by other cells and escaping into the environment because the XNA would not be recognised by other cells (Schmidt, 2010).

#### 1.1.6.2 Stability of sensor

Biosensors will need to be able to be stored for long time periods before use without any change in the performance of the sensor in order to be viable commercial products. A large amount of research has been done into improving the shelf life of biosensors as not only is long storage time required but also storage in ambient conditions. Biosensors are attractive for use in a low resource setting where cold chain storage is not necessarily feasible.

Lyophilisation is a key method researched that has shown promise for storing biosensor for long time periods. Freeze-dried cells have been shown to be able to be stored for around 3 months (Watstein and Styczynski, 2018, Siegfried et al., 2012, Struss et al., 2010, Yagur-Kroll et al., 2015b). However specific storage conditions at 4°C or -20°C are still required to achieve the maximum storage lifetime (Yagur-Kroll et al., 2015b, Struss et al., 2010). Cell-free biosensors which are an increasingly common method of constructing a biosensor also show good stability under lyophilisation (Pardee et al., 2016). This has shown to be able to increase the shelf life of cell-free sensors, with freeze-dried cell-free extract being able to be stored at room temperature for a up to a year (Magro et al., 2017, Pardee et al., 2016). Cell-free sensors are often stored on paper during the freeze-drying process which allows easy use.

Encapsulation has also been shown to be able to extend the lifetime of cells. *E.coli* has been shown to be able to be stored in alginate beads at 4°C for over a month (Li et al., 2017b), whilst encapsulation of other slower growth organisms within a material allowed storage at room temperature for months (Power et al., 2011). This suggests that using alternative organisms could be a good way to extend the shelf life of biosensors.

Other bacterial species are capable of forming spores that allow long term survival in adverse conditions. Using these bacterial species means that the cells could be induced to sporulate for storage and then reactivated when sensing is required (Schulz-Schönhagen et al., 2019). Studies into this have shown that the spores can survive for a year in a range of temperatures and humidity (Sangal et al., 2011), making this a good option for increasing the shelf life without requirements for specific storage conditions (Schulz-Schönhagen et al., 2019).

There has been progress in improving the storage lifetimes of biosensors and the conditions required but the need for reactivation of the biosensor is less desirable in a commercial product because it adds another step in the use of a device. In the case of spores this is significant as this is a necessary step but freeze-dried sensors can often be reactivated solely by the process of taking the sample, which would be convenient.

Stability of the response under different working condition is also important. The output from the sensor needs to remain the same despite any variation in the conditions to ensure accurate quantification of the molecule of interest. The construction of reactors which can maintain the cell at a desired density and growth state in a defined medium with the molecule of interest diffusing into the device is one method of ensuring the robustness of the results. This also allows multiple measurements to be taken from the same device which would be very important for some applications (Buffi et al., 2016).

Ensuring each part of the sensor is maintained at the same level between sensors and there is no intra sensor variability is also important. The use of feedback in the genetic circuits has also been studied in the literature to ensure that the expression levels from the genes remains the same despite variations in the copy number which could be a significant cause of variation in cell-based biosensors (Becskei and Serrano, 2000).

A key factor which can impact stability is burden. Adding additional DNA and genetic circuits to cells generates burden because the cellular machinery is

diverted from growth and maintenance to the expression of these new genes. This can lead to growth defects and unexpected responses from the genetic circuit (Qian et al., 2017, Borkowski et al., 2016). Increased understanding of burden and its causes means that sensors are being designed taking burden into consideration and attempt to reduce it, including programs which can automate this (Nielsen et al., 2016). Genetic circuits which generate too high burden show less stability, with the output of the sensor decreasing over time. Over time a high burden sensor's output is lower because the cell reduces the expression as it takes too much from growth and maintenance (Liu et al., 2018a).

## 1.1 Wearable devices

Monitoring biomarkers is crucial in healthcare for diagnosing disease, monitoring treatment and monitoring general health (Mimee et al., 2018, Magro et al., 2017, Watstein and Styczynski, 2018). Traditionally testing biomarkers is done by taking a sample from the patient, frequently blood, and sending the sample to a centralised laboratory to test. However, this limits the accessibility of these tests because it requires the samples to be taken within a healthcare setting and requires specialised laboratory facilities and trained personnel to carry out the testing of the samples. Being able to carry out testing within community settings, the home, elderly care facilities or schools, and at the time of seeing an individual with results on the spot would avoid the need for follow-on appointments for test results and speed up diagnostics. It would improve access to health care in low-resource settings where the infrastructure for traditional biomarker testing is hard to access. It could allow treatment for the correct disease to start sooner potentially improving outcomes (Bonawitz et al., 2015). In more developed countries it can also increase the level of testing by providing easier access and reducing the likelihood of missed appointments (El-Osta et al., 2017). Avoiding the need to send samples to a laboratory for testing increases the speed of results which allows for faster treatment and could reduce wait times within

healthcare systems, which is an ongoing challenge (Goldstein et al., 2019). Healthcare costs are also increasing and methods to reduce costs are increasingly important; point-of-care testing also has the potential to reduce healthcare costs (El-Osta et al., 2017).

Frequent or continuous monitoring gives a much deeper understanding of an individual's own normal ranges and cycles. This would allow earlier detection of negative states which could reduce costs and give the information required for personalised medicine. Wearable devices which can monitor continuously and allow data collection without input from either the individual or medical professionals would allow this (Kim et al., 2014, Sempionatto et al., 2017). Wearable devices have a large potential in both of these cases but currently the majority of wearable devices available commercially that can monitor continuously are only able to monitor physical markers of health such as heart rate and blood pressure, although some new monitors have been developed such as continuous glucose monitors but these require implantation. In order to be able to truly understand inter- and intra-individual variability and changes which signify changes in health more markers need to be monitored expanding these to include chemical markers. Sweat would also allow biomarkers to be monitored. The increased interest in using sweat as alternative source of biomarkers has led to lots of research into devices for monitoring biomarkers (Gao et al., 2016, Anastasova et al., 2017, Koh et al., 2016, Kim et al., 2019).

Currently the majority of devices use electrochemical detection methods for monitoring biomarkers. This allows fast, sensitive detection of biomarkers, however electrochemical sensors have some disadvantages. Electrochemical sensors work by converting the biological sensing often through enzymes or antibodies into a detectable change in electrical current. This method of biosensing has disadvantages in the sensor elements used, such as antibody cross reactivity and the instability of these proteins. This electrical sensing is also easily affected by many other factors such as temperature and pH which complicates the development of wearable

electrochemical sensors as other electrodes and measurements are required to account for these factors (Tseng et al., 2018). The cost to develop and produce these wearable sensors is also high. Stretch and strain also alters the conductivity of electrodes which is a challenge when developing wearable devices which will withstand high levels of stretch and strain. Electrodes which are insensitive to stretch and strain have been developed but are more complex to produce (Zhao et al., 2019).

Another important consideration if wearable devices are to be taken up and used is that they need to be comfortable to wear. Breathable, flexible materials need to be used so that the skin is able to breathe and move as normal. Such materials must also allow a high degree of contact with the skin as this is important for the device in taking up the sample and minimising the risk that contaminants could enter the sample (Heikenfeld, 2016, Boysen et al., 1984). Many materials exist which have these properties. Hydrogels are a popular choice because of their ability to absorb a large volume of water to swell which also allows, buffers and other chemicals that are important for the function of the sensor to be absorbed into the device. Hydrogels also have highly tuneable physical properties in terms of strength and stretchability. It is highly important that a wearable device can not only deal with the stretch and strain from movement of the wearer but can then return to normal and withstand repeated rounds of movement (Kolewe et al., 2015, Killion et al., 2011, Liu et al., 2017, Lei et al., 2020). A wearable device will also require a high level of conformation and contact with the wearer to ensure that sample enters the device effectively in order to provide accurate quantification of biomarkers.

### 1.1.1 Sweat as a source of biomarkers

Traditionally blood has been the gold standard for testing biomarkers. However there are challenges in using blood samples particularly outside a healthcare setting due to the risk of infection when taking the samples. Obtaining a blood sample also generates discomfort which particularly when

repeated testing is required often results in non-compliance. Blood testing is not suitable for wearable devices. Other body fluids can be sampled non-invasively such as tears, saliva and urine and have been studied due to their relationship to blood. However passive sampling of these is less straightforward. For tears contact lenses can be used and for saliva a mouthguard is an option, but are not necessarily comfortable for the user. Sweat however can be sampled passively with no risk of infection or discomfort making it easy to sample frequently. Sweat also contains a high number of different potential biomarkers, making it a possible alternative to the traditional blood source of biomarkers.

Sweat glands are found all over the body making sweat samples easy to obtain. There are three types of sweat gland: eccrine, apocrine and apoeccrine. Eccrine sweat glands are found all over the body, so eccrine sweat has been these focus of using sweat as a source of biomarkers due to the ease of obtaining samples (Baker, 2019a). Eccrine sweat contains many different molecules and chemicals and some of the potential biomarkers in sweat already identified are highlighted in **Table 1.1**. The majority of biomarkers in sweat have been transported from blood through either passive diffusion from or active transport from blood as a waste product to be excreted in sweat. Some molecules found in sweat are produced in the sweat gland as part of sweat production and secretion (Sonner et al., 2015). The fact many components of sweat have moved from blood means potentially biomarkers in sweat will correlate to blood. Consequently, sweat is thought to have great potential as a source of biomarkers. But there are still some obstacles as the correlations between blood levels and sweat levels are not well understood because the study of biomarkers in sweat is only recent. Some biomarkers such as cortisol have been shown to have a correlation between blood and sweat (Torrente-Rodríguez et al., 2020), whilst for others the correlation is debated. For lactate some say there is a correlation (Sakharov et al., 2010) and others suggest that the correlation maybe conditional, such as only over a working muscle (Karpova et al., 2020) or not at all (Green et al., 2000, Derbyshire et al., 2012). Another concern is that

there is a delay of up to twenty minutes between changes in blood levels and sweat levels of biomarkers (Tamada et al., 1995, La Count et al., 2019). Depending on the biomarker this delay may not be an issue and the information will still be highly useful but for other biomarkers this delay could mean changes are not picked up until they are already detrimental such as changes in glucose levels in an individual with diabetes. However, trend data also gives important data and depending on the biomarker if an upward trend is recorded it may act as an early warning.

**Table 1.2: Summary of some of the biomarkers in sweat for monitoring general health and disease.** The table gives biomarkers secreted in sweat, what information can be determined from the biomarkers and the concentration range found in sweat.

| Biomarker | Sensing Application | Concentration Range | Reference |
|---|---|---|---|
| Glucose | Monitoring glucose levels in diabetics | 0.01-1 mM (diabetic)<br>0.06-0.11 mM (healthy) | (Bruen et al., 2017, Lee et al., 2017b) |
| $Na^+$ ions | Changes can indicate hydration status | 0-120 mM<br>Most around 30-60 mM | (Lee et al., 2017a, Baker, 2017, Bates and Miller, 2008, Lara et al., 2016) |
| $K^+$ ions | Can be used to monitor hydration | 2-10 mM | (Lee et al., 2017a, Baker, 2017, Vairo et al., 2017) |
| Lactate | Monitoring muscle energy levels<br>Monitoring oxygen delivery in the body | 5-120 mM | (Lee et al., 2017a, Derbyshire et al., 2012, Sakharov et al., 2010, Jia et al., 2013) |

| Biomarker | Sensing Application | Concentration Range | Reference |
|---|---|---|---|
| Tryptophan | Muscle fatigue | 2-25 µM | (Lee et al., 2017a), (Delgado-Povedano et al., 2016, Mark and Harding, 2013) |
| Cortisol | Stress on the body e.g. due to intense training<br>Monitoring circadian rhythms | 0.02-2.0 ng/mL | (Lee et al., 2017a, Jia et al., 2016) |
| Urea | Elevated levels indicated kidney failure | Below 65 mM in elderly is healthy | (Al-Tamer and Hadi, 1994, Mehta, 2008) |
| | Small increases can signify dehydration | Below 40 mM for younger people | |
| Nitrate | Converted to NO in body- which decreases in hypoxic conditions<br>NO also important for metabolism and cardiovascular function- dysregulation in either direction can lead to disease | Similar to blood plasma ~40 µM (range in blood 16-52 µM) | (Weller et al., 1996, Ma et al., 2018b, Neilly et al., 1995) |
| Nitrite | Nitrate in sweat reduced by bacteria to nitrite | Around 4 µM | (Weller et al., 1996) |

| Biomarker | Sensing Application | Concentration Range | Reference |
|---|---|---|---|
| Nitric Oxide | Produced from nitrite on skin | pM per min | (Weller et al., 1996) |
| Histamine | Important in allergic reactions<br>Role in environmental stress response | Around 5-20 µg/l | (Garden, 1966) |
| TNF-α | Monitoring stress on the body | 0.04-0.15 pg/mL | (Hladek et al., 2018, Lee et al., 2017a) |
| IL-6 | Increased levels linked to poorer cancer prognosis | 0.03-0.15 pg/mL | (Hladek et al., 2018) |
| IL-10 | Levels linked to tumour size, can give an indication of response to treatment | 0.03-0.1 pg/mL | (Hladek et al., 2018, Zhao et al., 2015) |

## 1.2 Biomaterials

Generating materials with extra functionality is a big area of research which would allow properties previously unattainable to be added to materials, such as self-healing properties. Biomaterials can be materials which are produced using biological approaches or materials which can be combined with biological parts to add new characteristics and functions and there is a large area of research to achieve this.

### 1.2.1 Smart materials

Smart materials are materials capable of detecting and responding to the environment, such as detecting pollution in the environment (Gadore and Ahmaruzzaman, 2021) or delivering drugs in medicine (Mazidi et al., 2022). This is an area where biomaterials could have many advantages due to the natural ability in biology for sensing and responding to the environment.

In medical applications smart materials could allow dressings for wounds or medical implants to not only help with healing or act as scaffold but to also monitor how healing is progressing. They could monitor how a disease is progressing and provide information on this to medical professionals. Then based on the information sensed the smart materials can respond with the production or release of chemicals to correct and treat the disease (Su et al., 2010). Smart materials can also be used to generate monitoring devices for biomarker detection and quantification (Arakawa et al., 2016, Zhao et al., 2019). In this case the specific materials used can be chosen to have high biocompatibility and low immunogenicity to generate devices that are highly comfortable for long term wear and to maintain the biological parts.

When creating these devices, 3D printing allows materials to be printed to specific shapes which allows devices to be generated that will conform to the desired location and application of the biomaterial. Advances in 3D printing means this printing can be done directly onto living tissue to conform to the 3D shape of the tissue (Zhu et al., 2018).

## 1.3 Project objectives

Monitoring the levels of different biomarkers is important for understanding the health and physiological state of an individual. Being able to monitor biomarkers frequently and outside of a healthcare setting would allow greater understanding of normal fluctuations in biomarker levels and those fluctuations which signify changes to an individual’s physiological state. Wearable devices capable of monitoring biomarker levels in sweat offer a

good method for carrying out frequent monitoring of biomarkers because this allows for passive monitoring of biomarkers and increases the level of monitoring which can be undertaken. Current research is looking to develop wearable sensing devices based on electrochemical outputs using either biosensors or completely electrochemical sensors which provides fast sensitive detection but faces challenges in power requirements, results being affected by changes in temperature, strain, humidity and pH which need to be controlled for and the high cost to produce the devices. Many tools and new technologies have been developed for the construction of biosensors which are highly sensitive and specific to the molecule of interest. Biosensors which use alternative outputs such as optical outputs are also cheap to produce and less affected by changes in conditions such as humidity and strain. Therefore, biosensors could provide a good alternative for detecting biomarkers of human health and physiological state in sweat. Work into biomaterials also means that these biosensors could be used to functionalise a material to generate a wearable device.

My PhD project aims to develop a proof of concept wearable device for monitoring biomarkers of human physiological status and health using a biomaterial that contains a range of biosensors. Biosensors for monitoring potassium, lactate, tryptophan, cortisol, histamine and testosterone will be developed and optimised using synthetic biology tools to detect the concentration ranges found in sweat. A range of different biosensing approaches including cell-based genetic circuits and single molecule approaches will be studied to determine the best approach to develop biosensors that have the desired characteristics for a wearable device, including the response time and the possibility to take multiple measurements.

These biosensors will be combined with hydrogel materials to look into the effect of encapsulation and how the impact of encapsulation on the sensor can be minimised to ensure the required characteristics are maintained.

Finally, these encapsulated sensors will be used to develop a wearable device which will be used to study the ability of the device to function on human skin and to develop an accompanying App to simplify response detection and results recording.

# 2 Materials and methods

## 2.1 Materials

### 2.1.1 Growth media

The growth media used in the study are listed in **Table 2.1**. Media were sterilised by autoclaving at 121°C for 15 minutes or by filtration using a 0.22 µm filter (SLGPO33RS, Miliipore).

**Table 2.1: Growth media used in this study**

| Medium | Ingredients | Sterilisation | Use |
|---|---|---|---|
| LB | 10 g/L peptone, 5 g/L NaCl, 5 g/L yeast extract | All components were combined and autoclaved. | Culture of bacteria for DNA extraction. |
| LB Agar | 10 g/L peptone, 5 g/L NaCl, 5 g/L yeast extract, 16 g/L agar | | Culture of bacteria on solid media. |
| M9 media with 0.4% glycerol | 11.28 g/L M9 salts (M6030, Sigma-Aldrich), 1 mM thiamine hydrochloride, 0.2% (w/v) casamino acids, 2 mM $MgSO_4$, 0.1 mM $CaCl_2$, 0.4% (v/v) glycerol | All components except for thiamine hydrochloride, which was filter sterilised, were autoclaved separately and components. mixed fresh each time. | Characterisation of biosensors and swelling of hydrogel when using encapsulating cells, except for the tryptophan biosensor. |

| Medium | Ingredients | Sterilisation | Use |
|---|---|---|---|
| M9 medium with 0.4% glycerol and homemade amino acid solution | 11.28 g/L M9 salts (M6030, Sigma-Aldrich), 1 mM thiamine hydrochloride, 2 mM $MgSO_4$, 0.1 mM $CaCl_2$, 0.4% (v/v) glycerol, 1x homemade amino acid solution containing no tryptophan (see **appendix 1** for the full concentrations of all amino acids) | All components were autoclaved separately, except for thiamine hydrochloride and the homemade amino acid solution which were filter sterilised. The components were then mixed fresh each time. | Characterisation of tryptophan biosensor and swelling of hydrogel when using encapsulating cells. |

### 2.1.2 Antibiotics

The antibiotics used in bacterial growth are list in **Table 2.2**. All antibiotics were sterilised by filtration using 0.22 µm filters.

**Table 2.2: List of antibiotics used in this study.**

| Antibiotic | Concentration | Stock concentration | Solvent |
|---|---|---|---|
| Ampicillin | 100 µg/ml | 100 mg/ml | $ddH_2O$ |
| Kanamycin | 50 µg/ml | 50 mg/ml | $ddH_2O$ |
| Chloramphenicol | 25 µg/ml | 25 mg/ml | Ethanol |

### 2.1.3 Bacterial strains

For this project *E. coli* TOP10 was used for all cloning and cell-based assays. To generate the cell lysate for cell-free BL21 (DE3) Δlac.

### 2.1.4 Plasmids and DNA

Key plasmids for the optimised sensors are listed below in **Table 2.3**. The full DNA sequences of each part is given in **Appendix 1**. The sequences of the aptamers used are giving in **Table 2.4**.

**Table 2.3: List of optimised sensors used for identified biomarkers**

| Name | Use | Genetic parts |
|---|---|---|
| Lactate sensor | Plasmid containing the sense and respond genetic circuit to detect lactate. | J23101 RBS 32 LldR (reverse) $P_{LldR(117)}$ RBS 30 GFP |
| Dual lactate sensor | Plasmid containing the sense and respond genetic circuit to detect lactate and constitutive mRFP. | J23101 RBS 30 or 32 mRFP J23101 RBS 32 LldR (reverse) $P_{LldR(117)}$ RBS 30 GFP |
| Dual lactate sensor mNeon | Plasmid containing the sense and respond genetic circuit to detect lactate with mNeonGreen reporter and constitutive mRFP. | J23101 RBS 30 or 32 mRFP J23101 RBS 32 LldR (reverse) $P_{LldR(117)}$ RBS 30 mNeonGreen |
| Optimised tryptophan sensor | Plasmid containing the sense and respond genetic circuit to detect tryptophan. | J23109 RBS 33 TrpR EK49 (reverse) $P_{TrpO}$ RBS 30 GFP |
| Dual trp sensor | Plasmid containing the sense and respond genetic circuit to detect tryptophan and constitutive mRFP. | J23101 RBS 30 or 32 mRFP J23109 RBS 33 TrpR EK49 (reverse) $P_{TrpO}$ RBS 30 GFP |

| Name | Use | Genetic parts |
|---|---|---|
| Dual trp sensor mNeon | Plasmid containing the sense and respond genetic circuit to detect tryptophan with mNeonGreen reporter and constitutive mRFP. | J23101 RBS 30 or 32 mRFP J23109 RBS 33 TrpR EK49 (reverse) $P_{TrpO}$ RBS 30 mNeonGreen |
| AvT88 | Constitutive expression of Avidin mutant for detecting testosterone with cpGFP inserted after the 88$^{th}$ amino acid. | J23101 RBS 30 Avidin-Testosterone cpGFP insertion 88$^{th}$ amino acid |
| AvC88 | Constitutive expression of Avidin mutant for detecting cortisol with cpGFP inserted after the 88$^{th}$ amino acid. | J23101 RBS 30 Avidin-Cortisol cpGFP insertion 88$^{th}$ amino acid |
| AvC88.169 | Constitutive expression of Avidin mutant for detecting cortisol with cpGFP inserted after the 88$^{th}$ amino acid with a mutation in the linker region. | J23101 RBS 30 Avidin-Cortisol cpGFP insertion 88$^{th}$ amino acid with the first linker mutated from (YPDRVYIK to YPDRVYI**Q**) |
| AvC88.100 | Constitutive expression of Avidin mutant for detecting cortisol with cpGFP inserted after the 88$^{th}$ amino acid with a mutation in the linker region. | J23101 RBS 30 Avidin-Cortisol cpGFP insertion 88$^{th}$ amino acid with the second linker mutated from (KLEYEMAG to KLE**S**EMAG) |
| AM10 loop 5 | Constitutive expression of AM10 tick lipocalin with the | J23101 RBS 30 AM10 cpGFP insertion loop 5 |

| Name | Use | Genetic parts |
|---|---|---|
| | cpGFP inserted in loop 5 of the protein. | |

**Table 2.4: List of aptamer sequences with modifications made.**

| Name | Use | Sequence |
|---|---|---|
| MH064 | DNA oligonucleotide with 5’ FAM and 3’ TAMRA for sensing potassium with higher sensitivity. | /56-FAM/GGGTTAGGGTTAGGGTTAGGG/36-TAMSp/ |
| MH079 | DNA oligonucleotide with 5’ FAM and 3’ TAMRA for sensing potassium with increased loop size. | /56-FAM/GGGTTAAGGGTTAAGGGTTAAGGG/36-TAMSp/ |
| MH080 | DNA oligonucleotide with 5’ FAM and 3’ TAMRA for sensing potassium with increased loop size | /56-FAM/GGGTTATGGGTTATGGGTTATGGG/36-TAMSp/ |
| MH081 | DNA oligonucleotide with 5’ FAM and 3’ TAMRA for sensing potassium. | /56-FAM/GGGTAAGGGTAAGGGTAAGGG/36-TAMSp/ |

| Name | Use | Sequence |
|---|---|---|
| MH101 | DNA oligonucleotide with 5’ FAM. | /56-FAM/GGGTAAGGGTAAGGGTAAGGG |

### 2.1.5 Chemical Inducers

The different chemicals used for the sensor testing are listed in **Table 2.5**. All inducer chemicals were sterilised through filter sterilisation with 0.22 µm filter. All chemicals were ordered from Sigma-Aldrich and were analytical grade.

**Table 2.5: Chemical inducers used for characterisation of the biosensors.**

| Chemical | Stock concentration | Solvent | Use |
|---|---|---|---|
| Lithium lactate | 8 M | dd$H_2O$ | To induce the whole cell sense and respond lactate genetic circuit. |
| Potassium chloride | 2 M | dd$H_2O$ | To induce the potassium sensing aptamer. |
| Tryptophan | 50 mM | dd$H_2O$ | To induce the whole cell sense and respond tryptophan genetic circuit<br>To prevent leaky expression of the sensor in overnight cultures. |
| Hydrocortisone | 5 mg/ml | Ethanol | To induce the Avidin-Cortisol (AvC) cpGFP sensors. |

| Chemical | Stock concentration | Solvent | Use |
|---|---|---|---|
| Testosterone | 3 mg/ml | Ethanol | To induce the Avidin-Testosterone (AvT88) cpGFP sensors. |
| Histamine dihydrochloride | 2 mg/ml | dd$H_2O$ | To induce AM10 loop 5 cpGFP sensors. |

## 2.2 Methods

### 2.2.1 Bacterial growth and preparation

#### 2.2.1.1 Overnight growth

Overnight cultures of bacterial cells were grown in 5 mL LB, or 10 mL when growing bacteria containing a low copy plasmid that needed to be extracted, in a 30 mL Universal tube. For bacteria containing plasmids the appropriate antibiotic was added according to **Table 2.2**. These cultures were then incubated in a shaking incubator at 37°C 160 rpm (Infors multitron shaker). For each culture a single colony was picked from a LB agar plate. For circuit characterisation the plate was freshly streaked from glycerol stocks.

#### 2.2.1.2 Competent cell preparation

A 5 mL overnight culture of the TOP10 *E. coli* cells was used to generate competent cells was set up with no antibiotics. The following morning this culture was used to inoculate 200 mL fresh LB medium containing no antibiotics to an optical density (OD) of approximately 0.01 in a 500 mL Erlenmeyer flask. The culture was then left to grow at 37°C with 160 rpm shaking until the OD measured 0.3-0.4. At this stage the culture is transferred to frozen 50 mL falcon tubes and rested on ice for 10-20 minutes before being centrifuged at 3,011g for 8 minutes to pellet the cells. The supernatant was discarded and the cells were resuspended in 10 mL pre-cooled 50 mM

$CaCl_2$. The cells were then centrifuged again and resuspended as before. Then the cells were rested on ice for 30 minutes before being centrifuged once more. The supernatant was discarded and the cells were re-suspended in 2 mL 50 mM $CaCl_2$ with 15% glycerol. This was then transferred to frozen 1.5 ml microfuge tubes in volumes of 100 µl or 200 µl. The cells were then stored at -80°C.

### 2.2.2 DNA preparation and storage

#### 2.2.2.1 Plasmid extraction

Plasmids were extracted using Qiagen Miniprep kit (27106, Qiagen) according the manufacturer's protocol from 5 ml cultures grown overnight in LB with the appropriate antibiotic. For low copy number plasmids 10 ml cultures were used whilst still following the protocol for 5 ml cultures to improve the DNA yield. DNA was eluted in $ddH_2O$ and stored at -20°C. Extracted DNA was quantified using a DeNovix DS-11 spectrophotometer nanodrop blanked with the same $ddH_2O$ used to elute the plasmid from the DNA purification column.

#### 2.2.2.2 DNA preparation for cell-free reactions

Plasmids were extracted using ZymoPURE II Midiprep kit (D4201, Zymo Research) following the manufacturer's protocol for low copy plasmid. 100 mL cultures were grown overnight in LB in a 250 ml Erlenmeyer flask with the appropriate antibiotic and incubated at 37°C with shaking at 160 rpm. Following the midi prep the DNA was then cleaned up using NEB Monarch DNA cleanup kit (T1030, NEB) following the manufacturer's protocol. Nuclease free water was used to elute the DNA (W3500, Sigma-Aldrich), which was quantified on a DeNovix DS-11 spectrophotometer nanodrop. This two step purification method was used because this had been shown to

improve the response of cell-free transcription-translation systems (unpublished data from Wang lab).

#### 2.2.2.3 Oligonucleotide annealing

50 µl of each oligonucleotide at 100 µM were combined with 1x T4 DNA ligase buffer (M0202, NEB) and 1 µl T4 PNK (M0201, NEB) then incubated at 37°C for 30 minutes. Following this the oligonucleotides were heated to 100°C for 5 minutes before allowing to cool to room temperature slowly.

### 2.2.3 Sequencing

Sequencing reactions were sent to Source Bioscience according to their requirements, 5 µl of 100 ng/µl DNA and primers at 3.2 pmol/µl per reaction. The sequencing results were analysed using Benchling software. The oligonucleotides used as sequencing primers are listed in **Appendix 1**.

### 2.2.4 Plasmid construction

Plasmids were constructed using the Biobrick standard (Knight, 2003). Each part to be inserted into the plasmid backbone was designed with a prefix and suffix sequence containing EcoRI, XbaI, SpeI and PstI restriction sites. This allowed them to be sequentially cloned into the plasmid backbone at the desired position, with a maximum of two parts being able to be inserted at once as XbaI and SpeI produce complementary overhangs. So this allows parts to be inserted either before or after other parts depending on which sets of enzymes pairs are chosen to digest the plasmid and genetic part to be inserted. **Figure 2.1** illustrates how this method works.

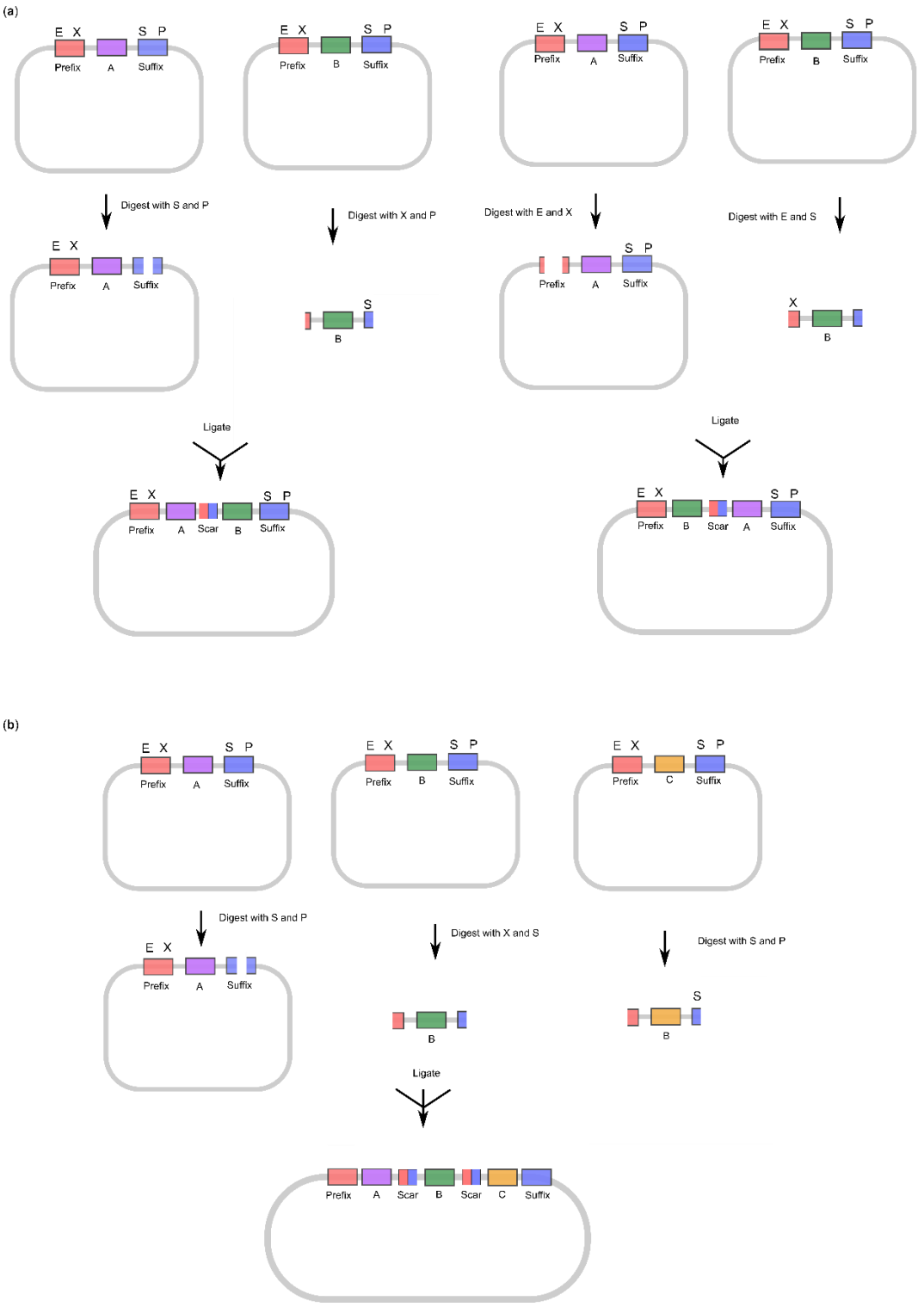


**Figure 2.1 Overview of Biobrick plasmid construction.** The diagram show how genetic parts can be added into a plasmid using Biobrick methodology. The prefix contains two restriction sites for EcoRI (E) and XbaI (X) whilst the suffix contains sites for SpeI/BcuI (S) and PstI (P) when digested XbaI and SpeI result in complementary overhangs allowing new parts to be added at desired locations resulting in a scar sequence, so that the restriction sites are only found in the prefix and suffix. (**a**) shows that by

selecting the appropriate pairs of restriction enzymes the plasmid can be opened at either the prefix or suffix to allow for one part to be inserted before or after parts already contained in the cloning site. (**b**) shows how three parts of the backbone and two inserts can be combined in one reaction using the full availability of restriction sites. Again the backbone is restricted at the prefix or suffix (in the diagram the suffix is digested) and then by using the X and S sites for one part and X and P for the second part both can be ligated into the backbone in the desired sequence (Knight, 2003).

#### 2.2.4.1 DNA synthesis

The long double stranded DNA sequences synthesised were produced by either IDT or ThermoFisher. Sequences containing a coding sequence were optimised to ensure codon usage matches *E. coli* and to remove BioBrick restriction sites (EcoRI, XbaI, SpeI and PstI) present outside of the prefix and suffix sequences. A few extra bases were added to the beginning and end of the DNA sequences to ensure that restriction enzymes were able to digest the prefix and suffix sequences for the following cloning steps.

Single stranded oligonucleotides for PCR or the assembly of short DNA fragments were ordered from IDT or Sigma when long oligonucleotides were required, which were ordered with cartridge purification. IDT oligonucleotides were ordered desiccated whilst oligonucleotides received from Sigma were ordered in water. Oligonucleotides used to assemble small fragments in plasmids were designed to contain the required overhangs, as the prefix and suffix which then were digested with the desired enzymes to allow for downstream cloning.

Oligonucleotides for aptamer sensors were ordered from IDT with the fluorescent dyes attached to the 5’ and 3’ end of the DNA sequences. These DNA sequences were ordered with polyacrylamide gel electrophoresis (PAGE) purification.

#### 2.2.4.2 Polymerase chain reaction

Polymerase chain reaction (PCR) to amplify DNA sequences for the construction plasmids was carried out using Thermo Scientific Phusion™ High-fidelity DNA polymerase according the manufacturer's protocol (F530S, Thermofisher). PCR reactions were carried out on Thermofisher Applied Biosystems Veriti Thermal Cyler or Proflex PCR System. For the majority of PCR 5x HF buffer was used for the reaction. Where long fragments such as an entire plasmid were being amplified or previous PCR attempts were unsuccessful, 5x GC buffer was used and if still unsuccessful then DMSO was added up to 1%. At this stage gradient PCR was also used to identify the optimal annealing temperature.

All of the primers used are listed in **Appendix 1**.

#### 2.2.4.3 Site-Directed mutagenesis

In order to generate small changes in the genetic constructs, such as changes to the constitutive promoter used to express transcription factor or the RBS, site-directed mutagenesis was used. Primers were designed which bound either side of the region which was to be changed, then one primer was designed to have an overhang which contained the mutation. These primers were then used to carry out PCR in the same manner as in 2.2.4.2 for the whole plasmid and then re-circularised as in 2.2.4.11

#### 2.2.4.4 Overlap extension PCR for random mutagenesis

In order to make multiple mutations overlap extension PCR (Ge and Rudolph, 1997) was used. Forward and reverse primers were designed to cover the whole coding sequence of the gene to be mutated. Primer pools which bind to both the forward and reverse strand at the region to be mutated were designed. First multiple PCR reactions using Thermofisher Phusion™ High-fidelity DNA (according to the manufacturer's protocol) were carried out

to generate the mutations. Fragment one uses the forward primer and the reverse primer pool for the first mutation region. Fragment two uses the forward primer pool for the first mutation region and the reverse primer pool for the second mutation region. The third fragment uses the reverse primer and the forward primer pool for the second mutation region. These reactions were then purified before the fragments were mixed together and a PCR with the forward and reverse primers was carried out to join the fragments together this process is shown in **Figure 2.2**. The final fragment was then cloned into a plasmid backbone using Gibson assembly for transformation.

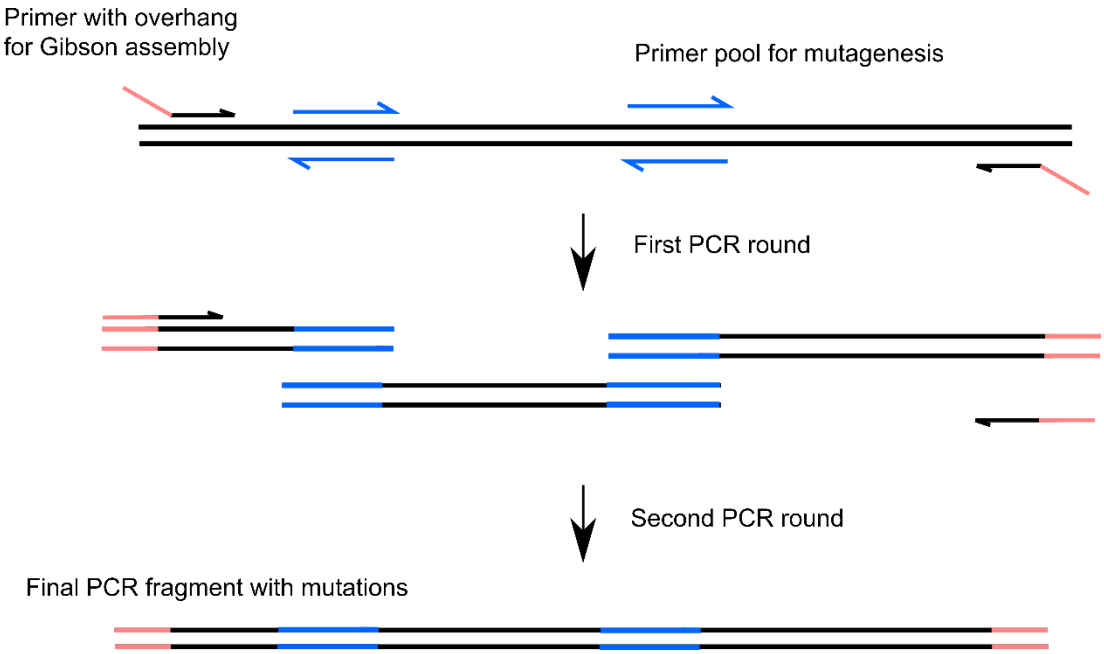


**Figure 2.2 Schematic of approach for overlap extension PCR.** Primer pools were designed for where the random mutagenesis is desired (shown by blue primer symbols) and then primers with complementary overhangs for Gibson assembly was designed for the primers at the end of the fragment to be constructed (black primer symbols with pink tail). The first round of PCR reactions amplifies each section of the fragment to introduce the mutations. Following the successful amplification of each small fragment these were combined and only the outside primers designed to make the full fragment were used with the complementary sections from each section ensuring that the separate fragments will anneal with each other to allow the full length to be amplified. This final full fragment is the product with the internal desired mutations (Ge and Rudolph, 1997).

#### 2.2.4.5 Gibson assembly

Primers were designed to contain 20 bases overlap with the neighbouring fragment. Desired sequences for assembly were then amplified by Phusion high-fidelity PCR and purified as described in 2.2.4.1 and 2.2.4.7. The purified fragments were then ligated together using 2x HiFi DNA assembly mastermix (E2621, NEB). DNA fragments were added to the reaction at a 1:2 ratio between the plasmid backbone and insert, using 50 ng of the plasmid backbone. The reaction was then incubated at 37°C for 30 minutes. Gibson assembly mix was then directly transformed (Gibson et al., 2009).

#### 2.2.4.6 Colony PCR

Colony PCR was used to identify colonies which contained plasmids with the correct size of insert for the final desired plasmid. Individual colonies were picked into 50 µl water and 0.5 µl of this was then added to the PCR reaction.

Colony PCR carried out using Promega GoTaq G2 (M7841, Promega), 20 µl reactions were set up with 1x GoTaq G2 buffer, 1 µM of both the forward and reverse primer (mostly commonly, VF2 and VR were used to PCR the entire insert), 0.2 mM each dNTP and 1.25 units of GoTaqG2 polymerase and water added up to 20 µl. The reaction was run using a touchdown protocol (Don et al., 1991). The first 10 cycles used an annealing temperature of 60°C then the following 20 cycles used an annealing temperature of 50°C. All other reactions settings followed the manufacturer's protocol.

The PCR reaction was then analysed using gel electrophoresis to check the correct size product was formed.

#### 2.2.4.7 Purification of PCR products

A small volume of the PCR reaction was analysed by gel electrophoresis to determine if the desired PCR product had been produced. If the desired size product was the only PCR product present on the gel, then the PCR reaction

was purified using either Promega Wizard reaction cleanup (A9281, Promega) columns or NEB Monarch reaction clean-up (T1030, NEB) columns according to the manufacturer's protocol.

If non-specific PCR products had also been formed then gel electrophoresis was used to separate the specific PCR product from the non-specific products. The band on the agarose gel of the correct size was then cut from the gel and the DNA extracted using either Promega Wizard gel extraction kit (A9282, Promega) or NEB Monarch gel extraction kit (T1020, NEB) according the manufacturer's protocol.

#### 2.2.4.8 Restriction digestion

Approximately 1 µg of DNA was digested with 1 µl each of the appropriate enzymes, usually the standard biobrick prefix and suffix enzymes (EcoRI FD0274, XbaI FD0684, SpeI/BcuI FD1254, PstI FD0614). Thermofisher FastDigest enzymes were used with 1x FastDigest buffer and water up to 20 µl reaction volume. If a plasmid backbone was being digested to insert parts, then 1 µl Fast AP was also added to remove the phosphates from the plasmid backbone to reduce re-ligation. The DNA products were then purified. Where only one product was formed or the cut-out bases were of a very short sequence (<10 bases) then Promega Wizard reaction cleanup (A9281, Promega) columns or NEB Monarch reaction cleanup (T1030, NEB) columns were used according to the manufacturer's protocol. If two products were formed then the reaction was run on a gel to separate the fragments and gel extraction using either Promega Wizard gel extraction kit (A9282, Promega) or NEB Monarch gel extraction kit (T1020, NEB) according the manufacturer's protocol was used for purification.

#### 2.2.4.9 Test digests

In cases where colony PCR failed, test digests were used to determine if the size of the insert in the plasmid was correct.

Approximately 500 ng of DNA was digested with 1 µl of each enzyme, usually a pair of the standard biobrick prefix and suffix enzymes (EcoRI, XbaI, SpeI, PstI). Thermofisher FastDigest enzymes were used with 1x FastDigest buffer and water up to the required volume. Reactions were incubated at 37°C for 30 minutes before being analysed by gel electrophoresis.

#### 2.2.4.10 Ligation

Ligation of DNA parts was carried out using NEB T4 DNA ligase (M0202, NEB) with 1x T4 DNA ligase buffer, 1 µl T4 DNA ligase, 6 µl of the insert and 3 µl of the plasmid backbone with water added up to 20 µl final volume. The reaction was incubated at room temperature for 30 minutes before directly transforming the ligation reaction.

#### 2.2.4.11 Plasmid recircularization

Where entire plasmids were amplified using PCR, the final PCR product was re-circularised before transformation into bacteria. First phosphates were added to the ends of the PCR product using T4 PNK (M0201, NEB). 12.5 µl of the purified PCR product was used with 1x T4 ligase buffer, 1 µl of the enzyme giving a 15 µl reaction volume. The reaction was incubated at 37°C for 30 minutes. Following the first step 1 µl of T4 DNA ligase, extra T4 DNA ligase buffer to ensure the buffer remained at 1x concentration and water up to 20 µl were added. The reaction was then incubated at room temperature for 1 hour. Finally FastDigest buffer was added to 1x concentration along with 1 µl of DpnI. The reaction was then incubated at 37°C for 30 minutes before transformation into bacteria.

#### 2.2.4.12 Transformation

Transformation of plasmids and cloned constructs was done using *E.coli* TOP10 cells, 50 µl of cells were used for one transformation. Cells were incubated with the DNA (100 ng of purified plasmid or up to 20 µl of the ligation or Gibson reaction was used) on ice for 30 minutes before heat shock at 42°C for 1 minute. Following heat shock the cells were immediately returned to ice for recovery for 3 minutes. After recovery 1 ml of LB was added to the cells and they were incubated at 37°C for 1 hour with 160 rpm shaking before plating onto LB-agar plates containing the correct selection antibiotic. LB-agar plates were left at 37°C overnight.

#### 2.2.4.13 Agarose gel electrophoresis

Separation of DNA fragments was carried out using an agarose gel of the appropriate percentage for the DNA length being analysed. Most commonly a 1% agarose gel was used. The agarose was dissolved in 1x TBE (20-6000-50, Thistle Scientific) by heating in a microwave. SYBR-safe was then added to the melted agarose to a 1x concentration (S33102, Life Techonologies), a 1 in 10,000 dilution. The dissolved agarose was poured into a gel tank containing a comb to provide enough wells for the number of samples being analysed. The gel was then run at 120 V for around 25 minutes (Bio-Rad PowerPac™ basic power pac with horizontal electrophoresis cell) to ensure good separation of bands before imaging using a Bio-Rad Gel Doc XR+ system (with filter 1 and SYBR safe mode). For the majority of agarose gels Hyperladder™ 1 kB ladder (BIO-33025, Bioline) was used. For the smaller DNA sizes being visualised NEB 1 kB plus was used.

The DNA being analysed was mixed with 6x loading dye (B7024S, NEB). For PCR reactions or digestions where available, reaction buffer containing loading dye was used to allow the sample to be loaded onto the gel directly.

### 2.2.5 Cell-free protein production

#### 2.2.5.1 BL21 Δlac lysate production

An overnight culture of 5 mL was set up placing one bacterial colony into the LB medium. This overnight culture was left to grow at 37°C with 160 rpm shaking. The following morning the OD of the culture was determined. Following this the culture was diluted 1:200 into 200 mL fresh LB in a 500 mL Erlenmeyer flask. This culture was incubated at 37°C with 160 rpm shaking for 4 hours. The culture was split into 50 mL falcon tubes (one of which needs to be weighed) for centrifugation at 3,300 g for 20 minutes at 4°C. From this point on cells were kept on ice. After centrifugation the supernatant was discarded and 10 mL of Buffer A (10 mM tris acetate, 14 mM magnesium glutamate, 60 mM potassium glutamate) is used to re-suspend the cells with all the cells transferred to one falcon tube. The cells were then centrifuged at 3300 g for 10 minutes at 4°C. The supernatant was discarded and the cells were re-suspended in 10 ml Buffer A and centrifuged as before. The supernatant was then discarded again and the tube weighed to determine the wet mass of the cell pellet (calculated by subtracting the weight of the empty tube from the new value). At this point the cells were frozen at -80°C overnight. Following this 1 mL of Buffer A with 2mM DTT was added to each 1 g wet mass, and the cells were re-suspended by vortexing. 1 ml was transferred to a new 2 ml microfuge and then sonicated at 50% amplitude with 10 secs on and 10 sec pause to a total energy of 400J, using Fisher Scientific FB120. The lysate was centrifuged at 12,000 g for 10 minutes at 4°C to pellet the debris. The supernatant was transferred to a new Eppendorf tube ensuring no debris was carried over. The run off reaction was then carried out at 37°C with shaking at 160 rpm for 1.5 hours, followed by centrifugation of the lysate at 12,000 g for 10 minutes at 4°C and the supernatant then transferred to a new tube. Dialysis of the lysate is carried

out using a Slide-a-lyzer dialysis cassette 10K MWCO (ThermoFisher, 66380) in Buffer A with 1 mM DTT for 3 hours at 4°C with stirring. Following this the lysate was centrifuged in the same way as previously and the supernatant transferred to a fresh tube. This lysate was then aliquoted in 25 µl stocks and frozen at -80°. This protocol followed was from (Laohakunakorn, 2020b)

#### 2.2.5.2 3-PGA energy solution

The energy solution was prepared as a 4x stock solution which was stored at -80°C in aliquots of 25 µl. **Table 2.6** gives the components for the 3-PGA energy solution with the stock concentrations and final concentration in the 4x energy solution. The final solution should be approximately pH 8. This is carried out according to the protocol from (Laohakunakorn, 2020a).

**Table 2.6: List of components used to produce 3-PGA energy solution.**

| Component | Stock concentration | Concentration in 3-PGA solution |
|---|---|---|
| HEPES | 2 M | 200 mM |
| ATP | 100 mM | 6 mM |
| GTP | 100 mM | 6 mM |
| CTP | 100 mM | 3.6 mM |
| UTP | 100 mM | 3.6 mM |
| tRNA | 43.75 mg/ml | 0.8 mg/ml |
| CoA | 65 mM | 1.04 mM |
| NAD | 175 mM | 1.32 mM |
| cAMP | 650 mM | 3 mM |
| Folinic acid | 33.9 mM | 0.27 mM |
| Spermidine | 1 M | 4 mM |
| 3-PGA | 1.4 M | 120 mM |
| amino acids | 50 mM | 6 mM |
| tyrosine | 50 mM | 3 mM |

| Component | Stock concentration | Concentration in 3-PGA solution |
|---|---|---|
| PEG-8000 | 50% | 8% |
| Mg-glutamate | 1 M | 42 mM |
| K-glutamate | 6 M | 400 mM |
| DTT | 1 M | 1 mM |
| Nuclease free water (W3500, Sigma-Aldrich) | | Used to make up to desired volume |

### 2.2.6 Sensor characterisation and analysis

#### 2.2.6.1 *In vivo* genetic sense and respond circuit sensors

Overnight cultures were diluted to OD 0.025 in fresh supplemented M9 media with the appropriate antibiotic. The diluted cells were then analysed using a plate reader (BMG FLUOstar) in a black clear flat bottom 96 well microplate (655096, Greiner Bio-One). 200 µl was used in each well made up of 196 µl of the cell culture or medium with 4 µl of the chemical inducer or solvent added (see **Table 2.4** for a full list of chemical inducers and the solvent). The microplate was then sealed using a breathable plate sealer (either AeraSeal Z707430-100EA, SigmaAldrich or Breatheeasy sealer Z380059, Diversified Biotech). The cells were incubated at 37°C with shaking at 1,000 rpm in a microplate incubator (AS-03020-00, Medical Supply Co. Ltd). Green fluorescent protein (GFP) was used as the reporter (excitation 485 nm and emission 520 nm gain 1000). Initial data analysis was carried out using BMG MARS data analysis software to carry out blank and negative control corrections. First the average value of the blank wells containing only media was subtracted from all wells, then the ratio between GFP values and OD (obtained from absorbance at 600 nm) was found and the average Fluorescence/OD value for the negative control (cells containing the empty

plasmid backbone) was then subtracted. Once sensors had been optimised a constitutive monomeric red fluorescent protein (mRFP) was added to the plasmid and data normalisation was carried out in the same manner but using the mRFP value (excitation 584 nm and emission 620 nm gain 1000) rather than OD to generate the ratio.

#### 2.2.6.2 DNA aptamer sensors

DNA aptamers were diluted to 0.2 µM in the desired buffer (either 5 mM Tris at pH 7.4 or pH 7.0 or 50 mM EDTA which had been dissolved in 2M Tris buffer). These were characterised in a black clear flat bottom 384 well microplate (Greiner Bio-One, 781906) with 25 µl per well. The plate was then sealed with a clear impermeable cover (E2796-0793, Starlab) before characterisation by microplate reader (BMG FLUOstar). The plate was incubated at either 25°C or 37°C, excitation 485 nm used with two emissions 520 nm and 590 nm gain 1000. Again BMG MARS data analysis software was used for the initial data normalisation. The average of the blank values was subtracted from each well before finding the ratio between the values for 590 nm emission and 520 nm emissions gain 1000. In this case there was no negative control to use for correction.

#### 2.2.6.3 Protein sensors

Single protein based biosensors were characterised in a cell-free transcription/translation system. Initially a commercial cell-free transcription-translation kit (Promega S30 extract for circular DNA, L1020) was used following the manufacturer's protocol scaled to a 5 µl reaction volume. The reaction was set up with 5 nM DNA for the sensor plasmid and negative control (an empty pSB3K3 backbone) and 20 nM for the positive control (constitutive GFP). A pre-incubation step was carried out to allow expression of the protein before induction. The exact pre-incubation method depended

on the sensor and is outlined for each sensor in chapter 4. Once the reaction was induced the mixture was incubated at 37°C.

When homemade cell-free reaction mixture was used the individual components were made at 4x concentration so that both the cell lysate and energy solution each made up a quarter of the final reaction volume with the remaining volume made up of the DNA to the required concentration and nuclease free water. The pre-incubation step was carried out in the same manner as for the commercial cell-free kit.

Cell-free transcription-translation experiments were set up in a low volume black 384 well microplate (Greiner BioOne, 788096) and sealed with an aluminium sealing foil (E2796-1100, Starlab).

### 2.2.7 Hydrogel Synthesis

Polyethylenedimethacrylate (PEGDMA) 1000 (15178, Polysciences) was dissolved in dd$H_2O$ to 50% w/w then the dissolved PEGDMA solution was purified using a 0.22 µm filter. The filtered solution was then protected from light using aluminium foil before the addition of the UV photo-initiator Igracure 2959, 2-Hydroxy-4′-(2-hydroxyethoxy)-2-methylpropiophenone (410896, SigmaAldrich) at 0.2% w/v. The hydrogel was then crosslinked in an Analytikjena UVP CL-1000L for 10 minutes to generate the solid hydrogel. The solid hydrogel was then swollen overnight with the appropriate medium or buffer for the sensor contained in it.

### 2.2.8 Wearable Device Construction

The wearable device was constructed from a silicone backing with the PEGDMA hydrogel crosslinked to the patch.

The silicone backing was prepared by spreading a thin layer of the silicone onto an acetate sheet (Amazon- Essential Arts A4 Acetate 240 Micron). The first layer of silicone was made from Sylgard 184 (1673921, Dow Corning)

produced according the manufacturer's protocol and was then left to set completely. Once this was set, the second layer of silicone was applied composed of Silgel 612 (WACSG612-1KG, Wacker) using a ratio of 1.5:1 of component A: component B, where a thin layer was spread on top of the first silicone layer. The setting step for both silicones can be sped up by heating the silicone patches. Once set the silicone was cut into the desired patch size and removed from the acetate, the silicone was treated with 10% w/v. benzophenone dissolved in ethanol for 5 minutes before being washed three times with ethanol and finally with dd $H_2O$. Following this the patches were quickly dried by blotting with lab tissue before applying the hydrogel. The silicone hydrogel patch was then crosslinked for 10 minutes in the UV crosslinker to ensure the hydrogel chemically bound to the silicone and to solidify the hydrogel. The whole device was then soaked in buffer or medium to swell the hydrogel. This method was adapted from (Liu et al., 2018b).

### 2.2.9 Wearable Device Characterisation

Excess media or buffer was removed from the container which held the wearable device. Images of the wearable device were then taken using the appropriate filters for the fluorescent proteins expected to be detected in the device. For detection of GFP or FAM a blue filter was placed over the flash and a green filter was placed over the camera (Lee colour filter catalogue Tokyo blue (71) and Twickenham green (736)). For RFP detection a green filter was place over the flash and a red filter placed over the camera (Lee colour filter catalogue Twickenham green (736) and light red (182)). For TAMRA detection a blue filter was used over the flash and a red filter over the camera (Lee colour filter catalogue Tokyo blue (71) and light red (182)) to allow for detecting the FRET pair formation The image was taken with a Samsung S20 plus using the pro mode. The only phone camera setting altered was the manual focus to ensure that the spots on the wearable device were in focus. In order to induce the sensors contained within the

wearable device the inducer chemical was added onto a piece of parafilm which the wearable device was then placed over.

### 2.2.10 Protein structure analysis

R package Bio3D (Grant et al., 2006) was used to examine the change in the dihedral angles between amino acids in a protein. In order to be able to determine the key areas of conformational change the crystal structure of the protein in the bound and unbound states were required to be uploaded from PDB to the R package.

The code developed alongside the package by (Grant et al., 2006) used to analyse the structures to obtain the change in dihedral angle as a graph and table is given in **Appendix 1**.

### 2.2.11 Data analysis

#### 2.2.11.1 Curve fitting

For the whole cell sense and respond circuits previous work within the lab had generated a mathematical model for individual transcription factors and their response behaviour to the ligand to generate an output (Wang et al., 2011). This model was used in data fitting the response curve, the equations used for data fitting are given in S2 and S4. From this, ordinary differential equations were developed to model the gene regulation. The output gene expression (G) was modelled as shown;

$$d[G]/dt = \alpha \cdot k1 + k1 \cdot [I]^n/(K_M^n + [I]^n) - d \cdot [G] \quad \text{(S1)}$$

$[I]$ gives the concentration of the inducer in the equations. $k1$ gives the rate constant for the variables and $K_M$ gives the binding coefficient for the inducer showing the concentration for half of the transcription factor to be bound to the inducer. $n$ is the hill coefficient and gives the degree of cooperativity in

the system, and $d$ is the constant for the degradation of the protein expressed. So in the equation S1 $\alpha \cdot k1$ is the basal constitutive activity of the promoter and $k1 \cdot [I]^n/(K_M^n + [I]^n)$ is the activity due to transcription activation, $d \cdot [G]$ shows the constitutive degradation of the output reporter.

At steady state this results in

$$f([I]) = [G]SS = \alpha \cdot k + k \cdot [I]^n/(K_M^n + [I]^n) \quad \text{(S2)}$$

In the steady state case $k = k1/d$ gives the maximum expression. This equation was used to fit the characterisation data of the biosensor systems to a dose response curve.

In the case of repressors, the equation becomes

$$d[G]/dt = \alpha \cdot k1 - k1 \cdot [I]^n/(K_M^n + [I]^n) - d \cdot [G] \quad \text{(S3)}$$

In this form $-k1 \cdot [I]^n/(KM^n + [I]^n)$ is the activity due to transcriptional repression.

At steady state this results in

$$f([I]) = [G]SS = \alpha \cdot k - k \cdot [I]^n/(K_M^n + [I]^n) \quad \text{(S4)}$$

For the aptamer sensors where only the binding of the ligand is responsible for the response, not the gene expression, the hill equation was used for the transfer function to fit the characterisation data.

$$y = a + (X^{slope} \cdot (b - a)/X^{slope} + EC50^{slope}) \quad \text{(S5)}$$

Where $EC50$ is the concentration of inducer required to generate 50% of the response, $a$ represents the basal expression of the output in this case basal fluorescence and $b$ shows the maximal response and $slope$ gives the steepness of the curve. $X$ represents the concentration of the biomarker.

#### 2.2.11.2 Data analysis of wearable device images

Initially to analyse the images taken of wearable device ImageJ was used to extract the red green blue (RGB) values of each spot. For GFP imaging the green value was then taken for each spot whilst for RFP imaging the red value was taken. When imaging the potassium aptamer, for FAM imaging the green value was taken and for TAMRA the red value was taken. The ratio between green and red was calculated.

This data analysis was then automated within a software App which also automatically detected the spots.

# 3 Whole cell synthetic biology enabled biosensors for detecting sweat biomarkers

## 3.1 Introduction

Whole cell sense and respond genetic circuits are an approach which is well suited for detecting molecules in human sweat due to their sensitivity and specificity. For biomarkers in human sweat the concentrations are generally at low levels, requiring high sensitivity. Sweat is also a very complex constituent sample where many different chemicals, metabolites etc. will be present (Baker, 2019a). Whole cell biosensors are well suited to dealing with this sample complexity as there are already the parts engineered and used to detect at physiological concentration ranges and in a specific manner.

Initially lactate, tryptophan, cortisol and testosterone were the biomarkers selected to study how well whole cell biosensors are suited to detect molecules of interest in human sweat as these are thought to show different aspects of an individual's physiological state as outlined in **Table 1.2**. To begin developing these sensors, the literature was searched to identify transcription factors and known responsive promoters. For lactate, whole cell biosensors have already been constructed so these parts were used as the initial basis (Trantidou et al., 2018). For the tryptophan sensor, *E. coli* metabolism is tightly regulated to ensure that amino acid synthesis only occurs when the amino acids cannot be obtained from the environment so these parts would be used in the construction of the biosensor. Mutant versions have also been made with stronger binding which could be useful in reaching the required sensitivity (Hurlburt and Yanofsky, 1990). Recently the bacterial interaction with the immune system and the chemicals that are released by an immune response has identified a promoter which is upregulated in *Salmonella typhimurium* in response to cortisol when infecting pigs (Verbrugghe et al., 2016). This provides the possibility of parts for generating a cortisol sensor using a whole cell bacterial system. For testosterone, a bacteria, *Comamonas testosteroni*, was identified which utilises testosterone as a carbon source so would have

promoters and proteins which are responsive to testosterone as part of its metabolism (Pruneda-Paz et al., 2004).

## 3.2 Lactate sensor

Lactate is produced in the body through anaerobic respiration and is found in high concentrations in sweat. Lactate can be produced through exercise, hypoxia and regular metabolic processes, including sweating (Buono et al., 2010, Li et al., 2022). Lactate concentrations in sweat range between 0-120 mM and are thought to change in response to changes in lactate found in blood or due to the build-up in muscles (Sakharov et al., 2010, Ohkuwa et al., 2009, Derbyshire et al., 2012).

LldR is the transcription factor responsible for binding to lactate and the interaction with the responsive promoter $P_{LldPRD}$. The transcription factor which forms a dimer binds to its operator site, with each DNA binding domain binding to one half of the operator site. LldR has been shown act as both a repressor and an activator through the mechanism shown in **Figure 3.1**. The LldR dimers are thought to oligomerise and loop DNA by binding to both operator sites to repress transcription when no lactate is present. Binding to lactate then destabilises this to remove the distal site binding and open the DNA (Aguilera et al., 2008).

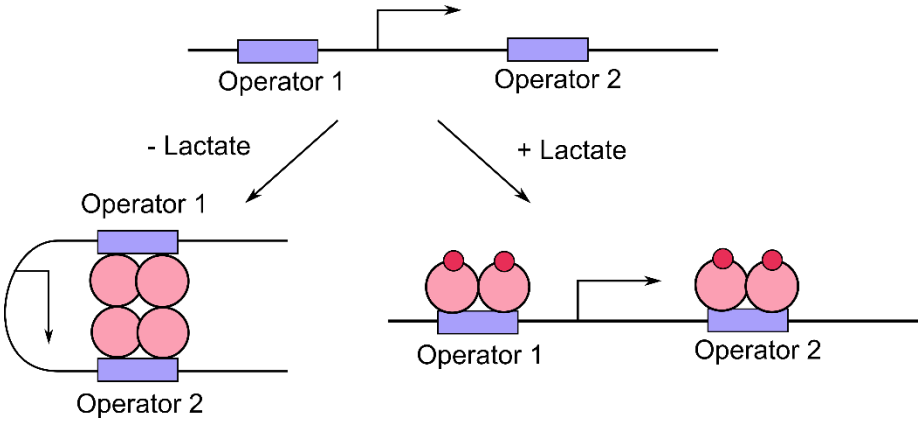


**Figure 3.1 Regulation of the lactate operon promoter.** The figure shows the structure of the lactate responsive promoter with one operator site present both upstream and downstream of the promoter. In

the absence of lactate, the LldR dimers are bound to the two operator sites and then oligomerise to loop the DNA and prevent transcription from the promoter. When lactate is present this binds to the LldR dimers resulting in the conformational change that prevents the oligomerisation and releases the DNA loop (Aguilera et al., 2008).

### 3.2.1 Development of a whole cell biosensor for lactate

First the sensor was constructed and characterised in TOP10 cells because this was different to previous work in the literature (Trantidou et al., 2018) so its function in a different bacterial strain needed to be tested, shown in **Figure 3.2a**.

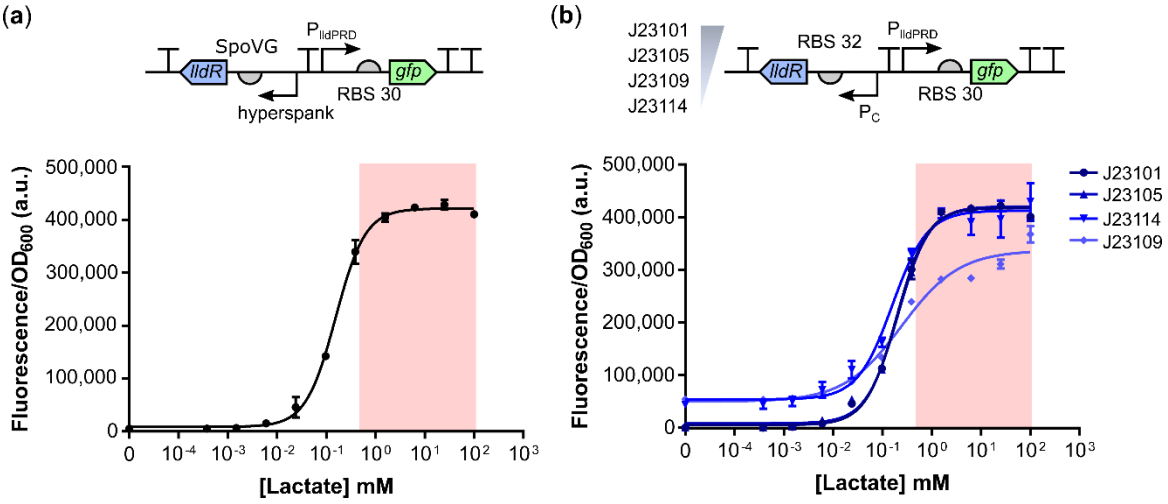


**Figure 3.2 Whole cell lactate sense and respond genetic circuit design and characterisation.** (**a**) The top panel shows a genetic construct constitutively expressing the LldR lactate responsive transcription factor expressed using *B. subtilis* promoter (hyperspank) and RBS (SpoVG) on pSB1A3. The lower panel shows a graph of the response to different concentrations of lithium lactate as identified from the literature. (**b**) The top panel shows the genetic construct for lactate sensing with the LldR protein expressed using *E. coli* RBS and different constitutive promoters from the Anderson collection (http://parts.igem.org/Promoters/Catalog/Anderson). The lower panel shows the graph of the responses from the different lactate sensor genetic constructs containing different strength promoters. For both graphs n=3 cells grown at 37°C with 1,000 rpm. Response taken 4 hours post-induction. The error bars show one standard error. The shaded red region highlights the concentration range of the inducer found in human eccrine sweat.

The whole cell sense and respond genetic circuit has very low leakiness and a high maximal output which is important for being able to detect the response in the wearable device. However, the response plateau's and flattens within

the physiological concentration range of lactate in sweat, which is shown by the red shaded area of the graph shown in the lower panel of **Figure 3.2a**. For a sense and respond genetic circuit to detect lactate to be suitable for use in the wearable device the sensitivity of the circuit needs to be decreased. A common way to optimise the sensitivity is to tune the level of the transcription factor present (Wang et al., 2015b). To optimise the sensitivity, a range of different strength constitutive promoters from the Anderson collection were cloned in front of the gene to express the transcription factor across the range of strengths achievable (http://parts.igem.org/Promoters/Catalog/Anderson) in order to change the level of the transcription factor. As LldR is both a repressor and an activator (Aguilera et al., 2008) the rules which have been identified on how the level of transcription factor would impact the response would not necessarily hold true. The promoters used are identified in the upper panel of **Figure 3.2b** and the response of these different versions are shown in the lower panel.

**Figure 3.2b** shows that using *E. coli* promoters and RBS to express the LldR transcription factor can give a good response in terms of leakiness and maximal response but there was no improvement to the sensing range. In **Figure 3.2b** the strong promoters J23101 and J23105 which would give high levels of the transcription factor had lower leakiness which suggests repressor activity whilst the reduced sensitivity seen in the version with the lower strength promoter J23109 showed activator like behaviour. This was important to test, as in the literature a *B. subtilis* promoter and RBS was used and the reasoning for this choice was unclear.

The time point used to determine the response of the lactate sensor to different concentrations of lactate could also impact the sensitivity of the sensor and potentially the maximum concentration which could be detected. The time course data at different concentrations of lactate for the different versions of the sensor is shown in **Figure 3.3**.

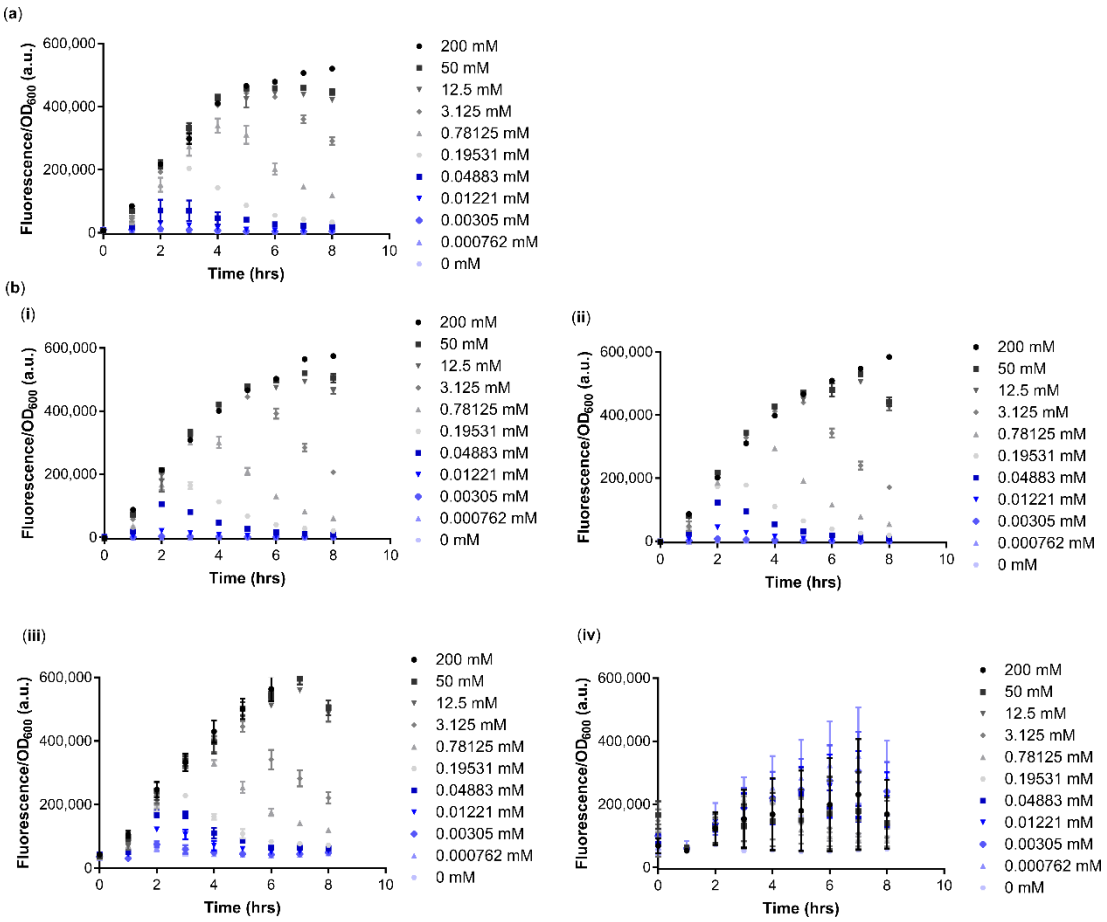


**Figure 3.3 Change in response to different concentrations of lactate over time.** The graphs show the change in the response of the sensor shown by fluorescence corrected for OD (optical density) over time. (**a**) shows the change for the initial construct identified from the literature (Goers et al., 2017) using *B. subtilis* promoter hyperspank and RBS SpoVG. (**b**) shows the change in the lactate sensors using *E. coli* promoters and RBS to control the expression. (**i**) shows the change in response over time for the lactate sensor using J23101 to express lldR. (**ii**) shows the change in response over time for the lactate sensor using J23105 to express lldR. (**iii**) shows the change in response over time for the lactate sensor using J23114 to express lldR. (**iv**) shows the response over time for the lactate sensor using J23109 to express lldR. For all graphs n=3, the sensors were grown at 37°C with 1,000 rpm. The error bars show one standard error.

For all the versions of the biosensor tested the change in the response over time is shown in **Figure 3.3**. For all of the different versions of the sensor tested at the lower concentrations of lactate the response begins to be lost after two hours and longer time intervals after this the decrease in response also begins to be lost at higher concentrations. This is likely due to the the lactate being utilised by the cells as part of their metabolism. However at later time points the difference in response at higher concentrations was more

detectable. Therefore four hours post-induction of the cells was chosen to balance the sensitivity of the response whilst still ensuring the higher concentrations could be differentiated.

However, when using the stronger promoters which gave the lowest basal expression and highest maximal expression, the growth of the cells was reduced at the highest lactate concentrations, shown in **Figure 3.4**. This suggests that the sensor was using too many of the cell's resources or the presence of the native promoter on the chromosome and its activation during sensing was leading to altered metabolism impacting the health of the cell. This burden to the cell needs to be avoided as much as possible as this can lead to the genetic circuit used in sensing and responding to lactate becoming unstable. This would negatively impact the function of the sensor.

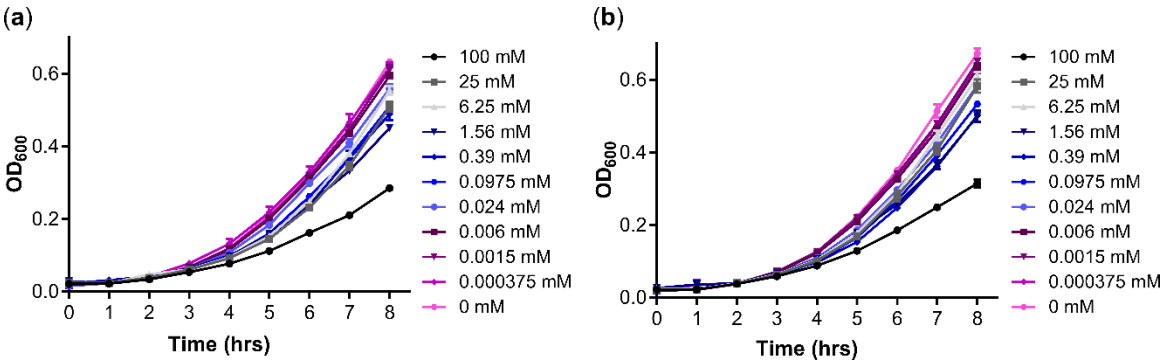


**Figure 3.4 Impact of different lactate concentrations on cell growth.** The graphs show the cell growth and optical density when different concentrations were added to the cell culture of the whole cell lactate sensor containing cells. (**a**) shows the change in growth for the sensors with LldR expressed using J23101. (**b**) shows the change in OD for sensors with LldR expressed using J23105. For all growth curves n=3 the cells were grown at 37°C with shaking at 1,000 rpm and the error bars show one standard error.

**Figure 3.4** shows that the cell growth decreased at the highest concentration of lactate. But this difference in optical density (OD) was not clear until the later time points at which the response for the sensor is taken, showing that for the response determined the OD for each concentration will be similar so this will have a similar effect on the response. However it would still be beneficial to optimise the sensor to reduce the impact on growth.

### 3.2.2 Optimisation of sensor

As the sense and respond genetic circuit on a high copy plasmid pSB1A3 (which has a pUC19-derived pMB1 origin of replication and has a copy number of 100-300 per cell) affected the growth of the cell at high lactate concentration the genetic circuit was moved to a medium copy plasmid backbone pSB3K3 (which has a p15A pMR101-derived replication origin giving a copy number of 20-30) and recharacterized to determine if this reduced the burden to the cell, shown in **Figure 3.5**.

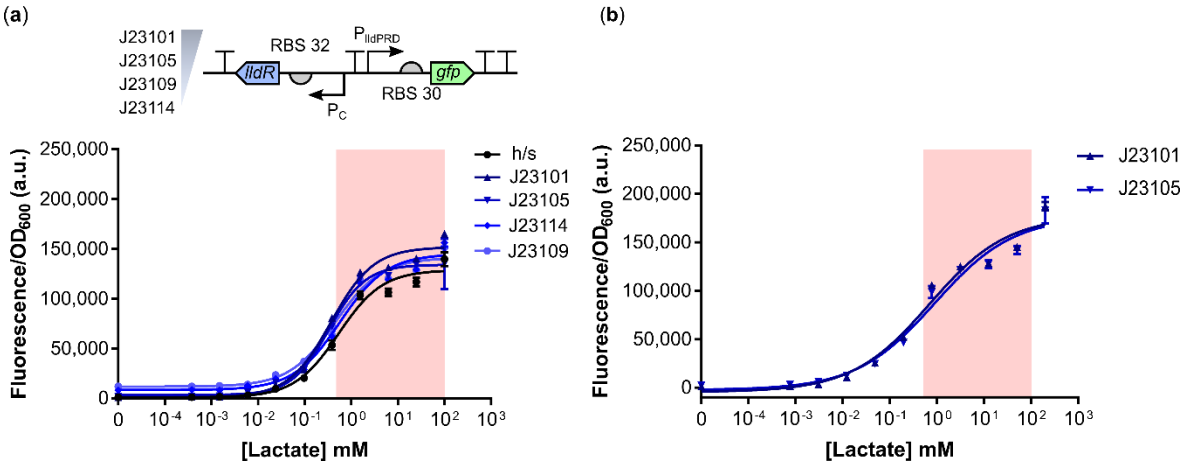


**Figure 3.5 Optimisation of the sense and respond lactate genetic circuit.** (**a**) The upper panel shows the genetic circuit construct for the lactate sensor which was transferred to the medium copy pSB3K3 plasmid. The lower panel shows the graph of the response curves for the lactate sensors on pSB3K3 with different strength constitutive promoters. (**b**) the graph shows the response of the two version of the lactate sense and respond genetic circuits which appear to show the best response when tested with higher lactate concentrations. The red shaded area shows the concentration range of lactate found in human eccrine sweat. For all genetic constructs n=3, cells grown at 37°C, 1,000 rpm shaking. Response shown 4 hours post-induction. The error bars show one standard error.

For the versions of the sensor using the strong promoters the response still seems to be increasing at the highest concentrations, unlike in the previous tests shown in **Figure 3.5a**. To see if this increase was in response to the higher lactate concentration or an artifact, the sensor was tested with higher lactate concentrations to see if the response continued to increase. Two versions of the sensors with a strong or medium strength constitutive promoter controlling the expression of LldR were tested because these should show a low level of leakiness with a high maximum response. The graph in **Figure**

**3.5b** shows that with higher concentrations of lactate an increase in the response could be seen. So the lactate sensor is now capable of detecting changes in lactate over the physiological sweat concentration range because the maximal expression has not yet been reached.

In preparation for using the lactate whole cell sense and respond genetic circuit in a wearable device, an alternative method for normalising the output of the sensor needed to be used. In the device OD of the cells would not be accurate as it would be affected by the materials used in the device itself. In addition, when being worn or placed on a surface to image, OD will not be measurable. A constitutive fluorescent protein expressed from the same plasmid will be used instead because although the protein will always be expressed, the exact level of expression will vary. This depends on a number of factors including the cell growth level and the plasmid copy number. These factors will also affect the output from the sensors, so by calculating the ratio between the two it should remain approximately the same for a particular concentration despite changes in the absolute levels. **Figure 3.6** shows the response curves of the lactate sensor using constitutive mRFP for the normalisation of the sensor output. To identify the best expression of mRFP for normalisation two different RBS strengths were tested.

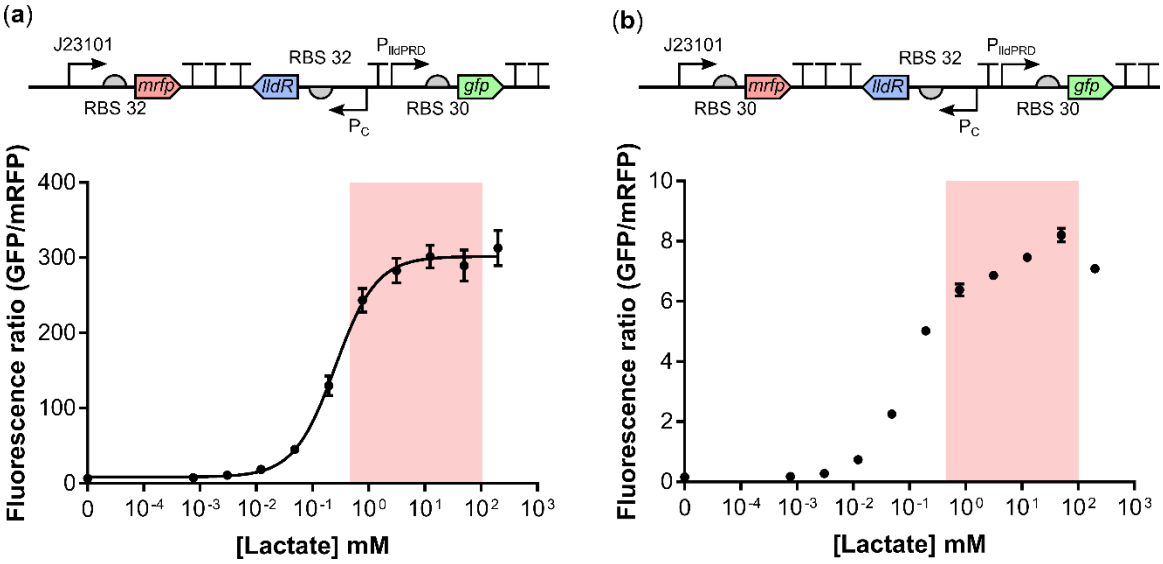


**Figure 3.6 Construction and characterisation of lactate sensor normalised to mRFP.** (**a**) shows the response curve of the whole cell lactate sense and respond circuit using a medium strength RBS (RBS

32) to express mRFP using a strong constitutive promoter (J23101). (**b**) shows the response curve for the whole cell lactate sense and respond circuit using a strong RBS (RBS 30) with a strong constitutive promoter (J23101) to express mRFP. Both versions of the sensors were characterised at 37°C with shaking at 1,000 rpm, n=3 with the red shaded area highlighting the physiological concentration range of lactate in human eccrine sweat. The response shown was taken 4 hours post induction, the error bars show one standard error.

For both versions of the sensor using constitutive mRFP the maximum concentration able to be detected appear to be less than when using OD. For the version with the medium strength RBS this appears to prevent the higher lactate concentrations to be quantified, shown in **Figure 3.6a**. However using the strong RBS the expression appeared to continue to increase up to the maximum concentration in the physiological sweat concentration ranges, shown in **Figure 3.6b**, but the maximal output was reduced. The better response range to lactate covering the whole physiological range suggests that having a higher level of constitutive mRFP is better for the lactate sensor normalisation when OD is not possible because it can still detect the required range of concentrations.

### 3.2.3 Orthogonality testing of sensor

Sweat is a highly complex sample with many different metabolites found within it. For the whole cell sense and respond genetic circuit to be able to be used for sensing in sweat it needs to be able to specifically detect lactate whilst being unaffected by the other chemicals that will be present.

Glucose is the other major carbon source that is found in sweat and is likely to have the potential to interfere with the response to lactate due to the global regulation that glucose can have on the metabolism. Glucose is found at much lower concentrations than lactate in sweat up to 0.1 mM in a healthy individual and up to 1 mM for an individual with diabetes. To test the impact of glucose on the sensor, it was tested against different concentrations of glucose without lactate and with lactate added, to see whether the glucose generated its own response or prevented the response to lactate as shown in **Figure 3.7**.

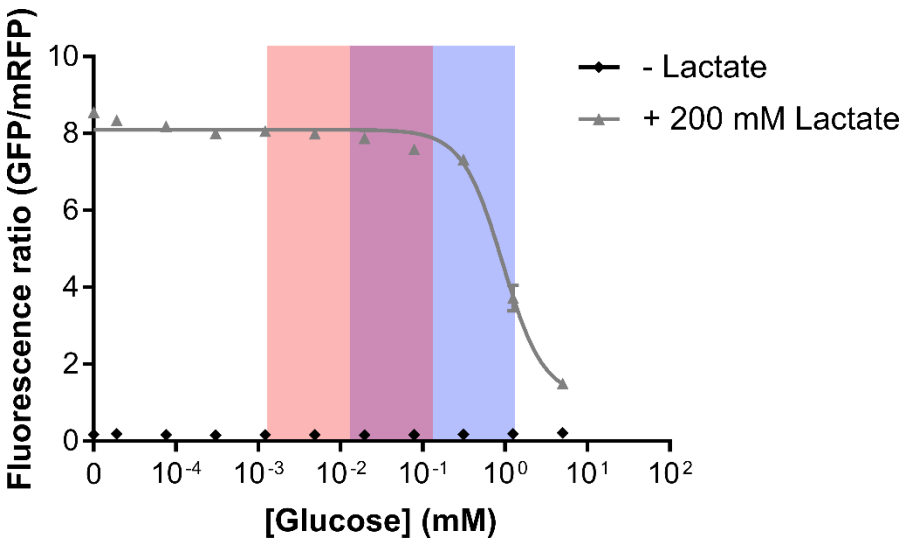


**Figure 3.7 Characterisation of lactate sensor response to glucose.** The graph shows the response of the dual lactate sensor with J23101 RBS 30 mRFP to different glucose concentrations both with or without lactate. The response to glucose when no lactate is present is shown by the black line (- Lactate) or with the maximal concentration of lactate previously characterised shown by the grey line (+200 mM Lactate). The sensor was characterised at 37°C with shaking at 1,000 rpm n=3. The red shaded area shows the levels of glucose found in eccrine sweat of a healthy individual whilst the blue shaded area shows the levels of glucose found in the eccrine sweat of a diabetic, with the response shown 4 hours post induction. The error bars show one standard error.

**Figure 3.7** shows that the lactate sensor does not produce a response to glucose itself, shown by the black line, but when high concentrations of glucose are present, shown by the grey line, the glucose results in the repression of the response to lactate. This was expected as the lactate sensor also responds to global catabolite repression. Previous work into this regulation has shown that the lactate operon is repressed by crp but also to some extent fruR (Gosset et al., 2004). For the glucose concentrations in sweat of a healthy individual this will not be a problem, but if this was to be used in a situation where higher concentrations of glucose are likely to be present such as for a person with diabetes this would be an issue, as shown by the decreasing output of the grey line throughout the blue shaded box. Further modifications to the lactate responsive promoter to remove the regulation by glucose have since been made (Zúñiga et al., 2021). The promoter was modified to remove the native sequence between the operator sites which removed regulation by ArcA in low oxygen environments along with further directed evolution to

remove the interaction by crp and fruR that results in inhibition in the presence of glucose. This engineered version of the promoter could therefore be added into the sensor in the future to prevent the impact of the glucose on the sensor if to be used for a person with diabetes.

The lactate sensor constructed has been shown to detect lactate at the concentration in sweat found in healthy individuals and the presence of other sugars will not cause any issues with the detection of lactate. For people with diabetes there could be issues, although if the disease is controlled then the individual's glucose levels should not be a problem.

## 3.3 Tryptophan sensor

Many different amino acids are present in sweat which have the potential to give information on a person's physiological state. Tryptophan is a key nutrient that plays a key role in the synthesis of many metabolites including melatonin and serotonin (Richard et al., 2009). This suggests that it would be a highly important metabolite to detect. Sweat tryptophan has also been shown to decrease in response to physical activity, so this suggests its use in monitoring exercise and an individual's response to exercise (Delgado-Povedano et al., 2016, Dunstan et al., 2016).

All bacteria are capable of synthesising their own amino acids when required due to a lack of that amino acid being present in their environment. However synthesising amino acids is highly energy intensive, so if the amino acid is present in their environment then bacteria will avoid synthesising their own. To do this, bacteria need to be able to sense the presence of the amino acid to ensure that the synthesis machinery can be repressed when not required (Yanofsky, 2004). Therefore to build a tryptophan biosensor genetic parts from *E. coli* were used to construct the sensor.

### 3.3.1 Initial construction and characterisation

For the initial construction of the tryptophan biosensor multiple versions were constructed using different mutants of the tryptophan responsive transcription factor (TrpR) which had been generated to give a higher sensitivity to tryptophan (Hurlburt and Yanofsky, 1990). The construct was designed by me but the initial cloning was carried out by an undergraduate intern, Yu Fu. These were tested because the levels of tryptophan found in sweat are in the micromolar concentration range, so sensitivity was likely to be an issue. The plasmid design for the initial sensor is shown in the upper panel of **Figure 3.8a**.

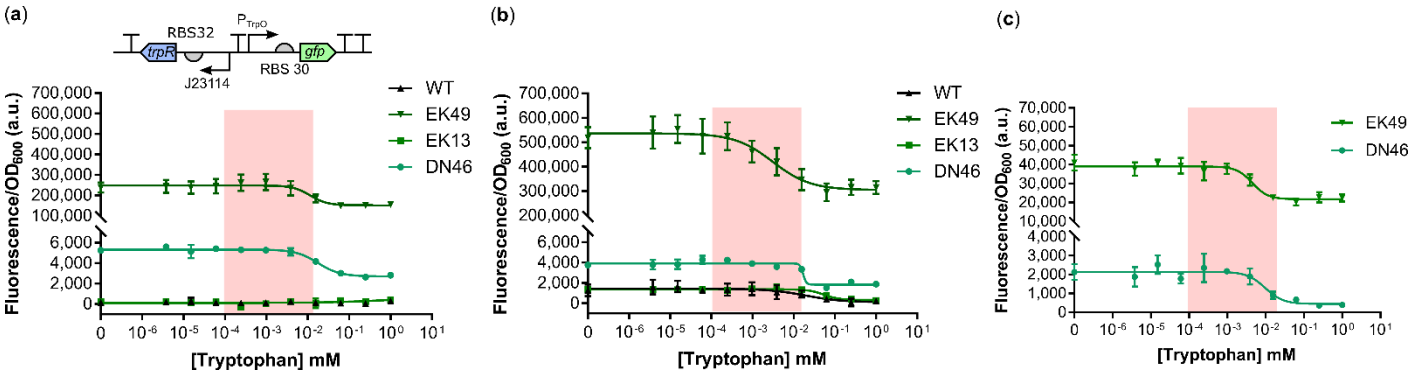


**Figure 3.8 Construction and characterisation of a tryptophan sense and respond genetic circuit.** (**a**) the upper panel shows the initial genetic construct for the tryptophan sense and respond genetic circuit using the *E. coli,* tryptophan responsive promoter ($P_{TrpO}$) to control expression of the reporter gene (*gfp*) and tryptophan binding transcription factor TrpR gene (*trpR*) expressed using a weak constitutive promoter from the Anderson collection (J23114). Four different versions using both the wild type TrpR and mutant TrpR were constructed. The lower panel shows the graph of the response curves of the different versions of the tryptophan sense and respond genetic circuits, the circuit containing the wild type TrpR (WT), the circuit containing a mutant TrpR with the 49$^{th}$ amino acid changed from glutamic acid to lysine (EK49), the circuit containing a mutant TrpR with the 13$^{th}$ amino acid change from glutamic acid to lysine (EK13) and the circuit containing a mutant TrpR with the 46$^{th}$ amino acid mutated from aspartic acid to asparagine (DN46). The cells were grown in M9 media with 0.4% glycerol but no casamino acids added. (**b**) the graph shows the response curve of the four different tryptophan sense and respond genetic circuits when grown in M9 media with 0.4% glycerol and added salts with no amino acids (40 mM dipotassium phosphate, 15 mM potassium phosphate, 7 mM ammonium sulphate, 0.4 mM magnesium sulphate and 1.5 mM sodium citrate) (**c**) the graph shows the response curves of the two best tryptophan sense and respond genetic circuits EK49 and DN46 grown in M9 media with 0.4% glycerol and homemade amino acid solution. For all experiments n=3, cell grown at 37°C 1,000 rpm shaking. The response taken at 7 hours post-induction. The error bars show one standard error.

Initial characterisation showed that two of the mutant versions of TrpR seemed to give a response to tryptophan. However there was a very high level of leaky expression, as shown by the response curves in **Figure 3.8a**. The version with the 49$^{th}$ amino acid changed from glutamic acid to lysine and the version with the 46$^{th}$ amino acid changed from aspartic acid to asparagine showed the best response curves. Due to the low level of change between the on and off states of working sensors alternative media were tested to see if the low OD of the cells when grown with no amino acids added to the media was the cause of the high fluorescence, because normalisation to OD would result in amplification even where there is low fluorescence, shown in **Figure 3.8b and c**. In **Figure 3.8b** M9 media without any amino acids added to the culture but supplementary salts added was used to see if having more salts would help with the cells ability to produce its own amino acids as this had been used in characterisation of cells expressing TrpR previously (Singleton et al., 1980). The versions of the sensors which were previously responsive in **Figure 3.8a** showed a much higher fluorescence and a larger change between on and off, however the leakiness of the sensor was still very high. The final media tested in **Figure 3.8c** used a homemade bespoke amino acid solution that contained no tryptophan, as the added salts had not improved the leakiness and it is only the presence of tryptophan in the media that could cause issues to the sensor's response. In this case only the two sensors which had previously worked were tested (EK49 and DN46). This did reduce the leakiness compared to the previous characterisation but it was still a large issue. The response of these sensors also required a far longer time to be detected compared to response time of the lactate biosensor. This could be due to the high level of leakiness and that for the repression to be detectable the cell needed to grow for longer to dilute the GFP already expressed. So the time course data of the tryptophan sensor was studied, shown in **Figure 3.9**.

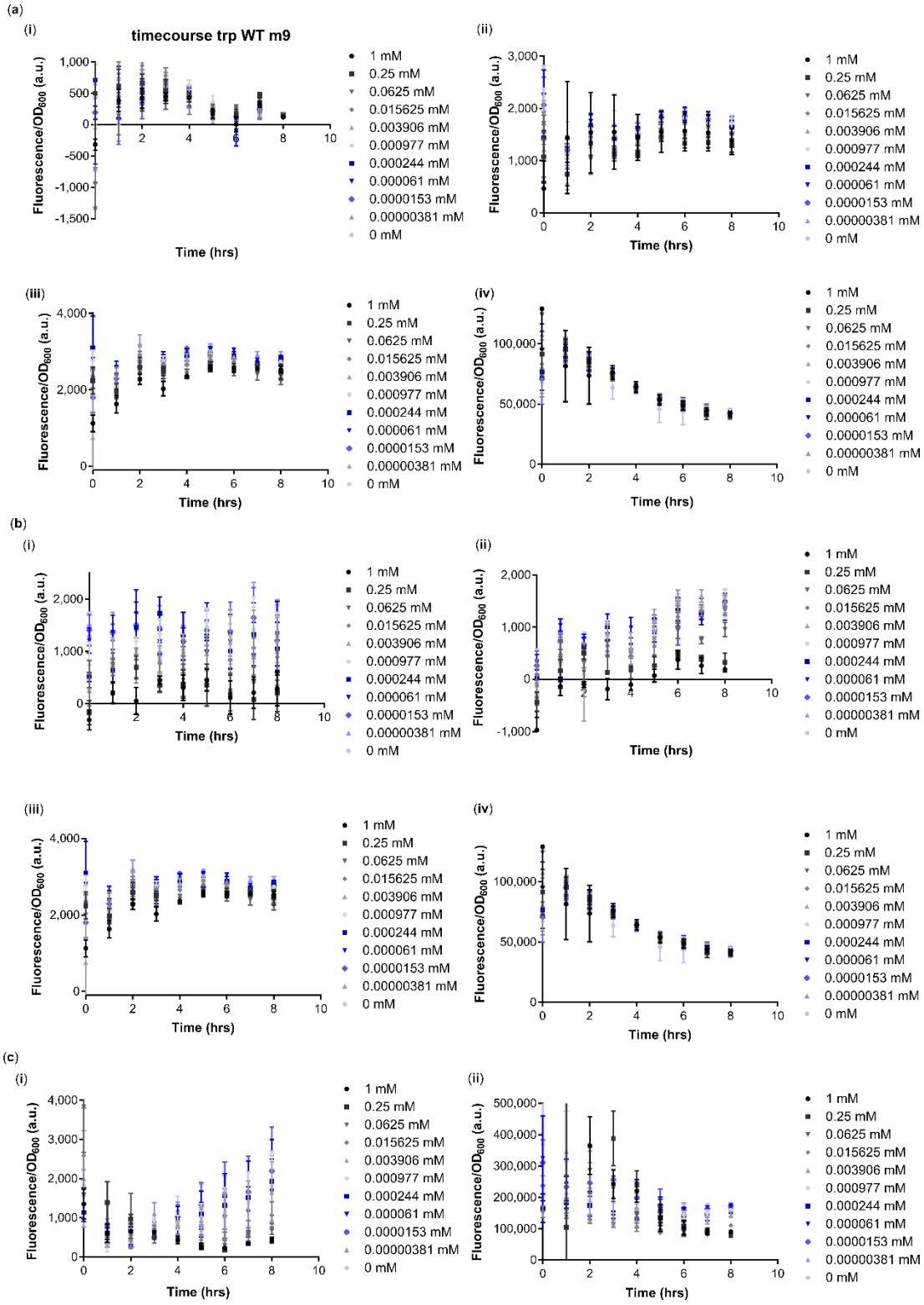


**Figure 3.9 Change in response over time of the tryptophan biosensors to different concentrations of tryptophan.** (**a**) shows the change in response over time when the biosensor is grown in M9 media with no amino acids added. (**i**) shows the response of the biosensor containing the wild type TrpR transcription factor. (**ii**) shows the response of the biosensor containing the mutant

version of TrpR EK13. (**iii**) shows the response of the biosensor containing the mutant version of TrpR DN46. (**iv**) shows the response of the biosensor containing the mutant version of TrpR EK49. (**b**) shows the change in response over time when the biosensor is grown in M9 media with no amino acids added but supplemented with extra salts. (**i**) shows the response of the biosensor containing the wild type TrpR transcription factor. (**ii**) shows the response of the biosensor containing the mutant version of TrpR EK13. (**iii**) shows the response of the biosensor containing the mutant version of TrpR DN46. (**iv**) shows the response of the biosensor containing the mutant version of TrpR EK49. (**c**) shows the change in response over time when the biosensor is grown in M9 media with a homemade amino acid solution which contains no tryptophan. (**i**) shows the response of the biosensor containing the mutant version of TrpR DN46. (**ii**) shows the response of the biosensor containing the mutant version of TrpR EK49. For all of the graphs n=3 the cells were grown at 37°C with 1,000 rpm and the error bars show one standard error.

In **Figure 3.9a and b** for some of the versions of the sensor show a decrease in the response over time suggesting that there is a large carry over of GFP that is expressed in the overnight culture as tryptophan present in the media is used up. This resulted in the response not being detectable at earlier time points due to the leaky expression overnight being masked. However for the functional sensors by hour 7 the level of dilution through the growth of the cells meant that the difference between the concentrations on tryptophan and whether this supressed GFP expression or not could be distinguished. For **Figure 3.9c** the response could begin to be distinguished earlier in comparison to **Figure 3.9 a and b** but the high response to begin with was still an issue.

### 3.3.2 Optimisation of sensor

Due to the high level of leakiness that had been seen in the sensor response, shown in **Figure 3.8,** the sensor was then moved to a medium copy plasmid from a high copy plasmid as it was likely that there were too many copies of the tryptophan responsive promoter for the repressor to be able to effectively repress the expression of GFP.

The initial characterisation on a medium copy plasmid showed no response to tryptophan at all. At this point it is likely that now the expression of the

repressor was too high, resulting in repression even when no tryptophan was present.

At this stage the options were either that the original constructs could be optimised to increase the TrpR expression to ensure there was a high enough level of TrpR present to be able to fully repress the promoter, or that the expression of TrpR on the medium copy plasmid could be lowered to prevent repression even when no tryptophan is present. The cloning for both methods was carried out. However, issues occurred generating the constructs for the high copy plasmid so this approach was stopped because this suggested that increasing the expression was overwhelming the cellular machinery or affecting the native metabolism.

A fairly weak promoter was already being used to expressed TrpR in the original construct (J23114) and there were only two alternative promoters, which when tested using constitutive GFP expression within the lab (unpublished data, Wang lab), that showed weaker activity. These two sensors were constructed as shown by the upper panel in **Figure 3.10a**. At this point the response of the sensor was tested in two different ways, by either growing the overnight cultures used in the characterisation of these new sensors with added tryptophan in the media to repress the GFP expression overnight or without this, to see how this impacted the leakiness (because as the amino acids in the medium for the overnight culture are utilised the sensors will begin to express GFP). As GFP is highly stable this GFP produced in the overnight remains in the cells so can result in fluorescence even when the sensors are fully repressed.

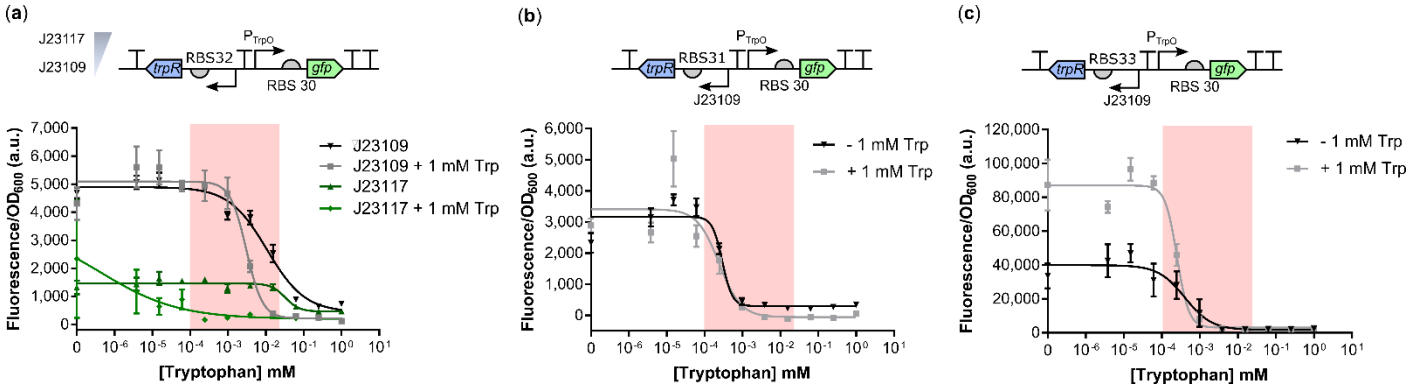


**Figure 3.10 Optimisation of the tryptophan sense and respond genetic circuit.** (**a**) the upper panel shows the sense and respond genetic circuits constructed to detect tryptophan using a medium copy plasmid pSB3K3. Two different constitutive promoters from the Anderson collection were tested with weak strengths (J23109 and J23117) with a medium strength RBS whilst the parts to express the reporter remained the same. The lower panel shows the graph of the response curves of the different tryptophan sense and respond genetic circuits with the two different promoters (J23109 and J23117). Also tested were the 2 circuits grown overnight in LB with 1 mM tryptophan added to see in this reduced the leakiness of the sensor (J23109 + 1 mM Trp and J23117 + 1 mM Trp). The response taken at 7 hours post-induction. (**b**) the upper panel shows the tryptophan sense and respond genetic circuit using a weak promoter (J23109) and a weaker RBS (RBS31). The lower panel shows the response curve of the genetic circuit either grown in LB overnight with no tryptophan (- 1 mM Trp) or grown overnight in LB with 1 mM tryptophan (+ 1 mM Trp). (**c**) the upper panel shows the tryptophan sense and respond genetic circuit with the TrpR tryptophan responsive repressor expressed using a weak constitutive promoter (J23109) and a weak RBS (RBS33). The lower panel show the response curve of the genetic circuit when grown overnight in LB without additional tryptophan (- 1 mM Trp) or with 1 mM tryptophan added to the LB (+ 1 mM Trp). For all graphs, the red shaded area shows the concentration range of tryptophan found in human eccrine sweat, n=3 with the cells grown at 37°C 1000 rpm shaking. For (**b**) and (**c**) sense and respond genetic circuit response taken at 4 hours post-induction. The error bars show one standard error

Lowering the expression level of TrpR did allow the response of the sensor to be recovered on the medium copy number plasmid, as seen in **Figure 3.10a** showing that too high expression of TrpR had resulted in the loss of the response. The response was best when using the weakest possible promoter J23109, so this version was used in further studies. Adding tryptophan to the overnight culture media did improve the response of the sensor with the sensor beginning to respond at a lower concentration. As reducing the expression of TrpR resulted in a large improvement of the response of the sensor on the medium copy plasmid potentially further reduction in the

expression level would improve the response further. As the weakest possible promoter was already being used in the sensor, the sensors were further optimised to use weaker RBS, as shown in **Figure 3.10b and c**. Initially the RBS was changed to RBS 31. This did not improve the response of the sensor compared to RBS 32, as shown in **Figure 3.10b**. Following this an even weaker RBS was used RBS33, as shown in **Figure 3.10c.** This resulted in a large increase in the maximal output of the sensor when no tryptophan was present whilst also responding to the desired concentrations of tryptophan and retaining low leaky expression.

For the opimised sensors with weaker RBSs the time to detect the response was much faster than previously, at four hours compared to seven. This is likely due to reduced expression of GFP in the overnight culture compared to previous versions of the biosensor. **Figure 3.11** gives the change in the response of the sensor over time to different concentrations of tryptophan.

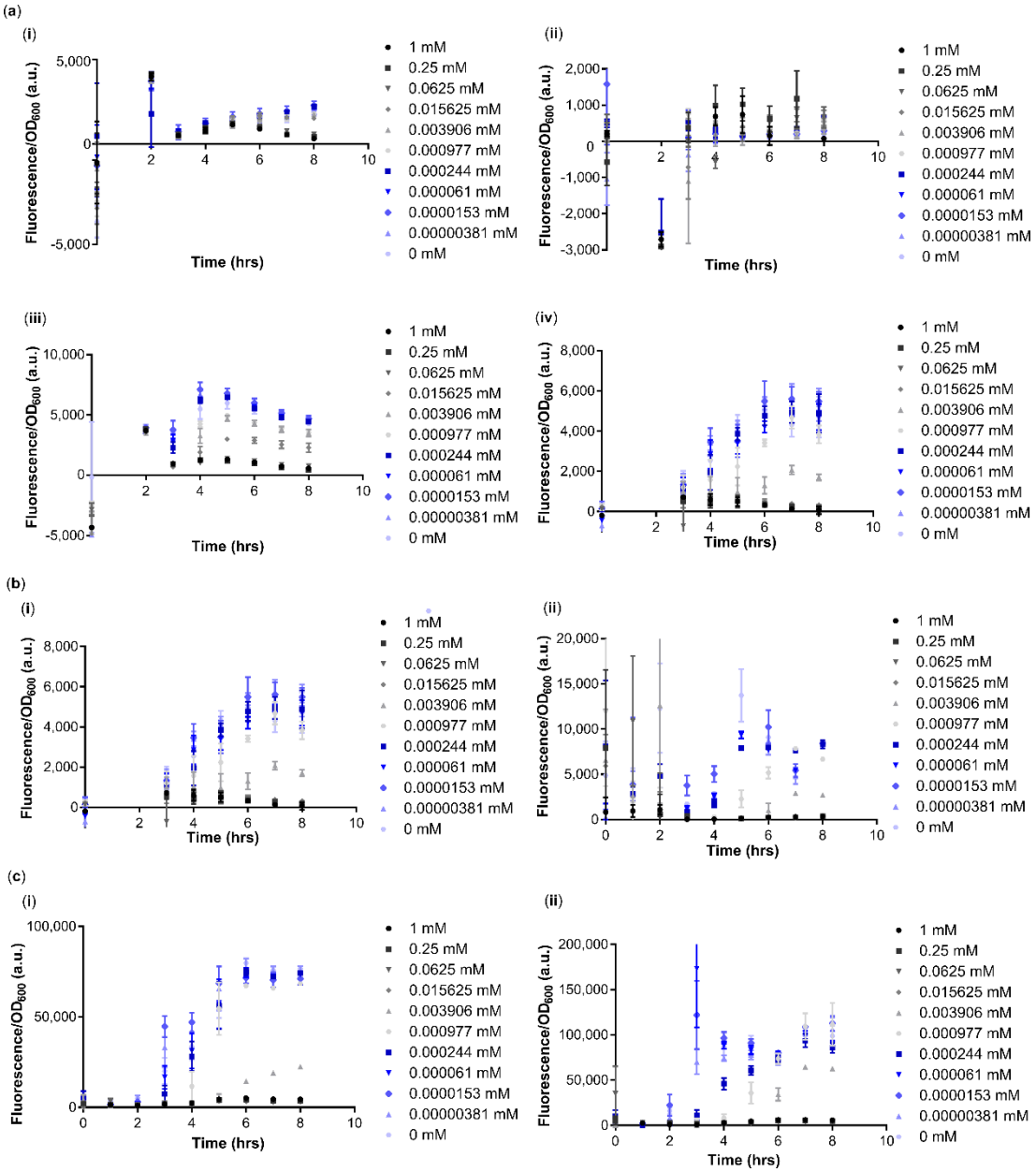


**Figure 3.11 Change in response over time of tryptophan biosensor on medium copy pSB3K3 plasmid backbone.** (**a**) shows the change in response over time of the tryptophan biosensor to different concentrations of tryptophan when TrpR EK49 is expressed with different constitutive promoters. (**i**) shows when TrpR EK49 is expressed using J23117 when the biosensor is grown overnight in LB medium as previously. (**ii**) shows when TrpR EK49 is expressed using J23117 when the biosensor is grown in LB medium overnight with 1 mM tryptophan added to the medium. (**iii**) shows when TrpR EK49 is expressed using J23109 when the biosensor is grown overnight in LB medium as previously. (**iv**) **ii**) shows when TrpR EK49 is expressed using J23109 when the biosensor is grown in LB medium overnight with 1 mM tryptophan added to the medium. (**b**) shows the change in response over time of the tryptophan biosensor with TrpR EK49 expressed using J23109 with RBS 31. (**i**) shows when the biosensor is grown in LB medium overnight as previously. (**ii**) shows when the sensor is grown in LB medium overnight with 1 mM tryptophan added. (**c**) shows the change in response over

time of the tryptophan biosensor with TrpR EK49 expressed using J23109 with RBS 33. (**i**) shows when the biosensor is grown in LB medium overnight as previously. (**ii**) shows when the biosensor is grown in LB medium containing 1 mM tryptophan overnight. For all graphs n=3 cells grown at 37°C with 1,000 rpm shaking. The error bars show one standard error.

**Figure 3.11a** shows that for the weakest promoter J23109 the response can begin to be seen at a much earlier time suggesting that there is a better balance between the promoter and transcription factor, so preventing repression of the response without the presence of tryptophan. But with the alternative promoter J23117 the GFP carried over disguised the response until later time points. Reducing the expression of the tryptophan further by weakening the RBS, shown in **Figure 3.11 b and c**, increased the response further allowing the earlier time point to be used for determining the response curve.

Having optimised the response of the tryptophan sensor to maximise the fold change of the sensors the versions with constitutive mRFP expression to use for normalisation were constructed and characterised, as shown in **Figure 3.12**.

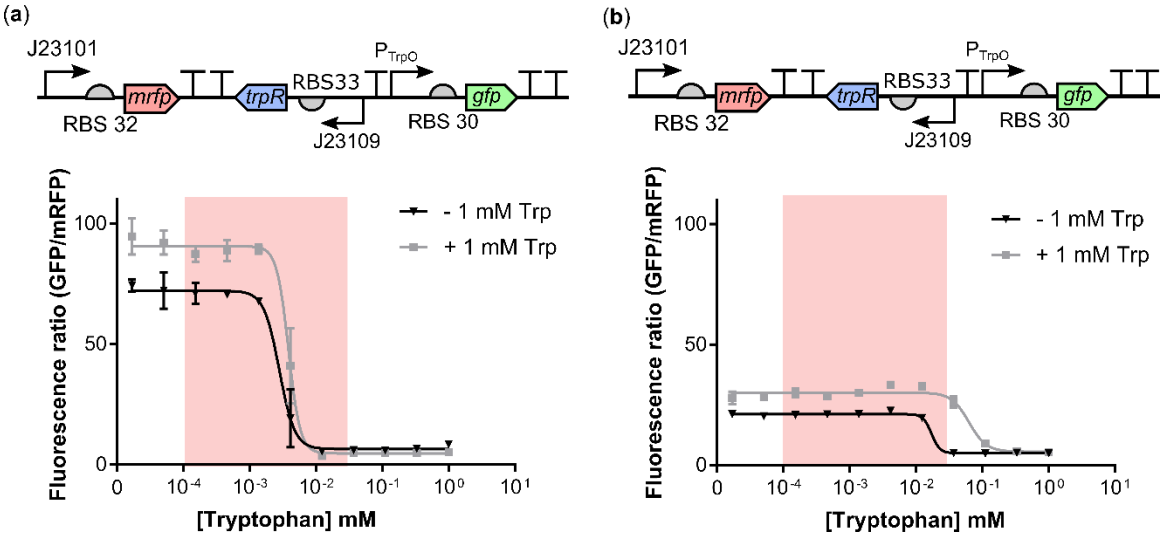


**Figure 3.12 Characterisation of mRFP normalised tryptophan whole cell biosensor.** (**a**) shows the response of the tryptophan sensor when J23101 RBS 32 mRFP is used to normalise the response to tryptophan. (**b**) shows the response of the tryptophan biosensor when J23101 RBS 30 mRFP is used for normalisation of the response. For both versions they were tested with 1 mM of tryptophan added to the overnight culture shown by the grey line (+ 1 mM Trp) and no tryptophan added to the overnight shown by the black line (-1 mM Trp), n=3 cell grown at 37°C with shaking at 1,000 rpm. The red shaded area

shows the region that corresponds to the concentrations of tryptophan that is found in human eccrine sweat. The response was taken 6 hours post-induction. The error bars show one standard error

For both versions of the sensor adding tryptophan to the overnight culture improved the maximal output of the sensor. **Figure 3.12a** shows the response when mRFP is expressed by J23101 and RBS 32. The response to tryptophan remained within the required range of concentration that needed to be detected. But there was reduced sensitivity compared to when the response was normalised to OD. When J23101 RBS 30 was used to express mRFP an even larger loss of sensitivity occurs, as seen in **Figure 3.12b**.

Using constitutive RFP fluorescence for normalisation also works for the tryptophan sensor and ensures that the sensor can work in the final device. But it appears to be better with RBS32 expressing the RFP for normalisation.

### 3.3.3 Orthogonality testing of sensors

The sensor's specificity also needs to be confirmed to ensure that when detecting biomarkers in sweat the response detected from the biosensor does reflect the concentration of tryptophan in sweat. The sensor was tested for a response to two other amino acids, tyrosine and phenylalanine, shown in **Figure 3.13**, because these are the most structurally similar so are most likely to be able to bind to TrpR within the binding pocket and result in off-target effects.

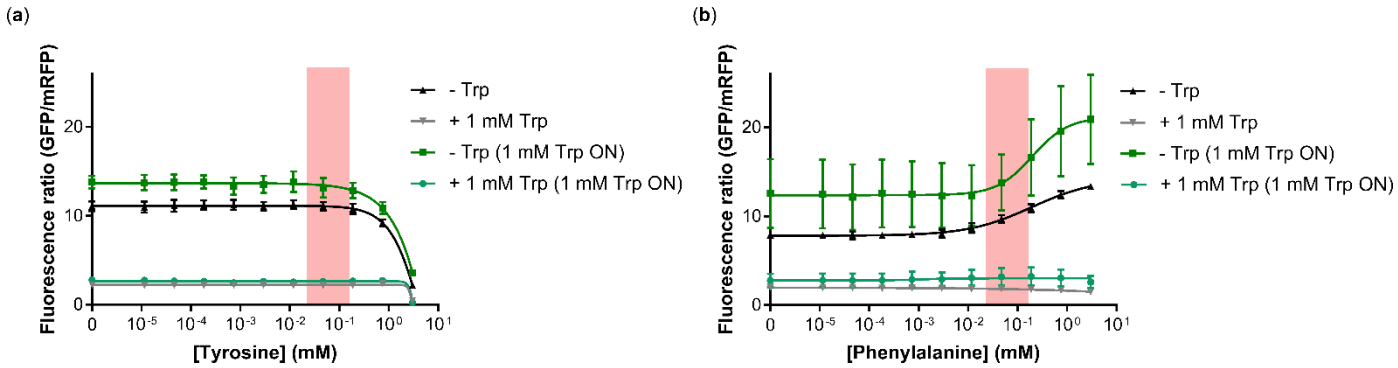


**Figure 3.13 Characterisation of tryptophan sensor with potential off-target biomarkers.** (**a**) shows the response of the tryptophan biosensor with J23101 RBS 30 mRFP to tyrosine without any tryptophan added during the day, without or with tryptophan in the overnight -Trp and -Trp (1 mM Trp ON) (black and dark green line) respectively, or with 1 mM tryptophan added to the sensor culture during the day without or with tryptophan added to the overnight + 1 mM Trp and + 1 mM Trp (1mM Trp ON) (grey and light green lines) respectively. (**b**) shows the response of the tryptophan sensor with J23101 RBS 30 mRFP to phenylalanine under the same four conditions as previously. For both n=3, cells grown at 37°C with shaking at 1,000 rpm. The red shaded area shows the concentration of the biomarker found in human eccrine sweat. The response shown was taken 5 hours post-induction. The error bars show one standard error.

**Figure 3.13a** shows that a very high concentration of tyrosine represses the sensor if no tryptophan is present, shown by the black and dark green lines. With tryptophan also present (shown by the grey and lighter green lines) the tyrosine does not prevent the tryptophan from generating the expected response from the sensor. But the repression of the response from both amino acids is combined at the highest concentrations of tyrosine. The concentration required to generate this repression is above the concentrations expected to be found in human sweat so this is not a concern. Phenylalanine increases the GFP expression from the tryptophan sensor at high concentrations when no tryptophan is present (black and dark green lines), as shown in **Figure 3.13b**. When tryptophan is added alongside phenylalanine the sensor it is still capable of repressing GFP expression even at the concentrations of phenylalanine that generates a response. Therefore, even though an increase in the response occurs when no tryptophan is present, the presence of phenylalanine does not appear to

impact the response to tryptophan, so should not cause issues for the final device when sensing sweat.

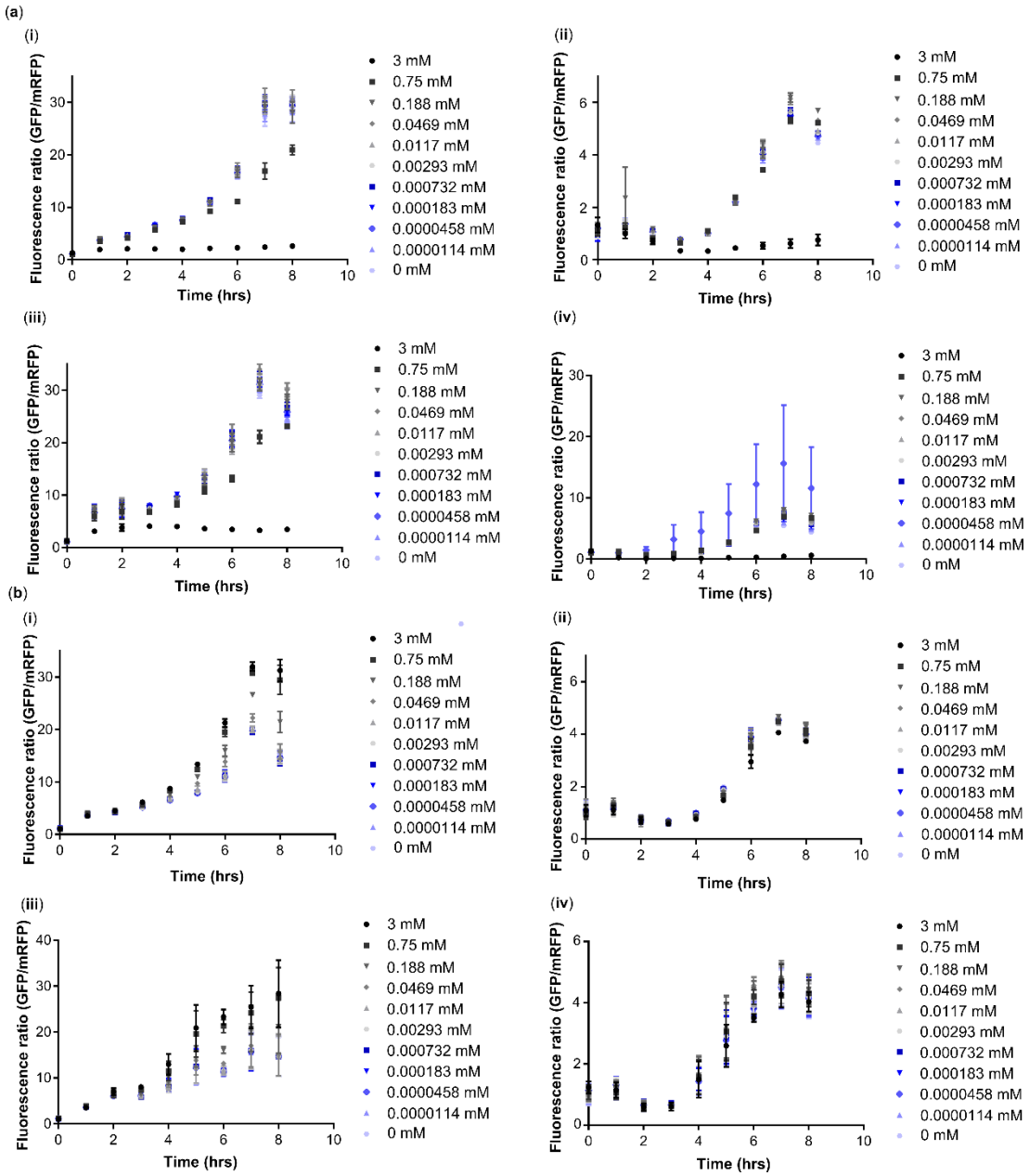


**Figure 3.14 The change in the response of the tryptophan sensor over time to different concentrations of alternative amino acids that had the potential to cause an off-target response.** (**a**) shows the response of the tryptophan to different concentrations of tyrosine. (**i**) shows the response over time when the sensor was grown overnight in LB medium and only induced with tyrosine. (**ii**) shows the response over time when the sensor was grown overnight in LB medium and was induced with 1 mM tryptophan as well as tyrosine. (**iii**) shows the response over time when the sensor was

grown overnight in LB medium with 1 mM tryptophan and only induced with tyrosine. (**iv**) shows the response over time when the sensor was grown overnight in LB medium containing 1 mM tryptophan and was induced with 1 mM tryptophan as well as tyrosine. (**b**) shows the response of the tryptophan to different concentrations of phenylalanine. (**i**) shows the response over time when the sensor was grown overnight in LB medium and only induced with phenylalanine. (**ii**) shows the response over time when the sensor was grown overnight in LB medium and was induced with 1 mM tryptophan as well as phenylalanine. (**iii**) shows the response over time when the sensor was grown overnight in LB medium with 1 mM and only induced with phenylalanine. (**iv**) shows the response over time when the sensor was grown overnight in LB medium containing 1 mM tryptophan and was induced with 1 mM tryptophan as well as phenylalanine. For all graphs n=3 the cells were grown at 37°C with shaking at 1,000 rpm. The error bars show one standard error.

**Figure 3.14** shows for all the graphs that by 5 hours post-induction the off that expected from TrpR and seen in the growth of the cells over time with different concentrations of tyrosine and phenylalanine, shown in **Figure 3.15**.

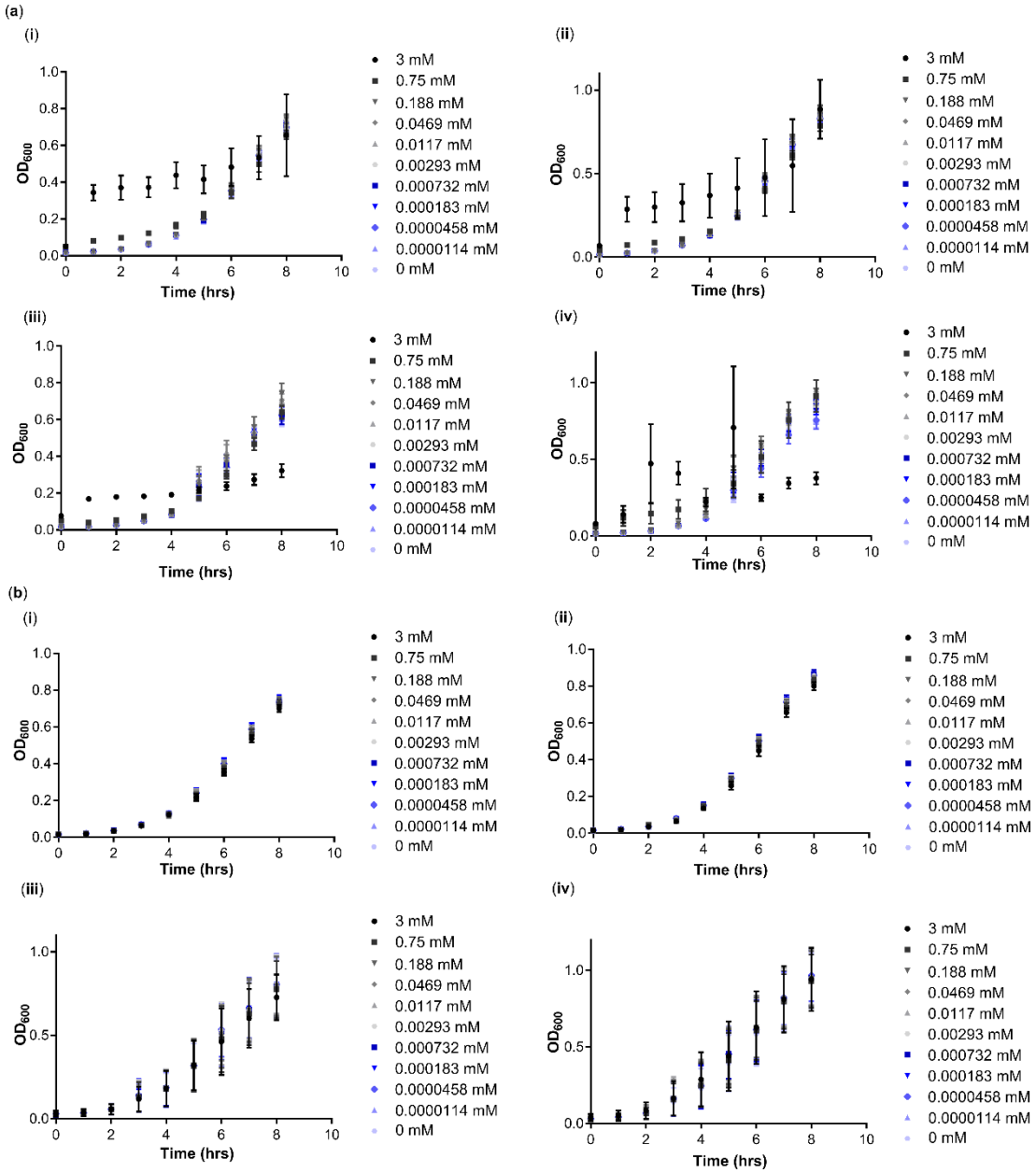


**Figure 3.15 Growth of the tryptophan biosensor with different concentrations of alternative amino acids that had the potential to cause an off-target response.** (**a**) shows the growth of the tryptophan biosensor with different concentrations of tyrosine. (**i**) shows the growth over time when the sensor was grown overnight in LB medium and only induced with tyrosine. (**ii**) shows the growth over time when the sensor was grown overnight in LB medium and was induced with 1 mM tryptophan as well as tyrosine. (**iii**) shows the growth over time when the sensor was grown overnight in LB medium with 1 mM and only induced with tyrosine. (**iv**) shows the growth over time when the sensor was grown overnight in LB medium containing 1 mM tryptophan and was induced with 1 mM tryptophan as well as tyrosine. (**b**) shows the growth of the tryptophan biosensors with different concentrations of phenylalanine. (**i**) shows the growth over time when the sensor was grown overnight in LB medium and only induced with phenylalanine. (**ii**) shows the growth over time when the sensor was grown overnight in LB medium and was induced with 1 mM tryptophan as well as phenylalanine. (**iii**) shows the growth

over time when the sensor was grown overnight in LB medium with 1 mM and only induced with phenylalanine. (**iv**) shows the growth over time when the sensor was grown overnight in LB medium containing 1 mM tryptophan and was induced with 1 mM tryptophan as well as phenylalanine. For all graphs n=3 the cells were grown at 37°C with shaking at 1,000 rpm. The error bars show one standard error.

For the tyrosine sensor the growth between the majority of the concentrations was very similar as shown in **Figure 3.15a** except for at the highest concentration of where the OD appear to be higher from the beginning for the sensors induced with only tyrosine. This could have changed the response determined because the higher number of cells could have impacted the RFP levels. But this would reduce the response so at the highest concentration the repression would appear more. As this is outside the concentration range expected to be seen in sweat this is not an issue for the sensor specificity. For the phenylalanine response an increase in the response at higher concentrations seen in **Figure 3.13b** was unexpected because TrpR is a repressor. Potentially one cause for the increase could be due to changes in the cell growth at these higher concentrations. **Figure 3.15b** shows that the growth of the cells at higher concentrations of phenylalanine was similar to the growth at other concentrations so the reason for the increase is unclear.

## 3.4 Steroid biosensors

Steroid hormones have a large role in determining an individual's health and physiological state due to their key role in the physiological response to stress. Cortisol and testosterone are both key hormones for monitoring an individual’s stress.

To date whole cell biosensors for steroid biosensors have focused on mammalian cells due to the presence of natural proteins which can respond to steroid hormones (Kang et al., 2021, Ryu et al., 2021). However mammalian cells will have a slower response time and the conditions required for the growth of the cells are more stringent and so are less suitable for developing a device which is to be worn.

### 3.4.1 Cortisol biosensor

Work into the interplay between the immune response and the hormones involved in this and the bacteria generating the immune response has identified that pathogenic bacteria can detect and respond to these hormones and alter their gene expression in response. *Salmonella typhimurium* has been shown to detect cortisol in infection of pig guts (Verbrugghe et al., 2016). A study into how cortisol changed gene expression showed an increase in proteins from a copper sensitivity locus suggesting this promoter was activated in response to cortisol. Two different methods of regulation have been identified for the copper sensitivity locus, a two-component system CpxR/CpxA and self-regulation through the ScSA protein from the Scs locus (Gupta et al., 1997).

A range of different biosensors to cover a range of transcription factor levels and both potential forms of regulation of the promoter were built. Two different versions of the promoter were also tested as the exact sequence was unknown. One was the extended version which was received from Sheppard lab at the University of Kent and an alternative version which was truncated to where there promoter was predicted to be using a program to analyse the sequence (de Avila e Silva et al., 2011). The different final versions of the sensor which were characterised are outlined in **Figure 3.16a**.

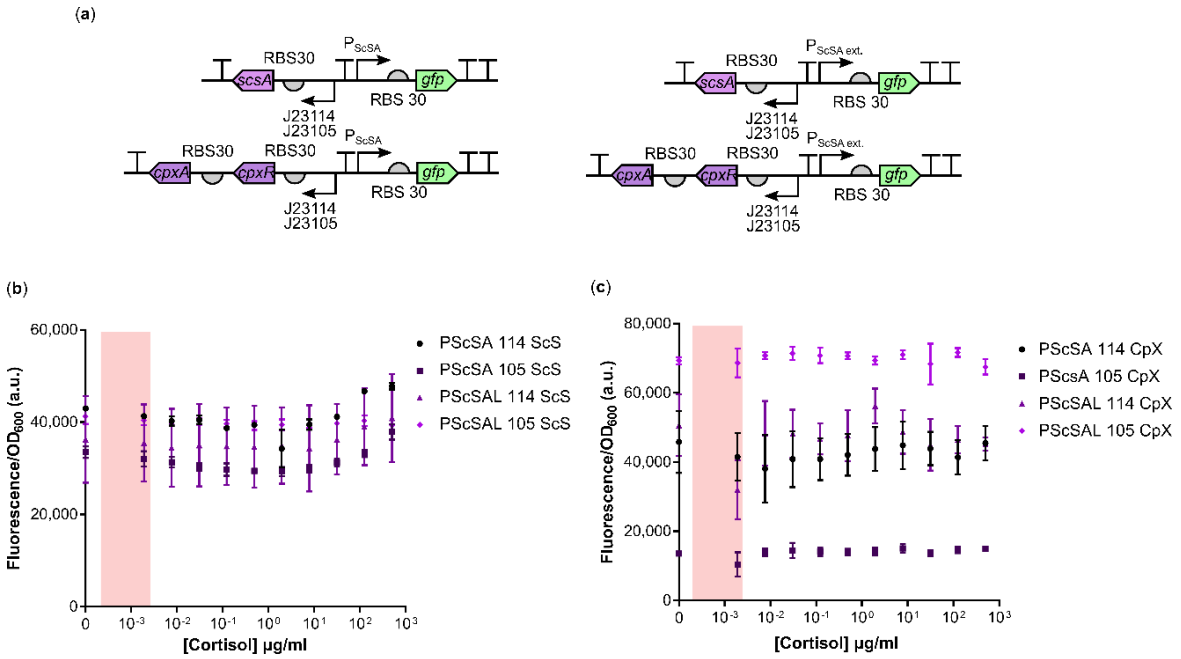


**Figure 3.16 Response of whole cell sense and respond cortisol sensors.** (**a**) shows the different genetic constructs that were built to generate a whole cell cortisol biosensor using two different strength promoters to express either ScsA or the two-component system CpXR/A. Two different versions of the responsive promoter were also tested due to the exact sequence of the promoter being unknown. (**b**) shows the response curve of the versions of the biosensor which used ScsA as the transcription factor. (**c**) shows the response curve of the sensor versions using the two-component system CpXR/A. For all sensors n=3 the cells were grown at 37°C with shaking at 1,000 rpm. The error bars show one standard error and the response was taken 5 hours post-induction.

In total eight different versions of the biosensors were constructed using the two different transcription factors with two different expression levels using either a medium or weak constitutive promoters. Alongside this two different versions of the responsive promoter were tested. The region within the genome which contains the promoter had been identified and this was then analysed using a program to predict where the likely -10 and -35 sites were (de Avila e Silva et al., 2011) to design the promoter. These constructs are highlighted in **Figure 3.16a**. The versions constructed using ScsA protein also showed an increase in fluorescence in response to cortisol seen in **Figure 3.16b** but with the two-component system no response could be detected, seen in **Figure 3.16c**. The ScsA versions showed very high leakiness which would need to be improved along with an improvement in the

sensitivity to cortisol to be able to reach the required response characteristics.

### 3.4.2 Testosterone biosensor

Within the environment *Comamonas testosteroni* utilises testosterone as a carbon source as part of its metabolism when other carbon sources are not available and so would have the ability to detect testosterone and control the expression of enzymes required to metabolise testosterone (Pruneda-Paz et al., 2004). **Figure 3.17a** outlines the genetic sense and respond circuits which were designed and characterised.

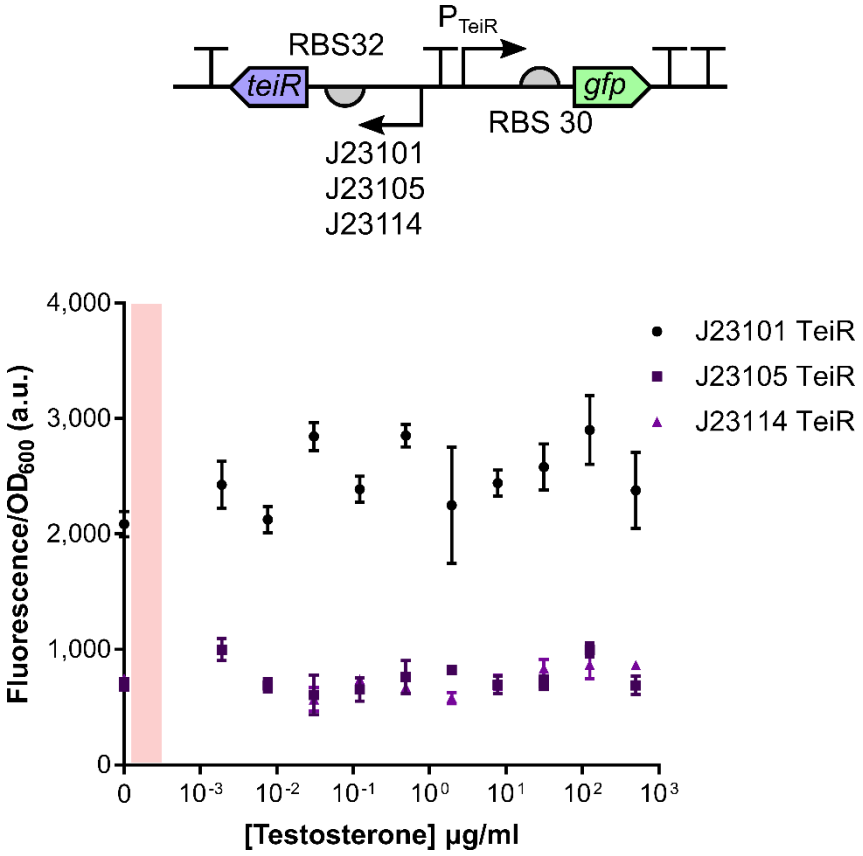


**Figure 3.17 Response of whole cell sense and respond testosterone biosensor.** The upper panel shows the genetic circuits that were constructed to generate the whole cell testosterone biosensors. The lower panel shows the response of the whole cell testosterone biosensor to testosterone. For all sensors n=3, the cells were grown at 37°C with shaking at 1,000 rpm. The error bars show one standard error and the response was taken 5 hours post-induction.

The initial constructs shown in **Figure 3.17** did not show a strong response to the testosterone in cells. Potentially the -10 and -35 sites present in the promoter were not able to recruit the polymerase well. Previous work in the literature has shown that replacing the -10 and -35 with a weak constitutive promoter can improve the response of a biosensor (Trantidou et al., 2018). This approach was tested with the testosterone biosensors using J23114 and J23117 added into the promoter, shown in **Figure 3.18**.

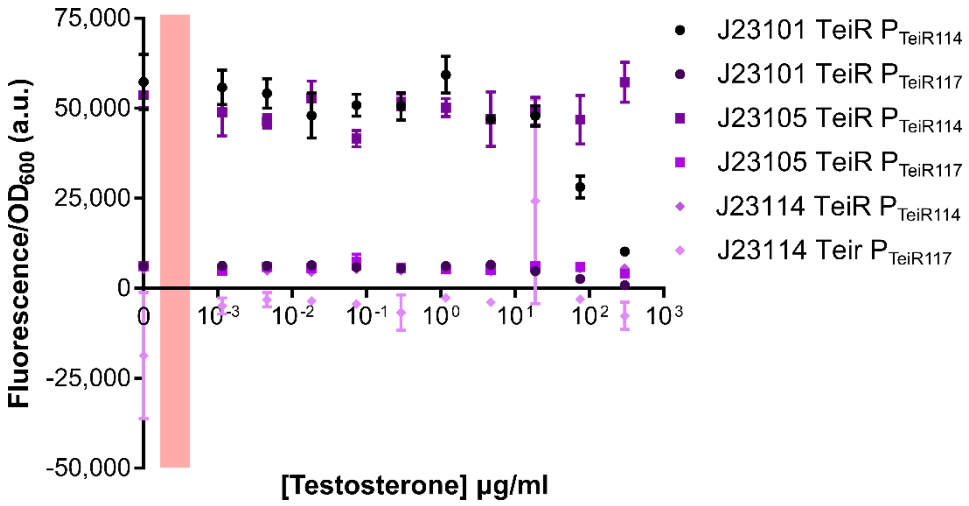


**Figure 3.18 Response of whole cell testosterone biosensors using synthetic testosterone promoters.** The figure shows the response of the whole cell testosterone biosensors to testosterone using synthetic testosterone responsive promoters with either J23114 or J23117 used to replace the -10 and -35 sites within the promoter. For all sensors n=3, the cells were grown at 37°C with shaking at 1,000 rpm. The error bars show one standard error and the response was taken 5 hours post-induction.

Altering the responsive promoter to try and improve the output did not show a strong improvement, as seen in **Figure 3.18**. This suggested that the current construct is not able to detect and respond to testosterone.

## 3.5 Discussion

Overall generating whole cell sense and respond genetic circuits works well for generating biosensors suitable for detecting biomarkers at the

physiologically relevant concentrations with the required specificity for use with complex samples.

Fluorescence is an easily detected output which is good when constructing and optimising biosensors. However as fluorescent proteins are highly stable with a half-life over 24 hours (Kitsera et al., 2007). This means that if multiple readings from the same sensor want to be taken then the fluorescent proteins will need to be actively degraded to ensure that when any new expression is triggered by biomarkers that a new response can be detected. This feature is something that needs to be considered as repeat readings are likely to be a desired characteristic in the final device. This adds more complexity to the sensor which would also likely affect the response of the sensor to the biomarker. Using a method that is easily reversible would be important for the future functionality of the wearable device. Cell-free biosensing methods exist that are far more suited to reversible detection so this is potentially a far more suitable method for biosensing in a wearable device than whole cell biosensors.

For the lactate and tryptophan biosensors optimisation was successful with the required sensing range being achieved and detection was within four hours which is a good speed for whole cell biosensors. For the steroid whole cell biosensors, the cortisol sensors showed some promise. The version using ScsA as the transcription factor showed an increase in fluorescence in response to cortisol. However the sensitivity was limited and a large improvement would be needed to reach the required sensitivity. The leakiness was also an issue with the fluorescence very high before the response which would also be an issue. For testosterone none of the sensor versions appeared to respond to testosterone. Previous work into biosensor development has shown that synthetic promoters can improve the output of a sensor (Trantidou et al., 2018) so this approach was also tested to see if it could help to generate a response to testosterone but no response could be detected in these versions either. Research in the literature has suggested that in gram negative bacteria the ability of some steroid hormones to cross

the cell wall is limited and this includes testosterone and cortisol to a lesser extent (Plésiat and Nikaido, 1992). This suggests that a whole cell approach to generating cortisol and testosterone biosensors may not be the best approach.

Another issue using whole cell biosensors is that the response time is fairly slow taking several hours to respond to a biomarker of interest. In a wearable device a fast response within minutes would be ideal as the user would want the results of the test as quickly as possible to be able to act on the information. Cell-free biosensing methods again have the possibility for generating the response much faster as this can be done based either on conformational changes or transcriptional only methods. Consequently cell-free biosensing methods will be explored for other biomarkers to see if these approaches can be used to generate faster responses which would be more suitable for the generation of a wearable device.

# 4 Biosensors using binding molecules

## 4.1 Introduction

Cell-free biosensing is a key area of research due to the removal of the biosecurity risk that has discouraged the use of whole cell biosensors. Cell-free biosensors also have potential advantages for commercial applications over whole cell biosensors in terms of better sensitivity and response speeds. When detecting biomarkers to determine information on physiological status and potentially provide warning indicators for changes in health and fitness, high sensitivity will be a key characteristic and fast detection of the biomarker would also be highly desirable. Being able to determine the information from the sensor quickly would allow faster action limiting negative symptoms and poor health outcomes. The cell-free biosensing approaches studied would also have the ability to take multiple measurements and this is an additional characteristic that would be highly important for the biosensors in the final wearable device to have.

To date it has not been possible to detect all biomarkers using whole cell biosensors due to the limited ability of the biomarker to enter the cell or the lack of knowledge of transcription factor and responsive promoter pairs for the specific biomarkers. This is an area where cell-free sensors could allow a wider range of biomarkers to be detected.

The aim of this chapter was to use biological molecules capable of binding with the biomarker as the basis of a sensing approach in order to expand the number of biomarkers that could be detected, focussing on molecules that have been shown to be hard to detect specifically and sensitively using whole cell biosensor approaches. For this I have focussed on potassium ions ($K^+$ ions), testosterone, histamine and cortisol. $K^+$ ions are hard for whole cell approaches to specifically detect separately from other positive ions. The main difference between positive ions is their size which affects the ability of a protein to bind an ion. But size does not prevent other ions that are a similar size or smaller from binding which means that the required level of

specificity cannot be achieved. For testosterone and cortisol whole cell biosensing approaches were investigated with the focus being to use bacterial cells for the sensing, but the availability of promoter and transcription factor pairs was limited. Possibilities for testosterone and cortisol were identified and tested (Verbrugghe et al., 2016, Göhler et al., 2008) but the response was not able to reach the required characteristics as the ability of steroid hormones to cross the cell wall is limited (Plésiat and Nikaido, 1992). The identification of a binding protein approach outlined in the introduction section 1.1.2.1 which had used a histamine binding protein in the design (Zhang et al., 2021b) suggested an alternative approach which would be better for detecting human hormones.

## 4.2 DNA aptamer for sensing potassium

Potassium is a key electrolyte as outline in **Table 1.2** of the introduction. The concentration of potassium in plasma and sweat has also been shown to be at similar levels suggesting this could be a good biomarker for the wearable device (Vairo et al., 2017). A key issue in detecting ions is ensuring a good level specificity from biological based systems. The behaviour between different positive ions of the same periodic group is similar and the main difference between these ions is the size of the ion itself. Although enzymes that require the ion for activity and transport channels exhibit a good level of specificity they will all still respond to sodium as well without preventing the function of the protein, so are not ideal specific sensing (Durdagi et al., 2013).

An alternative approach is the use of aptamers. Aptamers are short oligonucleotides of either DNA or RNA that fold into a specific 3D structure on binding to the molecule it detects. Because the interaction is based on this specific folding conformation and the pairings produced by the bases this method of sensing can be highly specific (Yoo et al., 2020). Therefore, this is a promising method for ensuring specific detection of potassium.

### 4.2.1 Initial characterisation

The initial design of the potassium aptamer was identified from the literature (Wu et al., 2016, Catherine et al., 2014, Ueyama et al., 2002). The sequence of the aptamer selected is shown in the upper panel of **Figure 4.1**. This sensor has shown a good response to potassium and had the closest sensing range to what would be required for sweat sensing but appeared to have a higher sensitivity than required. Tests on the specificity had also shown that a very high concentration of sodium was required to generate an off-target response which is also important for the aptamer to be suitable for sweat monitoring. The aptamer which had fluorescent dyes added to be able to detect the binding of the $K^+$ ion was used. At the 5' end a FAM dye was added and a TAMRA dye was added to the 3'. This meant that when the aptamer folded into the g-quadruplex the two dyes would be brought together to form a FRET pair that would allow the binding to be detected, shown in the upper panel of **Figure 4.1.** Previous work on the aptamer was carried out at room temperature using 5 mM Tris-HCl pH 7.4. In addition, a lower pH of pH 7.0 for the 5 mM Tris-HCl buffer was tested as the pH of sweat ranges from pH 5.0 to 7.0 depending on the sweat rate (Jadoon et al., 2015), so using a lower pH of the buffer would ensure that aptamer was able to function when exposed to sweat. Also, a higher temperature of 37°C was tested because human skin temperature could be much higher than room temperature. For all these different conditions the aptamer was diluted to 0.2 µM in the buffer and then induced with potassium chloride (KCl) immediately and the change in fluorescence for the FAM only and the FRET response from FAM and TAMRA read. The response of the sensor under these different conditions is shown in **Figure 4.1**.

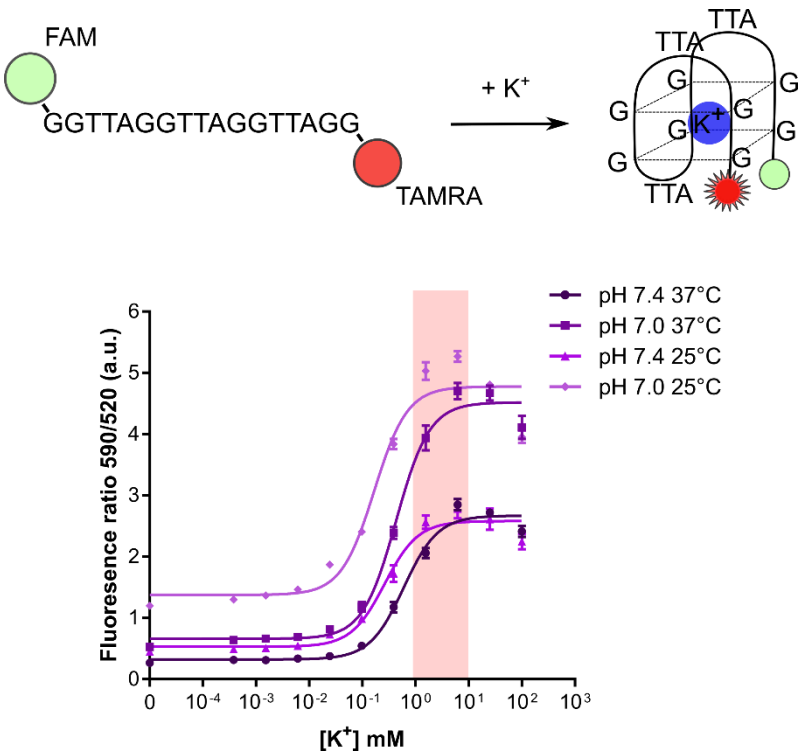


**Figure 4.1 Characterisation of potassium aptamer identified from literature.** The upper panel shows the sensing mechanism for potassium aptamers with the sequence annotated identified, an unstructured single stranded piece of DNA (ssDNA) with two different DNA dyes (FAM and TAMRA) attached to either end of the DNA strand. When potassium ions ($K^+$) are present the ssDNA binds to the ions to form a specific 3D structure which brings to 2 dyes close together allowing a FRET pair to form and this is used to detect the binding of $K^+$ to the aptamer. The lower panel shows the graph of the response curves of the potassium aptamer under different testing conditions. The aptamer was tested in 5 mM Tris-HCl buffer at two different pH (7.0 and 7.4) and under two different temperatures (25°C and 37°C). For all experiments 0.2 µM aptamer was used n=3, the response taken 6 minutes post-induction. The red shaded area shows the concentration range of $K^+$ ions found in human sweat. The error bars show one standard error of the results.

All of the conditions tested showed a good response to $K^+$ ions as seen in **Figure 4.1**. Changing the pH of the buffer used to dilute the aptamer had the largest impact on the response. Using a lower pH resulted in the response of the aptamer being shifted upwards with high basal expression but also higher maximal fluorescence so did not alter the fold change. But as a lower basal fluorescence level is preferable pH 7.4 was used for the ongoing work as at this pH the buffer should prevent the lower pH of sweat from affecting the aptamer. The temperature did not strongly affect the response. At pH 7.4, 37°C reduced the sensitivity slightly but this was outside of the required

sensing range so would not be an issue in the use of the sensor for the wearable device.

Although the sensor is suitable for detecting potassium and capable of functioning in the conditions that it is likely to be subjected to when sensing sweat, the sensitivity of the aptamer did not cover the range of concentrations that potassium is present in sweat. Therefore, the aptamer needed to be optimised to respond over these concentrations. In order to do this the sensitivity of the aptamer needed to be reduced to allow for higher potassium concentrations to be detected.

### 4.2.2 Optimisation of sensor

Previous work in the literature has shown several methods for altering the sensitivity of the aptamer to potassium. One method is to alter the size of the loop between the G bases that form the g-quadruplex. It has been shown that increasing the size of the loop reduces the sensitivity of aptamer to potassium (Wu et al., 2016). This method was the best approach for the aptamer design used in this work because it had already been shown to work for potassium aptamers with a FRET pair. Another way to increase the size of the loop would be to use purine bases rather than pyrimidine bases due to their larger size.

New sequences of the potassium aptamer with more bases were designed to increase the number of bases between the GGG sequences which bind the $K^+$ ions. The Gs are the DNA bases involved in binding to K+ ions so were not altered, cytosine bases (C) were also not used because they would be able to pair with G which could disrupt the folding. These new sequences were then characterised to see if this altered the concentration ranges detected by the aptamer as shown in **Figure 4.2**.

(**a**)

| | |
|---|---|
| Original | GGTTAGGTTAGGTTAGG |
| MH079 | GGTTAAGGTTAAGGTTAAGG |
| MH080 | GGTTATGGTTATGGTTATGG |
| MH081 | GGTAAGGTAAGGTAAGG |

(**b**)

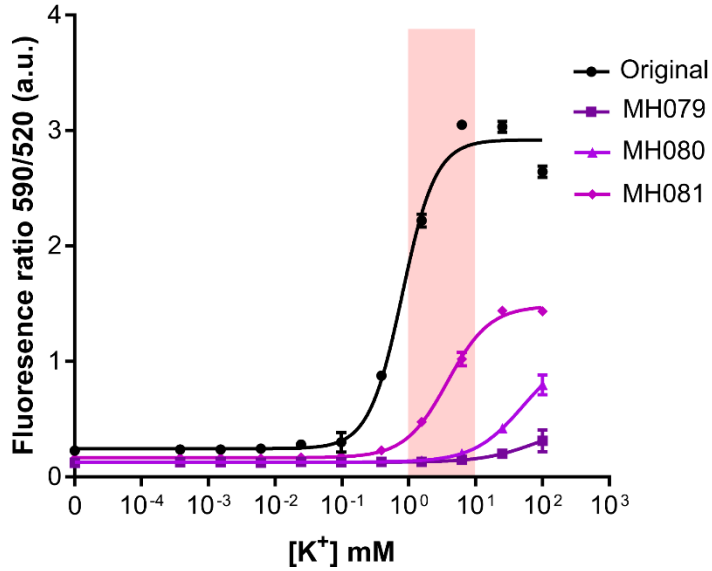


**Figure 4.2 Optimisation of the potassium aptamer sensitivity.** (**a**) gives the sequences of the original potassium aptamer tested and the mutant versions that were designed (MH079, MH080 and MH081). For the mutant versions the additional base or changed base are highlighted in red. (**b**) The graph shows the response curve of potassium aptamers containing the different sequences designed to alter the sensitivity of the potassium aptamer compared to the original sequence shown in black (Original $(GGGTTA)_3GG$). Initially an extra base was added between the series of Gs to increase the loop size (MH079 $(GGGTTAA)_3GG$) and MH080 $(GGGTTAT)_3GG$)). A third sequence was designed which kept the number of bases the same but altered the sequence of the bases and used purine bases which are larger (MH081 $(GGGTAA)_3GG$)). For the experiment n=3, aptamers diluted to 0.2 µM in 5 mM Tris-HCl pH 7.4 at 37°C. The response taken 6 minutes post-induction. The red shaded region highlights the concentration range of $K^+$ ions found in human eccrine sweat. The error bars show one standard error of the results.

All of the new sequences tested did reduce the sensitivity of the potassium aptamer as shown in **Figure 4.2,** with the new sequences shown in **Figure 4.2a**. Adding in an extra base, either an A or T reduced the sensitivity of the aptamer too much with the response occurring at higher concentrations of KCl than are found in human sweat. Altering the bases used to generate the loop to make it bigger reduced the sensitivity of aptamer less and resulted in

an aptamer that responds over the correct concentration range of KCl, shown in **Figure 4.2b**. However, this also resulted in a large decrease in the maximal output of the potassium aptamer which could potentially be an issue when using less sensitive equipment in the device. When the $K^+$ ions bind to the aptamer the folding can occur in more than one way. If the folding results in a parallel helix this will bring the two fluorescent dyes together to generate the FRET pair for detecting the result. Alternatively, the folding can result in an anti-parallel helix which means that the dyes are on opposite sides and the dyes are held away from each other so the FRET pair is not formed (Wu et al., 2016, Marchand and Gabelica, 2016), shown in **Figure 4.3**. This can occur when two $K^+$ ions bind into the g-quadruplex rather than one $K^+$ ion. Increasing the size of the loop makes this more likely to occur which could explain why the maximal fluorescence is reduced.

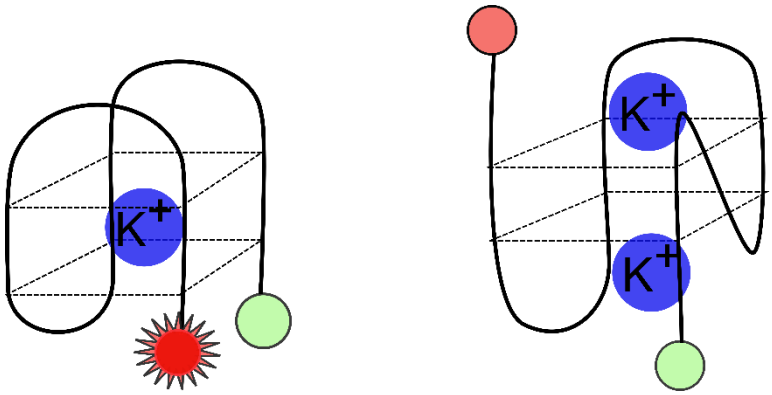


**Figure 4.3 Possible folding structures of the potassium aptamer.** The left folding structure is the desired structure which results in the two fluorescent dyes brought together to form a FRET pair. On the right shows an alternative folding structure which fits two potassium ions which can occur when using the aptamer and would prevent the FRET pair formation. Figure adapted from (Wu et al., 2016, Marchand and Gabelica, 2016).

### 4.2.3 Orthogonality testing of sensor

Although the desired sensing range had been achieved, there are many other positive ions found in human sweat which have the potential to non-specifically bind to the optimised aptamer MH081, shown in **Figure 4.2.** The sequence changes could in addition to sensitivity impact its specificity.

Sodium, magnesium and calcium ions are found in varying concentrations in human sweat, so these ions were tested against the aptamer using the concentrations found in human sweat. The aptamer was then also tested with a high concentration of potassium in combination with the other ions to ensure they did not prevent the response to potassium, shown in **Figure 4.4**.

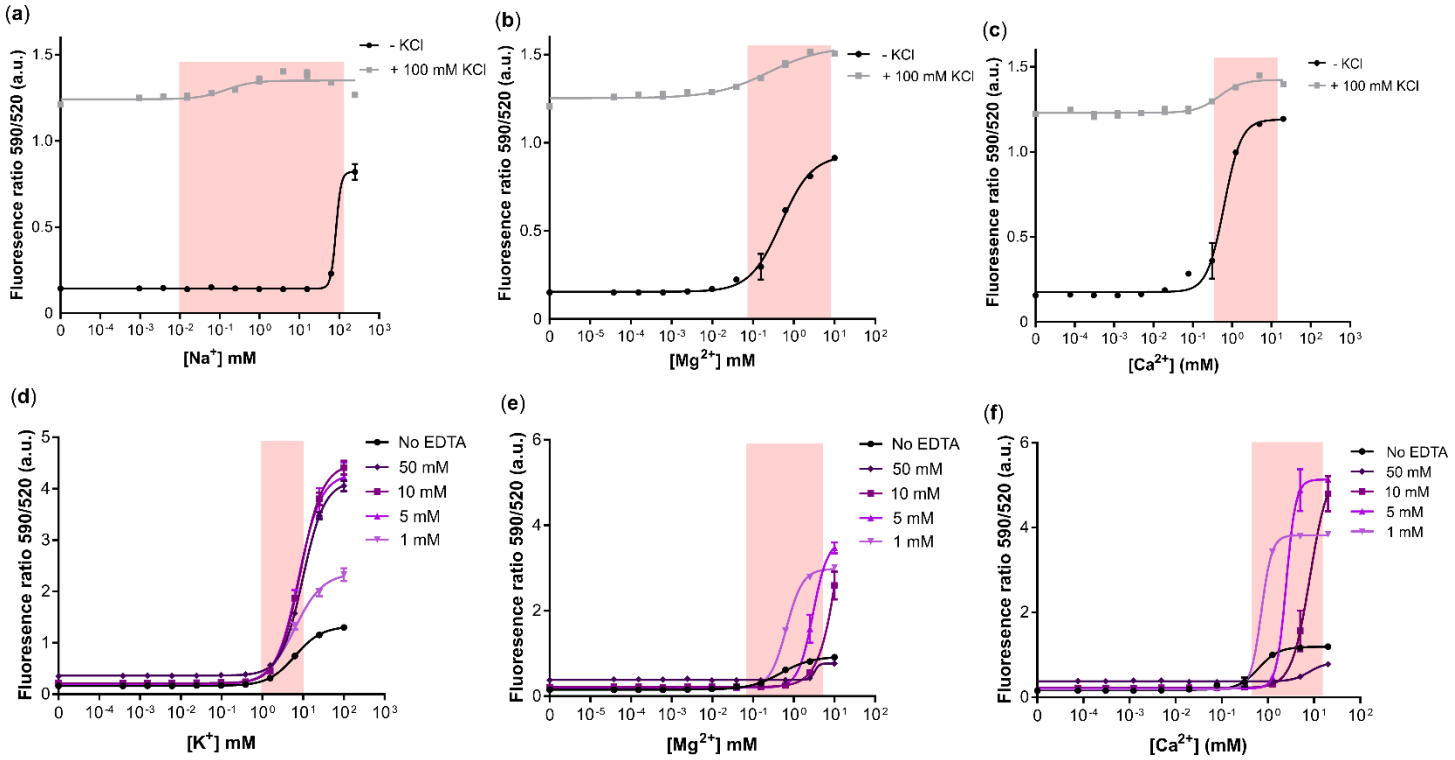


**Figure 4.4 Characterisation and optimisation of the potassium aptamer specificity.** The potassium aptamer was tested with other cations found in human sweat to see if the potassium aptamer response would be affected by these ions either through preventing the aptamer from responding to potassium or by generating a response itself. (**a**) shows the response of the potassium aptamer to sodium ions ($Na^+$) without potassium ions (- KCl, black line) and with the maximum concentration of potassium previously tested (+ 100 mM KCl, grey line). (**b**) shows the response of the potassium aptamer to magnesium ions ($Mg^{2+}$) without potassium ions (- KCl, black line) and with potassium ions (+ 100 mM KCl, grey line). (**c**) shows the response of the potassium aptamer to calcium ions ($Ca^{2+}$) without potassium ions (- KCl, black line) and with potassium ions (+ 100 mM KCl, grey line). (**d**) shows the response of the potassium aptamer when increasing concentrations of EDTA dissolved in Tris buffer were used as the buffer compared to 5 mM Tris-HCl pH 7.4 (No EDTA). (**e**) shows the response of the potassium aptamer to magnesium ions ($Mg^{2+}$) with increasing concentrations of EDTA present in the buffer compared to the response of the aptamer to $Mg^{2+}$ with no potassium ions present and the original buffer (No EDTA). (**f**) shows the response of the potassium aptamer to calcium ions ($Ca^{2+}$) with increasing concentrations of EDTA in the buffer compared to the response of the potassium ion to $Ca^{2+}$ with no potassium ions present (No EDTA). For all experiments

the aptamer was diluted to 0.2 µM, for 1 mM and 5 mM EDTA, the concentration of Tris used to dissolve the EDTA was 5 mM whilst for 10 mM and 50 mM EDTA the tris concentration required to dissolve the EDTA was higher. The experiment was carried out at 37°C, n=3 with the response taken 12 minutes post-induction. The red shaded area in all graphs show the concentration range for each ion found in human sweat. The error bars show one standard error.

For all the different ions tested none of the off-target ions prevented the response to potassium shown in **Figure 4.4a-c** by the grey line. However, the aptamer also responded to the non-target ions. For sodium the aptamer response happens at concentrations higher than are found in sweat, shown by the black line in **Figure 4.4a**, so it is unlikely to be an issue when using the aptamer as a $K^+$ sensor. For both magnesium and calcium ions the response from the aptamer occurs over the physiological concentration ranges in human sweat, shown by the increase in the black line through the red shaded areas in **Figure 4.4b and c**. This would be an issue when using the aptamer within the final sensor device, as these divalent cations would also be present and affect the reliability of the response. Currently magnesium and calcium ions are not of interest for detection, therefore removing these ions to prevent the interaction could be used to stop this undesired response. As a result, the buffer used to characterise the aptamer was altered to include EDTA which would chelate the divalent ions and prevent the aptamer from responding to the off-target ions. Initially to check this approach the potassium aptamer was tested with different concentrations of EDTA as shown in **Figure 4.4d**. Adding EDTA free acid dissolved in Tris to the buffer amplified the response of the potassium aptamer to KCl. The cause of the amplification is unclear but the pH has been shown to be important in how much fluorescence can be detected from the dyes so this could play a role (Gracie et al., 2014) and using the higher concentration of EDTA would alter the pH. This amplification would also improve the detection ability of the potassium aptamer when in the wearable device so was not an issue. This shows chelating the 2+ ions from the sweat entering the device will work to stop the off-target response. The response of the aptamer to magnesium and calcium ions with different concentrations of EDTA was then tested to see if this would prevent the aptamer from responding to these ions,

shown in **Figure 4.4e and f**. For magnesium either 10 mM or 50 mM was enough to chelate out the ions and prevent the off-target response at physiological concentration ranges in sweat, seen by the increase in the lines occurring outside of the red shaded area in **Figure 4.4e**. For calcium a higher concentration of EDTA was required to prevent the off-target response, only the 50 mM EDTA was able to prevent the response in the physiological concentration ranges shown by the dark purple line in **Figure 4.4f**. For all future work 50 mM EDTA dissolved in Tris will be used as the buffer.

## 4.3 cpGFP protein sensors

Another method that can be used in generating biosensors that use a conformational change to generate the response is by creating engineered proteins that contain a circular permuted fluorescent protein within a binding protein responsive to the molecule of interest. When the molecule of interest binds to the protein the conformational change that occurs also causes the circular permuted fluorescent protein to change conformation, which results in an ability to generate fluorescence that can be detected. In order to generate sensors of this type a binding protein for the molecule of interest needs to be identified as do sites within the protein structure where the circularly permuted fluorescent protein can be inserted and to allow it to function as a sensor. To find such insertion site regions which have large changes the dihedral angles of the bound and unbound structure of the protein can be analysed to identify regions which will allow the conformation change to be transferred to circularly permuted GFP (cpGFP) for response detection. The maturation of circularly permuted fluorescent proteins has been shown to be much slower than that of the unpermuted fluorescent protein but is not dependent on the protein which it has been inserted into (Kostyuk et al., 2019, Kroning et al., 2021) so the response is dependent on the conformational change which could allow for multiple measurements. This method is shown in **Figure 4.5** (Marvin et al., 2011, Zhang et al., 2021b) and is explained in section 1.1.2.1 in the introduction in more detail.

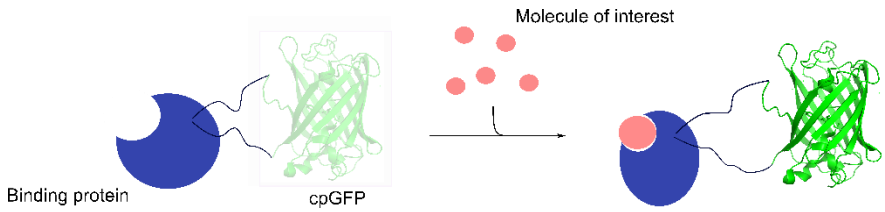


**Figure 4.5 Circularly permuted GFP (cpGFP) sensing mechanism.** The figure shows the method of response generation in cpGFP binding protein-based sensors. When none of the molecule of interest is present the binding protein is in the unbound conformation, which means that the linkers pull the cpGFP out of the GFP conformation preventing fluorescence. When the molecule of interest is present the binding protein changes to the bound conformation. This change is then transferred to the cpGFP through the linker to pull it into the proper conformation to allow fluorescence once the fluorophore has matured, which occurs at a slower rate than in unpermuted fluorescent protein but independent of the conformational state of the binding protein (Zhang et al., 2021b, Marvin et al., 2011, Kroning et al., 2021, Kostyuk et al., 2019).

Three different biomarkers were chosen to study this approach. histamine, cortisol and testosterone. The work into developing whole cell biosensors for cortisol and testosterone in Chapter 3 showed that entry of steroid hormones into the cell could be an issue for the cortisol and testosterone monitoring. None of the work carried out so far in the project had looked to generate a histamine biosensor but it also would provide useful information on an individual's physiological state, as outlined in **Table 1.2** in the introduction.

Currently in the literature the biosensors produced to detect these biomarkers all use mammalian proteins or cells, or use electrochemical sensors with antibodies, both of which limits the use of these biosensors in the field. Mammalian cells and proteins require more specific conditions and are not well suited to storage methods such as freeze drying, which is frequently employed when developing biosensors (Zhang et al., 2017a). Antibodies more recently have been shown to have large variability between batches and can often also bind to other targets not just the biomarker of interest, both of which would be significant problems in developing biosensors (Baker, 2015).

### 4.3.1 Identifying insertion points

A binding protein from ticks known as AM10 which is a lipocalin (a group of proteins that bind to molecules that play a role in the immune response to prevent the immune signalling) with suitable sites to insert the cpGFP for histamine had already been identified in the literature, but had not been tested (Zhang et al., 2021b). The approach used in the literature to identify the insertion sites was also used for cortisol and testosterone. The approach compares the dihedral angles between amino acids in bound and unbound state to identify where large conformational changes occur. Avidin mutants with altered specificity to steroid hormones (Lehtonen et al., 2016) were chosen as the binding protein because the avidin proteins will be able to be produced by *E. coli* cells or cell-free lysate. Avidin is also a well-studied protein with detailed structures available that allow for rational prediction of insertion sites. Although the structures studied are not those of the mutants, only a few point mutations were made to alter the specificity, the change in the structure for the unbound state should be small but this could be larger in the bound state. However the approach above would still give a starting point of regions to explore. The analysis was carried out using a program called Bio3d using R (Grant et al., 2006). The graph of the conformational changes is shown **Figure 4.6**.

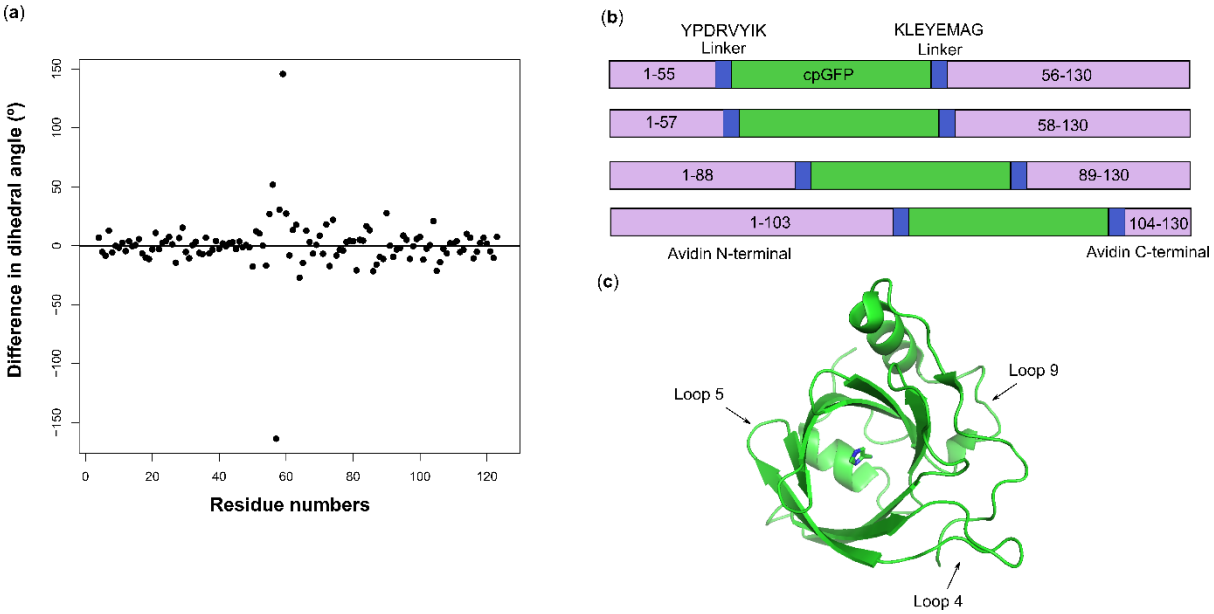


**Figure 4.6 Change in dihedral angles within avidin amino acid sequence.** (**a**) The graph shows the change in the dihedral angle between adjacent amino acids of the unbound and bound structures of avidin. Using 1RAV (10.2210/pdb1RAV/pdb (Nardone et al., 1998)) and 1AVD (10.2210/pdb1AVD/pdb (Pugliese et al., 1993)). (**b**) shows the final linear design of the four versions which would be used for the avidin based sensors. The amino acid sequence of each linker is given as well as the number of amino acids present in the N and C-terminals of the avidin either side of the cpGFP insertion. (**c**) shows the crystal structure of AM10 with the three loops where cpGFP was inserted which are shown by arrows, adapted from (Zhang et al., 2021b).

**Figure 4.6a** shows that there are a few regions where the conformational change occurs within the protein. The four largest changes in angle were chosen from the accompanying data table produced by the Bio3d programme (given in **Appendix 2**) (Grant et al., 2006). From this the different versions of the sensors for cortisol and testosterone were designed to incorporate the circularly permuted fluorescent protein with a linker sequence after the identified amino acid residue that had been selected from the literature as an optimal sequence (Zhang et al., 2021b), The four versions each designed for cortisol and testosterone are shown in **Figure 4.6b**. The three versions that had been suggested for the histamine sensor were also constructed (Zhang et al., 2021b), and the regions of insertion are shown in **Figure 4.6c**.

### 4.3.2 Initial characterisation

Once these different versions had been constructed an initial test to determine which versions of the sensors were functional in cell-free was carried out, shown in **Figure 4. 7**. For the initial test the plasmid was combined with the cell-free transcription translation system. Once loaded into a microplate the inducer was added immediately and the reaction was incubated at 37°C. For all the proteins there appeared to be insertion sites suitable to generate a sensor.

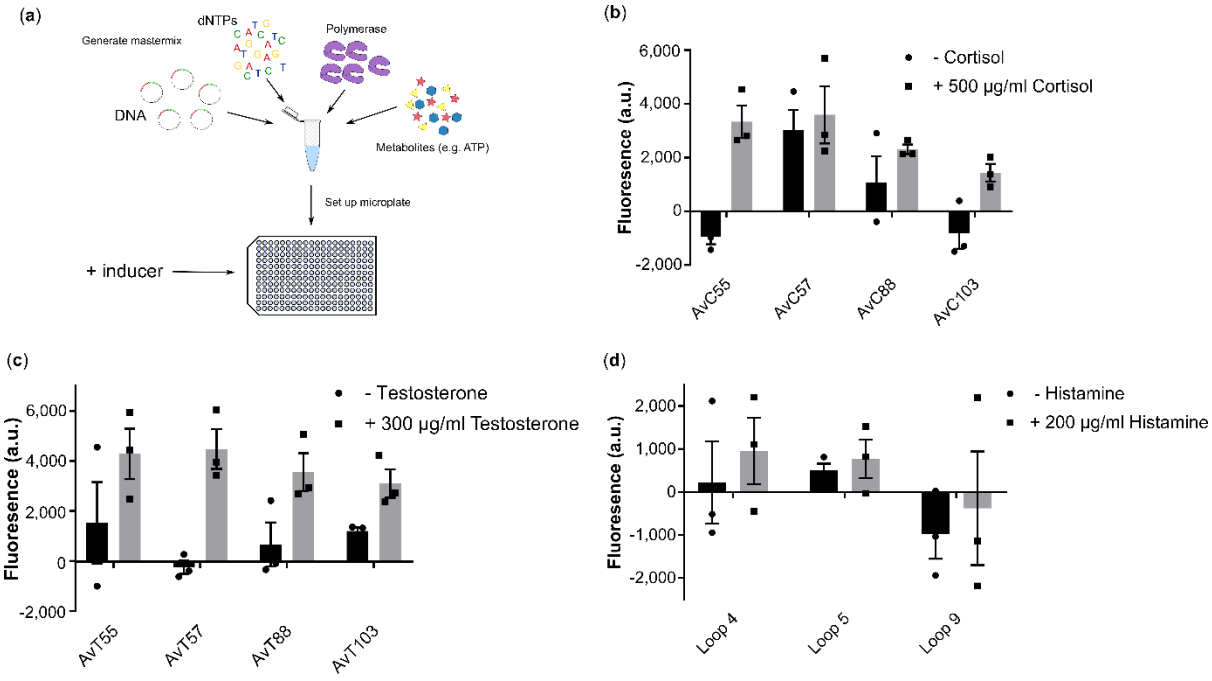


**Figure 4.7 Identification of functional cpGFP sensors for cortisol, testosterone and histamine.** (**a**) shows how the cell-free reactions were set up by generating a mastermix for each reaction which was then transferred to a microplate and induced immediately. The graphs show the change in fluorescence between uninduced and induced cell-free reactions of the possible biosensors with cpGFP inserted at different positions within the binding proteins. (**b**) shows the change in on (+ 500 µg/ml Cortisol, grey bars) and off (-Cortisol, black bars) fluorescence for the potential cortisol sensors. (**c**) shows the change in fluorescence of the on (+ 300 µg/ml Testosterone, grey bars) and off (-Testosterone, black bars) states of the potential testosterone sensors. (**d**) shows the change in the on (+ 200 µg/ml Histamine, grey bars) and off (- Histamine, black bars) fluorescence of the potential histamine sensors identified from the literature. For all n=3 and the cell-free reactions were incubated at 37°C. The response was taken 2 hours post induction for (**a**) and (**b**) whilst for (**c**) the response was taken 8 hours post induction. The error bars show one standard error.

**Figure 4.7** shows that for all the cpGFP biosensors being explored that there was a suitable insertion site into the binding protein. In **Figure 4.7b** the change in fluorescence for the cortisol binding protein with the cpGFP inserted after the 55$^{th}$ amino acid was statistically significant with a p-value of 0.0124 and after the 88$^{th}$ amino acid was not statistically significant, but had the second largest fold change of 2.1 after the one with insertion at the 55th amino acid. **Figure 4.7c** shows that the change in fluorescence for the testosterone binding protein with insertion of the cpGFP after 57$^{th}$ amino acid was statistically significant with a p-value of 0.0193 and after the 88$^{th}$ amino acid had the second largest fold change of 5.4 after the insertion at 57th amino acid. For histamine, insertion of cpGFP into loop 4 or loop 5 of the AM10 protein had the largest fold change in fluorescence with loop 4 insertion having a fold change of 4.4 and loop 5 had a fold change of 1.5, although no statistically significant result between induced and uninduced was seen. These two versions will be carried forward to see if optimisation approaches could improve the response, shown in **Figure 4.7d**.

### 4.3.3 Optimisation

Following the initial characterisation and identification of functional versions for the sensors, different DNA concentrations of the plasmid containing the genetic sequence of the sensor were added to the cell-free reaction because the concentration of the plasmid DNA would have an effect on the final protein concentration present in the cell-free reaction. Using mathematical modelling to study how the change in protein concentration would alter the response showed that reduced protein concentration appeared to increase sensitivity but reduced the output. Therefore this could be used to ensure that the sensors respond at the required range. The calculations used are shown in **Appendix 2.** The graphs obtained from modelling are shown in **Figure 4.8a.** The impact on the sensors of the different DNA concentrations is shown in **Figures 4.8 b - d**.

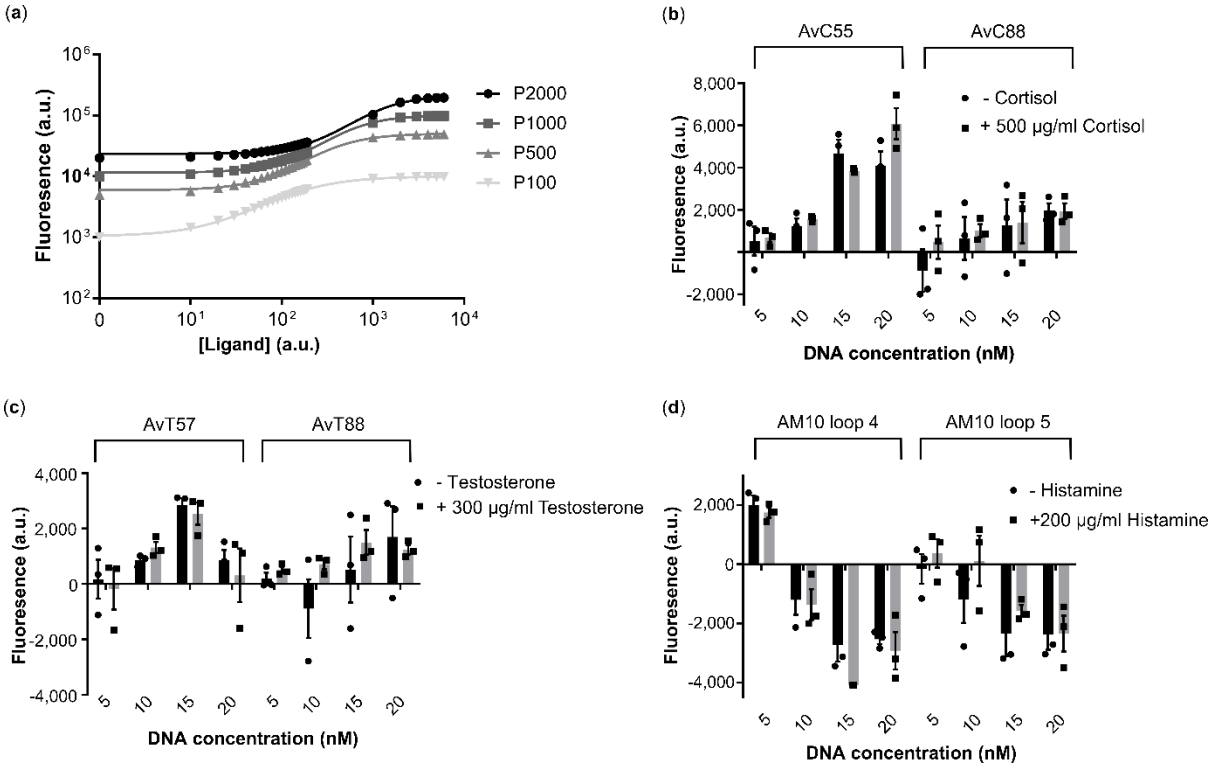


**Figure 4.8 Optimisation of DNA concentration for cell-free reactions**. (**a**) shows the response curves of simulated response for a binding protein cpGFP biosensor when different amounts of protein were present. (**b**) shows the change in fluorescence without cortisol (- Cortisol, shown by the black bars) and with 500 µg/ml cortisol (+ 500 µg/ml Cortisol shown by the grey bars) at four different DNA concentrations for both the AvC55 and AvC88 versions of the cpGFP cortisol sensor.(**c**) shows the change in fluorescence without testosterone (- Testosterone, shown by the black bars) and with 300 µg/ml cortisol (+ 300 µg/ml Testosterone shown by the grey bar) at four different DNA concentrations for both the AvT57 and AvT88 versions of the cpGFP testosterone sensor. (**d**) shows the change in fluorescence without histamine (- Histamine, shown by the black bars) and with 200 µg/ml histamine (+ 200 µg/ml Histamine shown by the grey bars) at four different DNA concentrations for the versions of the histamine sensors with cpGFP inserted at loop 4 and loop 5 of the protein. For all the sensors n=3, the cell-free reactions were incubated at 37°C. The response was taken 2 hours post-induction for (**b**) and (**c**) and 4 hours post-induction for (**d**). The error bars show one standard error of the results.

None of the results showed any statistical significance but the presence of less protein in the system appears to improve the sensitivity of the biosensors when simulating the response. This suggested that using the lower concentration of the plasmid would be better, as shown in **Figure 4.8a.** Comparing the 5 nM results for the two insertion sites in for the cortisol sensors shown in **Figure 4.8b** suggests that AvC88 would be better because the basal fluorescence is much lower. For the testosterone sensors shown in

**Figure 4.8c** AvT88 appears to be better because when testosterone was added no fluorescence was seen for AvT57. For the histamine sensor in **Figure 4.8d** the insertion into loop 5 resulted in a much higher fold change whilst for loop 4 there was a decrease in fluorescence when histamine was added.

Following this the sensors were then characterised to determine the response to different concentrations of the biomarker to begin to determine the sensitivity of the sensors, shown in **Figure 4.9**. At this point a pre-incubation step before induction with the biomarker was also added to the experiment to see if this would reduce the time for the response to be generated by the protein being expressed before the inducer is added. This workflow is shown in **Figure 4.9a**. Previous work has shown this reduced the time for the response to be detected (Pandi et al., 2019).

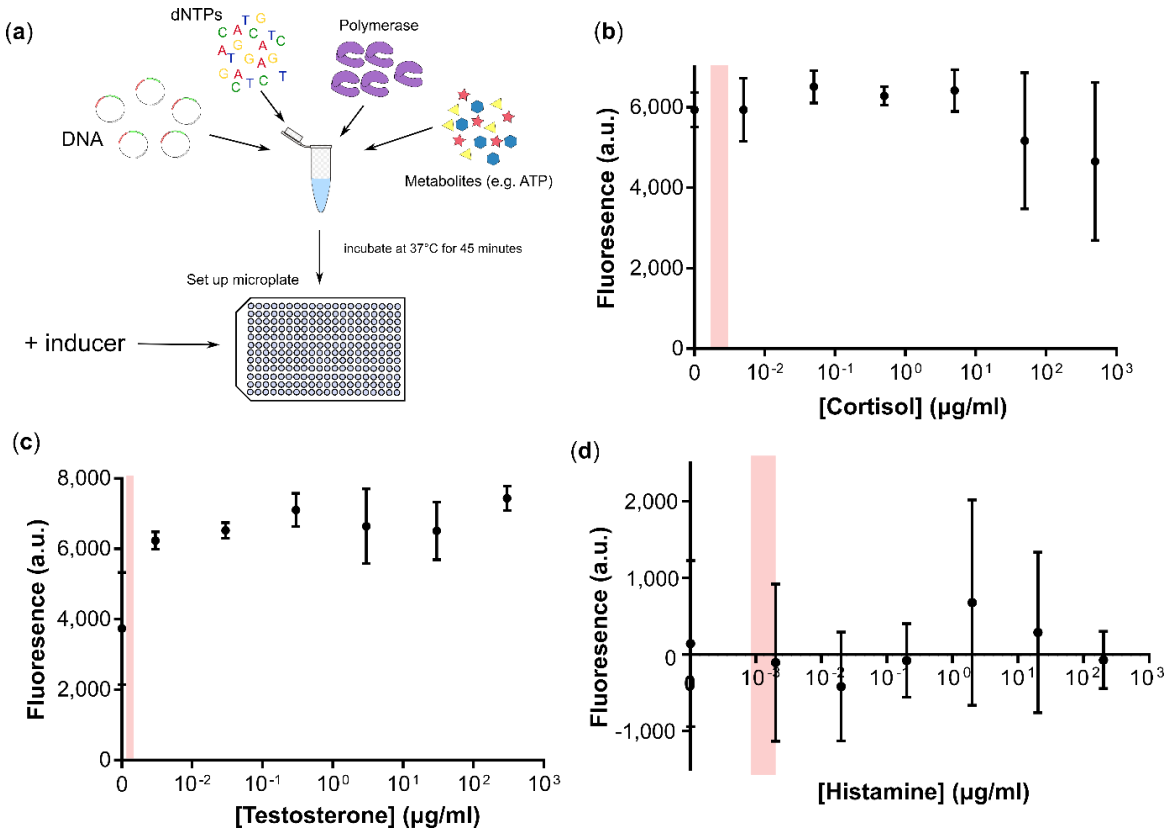


**Figure 4.9 Characterisation of cpGFP sensors response to biomarkers.** (**a**) shows the new approach for the set up of the experiment where all components of the cell-free reaction are added and then incubated for 45 minutes at 37°C before addition to the microplate, at which point the reaction was induced with the molecule of interest. The fluorescence would then be measured to detect the

response. (**b**) shows the response of AvC88 to different cortisol concentrations. (**c**) shows the response of AvT88 to different concentrations of testosterone. (**d**) shows the response of the AM10 loop 5 sensor to different concentrations of histamine. For all sensors n=3. For all curves the response was taken 4 hours post-induction. The error bars show one standard error.

For all of the sensors in **Figure 4.9** the response to the inducer was not strong, with only the testosterone sensor, shown in **Figure 4.9c**, appearing to have a response in the desired concentration range. Carrying out a t-test comparing the uninduced and maximum response for the testosterone gave a p-value of 0.0858 (to 3 significant figures), so the results are significant at a 90% test level. No statistical significance between the uninduced and maximal response was seen for cortisol and histamine. To improve the response across all sensors, the next step in the optimisation of the biosensors is to alter the linker sequence. The linker sequence has a large impact on the ability of the conformational change to be transferred from binding protein to the cpGFP (Kostyuk et al., 2019). So, random mutagenesis of the linker sequence was carried out for the version of the biosensor which as a result of the work on optimisation already carried out appeared to have the strongest response, and this is shown in **Figure 4.10.**

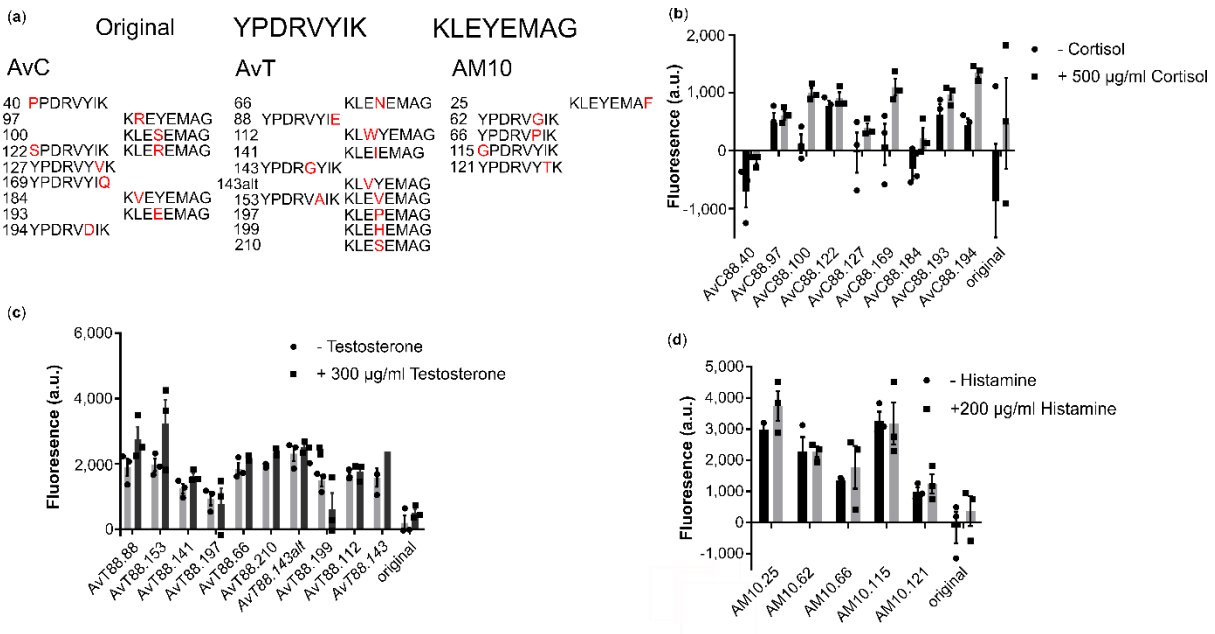


**Figure 4.10 Characterisation of cpGFP sensor mutants.** (**a**) shows the original linker amino acid sequences and the mutations that were identified for each sensor and tested. The specific mutations are highlighted in red. The graphs show the difference between on and off fluorescence of cpGFP

sensors with random mutations made to the linker sequences between the binding protein and cpGFP. (**b**) shows the response of mutants made to AvC88 cortisol sensors without cortisol (- Cortisol, black bars) or with cortisol (+500 µg/ml Cortisol, grey bars) compared to the original sensor. (**c**) shows the response of mutants made of the AvT88 testosterone sensor without testosterone (- Testosterone, black bars) or with testosterone (+300 µg/ml Testosterone, grey bars) compared to the original sensor. (**d**) shows the response of AM10 loop 5 histamine sensor mutants without histamine (- Histamine, black bars) or with histamine (+ 200 µg/ml Histamine, grey bars) compared to the original sensor. For all sensors n=3, the cell-free reaction was incubated for 45 minutes at 37°C before induction, post-induction the reactions were incubated at 37°C. The response was taken 30 minutes post-induction for (**b**) and (**c**) and 2 hours post-induction for (d). The error bars show one standard error of the results.

**Figure 4.10** shows the on and off fluorescence for the mutant versions of the sensors. The possible mutants were sequenced before characterisation to ensure that each possible mutant was tested only once in the cell-free and then numbered after the colony number they were identified from. For the cortisol sensor three mutant versions were identified that appeared to have a better response to cortisol than the original version, shown in **Figure 4.10b**. These three versions AvC88.100, AvC88.169 and AvC88.194 will be characterised to see if this improves the response to cortisol. AvC88.100 and AvC88.194 showed a significant difference between the on and off states with p-values of 0.0748 and 0.0290 respectively whilst AvC88.169 had the largest fold change of 10, so these three versions were selected to continue with optimisation. Both **Figure 4.10c and d** show that no mutants for the testosterone and histamine sensors resulted in an improved response, so other approaches to optimisation will be studied. The testosterone mutant AvT88.210 showed a statistically significant change between the on and off but the fold change was lower so it does not suggest an improved response, whilst for the histamine mutants sensor none of the responses showed a statistical significance.

These new versions of the avidin cortisol sensors were then tested for their response to different cortisol levels to see if they gave an improved response across concentrations, shown in **Figure 4.11**.

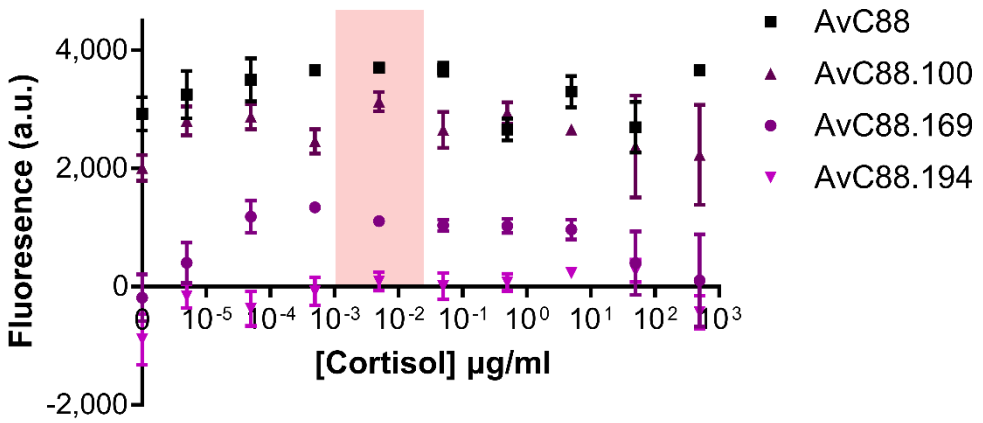


**Figure 4.11 Characterisation of the response of the avidin mutants to different cortisol concentrations.** The graph shows the change in fluorescence of the AvC88 sensors to different cortisol concentrations. The previously identified mutants that had shown an improved response to cortisol were tested and compared to the original sensor's response (black square symbols). The red shaded region highlights the concentrations found in human eccrine sweat. For all the sensors n=3, the cell-free reactions to generate the cortisol sensors were incubated for 45 minutes at 37°C before induction with cortisol, post-induction the reactions continued to be incubated at 37°C. The response was taken 2 hours post-induction. The error bars show one standard error of the results.

The mutants AvC88.100 and AvC88.169 showed a high sensitivity to cortisol, seen in **Figure 4.11,** with an increase seen at the pg/ml to ng/ml concentrations compared to no cortisol added. However, at higher concentrations there is a negative effect on the fluorescence which appears to occur over the desired concentration range, so the sensitivity needs to be adjusted to prevent this. Currently the AvC88.194 did not appear to respond to cortisol.

The cortisol sensors were still not able to detect over the required concentrations and mutants for the testosterone and histamine sensors that would potentially have a better response had not been found. So alternative forms of optimisation needed to be carried out. The next step was to test alternative methods of pre-incubation of the cell-free reaction before induction to produce the sensing protein within the cell-free reaction, shown in **Figure 4.12**.

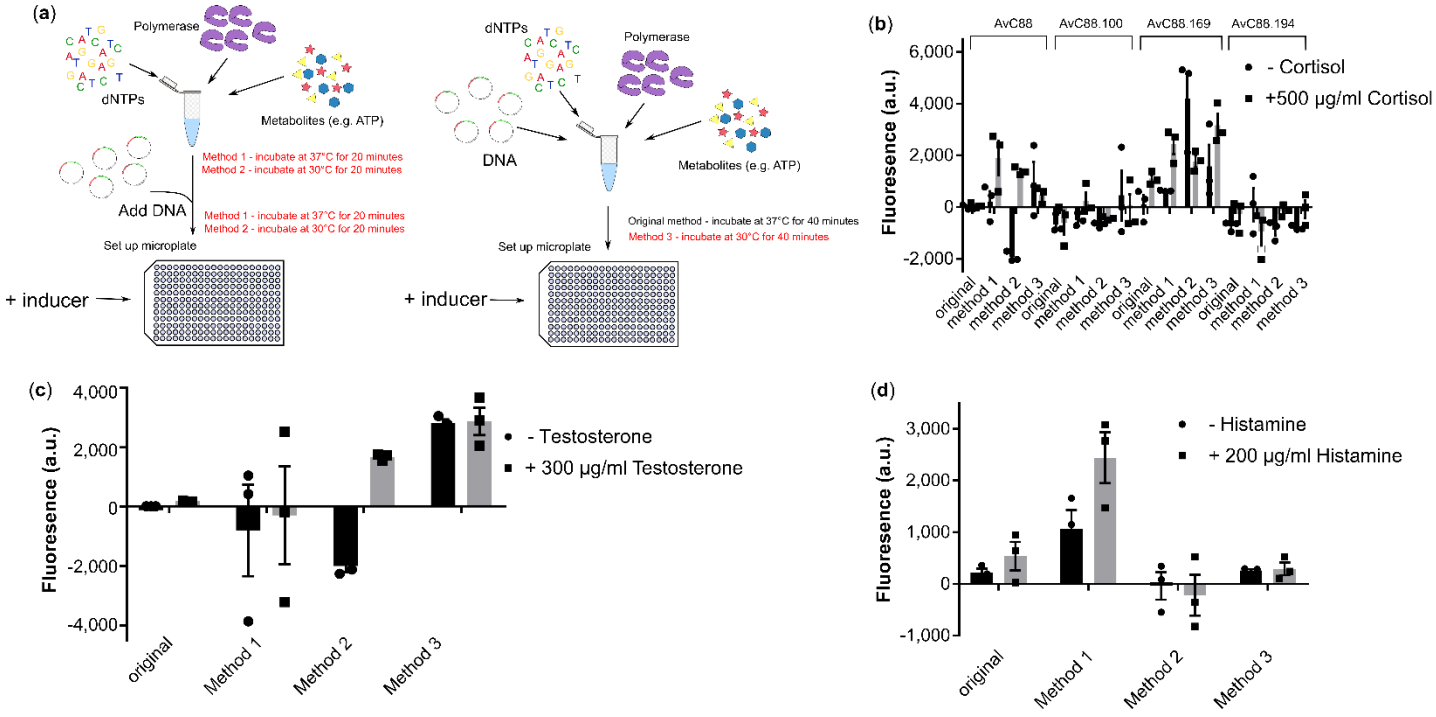


**Figure 4.12 Testing alternative pre-incubation methods to improve the response of cell-free cpGFP sensors.** The graphs show the change in fluorescence between the on and off states of the cpGFP sensors when different pre-incubation methods were used. (**a**) Three different methods were tested. For method 1 the cell-free reactions were incubated for 20 minutes at 37°C without the DNA added, following this the DNA was added and the reaction was incubated for a further 20 minutes before induction. For method 2 the cell-free reaction was set up with all components including the DNA and incubated at 30°C for 40 minutes. Method 3 was carried out in the same manner as method 1 but with all of the incubation carried out at 30°C. (**b**) shows the fluorescence detected for all of the AvC88 versions identified without cortisol (- Cortisol, black bars) and with cortisol (+ 500 µg/ml Cortisol, grey bars) when the different pre-incubation methods are used compared to the original set up method. (**c**) shows the change in fluorescence without testosterone (- Testosterone, black bars) and with (+ 300 µg/ml Testosterone, grey bars) when the different pre-incubation methods are used compared to the original method for the AvT88 sensor. (**d**) shows the change in fluorescence without histamine (- Histamine, black bars) and with (+ 200 µg/ml Histamine, grey bars) of the AM10 loop 5 sensor when the different pre-incubation methods were used. For all sensors n=3 and the cell-free reactions were incubated at 37°C post-induction. For (**b**) the response was taken 1 hour post-induction and for (**c**) and (**d**) the response was taken 2 hours post-induction. The error bars show one standard error of the results.

Altering the pre-incubation step for all of the different cpGFP sensors which had shown a response so far did improve the response, as shown in **Figure 4.12**. For the cortisol sensors and histamine sensor shown in **Figure 4.12b**

**and d,** method 1 where the reaction is incubated without DNA for 20 minutes before adding the DNA and incubating for a further 20 minutes all at 37°C gave the most improvement to the response except for the mutant number 194 (AvC88.194) which worked best with method 3 which used the same approach but at 30°C. For AvC88 and AvC88.169 a clear increase in the maximal output can be seen for this method compared to the original approach whilst for AvC88.100 and AvC88.194 a change in the output is much less clear. For the testosterone sensor shown in **Figure 4.12c** the best method for pre-incubation was at 30°C. Potentially because this lower temperature improves the production and folding of the protein due to the reduced speed of translation which is suggested within the manufacturer's protocol (https://www.promega.co.uk/-/media/files/resources/protocols/technical-bulletins/0/e-coli-s30-extract-system-for-circular-dna-protocol.pdf?la=en). Incubating the reaction without the DNA for the sensor added could allow any incomplete translation to be completed, free the ribosomes and readying the lysate for the production of the sensor protein which has be shown to be crucial to allow expression of proteins from native promoters (Silverman et al., 2019). This is usually carried out in lysate production but a short extra amount of time could make more ribosomes available, as the 20 minute incubation without the plasmid DNA did show an improved response. **Table 4.1** summarises the incubation method that would be used for the future work for each sensor.

**Table 4.1: The table summarises the optimised pre-incubation methods that were used for each sensor in the remaining work.**

| Sensor | Pre-incubation method |
|---|---|
| AvC88 | Method 1: the cell-free reactions were incubated for 20 minutes at 37°C without the DNA added, following this the DNA was added and the reaction was incubated for a further 20 minutes before induction |
| AvC88.100 | Method 1: the cell-free reactions were incubated for 20 minutes at 37°C without the DNA added, following this |

| Sensor | Pre-incubation method |
|---|---|
| | the DNA was added and the reaction was incubated for a further 20 minutes before induction |
| AvC88.169 | Method 1: the cell-free reactions were incubated for 20 minutes at 37°C without the DNA added, following this the DNA was added and the reaction was incubated for a further 20 minutes before induction |
| AvC88.194 | Method 3: the cell-free reactions were incubated for 20 minutes at 30°C without the DNA added, following this the DNA was added and the reaction was incubated for a further 20 minutes again at 30°C before induction |
| AvT88 | Method 2: the cell-free reaction was set up with all components including the DNA and incubated at 30°C for 40 minutes. |
| AM10 loop 5 | Method 1: the cell-free reactions were incubated for 20 minutes at 37°C without the DNA added, following this the DNA was added and the reaction was incubated for a further 20 minutes before induction |

Following this determination of the best method for pre-incubation the response curves were characterised again to see if the optimised pre-incubation would improve the response and help to move the response towards the required range, shown in **Figure 4.13**.

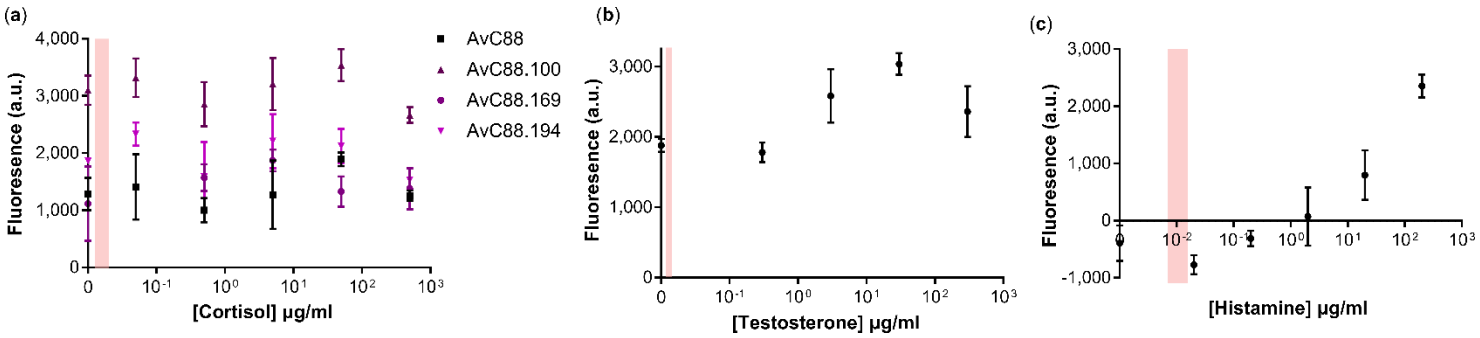


**Figure 4.13 Characterisation of the cpGFP sensor response to different concentrations of biomarker using the optimised pre-incubation method.** (**a**) shows the response of the AvC88

cpGFP sensor and mutant versions when the reaction was set up with the optimised pre-incubation step to different concentrations of cortisol. (**b**) shows the response of AvT88 to different concentrations of testosterone when using the optimised pre-incubation method. (**c**) shows the response of AM10 loop 5 sensors to different concentrations of histamine using the optimised pre-incubation step. For all sensors n=3 and the cell-free reaction was incubated at 37°C post-induction. The red shaded area shows the concentration range found in human eccrine sweat. For all the graphs the response was taken 2 hours post-induction. The error bars show one standard error of the results.

Altering the pre-incubation method did not appear to improve the response for the cortisol sensors as no clear response could be seen for any of the versions shown in **Figure 4.13a**. However, for both the testosterone and histamine sensors a response to the different concentrations of the biomarker is seen, shown in **Figure 4.13b and c**. For the testosterone sensor the sensitivity appeared to be lost compared to previous tests, as seen in **Figure 4.13b.** However, when compared to **Figure 4.9c** the error bars appeared to be reduced suggesting that pre-incubation at 30°C could be better for the testosterone sensor, but further work to improve sensitivity would be required. For the histamine sensor no response had previously been detected from the sensors shown in **Figure 4.9d** but with the new pre-incubation method a strong response could be detected as seen in **Figure 4.13c,** although further optimisation is required to improve the sensitivity.

Commercial cell-free lysate is highly expensive to purchase which would not be viable for commercial production of a wearable device where large volumes of the lysate are likely to be required. Having shown that the sensors work, they were then tested in homemade cell-free lysate to compare their function because homemade cell-free lysate would allow commercial scaling up where larger volumes would be used. The result of the of the comparison is shown in **Figure 4.14**.

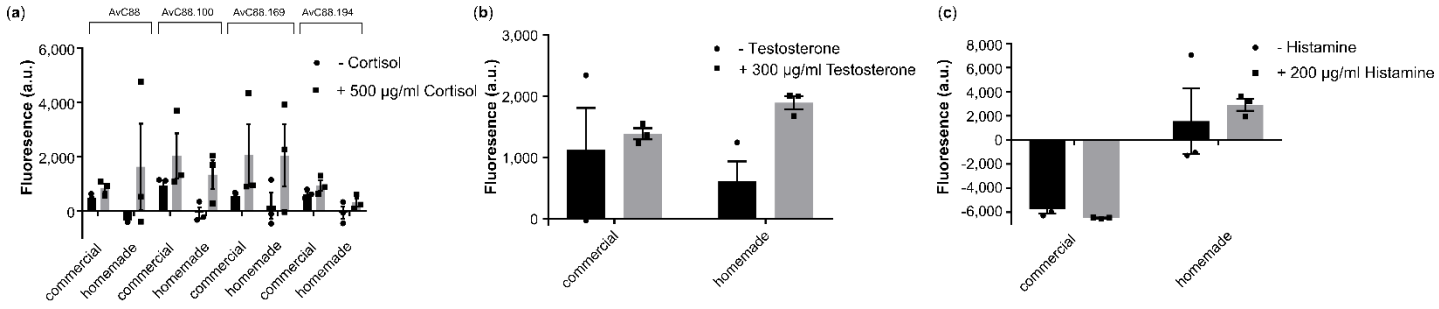


**Figure 4.14 Comparison of cpGFP sensor response in commercial and homemade cell lysate.** (**a**) shows the change in fluorescence without cortisol (- Cortisol, black bars) and with (+ 500 µg/ml Cortisol, grey bars) for the four versions of the AvC88 sensors in both homemade and commercial lysate. (**b**) shows the change in fluorescence of the AvT88 sensor without testosterone (- Testosterone, black bars) and with (+ 300 µg/ml Testosterone, grey bars). (**c**) shows the change in fluorescence of the AM10 loop 5 sensors without histamine (- Histamine, black bars) and with (+ 200 µg/ml Histamine, grey bars). For all sensors n=3 and the cell-free reactions were incubated at 37°C post-induction. For (**a**) and (**b**) the response was taken 1 hour post-induction and for (**c**) the response was taken 6 hours post-induction. The error bars show one standard error of the results.

All of the sensors tested in homemade cell lysate retained their function or saw an improvement between the on and off state, as shown in **Figure 4.14**. For the cortisol sensors in **Figure 4.14a** the basal expression was reduced which improves the dynamic range of the sensor, although the on state had very large error bars. For the testosterone sensor the basal and maximal outputs were both improved, as seen in **Figure 4.14b**. For the histamine sensor in the comparison test no response was seen for the commercial lysate shown in **Figure 4.14c** but the response was detectable in the homemade lysate. This comparison test suggests that homemade lysate is suitable for all the sensors and will be used going forward.

The next step was to see if changing to a new homemade lysate had an effect on the response of the sensors and could improve the sensitivity to their biomarker. The response curves are shown in **Figure 4.15**.

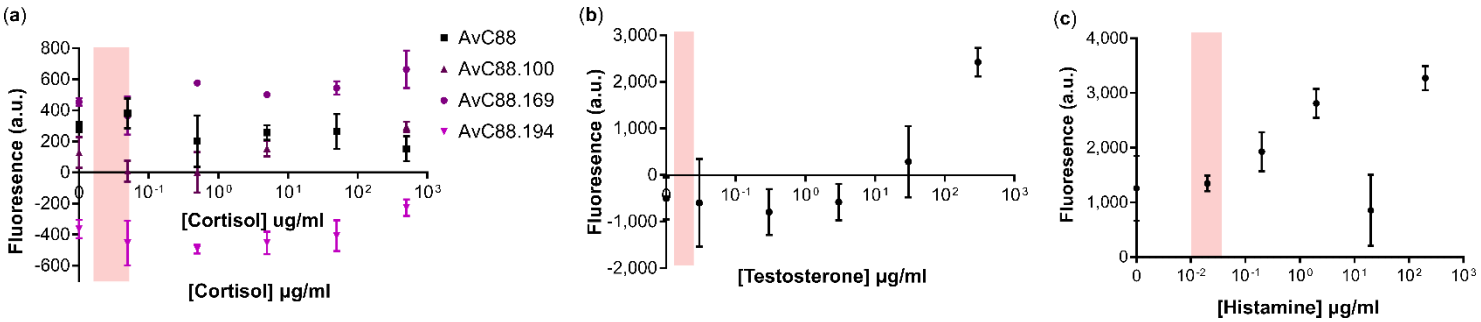


**Figure 4.15 Characterisation of the cpGFP sensors response to biomarkers in homemade cell lysate.** (**a**) shows the response curve of the AvC88 sensor (black squares) and mutants to different concentrations of cortisol. (**b**) shows the response of the AvT88 to different concentrations of testosterone. (**c**) shows the response of the AM10 loop 5 to different concentrations of histamine. For all sensors n=3 and the cell-free reactions were incubated at 37°C post-induction, the red shaded area highlights the concentrations of biomarker expected to be found in human eccrine sweat. For all graphs the response was taken 2 hours post-induction. The error bars show one standard error of the results.

An increase in fluorescence in response to cortisol was seen for two of the mutant versions (AvC88.169 and AvC88.194), shown in **Figure 4.15a.** However the response was not within the required sensing range. For the testosterone sensors the basal expression was noticeably reduced but the response to testosterone was also not within the required sensing range, shown in **Figure 4.15b**. For the histamine sensor the sensitivity seemed to be unchanged, **Figure 4.15c** compared to **Figure 4.13c,** and was within the required sensing range. However the basal fluorescence was increased.

Since some of the cpGFP sensors had reduced output and sensitivity in the homemade cell lysate the DNA concentration used were reoptimized because in different lysates the DNA concentration can alter the response due to the difference in the protein expression. The reduced basal expression means that potentially higher DNA concentrations would improve the sensitivity and output of the sensor, shown in **Figure 4.16**.

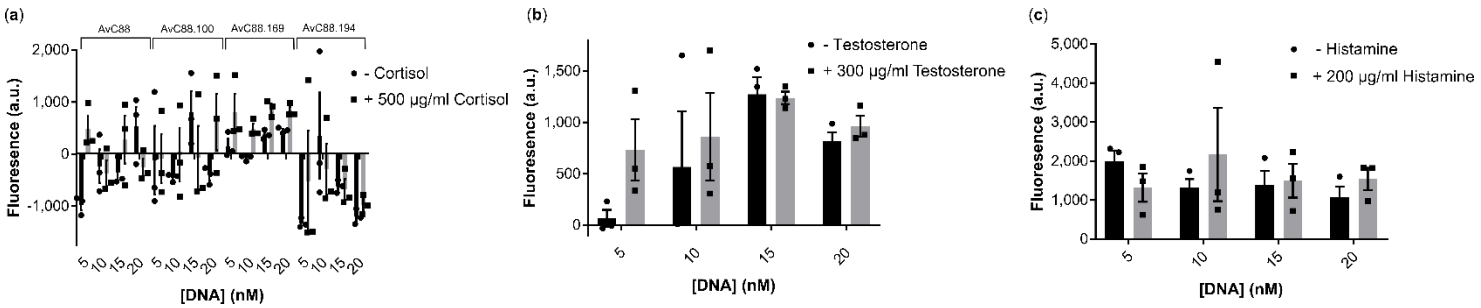


**Figure 4.16 Optimisation of DNA concentration in homemade cell lysate.** (**a**) shows the difference in fluorescence from AvC88 sensor and mutants without cortisol (- Cortisol, black bars) and with (+ 500 µg/ml Cortisol, grey bars) at different DNA concentrations. The response was taken 2 hours post-induction for AvC88, AvC88.100 and AvC88.194 whilst the response for AvC88.169 was taken 1 hour and 30 minutes post-induction (**b**) shows the changes in fluorescence of AvT88 without testosterone (- Testosterone, black bars) and with (+ 300 µg/ml Testosterone, grey bars). The response was taken 1 hour and 30 minutes post-induction (**c**) shows the change in fluorescence of the AM10 loop 5 sensor without histamine (- Histamine, black bars) and with (+ 200 µg/ml Histamine, grey bars). The response was taken 2 hours post-induction. For all sensors n=3 and the cell-free reaction is incubated at 37°C post-induction. The error bars show one standard error of the results.

For cortisol sensors, the original sensor and mutant 194 (AvC88.194) did not seen an improved response by altering the concentration of the plasmid, shown in **Figure 4.16a,** whilst for mutant 169 (AvC88.169) 10 nM DNA added to the cell-free reaction appeared to improve the change in fluorescence. Mutant 100 (AvC88.100) did not seem to have a particularly good response at any concentration, but possibly 10 nM did give the best change between on and off fluorescence. For testosterone, shown in **Figure 4.16b,** the previous concentration of 5 nM remained the optimal concentration of DNA to use in the cell-free reaction for maintaining the low basal fluorescence. None of the concentrations showed a particularly good response for the histamine sensors, shown in **Figure 4.16c,** however 10 nM showed the largest change between the on and off states. For the two AvC88 mutants (AvC88.100 and AvC88.169) and the histamine sensor using a higher concentration of DNA 10nM within the cell-free reaction the response curve for these sensors was re-characterised, shown in **Figure 4.17**.

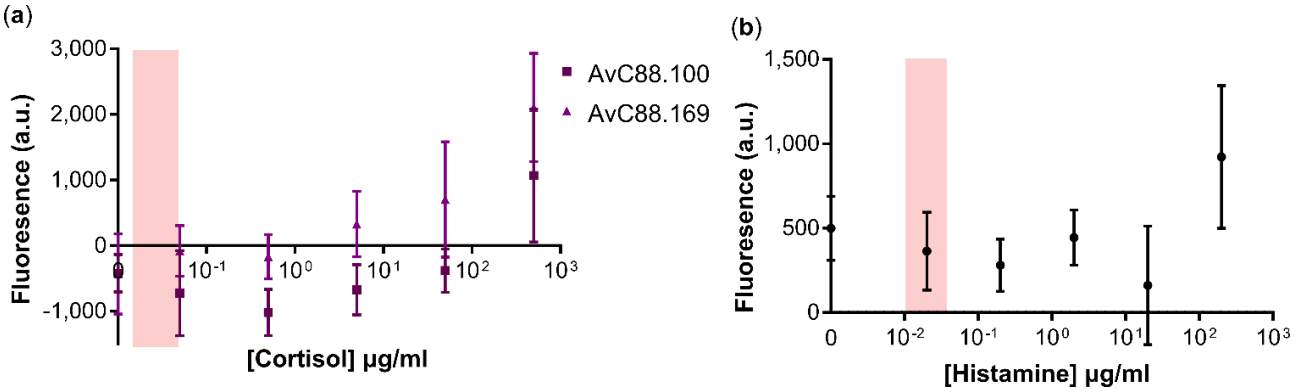


**Figure 4.17 Characterisation of cpGFP sensors response to biomarkers at the higher DNA concentrations of 10nM.** (**a**) shows the response of the AvC88 mutants 100 and 169 (AvC88.100 and AvC88.169) to different concentrations of cortisol. (**b**) shows the response of the AM10 loop 5 histamine sensors to different concentrations of histamine. For all sensors n=3 and the cell-free reactions were incubated at 37°C post-induction. For (**a**) the response was taken 6 hours post-induction and for (**b**) the response was taken 2 hours post-induction. The red shaded area shows the concentration range of the biomarker in human eccrine sweat. The error bars show one standard error of the results.

For the cortisol mutants shown in **Figure 4.17a** there was a clear response to cortisol with a larger output than previously in **Figure 4.15a**. However the sensitivity of the sensor was still not within the required sensing range for using on human sweat. Increasing the concentration of the DNA for the histamine sensor shown in **Figure 4.17b** did not improve the response as compared to **Figure 4.15c** so potentially 5 nM is better.

## 4.4 Discussion

Aptamers are a well-studied approach for using binding molecules to develop biosensors so appeared to be a good method. The potassium aptamer did allow for the detection of potassium ions at the desired concentrations for its use as a sensor for potassium ion levels in human eccrine sweat. The conditions required for the aptamer to be able to produce the required conformational changes are often highly specific which could pose a problem for sensors that are to be used in a wearable device as these could experience a wide range of different conditions (Wan et al., 2022). **Figure 4.1** shows that the aptamer could withstand changes to both the pH and the

temperature without losing its response, which is encouraging for the use of the aptamer within the wearable device. The highly programmable response and sensitivity of the aptamer is also very useful because this means that not only is the potassium aptamer able to detect potassium within the desired range but is also suitable for future further optimisation to be carried out in work on developing the wearable device. However for other aptamers this would need to be assessed on a case by case basis to see if they would also be suitable.

Using cpGFP inserted into a binding protein is a promising method for biosensor development because this could allow a generalised method for detecting almost any molecule of interest. The three cpGFP sensors developed showed that this method can work for detecting the molecule of interest. However, none of the optimisation that had been carried out to date was able to reach the desired level of sensitivity for their use as a sensor on human eccrine sweat. Mutating the linker regions did improve the output for the cortisol sensor, shown by **Figure 4.14b,** although not enough to reach the desired response curve characteristics. The library of mutants produced was not very large so only a limited number of the total possible mutations that could be made to the linker region were tested. More extensive study of the possible mutations for the testosterone and histamine sensors would be important in order to find alternative sequences that could improve these sensors. Further to this work, combining mutants to create sensors that contain multiple mutations would also be important to try for achieving an improved response.

The response of the sensors was also found to be different in different cell lysates when comparing commercial S30 lysate and BL21 DE3 homemade lysate. Therefore testing additional cell lysates from different strains could also improve the output of the sensors further due to their differing abilities for protein expression and folding (Rosano and Ceccarelli, 2014).

In other work to generate these forms of sensors using cpGFP inserted into a binding protein, the binding protein has also been mutated to improve the

sensitivity and fluorescent response. Although the sensors do not yet show high enough sensitivity to detect the required range in sweat there are still multiple different optimisation approaches that could be taken, suggesting that the response can still be improved further.

To produce these cpGFP sensors rational design was used with insertion sites identified through study of the protein structures. However this could also be carried out randomly to determine insertion sites where crystal structures are not available for analysis (Nadler et al., 2016). cpGFP sensors have many potential advantages for biosensing however there are significant challenges to producing biosensors using this approach. The first challenge is finding a suitable insertion point. When developing the sensors multiple insertion points were identified to increase the likelihood of the sensor working. Being able to analyse the structure and where the conformational changes occur will help by allowing rational selection but the exact impact of insertion at a point will not be known until it is carried out. A key potential issue with the insertion site is the effect on the stability of the protein which could prevent the molecule of interest from binding well or the stability of the response. The linker region has been shown to be highly important in transferring the conformational change from the protein to the cpGFP and hence to generate the response, this generates a challenge in optimisation of the sensor because the properties of the linker that are required to achieve transferring the conformational change will likely be specific to the protein meaning that generalised rules cannot be developed to speed future sensor development. The final key challenge will be optimising the sensor to achieve the required sensitivity and specificity of the sensor. Choosing proteins which have these desired characteristics initially will be highly important so as to avoid issues with these characteristics. But the insertion of cpGFP will likely impact the sensor sensitivity as the structure of the protein will be affected. Again optimisation will require protein engineering so this present a challenge as standardised approaches will not be available.

The time taken for the response to be detected in the cell-free reaction was highly variable between the different experiments which would be a large issue when using cell-free sensors within a wearable device. So when encapsulated within a wearable device optimisation would need to be addressed. A potential cause of these differences in response times is that different batches of cell lysate and energy solutions were used between experiments and the variability between batches is a well-known issue within cell-free work (Rhea et al., 2022, Dopp et al., 2019a). Producing larger batches would help to reduce this variability as it would allow the same batch to be used for more experiments. Testing a wider range of reaction and buffer conditions could also help to improve the response because alternative buffers have been shown to alter the protein production amount and speed (Banks et al., 2022a). Finally the cpGFP sensor proteins could be purified and used in a buffer system to reduce the variability between different test. This could also help to speed up the response time as the protein would not need to first be produced before responding.

# 5 Building a Wearable Device

## 5.1 Introduction

Easy to use devices for monitoring biomarkers that allow people to monitor themselves without training have become a key interest in research because point-of-care testing would improve access to monitoring and also reduce costs (Goldstein et al., 2019, El-Osta et al., 2017). Wearable devices are of particular interest because they would be easy to use and allow monitoring to occur passively in real time with no requirement for samples to be taken and then analysed separately. Any centralised analysis adds to the time taken to receive results and also limits how frequently tests can be carried out.

The majority of work in this area of wearable devices has focused on the development of electrochemical sensors but these have challenges in their use and development in terms of cost and ability to withstand the environment changes that the device will experience (Hoekstra et al., 2018, Zhao et al., 2019). The use of cell-based and cell-free biosensors encapsulated in a wearable patch could overcome these challenges and provide a cheap effective alternative.

The first aim was to develop a method to encapsulate the sensors which had been successfully developed and optimised within a hydrogel. Once a suitable method of encapsulation was identified this would then be used to start work toward the second aim to develop a wearable patch and to identify the conditions that would be required for sweat testing and which would give accurate monitoring results, and to determine whether the sensors could maintain the required sensing range. In addition work to build software to automate data capture via the smartphone would be carried out to improve the simplicity of the system and its use by untrained individuals.

## 5.2 Encapsulation of whole cell biosensors

Hydrogels were chosen for encapsulation because they are a polymer that once formed into a solid can absorb a large volume of liquid. This makes them highly suitable for encapsulating and maintaining biosensors as the liquid used to swell the hydrogel could be any buffer, media or reaction mixtures required for the sensors to work. Polyethylene glycol dimethacrylate (PEGDMA) was selected as the hydrogel to test due to its highly tailorable physical properties which depend on the concentration and length of PEGDMA chain (Killion et al., 2011). PEGDMA was also chosen due to its biocompatibility and suitability to be worn on the skin (Kolewe et al., 2015, Alcantar et al., 2000). The structure of PEGDMA and formation of PEGDMA hydrogels is outline in **Figure 5.1**.

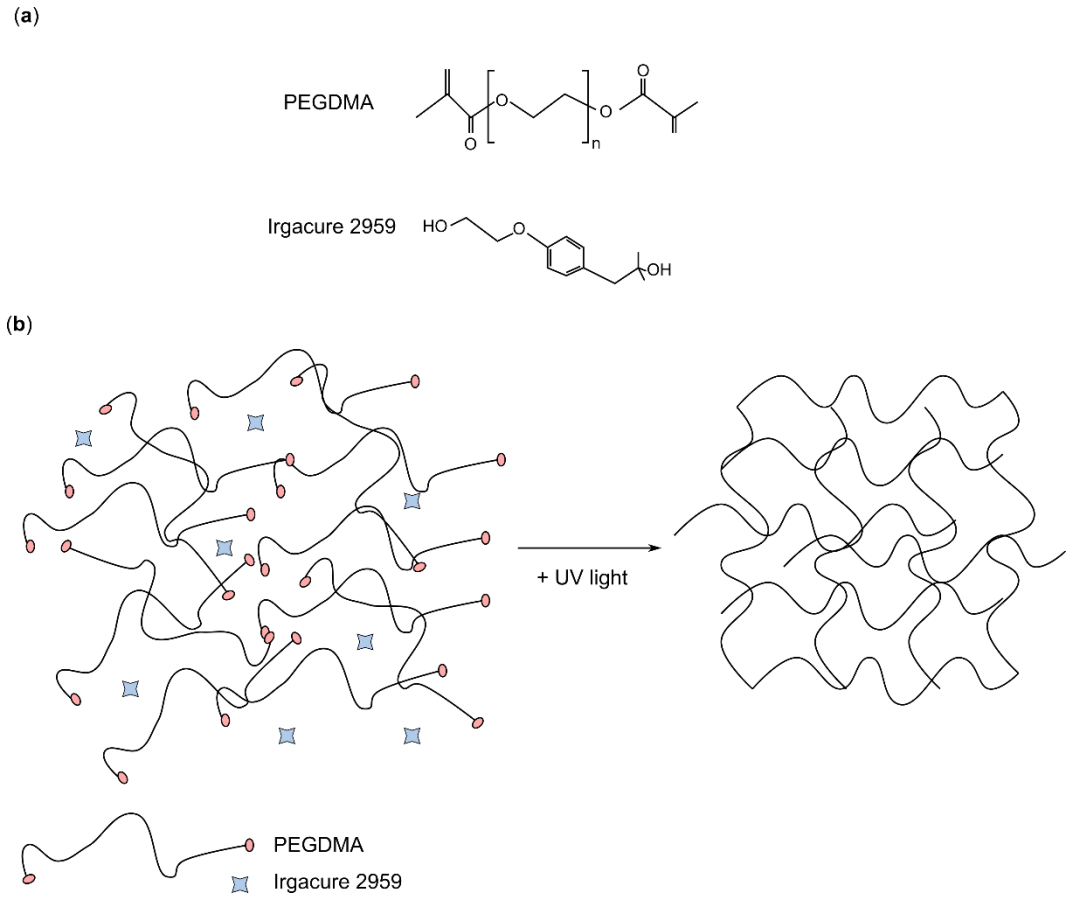


**Figure 5.1 Formation of a hydrogel using polydimethracrylate (PEGDMA) and Irgacure 2959.** (**a**) shows the chemical structures of PEGDMA and Irgacure 2959. The section within the square brackets of PEGDMA is repeated to generate the specific chain length. Irgacure 2959 is the photo initiator used when producing the hydrogel. (**b**) shows a schematic of how the solid PEGDMA hydrogel is produced. PEGDMA of the desired chain length is dissolved in water with Irgacure 2959 at the desired

concentration. This is then exposed to UV light which results in the release of free radicals from Irgacure 2959 which initiates the reaction of the methacrylate groups to crosslink the PEGDMA chains.

Initially to determine whether whole cell sense and respond genetic circuits would be capable of functioning within the hydrogel, cells constitutively expressing fluorescent proteins were encapsulated within the potential hydrogel compositions to see in which compositions the fluorescence from within the hydrogel could be detected, shown in **Figure 5.2a and b**. At the same time the number of cells able to escape from the hydrogel was also tested, shown in **Figure 5.2c,** because the escape of genetically modified organisms into the environment is considered a serious security issue. Encapsulation is method that has been considered for preventing escape.

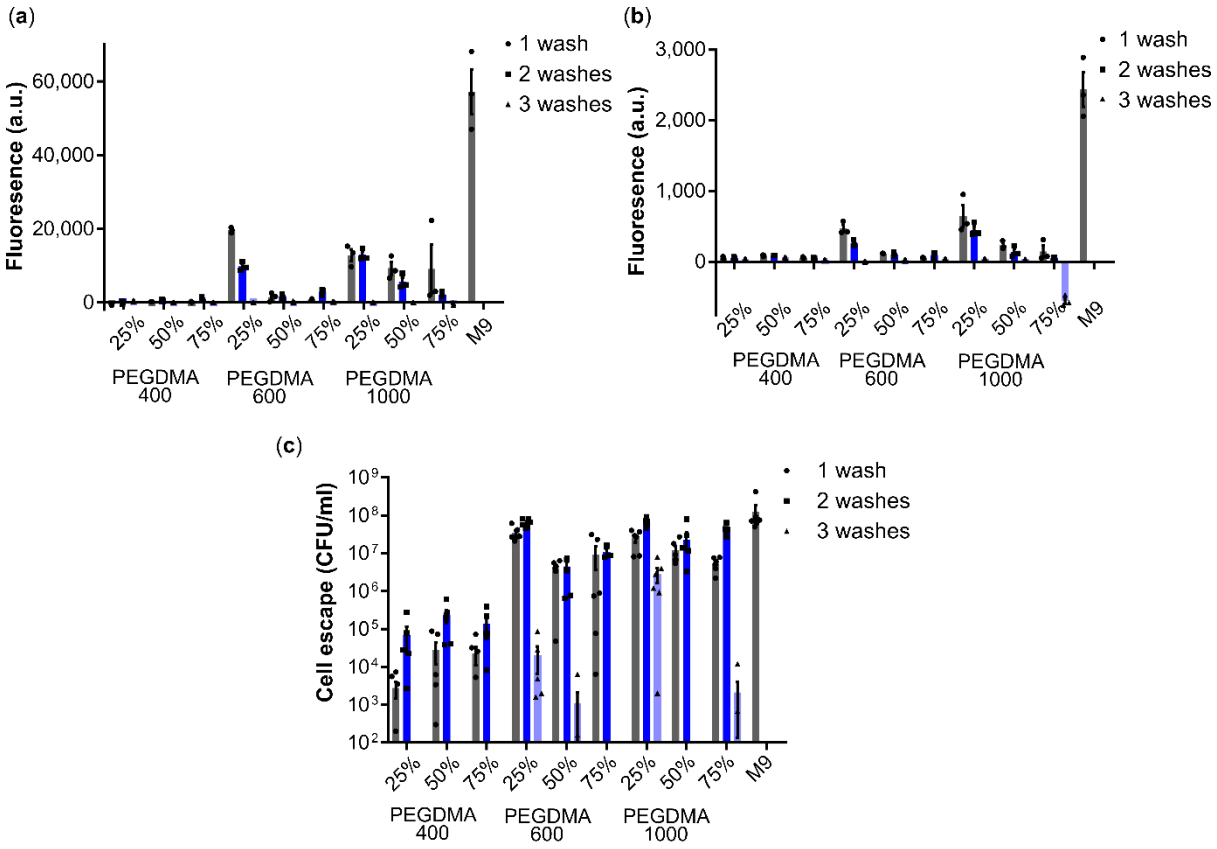


**Figure 5.2 Characterisation of cell growth in different PEGDMA hydrogels.** The figure shows the effect of the composition of the hydrogel on the detectable fluorescence and cell escape. (**a**) to determine which composition of PEGDMA hydrogel allowed the best cell growth, cells containing constitutively expressed GFP were diluted to OD 0.1 in the different hydrogels and cured. Three different lengths of PEGDMA chains and three different concentrations of the hydrogel as a percentage of the total weight

of the final solution were tested. The fluorescence of the cells in the hydrogel were compared to cells grown in M9 24 hours post UV crosslinking. (**b**) shows the fluorescence of constitutive mRFP expressing cell encapsulated in different hydrogel compositions in the same manner as in **Figure 5.1a**. (**c**) The different hydrogel compositions were also tested to see how well they contained the cells and prevented escape into the surrounding environment. The excess medium remaining on top of the hydrogel spots after 24 hours was removed to determine the number of colony forming units present in the medium of each composition. For all experiments n=3, 37°C. The error bars show one standard error.

Both GFP and mRFP constitutively expressing cells were encapsulated in 3 different chain lengths of PEGDMA at 3 different concentrations. Both the chain length and concentration would alter the pore size, which could impact the growth and viability of the cells which would in turn impact the fluorescence detected. **Figure 5.2a** shows the GFP fluorescence detectable from the hydrogel spots compared to cells diluted to the same level in M9 medium. **Figure 5.2b** shows the mRFP fluorescence that is detectable from the hydrogel in different composition**.** The longer PEGDMA chains allowed a higher level of detection of both mRFP and GFP, with PEGDMA 1000 resulting in much higher fluorescence than the other two chain lengths. Therefore, this would be the best composition for ensuring the function of the whole cell biosensors within the hydrogel. A lower concentration of the PEGDMA within the final hydrogel also seemed to improve the response with 25% w/w giving the strongest fluorescence.

Currently the regulations allowing genetically modified organisms (GMOs) to be removed from the laboratory are very strict and the GMOs need to be kept in a system that keeps them separate from the environment. Hydrogel encapsulation which prevents cell escape would be a step in generating a device that fits this requirement. The impact of washing the crosslinked hydrogel was tested to see if this impacted the fluorescence detected, because the fluorescence detected could be due to cells on the outside of the hydrogel rather than from those cells encapsulated inside the hydrogel. Washing should remove those cells on the surface so it would show whether the fluorescence was coming from cells within the hydrogel or on the surface, shown in **Figure 5.2c**. **Figure 5.2c** shows that encapsulation in the hydrogel was not enough to prevent cell escape even when washing is carried out to ensure no cells are

on the surface of the hydrogel. One wash should clear cells on the surface of the hydrogel but as additional washes continued to reduce fluorescence this suggests washing is removing cells from the hydrogel itself and this also suggests that encapsulation is not enough to ensure no cell escape occurs. To further examine the sensors within a hydrogel PEGDMA 1000 50% w/w was selected because with this composition the level of fluorescence was still detectable after one wash.

Using this hydrogel composition the response of the whole cell sense and response lactate circuit was tested under different set up conditions to see how the well the sensor responded and how much the encapsulation impacts the ability of the sensor, shown in **Figure 5.3**.

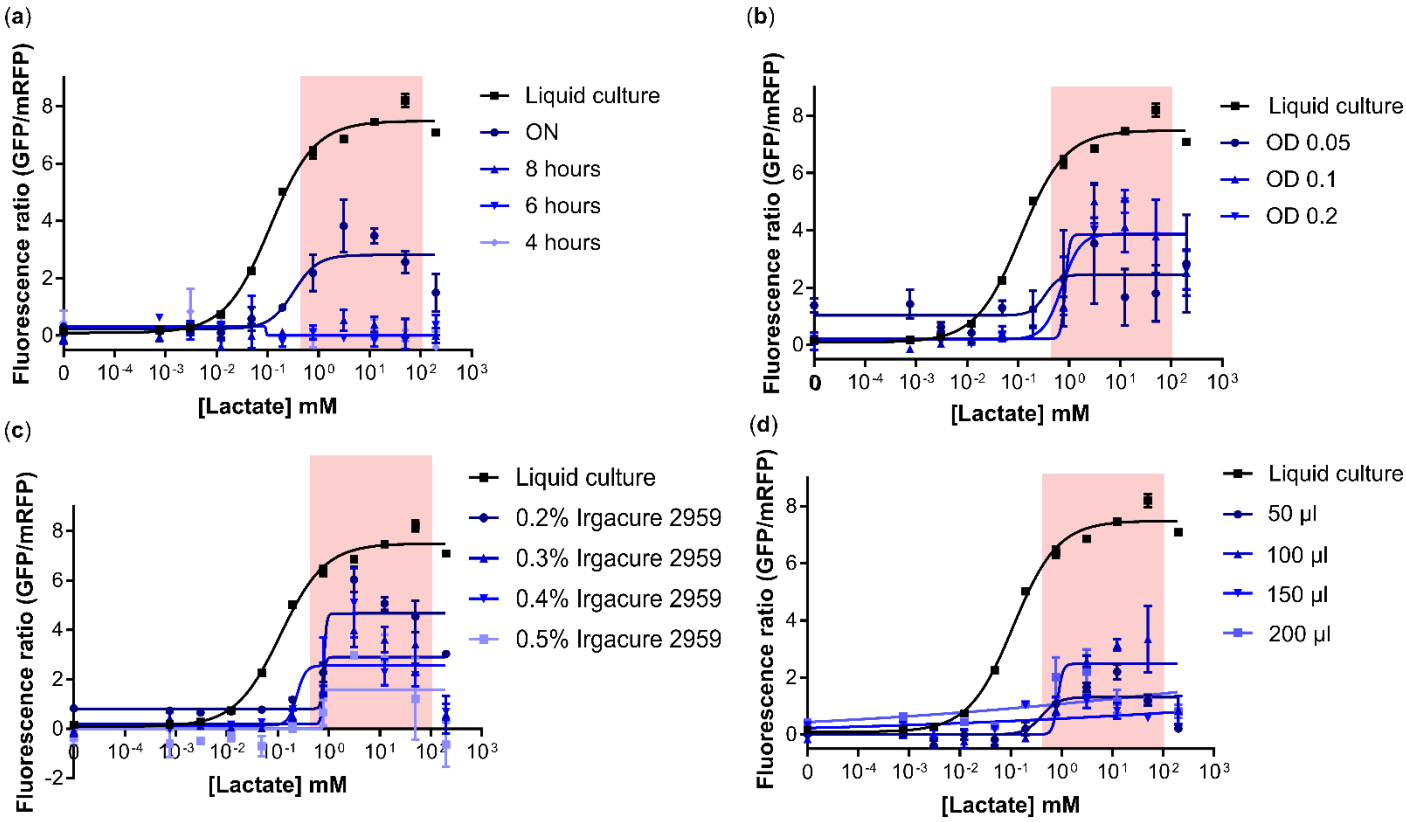


**Figure 5.3 Determination of the optimal conditions to encapsulate whole cell biosensors within a PEGDMA hydrogel.** The response curves show the impact of different hydrogel composition and encapsulation set up conditions on the response of the lactate sensor compared to the response curve of the lactate sensor in liquid culture. (**a**) shows the effect of the recovery time after cross-linking on the response of the sensor. (**b**) shows the impact of the starting density of the cells added to the hydrogel for encapsulation which was then recovered with the optimal condition identified so far from **Figure 5.3a**.

(**c**) shows the impact of different concentrations of Irgacure 2959 set up using the conditions identified from the previous tests from **Figure5.3a and b**. (**d**) shows the impact of using different volumes of M9 medium to swell the hydrogel containing the encapsulated cells. For all panels the cells grown at 37°C with no shaking n=3. The response is taken 5 hours post-induction. The error bars show one standard error.

Initially the amount of time the cells require to recover from the UV treatment and grow to the correct state for response to an inducer following the crosslinking of the hydrogel and for the biosensor response to be detectable was tested, as shown in **Figure 5.3a**. For this initial test the cell culture was diluted to OD 0.1 with 0.2% Irgacure 2959 and a three times volume of the hydrogel was used for swelling with media. **Figure 5.3a** shows that allowing the cells to recover overnight is required in order to ensure that the cells have recovered enough from the hydrogel formation for the response to lactate to be detected. Once this had been identified the starting OD was varied to see if altering this could further improve the response. A higher OD did improve the response, as seen in **Figure 5.3b,** so for all future experiments this higher starting OD of OD 0.2 will be used. No higher ODs were tested because at the volume of cells being added to the hydrogel if a higher OD was used this would start to have an effect on the concentration of the final PEGDMA solution (without other concentration steps to ensure the volume of culture added is reduced which could impact the cell's health themselves) which could affect other characteristics, see **Figure 5.2**. The next variable altered to see if it could improve the response of the sensor within the hydrogel was the concentration of the photo-inducible crosslinker Irgacure 2959, shown in **Figure 5.3c.** Higher concentrations could potentially speed up the crosslinking of the hydrogel. However higher concentrations did not help the response so this factor was not altered. Finally **Figure 5.3d** shows how the volume of media used to swell the hydrogel impacted the biosensor response curve, 100 µl appeared to be the best swelling volume for a 50 µl hydrogel spot.

Overall **Figure 5.3** shows that there is a reduction in the output of the sensor when encapsulated but optimisation of the conditions did allow for a

response to be detected and the impact of encapsulation would not prevent the sensor response.

Following the identification of the optimal composition of the hydrogel both versions of the lactate sensor were tested to see how the response compared to the response when in liquid culture, shown in **Figure 5.4**.

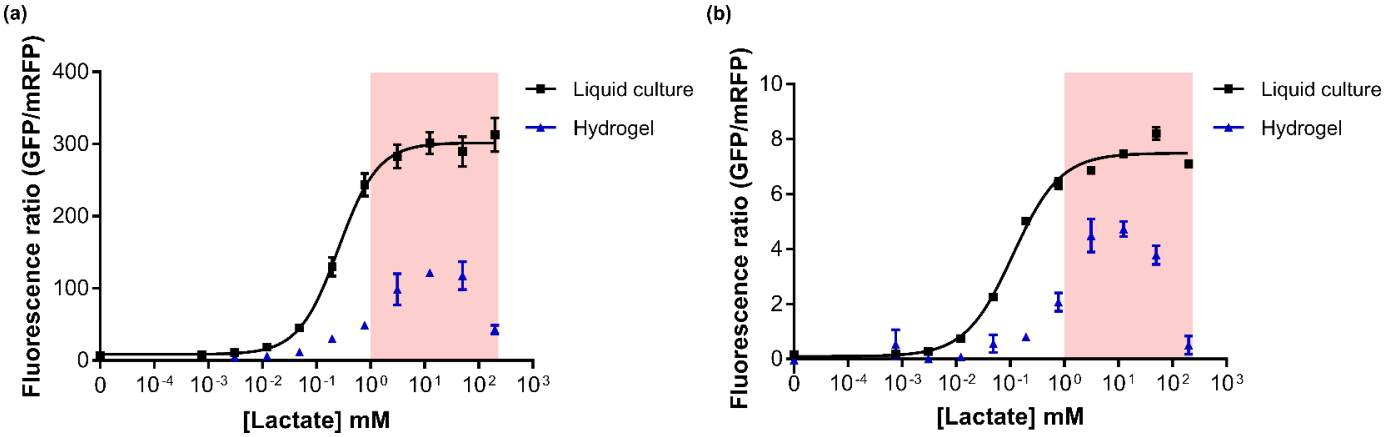


**Figure 5.4 Response of whole cell lactate sensor encapsulated in the optimised PEGDMA hydrogel.** (**a**) shows the response curve of the lactate sensor with J23101 RBS 32 mRFP for normalisation encapsulated within the optimal hydrogel condition identified (blue line) compared to the response of the sensor when grown in liquid culture (black line). (**b**) shows the response of the lactate sensor with J23101 RBS 30 mRFP for normalisation within the hydrogel (blue line) compared to in liquid culture (black line). For all response curves n=3 cells grown at 37°C, with liquid cultures shaking at 1,000 rpm. The response was taken 5 hours post-induction. The error bars show one standard error.

For both versions of the lactate sensors which contain constitutive mRFP the response when encapsulated was decreased, this was expected from the previous work shown in **Figure 5.3**. This impact on the maximal response was less for the version of the sensor with J23101 RBS30 mRFP, shown in **Figure 5.4b**. The sensor seems to have reduced sensitivity compared to the sensor grown in liquid culture, which is a more significant issue. Conversely the sensors with J23101 RBS 32 mRFP seem to have a larger reduction in the maximal output of the sensor when encapsulated in the hydrogel, as shown in **Figure 5.4a.** However, there was less of an effect on the sensitivity of the sensor. As both sensors have the potential to work in the final wearable device depending on which of the characteristics is the most important, testing will be carried out using both sensors to see which works

best. As well as the overall response being decreased the response at high concentrations drops for both versions, shown in **Figure 5.4**. The change in response over time was examined to see how the response of the sensor had changed when encapsulated in the hydrogel, shown in **Figure 5.5**.

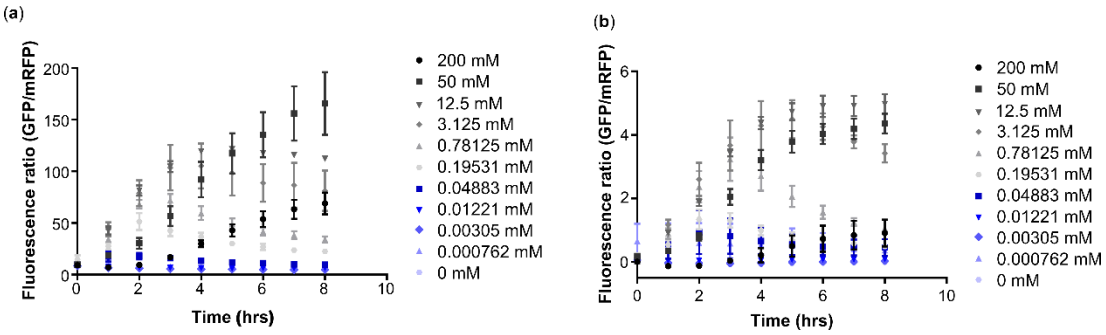


**Figure 5.5 Change in the response of the lactate sensor over time to different concentrations of lactate when encapsulated within the hydrogel.** (**a**) shows the change in response to different concentrations of lactate for the lactate biosensor with mRFP expressed using RBS 32. (**b**) shows the response to different concentrations of lactate for the lactate biosensors with mRFP expressed using RBS 30. For all n=3 cells grown at 37°C with the cells recovered overnight in the 50% PEGDMA 1000 (w/w) hydrogel. The error bars show one standard error.

When looking at how the response to each concentration changes over time similar behaviour to previous characterisation could be seen. For the lower concentrations where the response begins to decrease over time, shown in **Figure 5.5,** suggesting that the lactate is still being used up as a metabolite. For the highest concentrations looking at the response over time shows that attakes longer for the response to begin to increase and not until the 5 hour timepoint is the drop in response being seen in the response curve, shown in **Figure 5.4**. For the version using mRFP expressed using RBS 32, shown in **Figure 5.5a,** the response to the higher concentration does begins to increase at the later time points and did not appear to have reached a maximum, suggesting that at later time points potentially the drop in response would not be seen. Whilst for the version with mRFP expressed using RBS 30, shown in **Figure 5.5b,** for the highest concentration of 200 mM the increase in the response was not seen even at later time points. This suggests that it is not solely the reduced speed of the response causing the drop in the response at the higher concentrations.

The reduced speed in the response for higher concentrations could be due to the inducer solution not being able to diffuse into the hydrogel as well because the lactate solution becomes more viscous as the concentration increases. This could be tested by characterising the diffusion within the hydrogel using fluorescent molecules such as fluorescein with different concentrations added to the hydrogel to see how this alters the diffusion behaviour. The viscosity of the solution could also have an impact and so this would need to be accounted for and could be done through adding glycerol or a similar solution to the fluorescein at to mimic the viscosity more similarly. For the versions with mRFP expressed by RBS 30 where the delayed response is not seen for the highest concentration, this could suggest that expressing the higher level of mRFP for normalisation whilst also expressing the GFP in response to the lactate is causing too much burden for the cell, which would suggest using RBS 32 would be the better option.

Following the successful optimisation of the tryptophan sensor in chapter 3 showing that it should be able to function specifically in the conditions it will experience, the sensor was then tested in the hydrogel to see if this sensor would retain its functionality in the wearable device, shown in **Figure 5.6**.

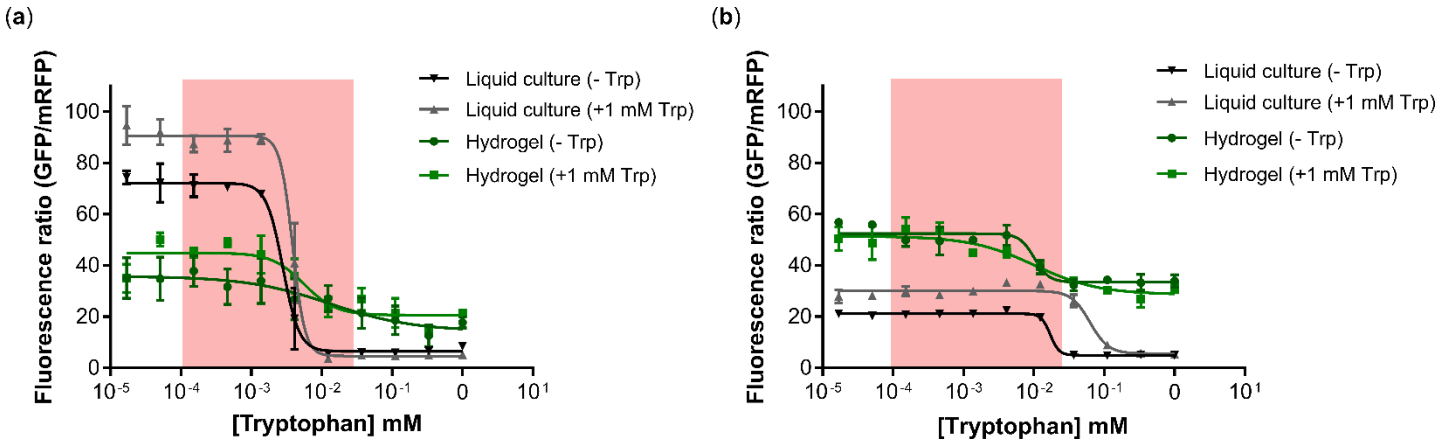


**Figure 5.6 Characterisation of the tryptophan biosensor encapsulated in 50% w/w PEGDMA 1000.** (**a**) shows the response of the tryptophan sensor with J23101 RBS 32 mRFP in the hydrogel without and with tryptophan in the overnight media, shown by the green lines, compared to the response of the sensor in liquid culture without and with tryptophan in the overnight, shown by the black and grey lines. (**b**) shows the response of the sensor with J23101 RBS 30 mRFP using the same line colours. For both graphs n=3, cells grown at 37°C with shaking at 1,000 rpm for the cells in liquid culture. The response within the hydrogel was taken 5 hours post induction. The error bars show one standard error.

As seen with the lactate sensor (**Figure 5.4**) the fold change of the sensor when encapsulated in the hydrogel is reduced compared to the sensor when in liquid culture, as shown in **Figure 5.6**. For the sensor with J23101 RBS 32 mRFP in **Figure 5.6a,** this is caused by a reduction in the maximal output and an increase in the leakiness at the high tryptophan concentrations. The sensitivity of the biosensor does not appear to be affected with encapsulation, with the response occurring within the physiological area. **Figure 5.6b** shows the response of the sensor with J23101 RBS30 mRFP. This version of the sensor did not have any reduction in the maximum fluorescence compared to liquid culture but did show a large increase in the leaky expression at high tryptophan concentrations. The sensitivity continued to match the requirements for detecting tryptophan levels in sweat, both when tryptophan is present in the overnight culture and in the media used in the recovery period after encapsulation (see **Figure 5.3**).

Either version can be used in the final wearable device because both of the sensors, as shown in **Figure 5.6,** will both respond over the required concentration ranges for sweat. But the version with J23101 RBS 32 mRFP may be better due to the lower leaky expression, as high leakiness may make the response harder to detect in the final wearable device.

## 5.3 Encapsulation of molecular binding sensors

Following the optimisation of the whole cell biosensors in the hydrogel, the composition previously identified as most suitable for sensor response was used to test the potassium aptamer.

Initially two concentrations of the potassium aptamer were tested, the same concentration as in the liquid buffer and a slightly higher concentration than in the liquid buffer, shown in **Figure 5.7a**. However, the sensitivity of the response was decreased which would not be ideal for the final device. Higher concentrations could potentially improve the sensitivity so a range of higher concentrations were tested, shown in **Figure 5.7b.**

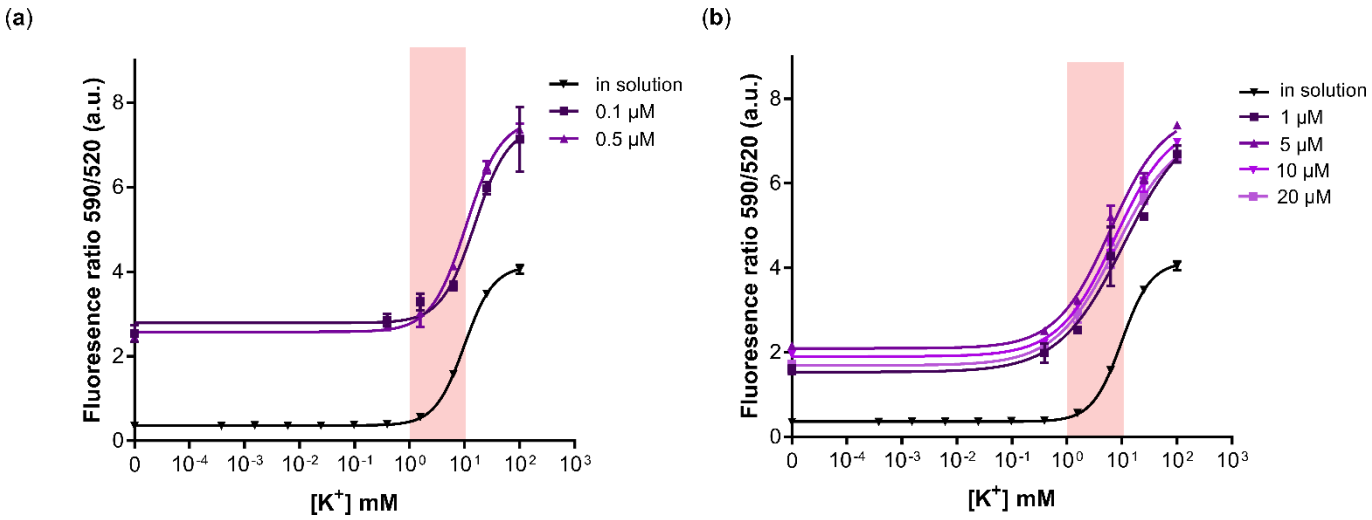


**Figure 5.7 Encapsulation of potassium aptamer within PEGDMA hydrogel.** (**a**) shows the response of the potassium aptamer when encapsulated in PEGDMA 1000 50% w/w hydrogel compared to 0.2 µM in the liquid buffer. (**b**) shows higher concentrations of the potassium aptamer encapsulated in PEGDMA 1000 50% w/w hydrogel compared to liquid buffer. The red region highlights the concentration in human eccrine sweat. The response was taken 30 minutes post-induction, n=3 37°C. The error bars show one standard error.

**Figure 5.7b** shows that at higher concentrations the potassium aptamer was able to respond to potassium ions whilst encapsulated within the hydrogel. For all the concentrations there was a noticeable increase in the basal fluorescence. 1µM of the potassium aptamer within the hydrogel seemed to have the smallest increase in the basal fluorescence suggesting this could be optimal. Taking the response at 30 minutes post-induction was noticeably slower than when testing the aptamer diluted in the buffer. The reduction in the speed of response was likely due to the diffusion of molecules within the hydrogel being slower and resulting in the response slowing, because it takes longer for the aptamer to interact with the potassium ions. To identify the timepoint to use for determining the response curve the change in the response over time was studied as shown in **Figure 5.8**.

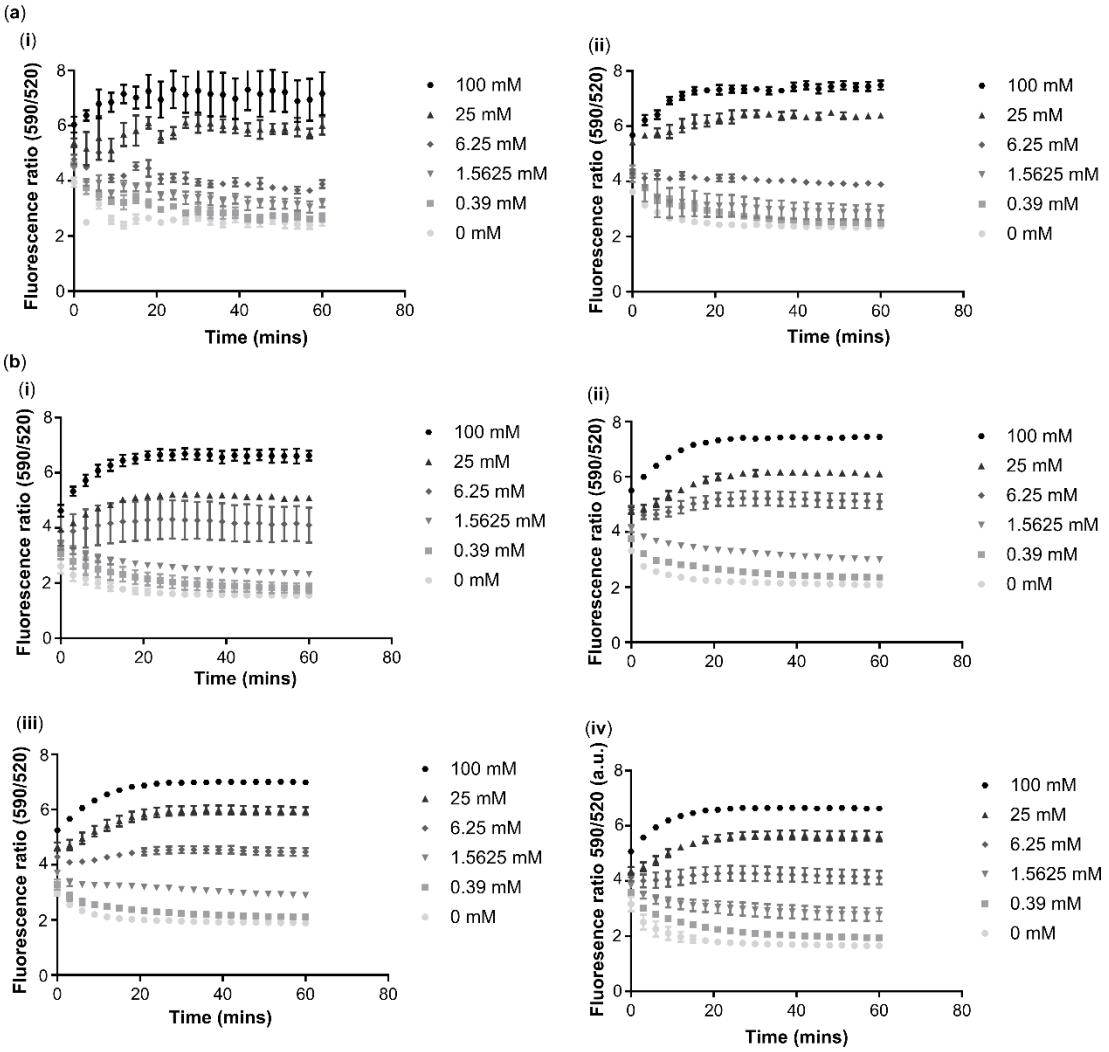


**Figure 5.8 Change in response over time of the potassium aptamer to different concentration of $K^+$ ions when encapsulated in 50% PEGDMA hydrogel (w/w).** (**a**) shows the response over time of the potassium aptamer in **Figure 5.6a**. (**i**) shows the response of 0.1 µM DNA aptamer encapsulated within the hydrogel. (**ii**) shows the response of 0.5 µM DNA aptamer encapsulated within the hydrogel. (**b**) shows the response over time of the potassium aptamer in **Figure 5.7b**. (**i**) shows the response of 1 µM potassium aptamer encapsulated within the hydrogel. (**ii**) shows the response of 5 µM potassium aptamer encapsulated within the hydrogel. (**iii**) shows the response of 10 µM potassium aptamer encapsulated within the hydrogel. (**iv**) shows the response of 20 µM potassium aptamer encapsulated within the hydrogel. For all graphs n=3 aptamer incubated at 37°C. The error bars show one standard error.

**Figure 5.8** shows that for all of the concentrations of the potassium aptamer the response could be detected very quickly after the induction of the hydrogel. However the response did not reach its steady state response until later time points. For the higher concentrations of the potassium aptamer in

the hydrogel, shown in **Figure 5.8b,** this steady state was reached faster with the highest concentration. In **Figure 5.8b iv** this took less than 20 minutes but for lower concentrations it took longer for the aptamer to reach a steady state. Whilst for the lowest concentrations tested this steady state was not achieved properly, as seen in **Figure 5.8a**.

## 5.4 Wearable device optimisation

Once three sensors had been shown to be functional within the hydrogel the next step was to test an entire wearable device that combines the hydrogel with a backing. Silicone had been chosen because this would allow the patch to be self-adhesive and it would help to avoid any irritation associated with glues being used for adhesion on skin. The flexibility of the silicone material would also ensure that movement is not impeded.

### 5.4.1 Initial construction of silicone hydrogel patch

In the literature a combination of two different silicones has been used to ensure that the patch has the strength to withstand movement and stretching but also remain adhesive (Liu et al., 2018b). Sylgard 184 (Dow) was used to provide the physical strength and is the first layer. The second layer which generates the adhesive properties is SilGel 612 (Wacker) and for this layer the ratio between the two components used to generate the material can be varied to alter its properties. The first step was to try different ratios of the components to see how this affected the ability of the hydrogel to be crosslinked to the silicone.

The spots were crosslinked to the patch made of the different silicone ratios. Immediately after crosslinking the hydrogel all of the spots were crosslinked to the different silicone compositions These patches were then left to swell overnight (as this would be needed when the sensors are encapsulated to ensure and maintain the functionality of the sensor, see **Figure 5.3**) to see if

the spots remained attached after the overnight swelling. For all of the different ratios tested for producing the SilGel 612 layer, the spots are able to remain linked to the hydrogel after swelling. The other characteristic that was determined at this stage was that the spots did not spread when added to the patch for crosslinking. This resulted in spots that stood out from the patch noticeably when crosslinked. However this could impact the ability of the patch to remain in contact with the skin of the wearer. The profile of spots may need to further optimised in the future.

The other attribute that is important to consider would be how comfortable the patch would be to wear.

**Figure 5.9 Characterisation of the physical characteristics of the 0.5:1 ratio silicone.** The image shows how the patch made using 0.5:1 silicone behaves when touched.

**Figure 5.9** shows that when the silicone patch with 0.5:1 (component A: component B) of SilGel 612 was touched with a pipette tip the silicone had retained a more liquid texture, shown by the filament of the silicone which remains attached to the pipette tip as it is removed, highlighted by the red circle within **Figure 5.9** and the zoomed in inset at the bottom of the picture.

This suggests that 0.5:1 would not be suitable because this level of stickiness would be uncomfortable for the user and would leave a residue which could

be irritating to the user. Neither 1:1 or 1.5:1 showed this same property so could be suitable to use.

To ensure good readings from sweat the silicone patch needs to maintain good contact with the skin over the whole patch. **Figure 5.10** shows that ability of the patch to remain attached to a gloved hand in different positions and flexing situations to study the adhesive properties and simulate adhesion under movement in order to check this approach to patch composition was suitable for continuing with in the development of the wearable device. The hand was chosen because this would allow easy determination of how well it is stuck and is a region that undergoes large changes during movement. If the patch can remain well stuck on the hand it would also work to remain stuck in other places. In the future this would need to be tested on skin in human trials in the future once the device has been optimised for sensing.

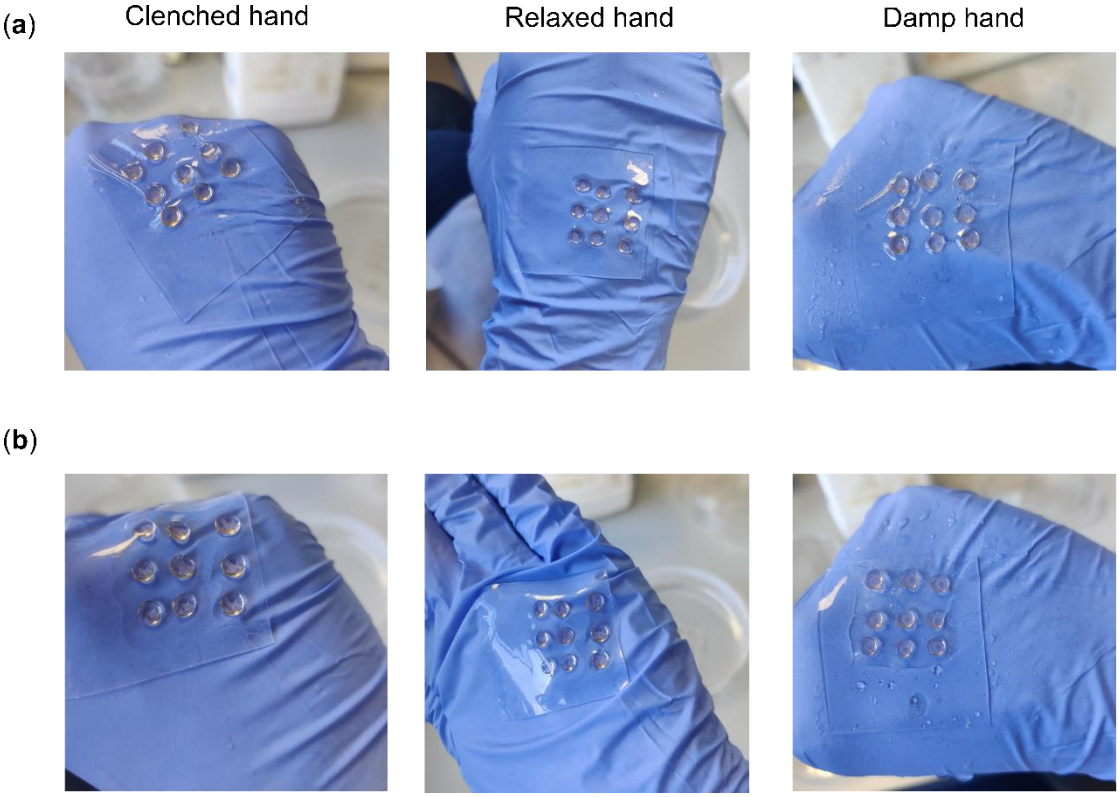


**Figure 5.10 Characterisation of the ability of silicone hydrogel patch to adhere to a surface.** (**a**) shows the ability of the silicone patch made using the 1:1 SilGel 612 ratio to attach to a gloved hand in held in different flexing positions and comparing wet and dry situations. (**b**) shows the ability of the

silicone patch made using the 1.5:1 SilGel 612 ratio to attach to a gloved hand in held in different positions and comparing wet and dry situations.

The two different compositions which appeared to be potentially suitable were tested. The ability of 1:1 SilGel 612 ratio to remain stuck to a surface under different conditions is shown in **Figure 5.10a**. The patch remained well stuck under all of the conditions tested, including when the surface was damp. This feature is important as when the patch is used to detect biomarkers in sweat the skin is likely to be damp. **Figure 5.10b** shows the patch made using 1.5:1 ratio for SilGel 612. On the dry glove the patch stuck well in both the clenched and relaxed positions but on damp skin the patch around the spot began to lift. This suggests that 1:1 ratio would be better, but it was much harder to remove once stuck which could reduce the comfort of the wearer. The patch of 1.5:1 ratio could potentially still provide enough adhesion if the spots were changed to ensure that they had less height because a lower profile would make it easier for the patch to remain stuck whilst still ensuring that the patch remains comfortable for the wearer and still easy to remove and re-attach.

For ongoing testing on the function of the sensors within the patch the ratio of 1.5:1 was used because the patches were easier to handle and this would speed up the next steps of work.

### 5.1.1 Testing with cell-based construct

Following the success of optimising the physical properties of the patch the next step was to test that cells could successfully be grown within the device.

First constitutive fluorescent proteins were tested to determine how well fluorescent proteins could be detected by a phone camera and if there needs to be a certain size of spot on the patch for it to be detectable, shown in **Figure 5.11**. For each spot size the same patch was imaged for both red and green fluorescence to also show that each fluorescent protein could be specifically detected by the filters. The top panel shows the four patches

imaged for green fluorescence whilst the bottom panel shows the same four patches imaged for red fluorescence. Images were taken with filters within a dark box to ensure the light emission was able to be detected. For imaging GFP Tokyo blue filter from Lee filters was used over the flash which has a transmission peak around 445 nm (https://leefilters.com/colour/071-tokyo-blue/) and Twickenham green filter which has a transmission peak around 530 nm was used over the lens (https://leefilters.com/colour/736-twickenham-green/). For imaging mRFP Twickenham green was placed over the flash and the light red filter which has a transmission peak around 640 nm and above was placed over the lens (https://leefilters.com/colour/182-light-red/). These spectra are shown in **Appendix 3**.

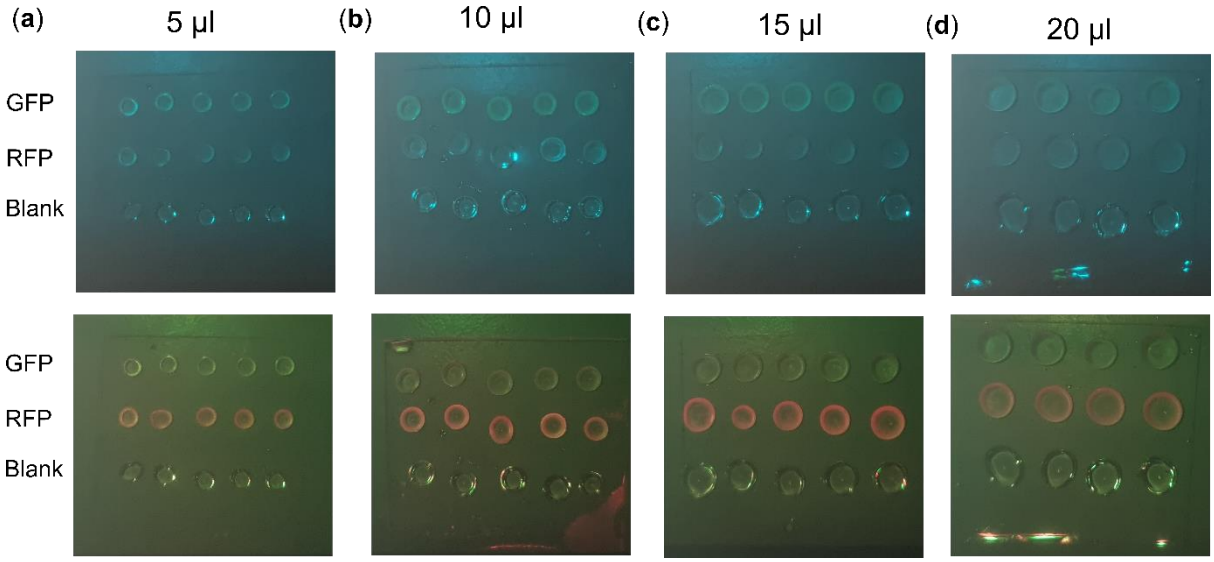


**Figure 5.11 Characterisation of different hydrogel spots volumes containing constitutively expressed fluorescent proteins.** The first row in the patches has GFP expressing cells contained within the spots the middle row shows mRFP expressing cells within the hydrogel spots and the bottom row shows hydrogel spots containing no cells. (**a**) shows the ability to image GFP and mRFP when using 5 µl hydrogel spots. (**b**) shows the ability to image GFP and mRFP when using 10 µl hydrogel spots. (**c**) shows the ability to image GFP and mRFP when using 15 µl hydrogel spots. (**d**) shows the ability to image GFP and mRFP when using 20 µl hydrogel spots. To image the green fluorescence filters were obtained from the Lee colour catalogue with Toyko blue over the flash and Twickenham green over the camera lens. For red fluorescence Twickenham green was placed over the flash and light red was placed over the camera lens. A dark box was then used to shield the patches from light during imaging to allow fluorescence to be detected. Patches produced and swollen overnight before excess media removed and then the patches were incubated for further 5 hours at 37°C.

**Figure 5.11** shows how fluorescent proteins can be detected in the wearable device. Four different spot sizes were tested of 5 µl, 10µl, 15 µl and 20 µl, seen in **Figure 5.11a, b, c and d** respectively. For GFP the strongest fluorescence appeared to be for the spots that were 10 µl or 15 µl, in the top panel of **Figure 5.11b and c** the change in the green pixel values compared to the blank for these two spots sizes were statistically significant with p-values of 0.0271 and 0.0218 respectively. The green colour that forms the top row of spots can be easily distinguished from the other two rows of spots which should not have any response when imaging GFP. The response for 5 µl was not significantly different from the green values of the blank and 20 µl was much harder to distinguish visually even though it was statistically significant, shown in **Figure 5.11a and d**. For mRFP shown in the lower panel of **Figure 5.11** overall the mRFP response was better detected by the phone camera with all the spot sizes having a statistically significant change in the red pixel data compared to the blanks. Visually the response appeared weakest in the 20 µl spot seen in **Figure 5.11d** and the 5 µl spots also showed a weaker response in **Figure 5.11a** compared to **Figure 5.11b and c**. Therefore 10 or 15 µl spots were used in future experiments.

The initial test was to determine if fluorescent proteins could be detected used a strong constitutive promoter (J23101) and a strong RBS (RBS 30). However, using a medium strength RBS to express the mRFP might be required to achieve the desired response of the sensor response, shown in **Figures 5.4 and 6.** Therefore knowing whether a weaker level of mRFP expression could be detected by the camera phone is also important, shown in **Figure 5.12,** as the biosensors have been shown to be able to function better with the reduced mRFP expression within the wearable device.

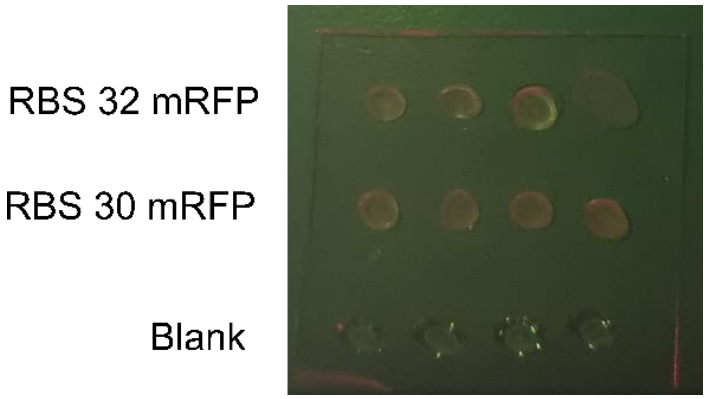


**Figure 5.12 Comparison of different mRFP expression levels in the wearable device.** The image shows a wearable device containing constitutive mRFP with different strength RBS being used to express the mRFP. To image red fluorescence twickenham green was placed over the flash and light red was placed over the camera lens. A dark box was then used to shield the patches from light during imaging to allow fluorescence to be detected. Patches produced and swollen overnight before excess media removed and then the patches were incubated for further 5 hours at 37°C.

Using a weaker RBS to express mRFP in the wearable device did reduce the fluorescence detected from the spots, shown in **Figure 5.12,** although the red fluorescence could still be detected. This was expected because the number of mRFP protein molecules would be less. However, because the red fluorescence was much more easily seen when using RBS 30 this would be used for work in optimising the wearable device and biosensor at this stage.

Having shown that cells can produce fluorescent proteins which the phone camera could detect using filters and a dark box then the next step is to test the optimised whole cell biosensors within the device to determine the sample volume required to be able to detect a response. The lactate sensor was initially tested, shown in **Figure 5.13**.

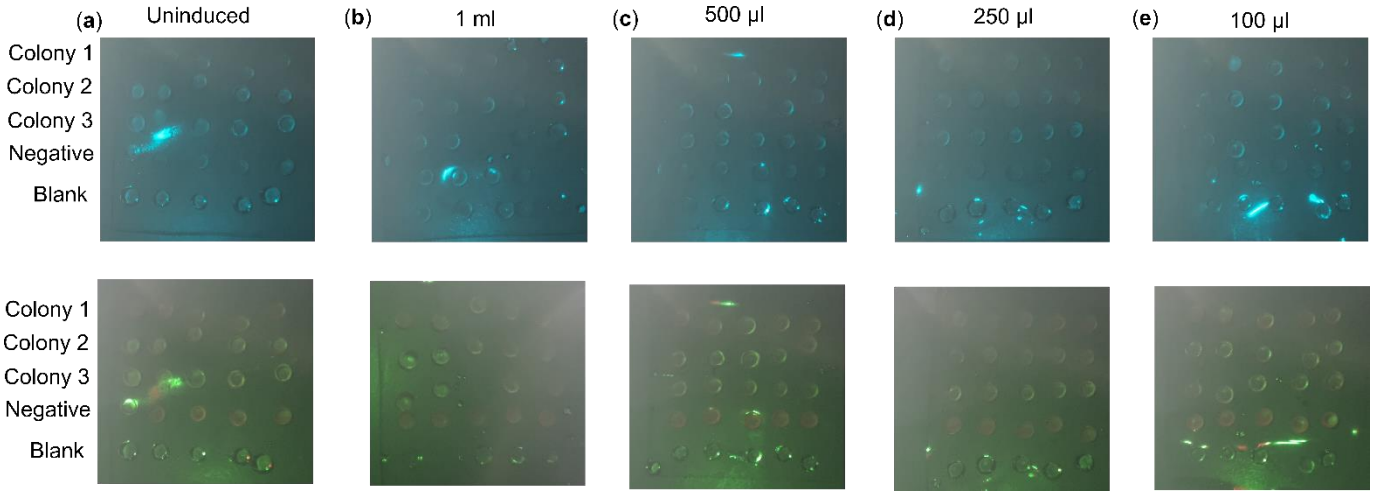


**Figure 5.13 Optimisation of sample volume requirement for wearable device containing the lactate sensor.** The images show the fluorescence of the patch which had been induced with different volumes of lactate. The upper panel shows the patch imaged to detect GFP and the lower panel shows the patch imaged to detect mRFP. Each row of the patches was laid out the same as in the first image. (**a**) shows the patch which was induced with water added rather than lactate. (**b**) shows the patch where 1 ml 1 M lactate was used to induce. (**c**) shows the patch where 500 µl 1 M lactate was used to induce and (**d**) shows the patch where 250 µl 1 M lactate was used to induce. (**e**) shows the patch where 100 µl 1 M lactate was used to induce the patch. 10 µl spots were used to produce the patch. The images were 8 hours post-induction. To image the green fluorescence filters were obtained from the Lee colour catalogue with Tokyo blue over the flash and Twickenham green over the camera lens. To image red fluorescence Twickenham green was placed over the flash and light red was placed over the camera lens. A dark box was then used to shield the patches from light during imaging to allow fluorescence to be detected.

High concentrations of lactate were used to induce the device because there would be a dilution effect as the sample enters the device and at this point the focus was to show that the sensors could produce a response within the patch. The lower panel of **Figure 5.13a** shows the constitutive expression of mRFP which is used to normalise the response to account for growth or plasmid copy number differences between spots. For all patches **Figures 5.13** there was a detectable mRFP expression for the three colonies of the sensor, and the negative control which only express mRFP that shows that the cells were growing within the patch. However no green fluorescence could be seen in the induced patches shown in **Figures 5.13b-d** and there was no statistically significant difference in the GFP/mRFP ratio when

compared to the uninduced patch. This could either be because the output is not strong enough to be detect or the cells are not responding.

A wearable device containing the tryptophan sensor was then constructed as this would have the highest GFP expression when no tryptophan is present. Testing this would allow it to be determined whether the lack of detection of GFP fluorescence for the lactate sensor was due to no response to the inducer or whether there is a response but it is just not detectable, shown in **Figure 5.14**.

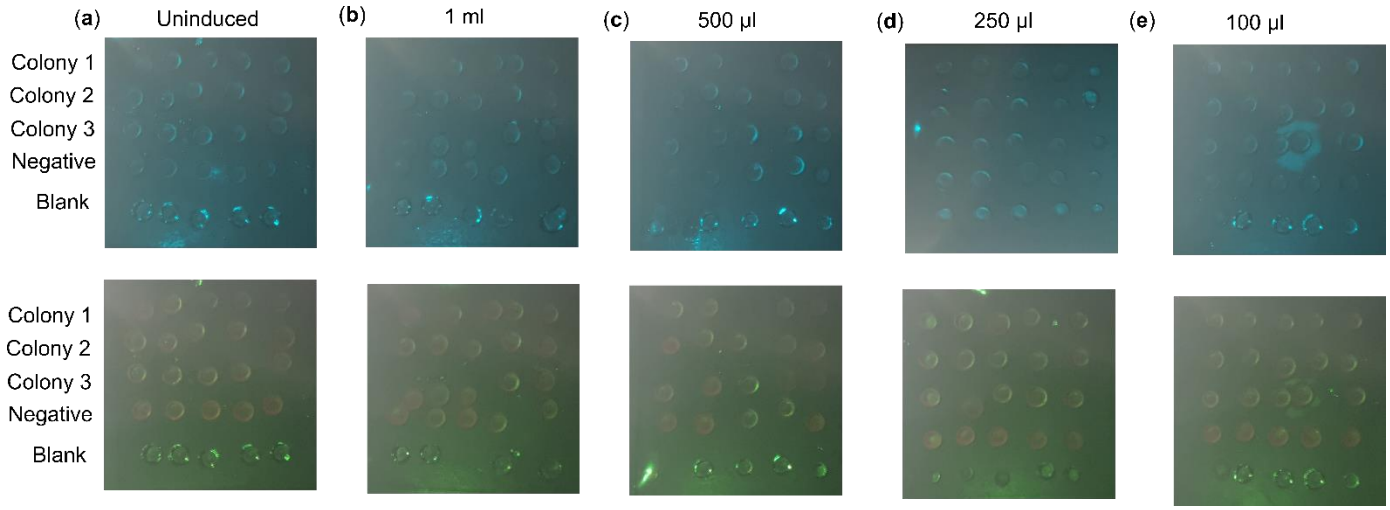


**Figure 5.14 Optimisation of sample volume requirement for wearable device containing the tryptophan sensor.** The images show the fluorescence of the patch which had been induced with different volumes of tryptohan . The upper panel shows the patch imaged to detect GFP and the lower panel shows the patch imaged to detect mRFP. Each row of the patches was laid out the same as as the first image. (**a**) shows the patch which was uniduced, with water added rather than tryptohan. (**b**) shows the patch where 1 ml 50 mM tryptohan was used to induce. (**c**) shows the patch were 500 µl 50 mM tryptohan was added and (**d**) shows the patch where 250 µl 50 mM tryptohan was added. (**e**) shows the patch where 100 µl 50 mM tryptophan was added. 10 µl spots were used to produce the patch. To image the green fluorescence filters were obtained from the Lee colour catalogue with Tokyo blue over the flash and Twickenham green over the camera lens. To image red fluorescence Twickenham green was placed over the flash and light red was placed over the camera lens. A dark box was then used to shield the patches from light during imaging to allow fluorescence to be detected. The images were 8 hours post-induction.

**Figure 5.14** again shows that no green fluorescence was being detected when using the phone. All of the patches in the upper panel showed no green

fluorescence even for the uninduced patch in **Figure 5.14a**, despite red fluorescence being detectable in all of the patches which confirms that the cells and sensor plasmid are in the patches. This suggests that the green fluorescence cannot be detected by the phone camera. When testing the statistical significance **Figure 5.14b and c** showed a statistically significant change in the GFP/mRFP fluorescence ratio with p-values of 0.000000227 and 0.00158 respectively but the mean ratio is higher in the induced compared to the uninduced, which is not the desired response. The mean for the uninduced was 1.044 whilst for the 1 ml patch it was 1.177. A strong GFP fluorescence should be detected in **Figure 5.14a** which it is not. So improving the brightness of GFP would be important for detecting the expected response.

An alternative form of GFP, sfGFP, and alternative green fluorescent proteins mNeonGreen derived from *Branchiostoma lanceolatum* yellow fluorescent protein (LanYFP) (Shaner et al., 2013) which are both brighter were tested along with the GFP. These were tested in the same way as the initial test in **Figure 5.11.** The outcome of testing these different green fluorescent proteins is shown in **Figure 5.15**.

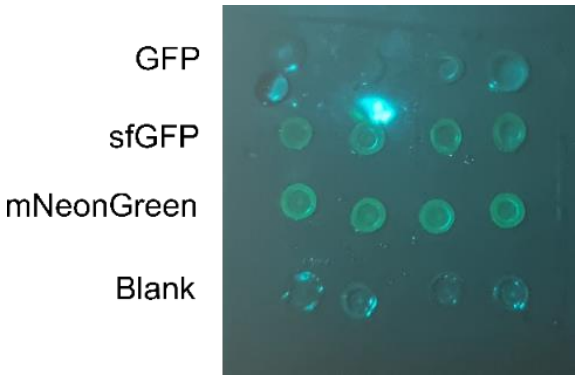


**Figure 5.15 Characterisation of alternative green fluorescent proteins in a hydrogel patch.** The image shows the green fluorescence from three different fluorescent proteins in 10 µl hydrogel spots used to make the patch. To image the green fluorescence filters were obtained from the Lee colour catalogue with Tokyo blue over the flash and Twickenham green over the camera lens. A dark box was then used to shield the patches from light during imaging to allow fluorescence to be detected. Patches produced and swollen overnight before excess media removed and then the patches were incubated for further 5 hours at 37°C.

Testing alternative fluorescent proteins showed that using a bright protein could improve the ability to detect the green fluorescence using the phone camera as shown in **Figure 5.15**. sfGFP in row 2 of **Figure 5.13** is much more visible than the GFP fluorescence, and row 3 show mNeonGreen was even brighter. The GFP row appeared to be less fluorescent than in the previous images taken in **Figure 5.11**, although this is likely to be due to the camera automatically adjusting its settings in the presence of the other brighter proteins.

As using a brighter protein was more clearly visible when taking images with the phone the whole cell biosensors were altered to replace the GFP with mNeonGreen. These new versions of the sensors were then tested within the wearable device. The outcome of testing the lactate sensor is shown in **Figure 5.16**.

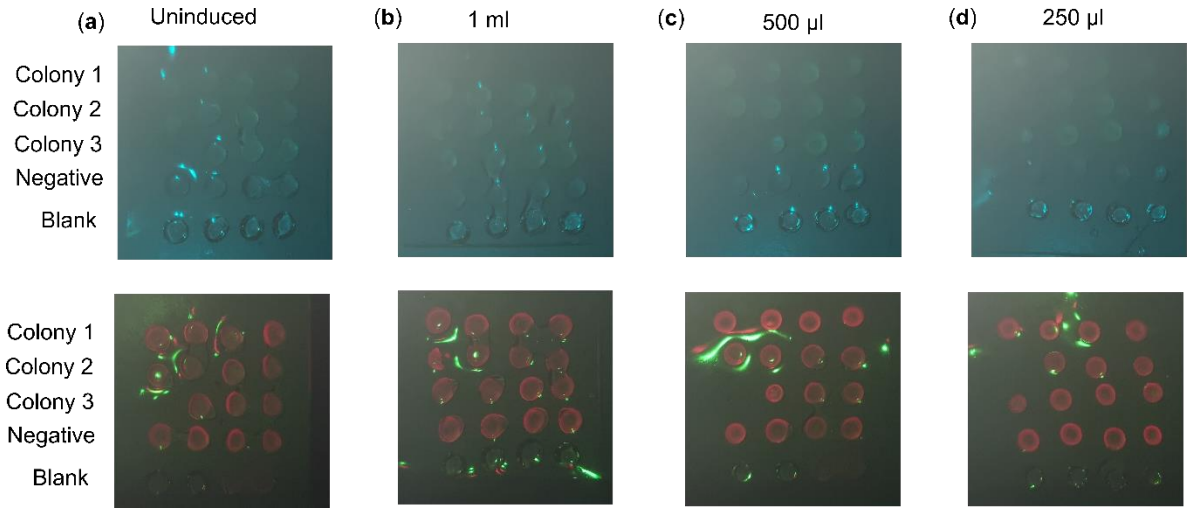


**Figure 5.16 Optimisation of sample volume requirement for wearable device containing the optimised lactate sensor.** The images show the fluorescence of the patch which had been induced with different volumes of lactate. The upper panel shows the patch imaged to detect mNeonGreen and the lower panel shows the patch imaged to detect mRFP. Each row of the patches was laid out the same as the first image. (**a**) shows the patch which was uniduced, with water added rather than lactate. (**b**) shows the patch where 1 ml 1 M lactate was used to inducer. (**c**) shows the patch were 500 µl 1 M lactate was added and (**d**) shows the patch where 250 µl 1 M lactate was added. 10µl hydrogel spots were used to generate the wearable device. To image the green fluorescence filters were obtained from the Lee colour catalogue with Tokyo blue over the flash and Twickenham green over the camera lens. To image red fluorescence Twickenham green was placed over the flash and light red was placed

over the camera lens. A dark box was then used to shield the patches from light during imaging to allow fluorescence to be detected. The images were taken 8 hours after induction.

Again the red fluorescence was clearly detectable in **Figure 5.16** showing that the cells and the plasmid containing the sensor was present in all the hydrogel spots on the patches. In the upper panel for **Figure 5.16c** there was potentially some green fluorescence visible in the three rows containing the sensor compared to **Figure 5.16a** which was uninduced and should not have any green fluorescence. When comparing the data there is a statistically significant difference in the mNeonGreen /mRFP ratio with a p-value of 0.0455 but the mean of the uninduced patch is higher at 1.175 whilst for the patch induced with 1 ml it was 1.11 which implied there is not a response to lactate. The fluorescence is also still very weak. A lot more optimisation would be needed to be able to generate enough of a response that would allow a response curve for detection at smaller concentrations of lactate to be determined.

To establish if the weakness of fluorescence was due to the response to lactate only being weak or if this is still a detection issue, the tryptophan sensor was again tested using mNeonGreen, shown in **Figure 5.17.**

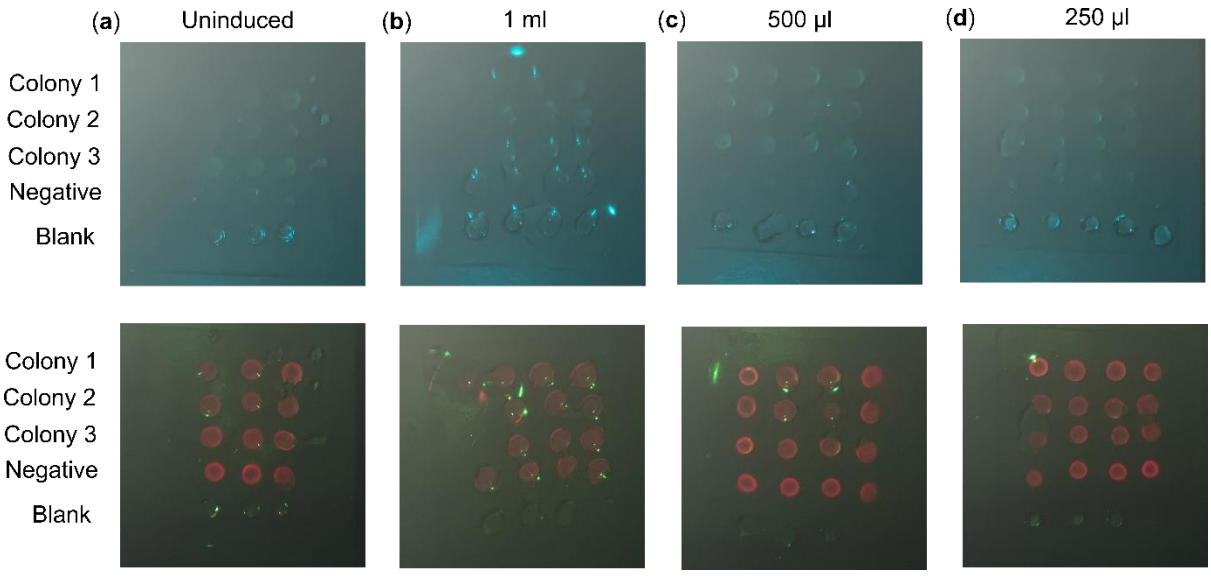


**Figure 5.17 Optimisation of sample volume requirement for wearable device containing the tryptophan sensor.** The images show the fluorescence of the patch which had been induced with different volumes of tryptohan . The upper panel shows the patch imaged to detect mNeonGreen and

the lower panel shows the patch imaged to detect mRFP. Each row of the patches was laid out the same as as the first image. (**a**) shows the patch which was uniduced, with water added rather than tryptohan. (**b**) shows the patch where 1 ml 50 mM tryptohan was used to inducer. (**c**) shows the patch were 500 µl 50 mM tryptohan was added and (**d**) shows the patch where 250 µl 50 mM tryptohan was added. To image the green fluorescence filters were obtained from the Lee colour catalogue with Tokyo blue over the flash and Twickenham green over the camera lens. To image red fluorescence Twickenham green was placed over the flash and light red was placed over the camera lens. A dark box was then used to shield the patches from light during imaging to allow fluorescence to be detected. The images were taken 8 hours after induction.

For the tryptophan sensor in **Figure 5.17** the green fluorescence from mNeonGreen was not strong in any of the images including the uninduced device in **Figure 5.17a**. This suggests that the ability to detect the green fluorescent protein is still an issue, no statistically significant result was seen in the mNeonGreen/mRFP ratio between the different induction volumes and uninduced as well.

### 5.1.2 Aptamer based wearable device

The TAMRA dye which is involved in the formation of the FRET pair which allows the interaction of the aptamer with potassium ions to be detected has its emission peak at a different wavelength to mRFP, mRFP has peak excitation and emission wavelengths of 584 nm and 607 nm (Campbell et al., 2002) whilst for TAMRA this is 559 nm 583 nm respectively (https://eu.idtdna.com/site/Catalog/Modifications/Product/1095). So the red filter light red which is used over the camera for mRFP may not work to detect the emission from the aptamer based sensor. Therefore this filter was tested along with an alternative filter dark amber from the Lee colour catalogue which allows through light of a wavelength closer to the emission wavelength of TAMRA as dark amber has a transmission peak around 610 nm and above (https://leefilters.com/colour/022-dark-amber/). The ability to detect the response using these two different filters is shown in **Figure 5.18**.

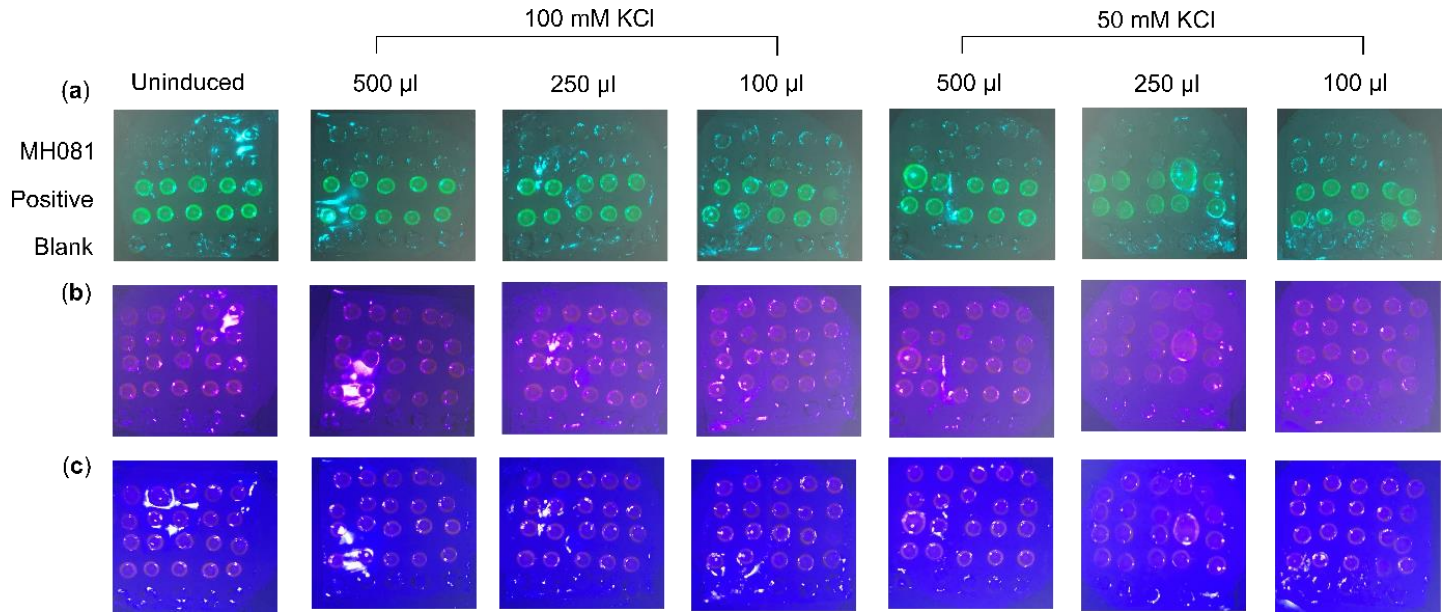


**Figure 5.18 Optimisation of the filter pairs for fluorescent detection of the potassium aptamer.** The images show wearable devices containing the potassium aptamer when imaged with different filter pairs to detect the dyes and FRET pair on the aptamer. MH081 is the potassium aptamer and MH101 shows the positive control aptamer with only the FAM dye on the 5' end and blank shows the hydrogel spot containing nothing. (**a**) shows the images when taken with the blue filter on the flash (Tokyo blue) and the green filter over the camera lens (Twickenham green). (**b**) shows the images when taken with the blue filter on the flash (Tokyo blue) and the red filter over the camera lens (light red). (**c**) shows the images when taken with the blue filter over the flash (Tokyo blue) and an alternative red filter (Dark amber). 10 µl hydrogel spots were used to produce the wearable device. A dark box was placed over the patches for imaging to shield them from light and allow the fluorescence to be detected. The images shown were taken 5 hours post-induction.

**Figure 5.18a** shows that when the patch is imaged using the filters for GFP the positive control has a strong output, which was the expected response as this oligonucleotide only has the FAM dye and this responds at the same wavelengths as GFP. If the FRET pair has not been formed then it would also be expected that green fluorescence would be seen in the top two rows of the patch such as for the uninduced patch. This could not be seen in any of the patches in **Figure 5.18a.** Potentially this could be due to the brightness of the positive control reducing the camera sensitivity. **Figure 5.86b** shows the patch imaged for detecting the output of TAMRA through the FRET pair using the light red filter which is used when imaging mRFP. It was not expected that the positive control would show fluorescence with this filter pair

because it should not be emitting light at the right wavelength. However the colour filters are not as specific as the laboratory grade filters used in laboratory equipment so other wavelengths could also be getting through the filter, the spectra for the filters in shown in **Appendix 3**. This is not necessarily an issue if the output for the sensor can be detected. Fluorescence can also be seen in the top row for the sensor. However, this appears to be the same in the induced and uninduced patches so is not necessarily due to a sensor response but because the FAM dye fluorescence is showing through. Using the alternative red filter Dark amber is shown in **Figure 5.18c.** Again the fluorescence could be seen in the positive control so some of the fluorescence from the FAM dye was leaking through. Fluorescence could be seen in the row of sensors containing spots but it did not appear to change between the induced and uninduced sensors which suggests that the fluorescence from the FAM dye is being detected rather than the formation of the FRET pair in response to potassium. When looking at the ratio between red and green fluorescence to look at the FRET pair, statistically significant changes were seen when using both of the different red filters compared to uninduced. The light red filter was chosen for future experiments to reduce the number of filters required to carry out imaging.

In the cell-based sensor wearable devices there seemed to be a large loss of sensitivity and this could also be an issue for the aptamer sensor device. So the initial DNA aptamer sequence was also tested in the device because this had a higher sensitivity to potassium. The function of this aptamer in the wearable device is shown in **Figure 5.19**.

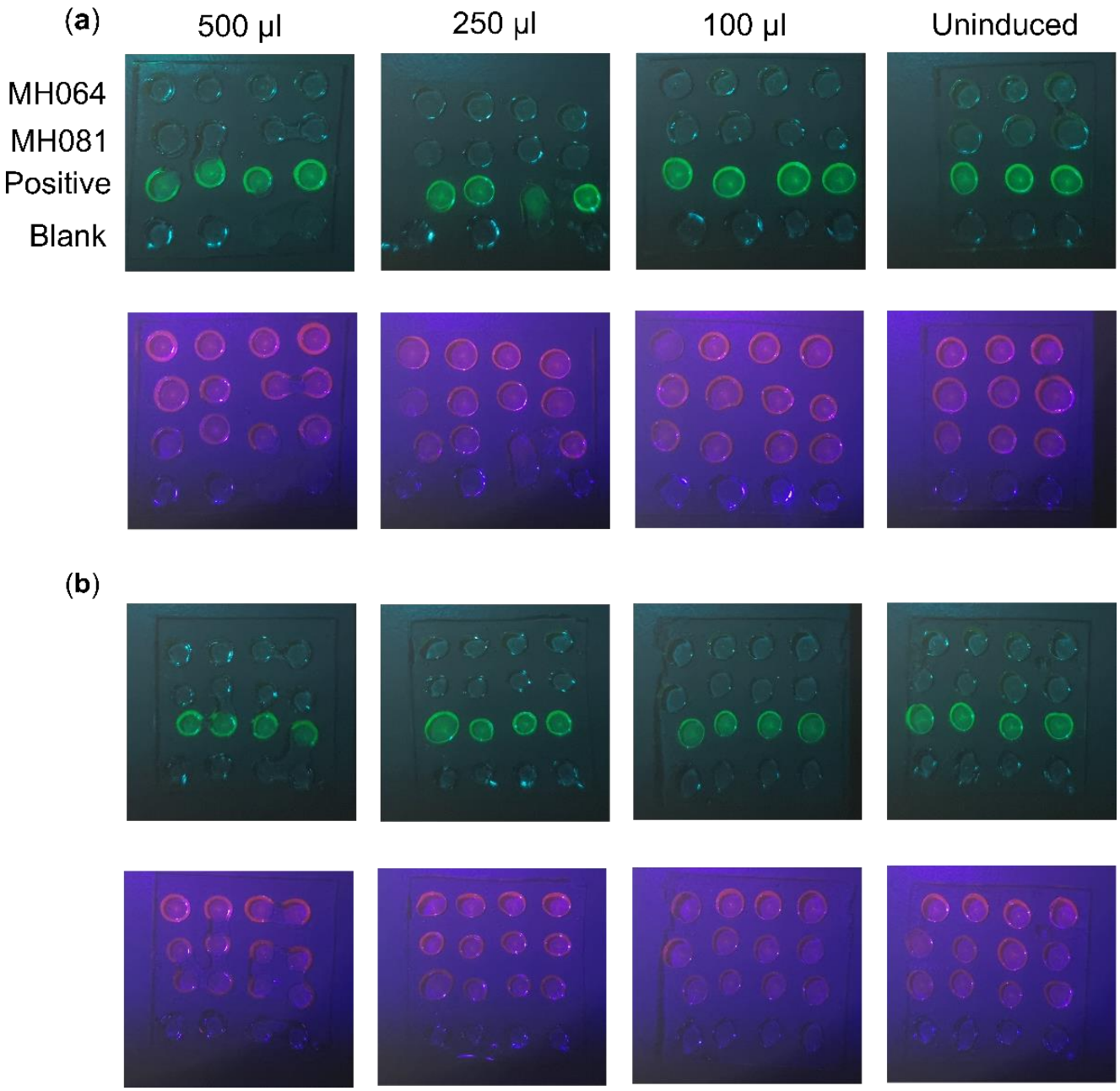


**Figure 5.19 Characterisation of different potassium aptamers with the wearable device.** The images show the fluorescence of the aptamers within the device. The upper panel shows the patches imaged with the blue filter over the flash (Tokyo blue) and the green filter over the camera (Twickenham green) and the lower panel shows the patch imaged with the blue filter over the flash (Tokyo blue) and the red filter over the camer (light red). A dark box was placed over the patches for imaging to shield them from light and allow the fluorescence to be detected. 1 M potassium chloride was used to induce the patches at the volumes shown above the images. (**a**) shows the original potassium aptamer (MH064) and the optimised potassium aptamer (MH081) in a wearable patch using 15 µl spots. (**b**) shows the original potassium aptamer (MH064) and the optimised potassium aptamer (MH081) in a wearable patch using 10 µl spots. The images are taken 6 hours after induction.

The two spot sizes 15 µl and 10 µl which had been shown to optimal when testing the cell-based devices were tested, shown in **Figure 5.19**. The far-right image in **Figure 5.19a** shows the 15 µl spot size in the uninduced patch for the row containing MH064. It appears that a faint green fluorescence can be seen and this suggests that some response is occurring, because when uninduced this should have the highest fluorescence from FAM because the FRET pair is not being formed so green fluorescence should be detectable. When looking at the FRET pair formation in the lower panel of **Figure 5.19a** the fluorescence from the MH064 row appears to be brighter than the positive control row (Positive) for the patch with 500 µl KCl added. This suggested that there is a response to the potassium added to the patch. This also appeared to also be true for the MH081 row. In **Figure 5.19b** these changes in fluorescence could be seen in MH064 but with less strength than in in 15 µl spots but no fluorescence could be seen for the MH081 row.

The images were analysed with ImageJ to confirm what could be seen visually and that there was a difference in the FRET fluorescence ratio of the two images. For the uninduced patch of 15 µl spots the ratio is 1.19 (farthest right images) and for the patch induced with 500 µl it was 1.31, the full table of values obtained using ImageJ is give in **Appendix 3**. There is a change in the values but it is so small that it cannot clearly be said this is a true response and more testing and optimisation would need to be carried out. This is not statistically significant when compared to the uninduced but the p-value is much smaller compared to the other induction volumes where visually there did not seems to be a response. The p-values were 0.120, 0.996 and 0.996 for 500 µl, 250 µl and 100 µl respectively.

## 5.5 Phone App and imaging set up

The aim for the wearable device is that outputs could be analysed without using a computer and separate software. So work was started to develop an App which would be capable of taking the image, recognising the spots within

the wearable device and extract the RGB values. The RGB values gives the intensity of the pixels in terms of red, blue and green to allow fluorescence to be analysed.

### 5.5.1 App design

**Figure 5.20** Shows the schematic design of an App which could be developed to automate data capture and analysis.

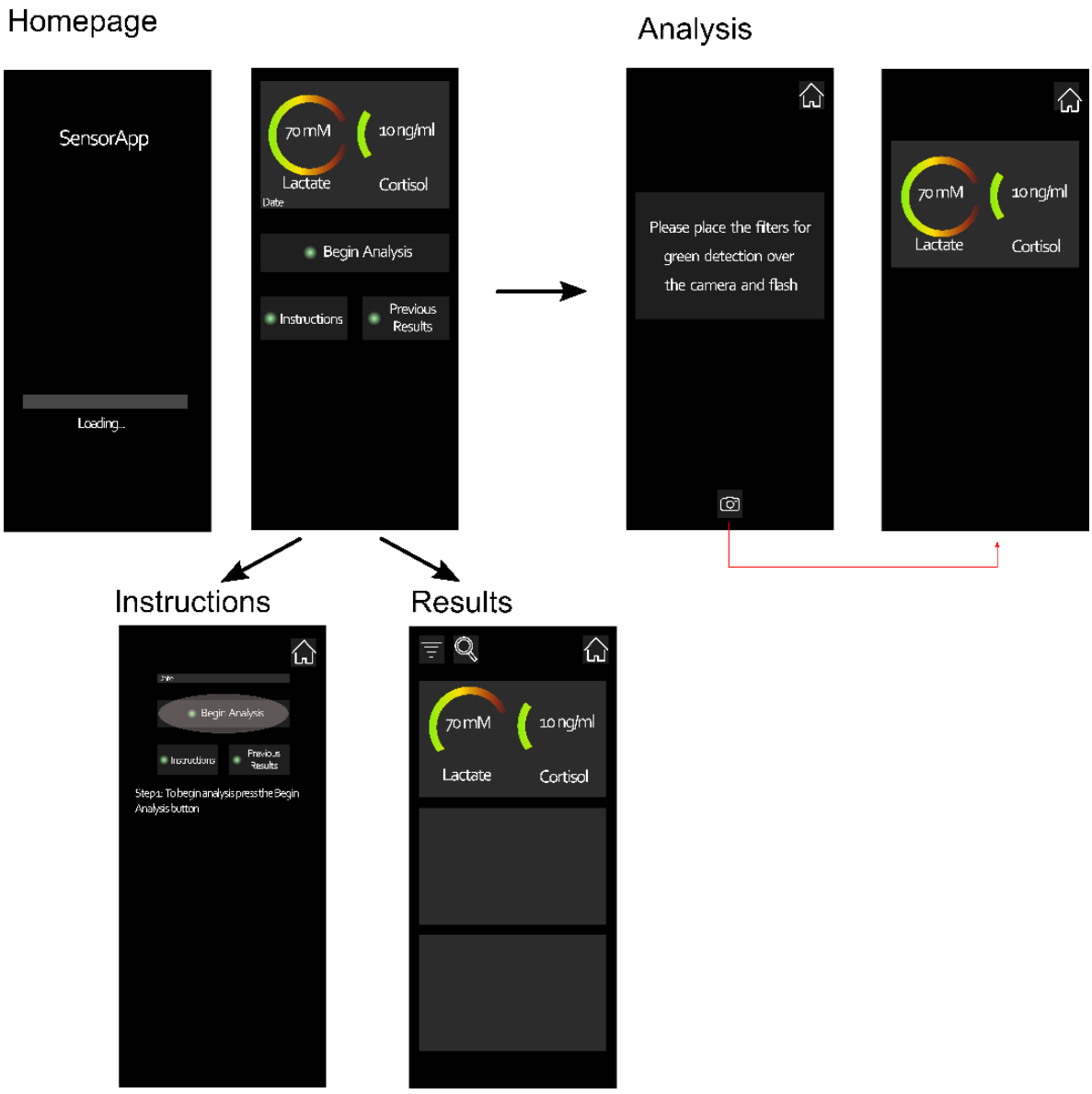


**Figure 5.20 Schematic of App design for automation of response detection.** The schematic highlights the design of the App including the pages which would be present along with the functionality

of the App. The black arrows indicated the different pages that can be opened through clicking the buttons of the app. The red line indicates an automatic change onto a new page when going through the analysis steps.

The App was designed to open on a homepage screen which would display the last response taken with the date of the result at the top of the screen. Below this would be three different buttons; one to start a new analysis, one to look at the instructions for carrying out analysis and looking at the stored results, and one button to take the user to all the previous results taken by the App.

On pressing the **begin analysis** button the user is taken to a screen which reminds the user of the correct filters for imaging the fluorescence of the sensor and a **camera button** to take the image. Once the first image is taken the user is shown another message to change the filters then to image the second fluorescent protein, such as the mRFP, which acts as the control before the **camera button** can be pressed again to activate the camera. Once the images have been taken the analysis is carried out in the same manner using ratios as used for the analysis in the laboratory and the results would be automatically displayed.

Initial work was carried out to develop this app and the code is give in **Appendix 3**. The outcome of using this App is shown in **Figure 5.21**.

(a)

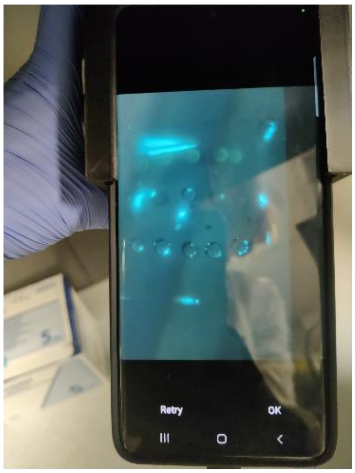


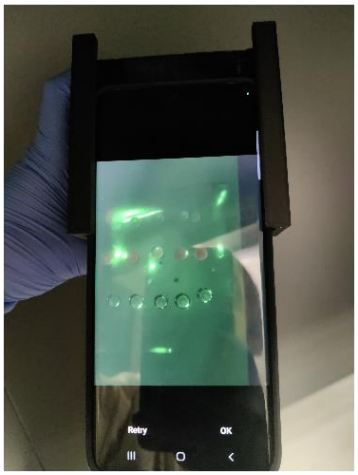


(b)

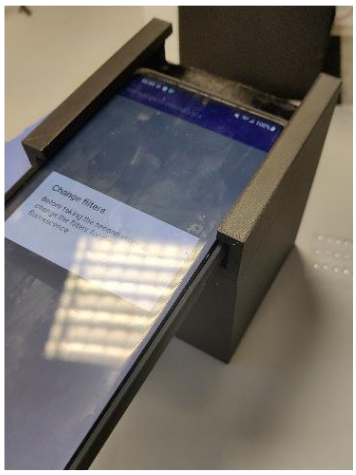


(c)

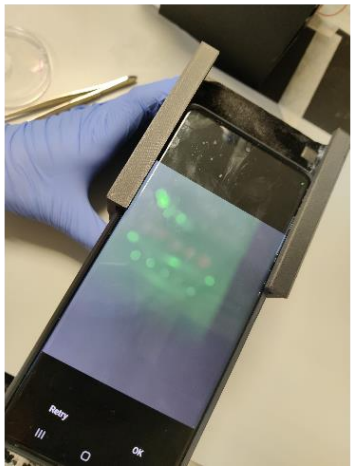


**Figure 5.21 Images of initial app in use.** The photographs show snapshots of the App in use at different points of the analysis method. (**a**) shows the images for the fluorescence taken by the App. (**b**) shows one of the pop-up messages to ensure the correct filter usage. (**c**) see shows a poor picture outcome with the App.

Using the App showed that images which displayed the fluorescence could be obtained using the App, shown in **Figure 5.21a**. **Figure 5.21b** shows that the App was capable of reminding the user about how to carry out the analysis and ensure the correct analysis. However, this test sequence also highlighted some issues with the App, **Figure 5.21c** shows that the focus of the camera could not be manually controlled whilst using the App which resulted in many out of focus images. The App in its current form also used fixed positions for where the pixel intensity would be extracted for the

fluorescence detection and as a result if the spots are not in the correct positions the analysis would not be detecting the output of the sensors. As a result of these issues, Ishan Mishra, a student in computer sciences, developed an alternative version of the App which could automatically detect the spots. This new version of the App took continuous images of the patch and used computer vision to automatically detect the spots. First an image with no filters for fluorescence was taken to determine the number of spots and their position within the patch, currently the user is required to give the number of rows and columns in the patch to aid in this. Then the first image for detecting fluorescence was taken. The red fluorescence would be detected first as it is a control and would allow any spots that did not work to be removed from the data sets because if no red fluorescence is detected then either the plasmid had mutated or been lost or the cell were not growing. Then the green fluorescence would next be detected, at which point the ratio between green and red would be determined in the same way as was done in the initial characterisation elements. To check the ratio was calculated using the red and green values from the same spots the position of the spot in the image determined from the first image was compared to the positions in the later images and if the difference in the x and y values was too large it is discounted. This currently cause challenges in extracting the red and green values because ensuring the same position after changing the filters in difficult.

### 5.5.2 Lighting optimisation

Whilst optimising the App, alternative sources of light to excite the fluorescent proteins and dyes to allow a response to be detect from the sensors were examined. As the green fluorescence could still not be strongly detected for any of the sensors in response to the biomarker in question, potentially the light from the camera flash was not strong enough at the correct wavelength for when the green fluorescent protein is not as highly expressed as when there is a strong constitutive promoter. Current phone flash LEDs do not emit

a large amount of light around 400 nm (Kimme et al., 2013) which is where light emissions are required for exciting green fluorescent proteins and this could be one reason for the lack of green fluorescence being detected shown in **Figure 5.22**.

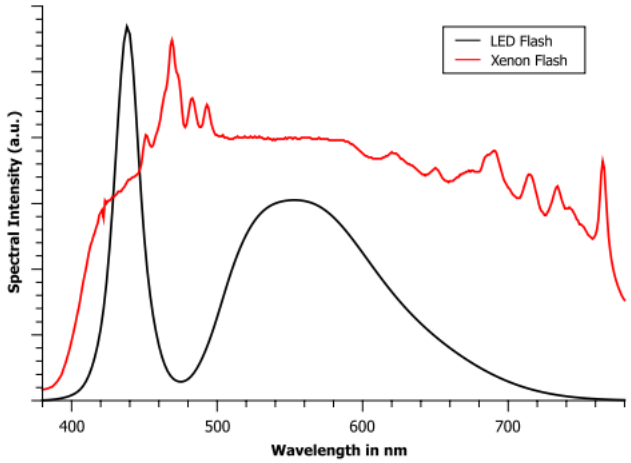


**Figure 5.22 Light spectra of LED phone flash.** The figure shows the spectra of light wavelengths found in a modern LED flash used in smartphones compared to a traditional Xenon flash. The figure is reproduced from (Kimme et al., 2013).

LEDs with a controllable light output were added to the dark box and were then controlled by the App via Bluetooth to see if this improved the fluorescence detection. Work in this area is still ongoing as further optimisation in the App's ability to detect the spots needs to be made before testing can begin.

## 5.6 Discussion

Work into encapsulation of the sensors showed that they can function within the hydrogel although the response was weakened compared to the response when in liquid format. When testing the constitutive fluorescent proteins, altering the chain length and concentration of the PEGDMA hydrogel had a large impact on the ability to detect fluorescence showing that longer chain lengths were better and as was a lower concentration. A hydrogel composition that worked for cell growth and fluorescence was identified and using

PEGMDA chain length 1000 at 50% w/w concentration was used for the remaining experiments. The encapsulation with this composition was not sufficient to ensure that the genetically modified organisms are kept separate from the environment and ensure no accidental release into the environment. In the UK there is not a defined level of escape considered acceptable but is considered rather on a case-by-case basis (Public General Acts, 1990, Statutory Instruments, 2002, Statutory Instruments, 2014). In the USA the NIH has set the guidelines for the level to be below $1x10^{-8}$ cells to survive when in conditions that mimic the environmental conditions in cell escape (Biotechnology Activities, 2019). So this would be a good measure to use. Using one or two washes did not significantly alter the number of cells that were left present in the liquid media after the hydrogel spot was left in medium overnight, suggesting leakage out of the hydrogel rather than just surface removal. This would therefore be an issue for the wearable device, but other methods for biocontainment could be looked at, such as kill switches (Chan et al., 2015, Stirling et al., 2017) although these are not specifically recognised in legislation. Altering the composition of PEGDMA also had an impact on the fluorescence and in future work the composition could be further improved by testing more concentrations or through a combination of different chain lengths (Rutz et al., 2015, Yuk et al., 2016, Fan and Gong, 2020).

Even in the optimised hydrogel composition the response from the whole cell biosensors was reduced. For the whole cell sensors within the identified hydrogel the reduced output could potentially be because the cells are not growing as well within the hydrogel compared to liquid culture. When only testing the hydrogel, this was not a problem because it could be mitigated by adjusting the conditions of the microplate reader. But in the wearable patch this weakened response could be an issue because at this point a camera phone will be used to detect the response and this will be less sensitive than the microplate reader.

Altering the composition of the set up for encapsulation did improve the response and certain factors seemed to have more effect than others further

exploration could improve the response further. Curing of the hydrogel requires UV light so it is likely that some cells are killed in this process. A 365 nm UV wavelength was used for crosslinking rather than 302 nm or 265 nm as these two wavelengths would both have a higher lethality to the bacterial cells due to their higher energy (Tyrrell and Peak, 1978, Vermeulen et al., 2008). However, it is still likely that some cells will die during crosslinking. Therefore, some recovery time will be important in allowing the cells to grow to a high enough density to be able to respond after the curing which was seen in **Figure 5.3a** but speeding the crosslinking to reduce exposure could also help. **Figure 5.3c** shows that increasing the concentration of the photo initiator did not improve the response and that lower concentrations are actually better. This is most likely due to the impact of the photo initiator itself on cell viability (Williams et al., 2005). Using different photo initiators could also help the ability of the cells grow and produce an improved response in the hydrogel as Irgacure 2959 has also been shown to inhibit cell growth. Irgacure 2959 is frequently used as the photo-initiator to crosslink hydrogels. However testing of different initiators suggests that alternative chemicals or a combination can be used to speed the reaction which would reduce the time of the UV treatment required for crosslinking and potentially reduce lethality (Han et al., 2020). The wavelength of 365 nm is not ideal to trigger the reaction for Irgacure 2959 but combination with VA-086 which is activated much better at this wavelength but has other undesirable characteristics and can then trigger the Irgacure 2959 to speed up the reaction (Han et al., 2020). The solubility of Irgacure 2959 in water is also limited which could be why using higher concentrations did not improve the response of the sensors as these higher concentrations were not actually dissolving into the PEGDMA and altering the speed of crosslinking. The final condition tested was the volume of cell media used to swell the hydrogel, shown in **Figure 5.3d**. There seems to be an optimal volume, if it is too low the biosensor does not respond as well, most likely because it does not provide enough nutrients for the cells to grow well. Too much media also reduces the response of the biosensor, potentially because it results in more cells ending up in the media

and being lost when the excess media is removed as has been already seen the hydrogel does not fully prevent cell loss.

Currently when producing the spots the final crosslinked spot sticks out from the patch noticeably and this is not ideal because it would impact how well the patch could stick to the individual wearing the device. But this could also affect the diffusion of the inducer into the patch. Potentially altering the set up to flatten the hydrogel before crosslinking would help ensure that this does not impact the contact of the patch to the individual and it would also increase the surface area of the spot compared to the volume. This would improve diffusion between the sample and spot which could help to improve the response.

For the potassium aptamer a reduced output did not seem to be an issue in the way it was for the whole cell sensors. This is probably because the biggest impact on the whole cell sensors was likely low growth of the cells. However for the potassium aptamer its concentration was highly important as higher concentrations saw increased basal fluorescence. The increase in basal fluorescence is likely due to the increased concentration of dyes present within the hydrogel because of the higher concentration of aptamer being used, leading to FRET pairs being generated just by the dyes bumping into each other within the hydrogel rather than from specific folding in response to potassium.

Initial tests using the cell-based sensors in the wearable device showed that GFP is not well detected by the phone. This is thought to be partly due to the wavelengths of light which are emitted by the camera phone flash not being well suited to exciting the GFP molecules (Kimme et al., 2013). As the GFP which had been used initially in the development of the sensors was not the brightest version possible, other green fluorescent proteins which would have a brighter output were tested and this did appear to improve the response. There was some green fluorescence detected when testing the sensors using the brighter proteins but there was still not a good and strong response to the inducer. Improving the imaging set up for the phone and adding an

alternative light source had the potential to help by better exciting the fluorescent protein. This has not yet been fully tested and work into allowing the phone to automatically detect and recognise the spots on the patch is still ongoing.

However the potassium aptamer also did not show a good response although the potential issue with the light source did not appear to be such an issue as the FAM dye could be easily detected in the positive control suggesting that there is another issue affecting the response from the sensors in the patch.

# 6. Summary and future directions

The use of wearable devices in non-invasive biomarker monitoring has become a large area of research due to the advantages their use can have in patient compliance, for allowing passive monitoring and the ease of monitoring outside of a medical setting. They would allow any analysis to be carried out without the requirement for a centralised testing lab which would make testing faster and more accessible. This approach has been shown to reduce costs to healthcare providers and early and frequent testing can reduce negative outcomes in patients (El-Osta et al., 2017, Goldstein et al., 2019). Sweat has recently become a key area of interest as a source of biomarkers due to its ease in sampling and the high number of biomarkers present (Baker, 2019b, Dunstan et al., 2016, Heikenfeld et al., 2019, Verde et al., 1982). So sweat has also become the focus of wearable devices because they could achieve passive sampling using easy to produce, comfortable devices. Although the relationship between blood and sweat concentrations of biomarkers still needs to be studied.

This project aimed to show the suitability of using synthetic biology approaches to build biosensors and to develop a wearable device suitable for sweat monitoring. The work in this project has shown that biosensors using a range of sensing mechanisms can be developed for specific biomarkers found in human eccrine sweat. The encapsulation work has shown that these biosensors can be encapsulated and retain their function, but there is a large amount of sensor optimisation required before these sensors are suitable for commercial applications. The overall work flow of the project is shown in **Figure 6.1**.

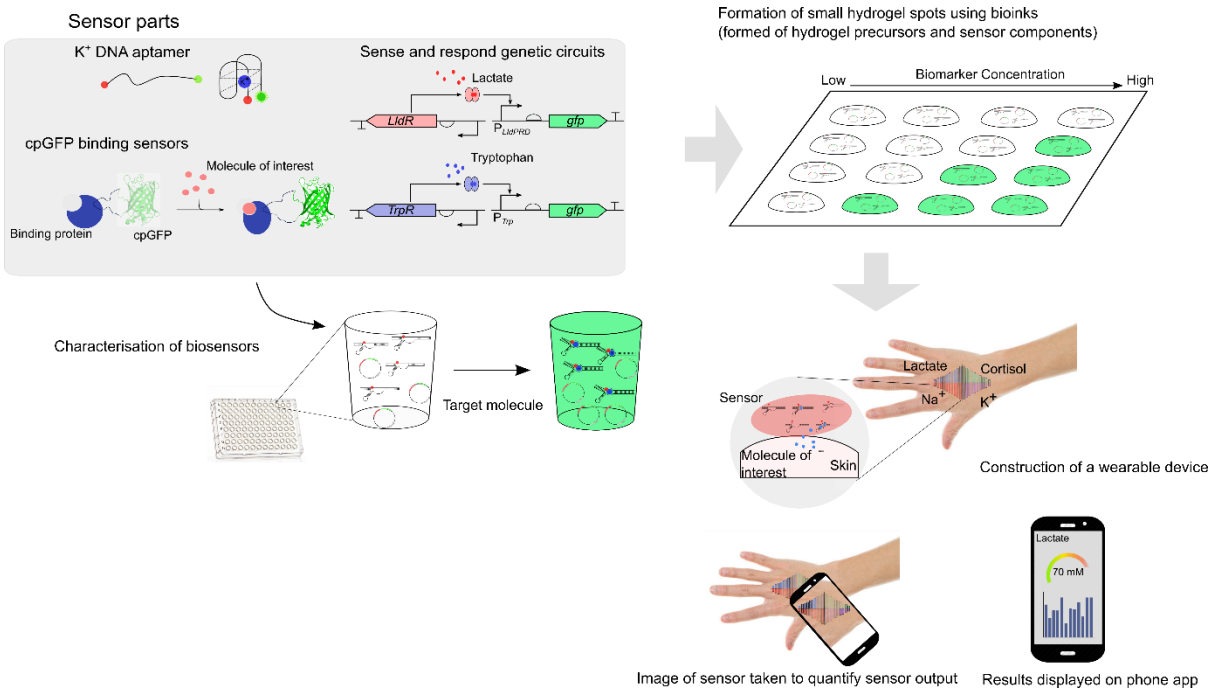


**Figure 6.1 Methodology to generate a biosensor wearable device.** The figure highlights the approach to generate optimised biosensors, initially using a microplate assay to detect fluorescence during optimisation. Following this the biosensors are transferred into hydrogel and further optimisation is carried out before using these hydrogel sensor combinations (bioinks) to generate the wearable device. The wearable device can be imaged using a phone and App to analyse the output and store data.

Initially whole cell biosensors were the focus of the development of biosensors for human biomarkers in sweat (Chapter 3). Two whole cell biosensors were successfully optimised to detect the concentrations of lactate and tryptophan in human sweat. The work also looked at developing whole cell biosensors for steroid hormones. Although some initial positive results were seen for cortisol, the limited uptake of steroid hormones in gram negative bacteria (Plésiat and Nikaido, 1992) suggests that whole cell biosensors would not be the best approach for detecting human steroid biomarkers. After also considering the biosecurity concerns that have limited the use of whole cell biosensors commercially, which is highlighted by the encapsulation work in Chapter 5, alternative biosensing approaches would be a more promising area to explore.

Following on from the whole cell approach, further sensors where designed and optimised using binding molecules to allow for cell free detection

(Chapter 4) and two different approaches were investigated one using DNA and the second proteins. Cell-free biosensing also has the advantage that it could improve sensitivity and response time, as whole cell sense and respond genetic circuits frequently rely on transcription and translation which requires hours to respond. When using a wearable device to look at biomarker levels and detect negative changes speed would be highly important.

The DNA aptamer showed a good strong response and fast detection time, within minutes, which shows that it is a good potential approach. But the requirement for specific conditions that aptamers often have could pose a problem in a device where conditions are less controlled and where changes in conditions can often affect the affinity to the target (Wan et al., 2022). The potassium aptamer showed the ability to tolerate some changes in the conditions it was exposed to, different pHs and temperatures, without preventing the ability of the aptamer to respond to potassium. This was encouraging but it would not necessarily be the case for other aptamers. So each aptamer would need to be separately tested.

Using binding proteins as the sensing method was then explored by adding a circularly permuted fluorescent protein into the protein to allow the binding of the biomarker to be detected. This approach allowed proteins which bind cortisol and testosterone to be engineered which would allow more sensitive detection because this avoids the issue of transport through the cell wall or membrane (Plésiat and Nikaido, 1992). This would also avoid the requirement to use mammalian parts or antibodies which have their own disadvantages in the development of biosensors (Baker, 2015). These two sensors are not yet able to detect the physiological concentrations of cortisol and testosterone in human sweat but the optimisation carried out to date shows that this method can be optimised to increase the fluorescent output of the sensor and its sensitivity.

The initial work into using mutagenesis to improve the response of the protein cpGFP sensors showed that for cortisol this approach could generate

mutants with improved characteristics. Mutant versions with improved characteristics could not be identified for the other sensors. As only a very small number of the possible mutations of the cpGFP sensors were tested, further testing of more mutations and combining with those mutations which had been shown to improve the response could generate mutants which further improve the response. Further testing and combining could also find mutants which improved the output for the other two cpGFP sensors for testosterone and histamine which were developed. In this project cell-free lysate was used to express the protein with these lysates being used to detect the biomarker. The cell-free reactions and output from the sensors showed high variability between different tests which would be a large problem in a wearable device where the response between different tests needs to be highly similar in terms of output and response time. Potentially switching to purifying the protein and maintaining the proteins within a buffer could remove this variability because the components would be far more defined and controlled. Further work to optimise the cell-free transcription translation systems could also be undertaken as large amounts of work in the literature have been carried out to reduce the variability between cell-free batches and to optimise the buffers and energy solutions to the specific requirements of the reaction (Dopp et al., 2019b, Rhea et al., 2022, Banks et al., 2022a). This cell-free cpGFP method of biosensing is highly promising. The results achieved were encouraging suggesting that the required sensing characteristics could be achieved. This is important because this method could be used as a general approach to develop cell-free biosensors that do not rely on transcription and translation, so should have a fast response time. Beyond the different approaches which could be taken to improve the current sensors that had been explored, expanding on the range of biomarkers which could be detected using the binding molecule with cpGFP approach would be useful in order to show that it is applicable more generally. Overall, the results of developing molecular sensors were encouraging and show that this approach is a good way to generate biosensors of human eccrine sweat. A particular advantage of the cpGFP sensor approach is that the sensors would

be able to take multiple measurements from one device which is a highly desirable characteristic for a wearable sensing device.

Having developed multiple sensors which were capable of detecting their biomarker at the physiologically relevant concentrations and with a high specificity to their biomarker, work was carried out to determine if these sensors could be used within a wearable device (Chapter 5). Several methods for encapsulating biosensors within hydrogels have been studied due to this being a large area of interest in research currently. However this has frequently focused on using example biosensors such as for IPTG or arabinose that are well characterised and have a strong response, which is good when studying methods of developing methods to generate wearable device (Liu et al., 2018b, Liu et al., 2017). But this would not necessarily translate to sensors for biomarkers. The first step was to look at encapsulation. The conditions for generating the hydrogel were optimised in order to minimise the impact of the hydrogel on the sensor output. A decrease in the maximal output was seen for whole cell sensors. For the potassium aptamer altering the concentration of the aptamer within the hydrogel could mitigate the decrease in the maximal output. This further suggests that pursuing cell-free methods would be the best approach. However more work could be carried out to further improve the whole cell biosensors within the hydrogel, as recent work on the photo-initiators have shown that using a combination of different photo-initiators can improve the crosslinking efficiency and reduce the time needed to expose the hydrogel to UV which could improve the cell survival (Li et al., 2017a, Nguyen et al., 2019, Han et al., 2020). But in the future work on generating the wearable device whole cell sensors would not be the focus because the molecular sensors had other advantages making them a better focus.

As the hydrogel optimisation allowed the sensors to function within hydrogel spots work to produce wearable patches was carried out and these were tested to see how the sensors would respond within a wearable device and whether responses can be recorded using a smartphone. There is a large

volume of literature on the development of wearable patches which was used to direct the development of the patch. The backing was produced using silicone which allows the use of adhesives to be avoided and this has advantages in reducing skin irritation which would be important for long term wear (Gisin et al., 2017). A key issue in developing the wearable device was the ability to detect green fluorescence because a green fluorescence response within the relevant concentration ranges could not be achieved from the sensors. Altering the light source would allow the excitation wavelengths at a higher intensity to be achieved because the necessary wavelengths are only weakly present in a phone flash (Kimme et al., 2013).

However this would add significant bulk to the dark box which is not ideal for a device that should be easy and simple to use. Alternatively other fluorescent proteins of different colours could be used as the output, since for mRFP a very strong output showed when using the phone to image. From the spectra of expected light wavelengths in a phone flash blue fluorescent proteins would also be an appropriate choice. This would be suitable for all sensors, as the output gene can be easily switched out for the whole cell biosensors and alternative circularly permuted fluorescent proteins exist which could be used to replace the cpGFP (Nagai et al., 2004, Kawai et al., 2004, Mehta et al., 2018). The switch for the aptamer would be simple as it would be a case of selecting different fluorescent dyes which could form a FRET pair. The other key area of future work would be to see if the diffusion of biomarkers into the patch could be improved. Fluorescein studies have been used in other work to determine how molecules move in the hydrogel (Hettiaratchi et al., 2018). These studies could be carried out for the hydrogel spots of the wearable device to see how well this is occurring. An initial approach to improve diffusion could be to flatten the spots. This would have several advantages for the wearable device. This would allow better contact between the wearable device and the individual’s skin which would be important for the device’s accuracy. This would also increase the surface area to volume ratio which should improve the diffusion of biomarkers into the device. Work into improving the hydrogel could also be carried out.

Different combinations of chain lengths or different chemicals to produce the hydrogel could be tested, as combinations of materials have been shown to improve hydrogel characteristics in other work (Liu et al., 2018b, Cellesi et al., 2002, Yang et al., 2013).

Overall, this work shows that both whole cell and cell-free biosensors can be developed to meet the required sensitivity for detecting biomarkers found in human sweat. The development of single protein based sensors provides the better potential method to generate a general biosensor approach and the initial work that has been carried out in this area is encouraging. There remains a large amount of work to optimise the sensors developed and this would be crucial to show the effectiveness of the approach, as well work on developing further examples of sensors. The work shows that the optimised sensors can be combined with materials to produce an encapsulated sensor which could be used to generate a wearable device, although these are not yet able to detect the relevant physiological concentrations.

Significant work is still required to optimise the wearable device before it would be suitable to test with human sweat and show that the required sensitivity could be achieved.

# Appendix 1: Chapter 2 Materials and Methods

**Appendix Table 2.1: The table gives the sequences of the primers that were used when sequencing plasmids during their construction**

| Name | Sequence | Use |
|---|---|---|
| MH027 | taaccagtaaggcaacccc | Forward sequencing primer PscsA extended |
| MH028 | TTGTTAGCAGCCGGATCT | Reverse sequencing primer PscsA extended |
| MH043 | gggaactacaagacacgtgc | Sequencing primer dual reporter promoters |
| MH130 | gcacgtgtcttgtagttccc | Reverse primer sequencing GFP |
| MH131 | gaacaatgttttccagtgctg | Forward primer sequencing EGF CpxA gene |
| MH132 | caaccagttcaacacgac | Forward primer sequencing EGF CxpA gene 2 |
| MH133 | cagaaccagtgcatcaac | Forward primer sequencing GFP CpxR gene |
| MH134 | agtcagtgagcgaggaag | Forward primer sequencing EGF plamisid backbone |
| VF2 | tgccacctgacgtctaagaa | Forward sequencing primer for biobrick plasmids |
| VR | attaccgcctttgagtgagc | Reverse sequencing primer for biobrick plasmids |

**Appendix Table 2.2: The table gives the sequences of primers used for construction of plasmid used in the project**

| Name | Sequence | Use |
|---|---|---|
| MH010 | CTTGTAGATAAAGTCAACAACTTTTGCA AAATGAATTGTGAGTGCTCACATTTACC CTCGAGTACTAGAGGGCTCACCTTCG | Forward primer SDM lactate sensor construct to add in hyperspank promoter and SpoVG RBS before lldR |

| | | |
|---|---|---|
| | GTGTGGCATAATGTGTGTAATTGTGAGC<br>GGATAACAATTTACTAGAGAAAGGTGGT<br>GAATACTAGATGATTGTTCT | Reverse primer SDM lactate sensor construct to add in hyperspank promoter and SpoVG |
| MH011 | GCCTCG | RBS before lldR |
| MH012 | TACTAGAGTCACACAGGAAAGTAC | Reverse primer SDM lactate sensor construct to change lldR promoter |
| MH013 | GCTAGCACAGTCCCTAGGACTGAGCTAG<br>CTGTAAATACTAGAGGGCTCACCTTC | Forward primer SDM lactate sensor construct to change lldR promoter (j23109) |
| MH014 | GCTAGCACAATCCCTAGGACTGAGCTAG<br>CTGTCAATACTAGAGGGCTCACCTTC | Forward primer SDM lactate sensor construct to change lldR promoter (j23117) |
| MH015 | GCTAGCATAATACCTAGGACTGAGCTAG<br>CTGTAAATACTAGAGGGCTCACCTTC | Forward primer SDM lactate sensor construct to change lldR promoter (j23101) |
| MH016 | GCTAGCATAGTACCTAGGACTGAGCTAG<br>CCGTAAATACTAGAGGGCTCACCTTC | Forward primer SDM lactate sensor construct to change lldR promoter (j23105) |
| MH039 | TCACACAGGAAAGTACTAGATGCGTAAA<br>GGAGAAG | Forward primer SDM insert RBS 32 to PScsA |
| MH040 | CTCTAGTACGCGAGTTATCTTAG | Reverse primer SDM insert RBS 32 to PSCsA |
| MH041 | TCACACAGGAAAGGAGCTCATGAGCAAA<br>GGAG | Forward primer SDM insert RBS 32 to PScsA MS |
| MH042 | CGCGAGTTATCTTAGCCAC | Reverse primer SDM insert RBS 32 to PSCsA MS |
| MH082 | TACTAGAGTGGCAAATATTCTG | Forward primer for SDM to change TrpR promoter |
| MH083 | TTTACAGCTAGCTCAGTCCTAGGGACTG<br>TGCTAGCCTCTAGTATCACACAGGAAAG | Reverse primer for SDM to change TrpR promoter (J23109) |

| | | |
|---|---|---|
| | TTGACAGCTAGCTCAGTCCTAGGGATTG | Reverse primer for SDM to change |
| MH084 | TGCTAGCCTCTAGTATCACACAGGAAAG | TrpR promoter (J23117) |
| | TTTACGGCTAGCTCAGTCCTAGGTACTA | Reverse primer for SDM to change |
| MH085 | TGCTAGCCTCTAGTATCACACAGGAAAG | TrpR promoter (J23105) |
| | TTTACAGCTAGCTCAGTCCTAGGTATTA | Reverse primer for SDM to change |
| MH086 | TGCTAGCCTCTAGTATCACACAGGAAAG | TrpR promoter (J23101) |
| | AATTCGCGGCCGCTTCTAGAGCTTTCCT | |
| | GTGTGACTCTAGTAGCTAGCATAGTACC | |
| MH092 | TAGGACTGAGCTAGCCGTAAATAC | J23105 Forward |
| | CTAGTATTTACGGCTAGCTCAGTCCTAG | |
| | GTACTATGCTAGCTACTAGAGTCACACA | |
| MH093 | GGAAAGCTCTAGAAGCGGCCGCG | J23105 Reverse |
| | AATTCGCGGCCGCTTCTAGAGCTTTCCT | |
| | GTGTGACTCTAGTAGCTAGCATAATACC | |
| MH094 | TAGGACTGAGCTAGCTGTAAATA | J23101 Forward |
| | CTAGTATTTACAGCTAGCTCAGTCCTAG | |
| | GTATTATGCTAGCTACTAGAGTCACACA | |
| MH095 | GGAAAGCTCTAGAAGCGGCCGCG | J23101 Reverse |
| | | Forward primer to change RBS |
| MH125 | TACTAGAGGCTAGCACAG | strength for TrpR EK49 109 3K3 |
| | TCACACAGGACCTCTAGTAATGGCCCAA | Reverse primer to change RBS33 |
| MH126 | C | for TrpR EK49 109 3K3 |
| | TCACACAGGAAACCCTCTAGTAATGGCC | Reverse primer to change RBS31 |
| MH127 | CAAC | for TrpR EK49 109 3K3 |
| | ATTAAAGAGGAGAAACTCTAGTAATGGC | Reverse primer to change RBS30 |
| MH128 | CCAAC | for TrpR EK49 114 1a3 |
| | | Forward primer to change RBS 30 |
| MH129 | TACTAGAGGCTAGCATTGTAC | for TrpR EK49 114 1a3 |
| | GTAGCACCTGTGATGTTGTTTATCCTGA | Forward primer gibson cpGFP loop |
| MH135 | TCGTGTTTATATCAAGG | 9 insertion |
| | TCAATCTGACCATTCAGACGACCCGCCA | Reverse primer gibson cpGFP loop |
| MH136 | TCTCGTACTC | 9 insertion |

| | | |
|---|---|---|
| | TGGAGTACGAGATGGCGGGTCGTCTGAA | Forward primer gibson AM10 loop |
| MH137 | TGGTCAGATTG | 9 insertion |
| | ATATAAACACGATCAGGATAAACAACAT | Reverse primer gibson AM10 loop |
| MH138 | CACAGGTGC | 9 insertion |
| | CCTATGTTAAAGGCAGCAATTATCCTGA | Forward primer gibson cpGFP loop |
| MH139 | TCGTGTTTATATCAAGG | 4 insertion |
| | GTCTGTGCTGCATCGTTAAAACCCGCCA | Reverse primer gibosn cpGFP loop |
| MH140 | TCTCGTACTC | 4 insertion |
| | TGGAGTACGAGATGGCGGGTTTTAACGA | Forward primer gibson AM10 loop |
| MH141 | TGCAGCACAGAC | 4 insertion |
| | ATATAAACACGATCAGGATAATTGCTGC | Reverse primer gibson AM10 loop |
| MH142 | CTTTAACATAGG | 4 insertion |
| | ATACCTATGGTAATTTAGGTTATCCTGA | Forward primer gibson cpGFP loop |
| MH143 | TCGTGTTTATATCAAGG | 5 insertion |
| | TGGGTCAGCTGATTACCGCTACCCGCCA | Reverse primer gibson cpGFP loop |
| MH144 | TCTCGTACTC | 5 insertion |
| | TGGAGTACGAGATGGCGGGTAGCGGTAA | Forward primer gibson AM10 loop |
| MH145 | TCAGCTGAC | 5 insertion |
| | ATATAAACACGATCAGGATAACCTAAAT | Reverse primer gibson AM10 loop |
| MH146 | TACCATAGGTATAGG | 5 insertion |
| | CGCTGCATGGCACCCAGAATTATCCTGA | Forward primer cpGFP avidin |
| MH147 | TCGTGTTTATATCAAGG | constructs insertion 55 |
| | TGGGTACGTTTGTTAATGGTACCCGCCA | Reverse primer cpGFP avidin |
| MH148 | TCTCGTACTC | constructs insertion 55 |
| | TGGAGTACGAGATGGCGGGTACCATTAA | Forward primer avidin constructs |
| MH149 | CAAACGTACCC | backbone insertion 55 |
| | ATATAAACACGATCAGGATAATTCTGGG | Reverse primer avidin constructs |
| MH150 | TGCCATGCAG | backbone insertion 55 |
| | ATGGCACCCAGAATACCATTTATCCTGA | Forward primer cpGFP avidin |
| MH151 | TCGTGTTTATATCAAGG | constructs insertion 57 |
| | GTCGGCTGGGTACGTTTGTTACCCGCCA | Reverse primer cpGFP avidin |
| MH152 | TCTCGTACTC | constructs insertion 57 |

| | | |
|---|---|---|
| | TGGAGTACGAGATGGCGGGTAACAAACG | Forward primer avidin constructs |
| MH153 | TACCCAGCC | backbone insertion 57 |
| | ATATAAACACGATCAGGATAAATGGTAT | Reverse primer avidin constructs |
| MH154 | TCTGGGTGCC | backbone insertion 57 |
| | GCCAGTGTTTTATTGATCGCTATCCTGA | Forward primer cpGFP avidin |
| MH155 | TCGTGTTTATATCAAGG | constructs insertion 88 |
| | TTCAGCACTTCTTTACCATTACCCGCCA | Reverse primer cpGFP avidin |
| MH156 | TCTCGTACTC | constructs insertion 88 |
| | TGGAGTACGAGATGGCGGGTAATGGTAA | Forward primer avidin constructs |
| MH157 | AGAAGTGCTGAAAAC | backbone insertion 88 |
| | ATATAAACACGATCAGGATAGCGATCAA | Reverse primer avidin constructs |
| MH158 | TAAAACACTGG | backbone insertion 88 |
| | TGTGGCTGCTGCGTAGCAGCTATCCTGA | Forward primer cpGFP avidin |
| MH159 | TCGTGTTTATATCAAGG | constructs insertion 103 |
| | TCATCACCAATATCATTAACACCCGCCA | Reverse primer cpGFP avidin |
| MH160 | TCTCGTACTC | constructs insertion 103 |
| | TGGAGTACGAGATGGCGGGTGTTAATGA | Forward primer avidin construct |
| MH161 | TATTGGTGATG | backbone insertion 103 |
| | ATATAAACACGATCAGGATAGCTGCTAC | Reverse primer avidin constructs |
| MH162 | GCAGCAGCCAC | backbone insertion 103 |
| | TTGACAGCTAGCTCAGTCCTAGGGATTG | Forward primer to generate |
| MH167 | TGCTAGCTCGTTCGCAATTGCGAGTC | synthetic PTeiR |
| | TTTATGGCTAGCTCAGTCCTAGGTACAA | Reverse primer to generate |
| MH168 | TGCTAGCTCGTTCGCAATTGCGAGTC | PTeiR(114) |
| | | Reverse primer to generate |
| MH169 | GCGCAACGATCGTCAATTAG | PTeiR(117) |
| | ATTAAAGAGGAGAAATACTAGATGGCTT | Forward primer to generate RBS |
| MH170 | CCTCCG | 30 mRFP |
| | | Reverse primer to generate RBS |
| MH171 | CTCTAGTAGCTAGCATAATACCTAG | 30 mRFP |
| | | Forward primer for overlap |
| MH172 | AAGGATGATTTCTGGAATTCG | extension of avidin and AM10 |

| | | |
|---|---|---|
| | | constructs to generate first fragment and final full length fragment |
| | | Reverse primer for overlap extension of avidin and AM10 constructs to generate final fragment and final full length fragment |
| MH173 | GTTTTTTTGCCGGACTGCAGCGGC | |
| | TAAAGAGGAGAAATACTAGATGCGTAAA | Forward primer to generate sfGFP fragment for Gibson assembly of |
| MH174 | GGCGAAGAGCTGTTC | Trp and lactate sensor with sfGFP |
| | GCCTGGCTCTAGTATTATTATTTGTACA | Reverse primer to generate sfGFP fragment for Gibson assembly of |
| MH175 | GTTCATCCATACCATG | Trp and lactate sensor with sfGFP |
| | TGAACAGCTCTTCGCCTTTACGCATCTA | Forward primer to generate Trp and lactate sensor fragment for Gibson assemblies to change |
| MH176 | GTATTTCTCCTCTTTAATCTCTA | reporter to sfGFP |
| | ATGGTATGGATGAACTGTACAAATAATA | Reverse primer to generate Trp and lactate sensor fragment for Gibson assemblies to change |
| MH177 | ATACTAGAGCCAGGCATC | reporter to sfGFP |
| | TCTTCTTCACCTTTAGAAACCATCTAGT | Reverse primer to generate Trp sensor fragment for Gibson assemblies to change reporter to |
| MH178 | ATTTCTCCTCTTTAATCTCTAGTAGTC | mNeonGreen |
| | GTATGGATGAACTGTACAAATAATAATA | Forward primer to generate Trp and lactate sensor fragment for Gibson assemblies to change |
| MH179 | CTAGAGCCAGGCATC | reporter to mNeonGreen |
| | GATTAAAGAGGAGAAATACTAGATGGTT | Forward primer to generate |
| MH180 | TCTAAAGGTGAAGAAGATAAC | mNeonGreen fragment for Gibson |

| | | |
|---|---|---|
| | | assembly of Trp and lactate sensor with mNeonGreen |
| | | Reverse primer to generate mNeonGreen fragment for Gibson |
| | ATTTGATGCCTGGCTCTAGTATTATTAT | assembly of Trp and lactate sensor |
| MH181 | TTGTACAGTTCATCCATACCC | with mNeonGreen |
| | | Reverse primer to generate lactate sensor fragment for Gibson |
| | CTTCACCTTTAGAAACCATCTAGTATTT | assemblies to change reporter to |
| MH182 | CTCCTCTTTAATCTCTAGTAGGAG | mNeonGreen |
| | TCAGATCTGCAGCGGCCGCTACTAGTAA | Forward primer to generate |
| MH183 | TGGTTTCTAAAGGTGAAGAAG | mNeonGreen as a BioBrick |
| | AGTCGTGAATTCGCGGCCGCTTCTAGAG | Forward primer to generate |
| MH184 | TTATTATTTGTACAGTTCATCCATAC | mNeonGreen as a BioBrick |
| | | Reverse primer for SDM to RBS 30 |
| | ATTAAAGAGGAGAAAGTACTAGATGGTT | on constitutive mNeonGreen |
| MH185 | TCTAAAGGTGAAG | plasmid expression |

**Appendix Table 2.3: Table of primer pools used in random mutagenesis of linker regions of cpGFP sensors, N denotes the base to be randomised, the pools were designed to randomise each amino acid in the linker sequence.**

| Name | Pool sequence | Use |
|---|---|---|
| MH001pp | CGCNNNCCTGATCGTGTTTATATCAAGGCCG | Forward primer for |
| | CGCTATNNNGATCGTGTTTATATCAAGGCCG | generating middle |
| | CGCTANCCTNNNCGTGTTTATATCAAGGCCG | fragment of overlap |
| | CGCTATNCTGATNNNGTTTATATCAAGGCCG | extension PCR of |
| | CGCTATCNTGATCGTNNNTATATCAAGGCCG | avidin constructs |
| | CGCTATCCTGATCGTGTTNNNATCAAGGCCG | |
| | CGCTATCCTGATCGTGTTTATNNNAAGGCCG | |
| | CGCTATCCTGATCGTGTTTATATCNNNGCCG | |
| MH002pp | NNNCGCCATCTCGTACTCCAGCTTG | Reverse primer for |
| | ACCNNNCATCTCGTACTCCAGCTTG | generating middle |

| | | |
|---|---|---|
| | ACCCGCNNNCTCGTACTCCAGCTTG | fragment of overlap extension PCR of avidin constructs |
| | ACCCGCCATNNNGTACTCCAGCTTG | |
| | ACCCGCCATCTCNNNCTCCAGCTTG | |
| | ACCCGCCATCTCGTANNNCAGCTTG | |
| | ACCCGCCATCTCGTACTCNNNCTTG | |
| | ACCCGCCATCTCGTACTCCAGNNNG | |
| MH003pp | NNNGATATAAACACGATCAGGATAC | Reverse primer to generate first fragment of overlap extension PCR of avidin constructs |
| | CTTNNNATAAACACGATCAGGATAC | |
| | CTTGATNNNAACACGATCAGGATAC | |
| | CTTGATATANNNACGATCAGGATAC | |
| | CTTGATATAAACNNNATCAGGATAC | |
| | CTTGATATAAACACGNNNAGGATAC | |
| | CTTGATATAAACACGATCNNNATAC | |
| | CTTGATATAAACACGATCAGGNNNC | |
| MH004pp | NNNCTGGAGTACGAGATGGCGGGTAATG | Forward prime to generate final fragment of overlap extension PCR of avidin constructs |
| | AAGNNNGAGTACGAGATGGCGGGTAATG | |
| | AAGCTGNNNTACGAGATGGCGGGTAATG | |
| | AAGCTGGAGNNNGAGATGGCGGGTAATG | |
| | AAGCTGGAGTACNNNATGGCGGGTAATG | |
| | AAGCTGGAGTACGAGNNNGCGGGTAATG | |
| | AAGCTGGAGTACGAGATGNNNGGTAATG | |
| | AAGCTGGAGTACGAGATGGCGNNNAATG | |
| MH005pp | GGTNNNCCTGATCGTGTTTATATCAAGGCCG | Forward primer for generating middle fragment of overlap extension PCR of AM10 constructs |
| | GGTTATNNNGATCGTGTTTATATCAAGGCCG | |
| | GGTTATCCTNNNCGTGTTTATATCAAGGCCG | |
| | GGTTATCCTGATNNNGTTTATATCAAGGCCG | |
| | GGTTATCCTGATCGTNNNTATATCAAGGCCG | |
| | GGTTATCCTGATCGTGTTNNNATCAAGGCCG | |
| | GGTTATCCTGATCGTGTTTATNNNAAGGCCG | |
| | GGTTATCCTGATCGTGTTTATATCNNNGCCG | |
| MH006pp | CTNNNCGCCATCTCGTACTCCAGCTTGTG | Reverse primer for generating middle |
| | CTACCNNNCATCTCGTACTCCAGCTTGTG | |

| | | |
|---|---|---|
| | CTACCCGCNNNCTCGTACTCCAGCTTGTG | fragment of overlap extension PCR of AM10 constructs |
| | CTACCCGCCATNNNGTACTCCAGCTTGTG | |
| | CTACCCGCCATCTCNNNCTCCAGCTTGTG | |
| | CTACCCGCCATCTCGTANNNCAGCTTGTG | |
| | CTACCCGCCATCTCGTACTCNNNCTTGTG | |
| | CTACCCGCCATCTCGTACTCCAGNNNGTG | |
| MH008pp | CGGCNNNGATATAAACACGATCAGGATAACC | Reverse primer to generate first fragment of overlap extension PCR of AM10 constructs |
| | CGGCCTTNNNATAAACACGATCAGGATAACC | |
| | CGGCCTTGATNNNAACACGATCAGGATAACC | |
| | CGGCCTTGATATANNNACGATCAGGATAACC | |
| | CGGCCTTGATATAAACNNNATCAGGATAACC | |
| | CGGCCTTGATATAAACACGNNNAGGATAACC | |
| | CGGCCTTGATATAAACACGATCNNNATAACC | |
| | CGGCCTTGATATAAACACGATCAGGNNNACC | |
| MH009pp | CACNNNCTGGAGTACGAGATGGCGGGTAG | Forward prime to generate final fragment of overlap extension PCR of AM10 constructs |
| | CACAAGNNNGAGTACGAGATGGCGGGTAG | |
| | CACAAGCTGNNNTACGAGATGGCGGGTAG | |
| | CACAAGCTGGAGNNNGAGATGGCGGGTAG | |
| | CACAAGCTGGAGTACNNNATGGCGGGTAG | |
| | CACAAGCTGGAGTACGAGNNNGCGGGTAG | |
| | CACAAGCTGGAGTACGAGATGNNNGGTAG | |
| | CACAAGCTGGAGTACGAGATGGCGNNNAG | |

**Appendix Table 2.4: Sequences of small parts used in the project**

| Name | Sequence | Use |
|---|---|---|
| J23114 (synthesised *de novo* with RBS 32) | TTTATGGCTAGCTCAGTCCTAGGTACAATGCTAGC | Weak constitutive promoter for the expression of transcription factors |

| | | |
|---|---|---|
| J23105** | TTTACGGCTAGCTCAGTCCTAGGTACTATGCTAGC | Medium strength constitutive promoter for the expression of transcription factors |
| J23101** | TTTACAGCTAGCTCAGTCCTAGGTATTATGCTAGC | Strong constitutive promoter for the expression of transcription factors and binding protein cpGFP sensors |
| J23109* | TTTACAGCTAGCTCAGTCCTAGGGACTGTGCTAGC | Weak constitutive promoter for the expression of transcription factor |
| J23117* | TTGACAGCTAGCTCAGTCCTAGGGATTGTGCTAGC | Weak constitutive promo |
| Hyperspank (synthesised *de novo* with SpoVG) | CTCGAGGGTAAATGTGAGCACTCACAATTCATTTTGCAAAAGTTGTTGACTTTATCTACAAGGTGTGGCATAATGTGTGTAATTGTGAGCGGATAACAATT | Constitutive promoter from *B. subtilis* |

| | | |
|---|---|---|
| PLld (synthesised *de novo* with RBS 30) | CTTTACCAGACATCTCCCCCCACAAGAATTGGCCCTACCAATTCTTCGCTTATCTGACCTCTGGTTCACAATTTCCCAATTAAAACTCACATCAATGTTGACAGCTAGCTCAGTCCTAGGGATTGTGCTAGCTCATTATCCCTACACAACACAATTGGCAGTGCCACTTTTACACAACGTGTGACAAGGAGATGAGCAACAGACTCATTACACGATGTGCGTGGACTCC | Synthetic promoter responsive to LldR and lactate |
| PTrpO (synthesised *de novo*) | TGGCAAATATTCTGAAATGAGCTGTTGACAATTAATCATCGAACTAGTTAACTAGTACGCAAGTTCACGTAAAAAGGGTATCGAC | Promoter responstive to tryptophan and TrpR |
| PScsA (Synthesised *de novo*) | AGAAGGTTGCGCAGCGCGCCGACATAACTTTACAGGGGAAAGGTTGCCAAAACCGCGCCAGTGGCTAAGATAACTCGCGTTAAACAGTGAGGGCGCA | |
| PScsAext. (gifted from Sheppard lab University of Kent and mutated to remove native RBS) | GCACTTCCCATGCTTCAGCAACCTCTTTGAAACGGGCTTCGGCATCGGGTTCTTTGCTGACATCTGGATGGTACTTGCGGGCCAGTCGGCGATAGGCGGTCTTAATCGTCTTGAGATCGTCCGTCGGTTTCACGCCCATAATGGCGTAATAATCCTTAAGTTCCATAGCATCATCTCGCTAAATCAATACATACAGAAGGGACCCCAAAAGGTTTCTCCACTAAGTGTAGGGTAAACCTGAAAAGTGCGTATGAAAACACCAGTTATATCATTAGTAAGAATAAATTACGTTGTTCGACTATCAGAAGGTTGCGCAGCGCGCCGACATAACTTTACAGGGGAAAGGTTGCCAAAACCGCGCCAGTGGCTAAGATAACTCGCG | |

| | | |
|---|---|---|
| SpoVG | AAAGGTGGTGAA | RBS from *B. subtilis* |
| RBS 30 | ATTAAAGAGGAGAAA | Strong RBS |
| RBS 32 | TCACACAGGAAAG | Medium RBS |
| RBS 31∗ | TCACACAGGAAACC | Weak RBS |
| RBS 33∗ | TCACACAGGAC | Weak RBS |
| *E. coli* his operon terminator | TCCGGCAAAAAAACGGGCAAGGTGTCACC ACCCTGCCCTTTTTCTTTAAAACCGAAAA GATTACTTCGCGTT | Transcriptional terminator |
| L32P55 (present in BioBrick plasmids) | CTCGGTACCAAAGACGAACAATAAGACGC TGAAAAGCGTCTTTTTTCGTTTTGGTCC | Transcriptional terminator |
| B0015 (synthesised *de novo* with transcription factors) | TATAAACGCAGAAAGGCCCACCCGAAGGT GAGCCAGTGTGACTCTAGTAGAGAGCGTT CACCGACAAACAACAGATAAAACGAAAGG CCCAGTCTTTCGACTGAGCCTTTCGTTTT ATTTGATGCCTGG | Transcriptional terminator |

∗ generated in plasmid through mutagenesis

∗∗produced through oligonucleotide annealing

**Appendix Table 2.5: The table gives the sequences of genes used in the construction of biosensors in the project.**

| Name | Sequence | Use |
|---|---|---|
| TrpR (amplified from TOP10 genome) | ATGGCCCAACAATCACCCTATTCAGCAGC GATGGCAGAACAGCGTCACCAGGAGTGG TTACGTTTTGTCGACCTGCTTAAGAATGC CTACCAAAACGATCTCCATTTACCGTTGT TAAACCTGATGCTGACGCCAGATGAGCG CGAAGCGTTGGGGACTCGCGTGCGTATT GTCGAAGAGCTGTTGCGCGGCGAAATGA GCCAGCGTGAGTTAAAAAATGAACTCGG CGCAGGCATCGCGACGATTACGCGTGGA TCTAACAGCCTGAAAGCCGCGCCCGTCG AGCTGCGCCAGTGGCTGGAAGAGGTGTT GCTGAAAAGCGATTGA | Wild type sequence of the transcription factor capable of binding tryptophan |
| TrpR DN46 (mutated from wild type) | ATGGCCCAACAATCACCCTATTCAGCAGC GATGGCAGAACAGCGTCACCAGGAGTGGT TACGTTTTGTCGACCTGCTTAAGAATGCC TACCAAAACGATCTCCATTTACCGTTGTT AAACCTGATGCTGACGCCAAACGAGCGCG AAGCGTTGGGGACTCGCGTGCGTATTGTC GAAGAGCTGTTGCGCGGCGAAATGAGCCA GCGTGAGTTAAAAAATGAACTCGGCGCGG GCATCGCGACGATTACGCGTGGATCTAAC AGCCTGAAAGCCGCGCCCGTTGAGCTGCG CCAGTGGCTGGAAGAGGTGTTGCTGAAAA GCGATTGA | Sequence of the transcription factor capable of binding tryptophan with a mutation at 64$^{th}$ amino acid from aspartic acid to asparagine |
| TrpR EK49 (mutated from wild type) | ATGGCCCAACAATCACCCTATTCAGCAGC GATGGCAGAACAGCGTCACCAGGAGTGGT TACGTTTTGTCGACCTGCTTAAGAATGCC TACCAAAACGATCTCCATTTACCGTTGTT AAACCTGATGCTGACGCCAGATGAGCGCA AAGCGTTGGGGACTCGCGTGCGTATTGTC | Sequence of the transcription factor capable of binding tryptophan with a mutation at 49$^{th}$ amino |

| | | |
|---|---|---|
| | GAAGAGCTGTTGCGCGGCGAAATGAGCCA<br>GCGTGAGTTAAAAAATGAACTCGGCGCGG<br>GCATCGCGACGATTACGCGTGGATCTAAC<br>AGCCTGAAAGCCGCGCCCGTTGAGCTGCG<br>CCAGTGGCTGGAAGAGGTGTTGCTGAAAA<br>GCGATTGA | acid from glutamic acid to lysine |
| TrpR EK13 (mutated from wild type) | ATGGCCCAACAATCACCCTATTCAGCAGC<br>GATGGCAAAACAGCGTCACCAGGAGTGGT<br>TACGTTTTGTCGACCTGCTTAAGAATGCC<br>TACCAAAACGATCTCCATTTACCGTTGTT<br>AAACCTGATGCTGACGCCAGATGAGCGCG<br>AAGCGTTGGGGACTCGCGTGCGTATTGTC<br>GAAGAGCTGTTGCGCGGCGAAATGAGCCA<br>GCGTGAGTTAAAAAATGAACTCGGCGCGG<br>GCATCGCGACGATTACGCGTGGATCTAAC<br>AGCCTGAAAGCCGCGCCCGTTGAGCTGCG<br>CCAGTGGCTGGAAGAGGTGTTGCTGAAAA<br>GCGATTGA | Sequence of the transcription factor capable of binding tryptophan with a mutation at 13$^{th}$ amino acid from glutamic acid to lysine |
| LldR* | ATGATTGTTCTGCCTCGTCGTCTGAGTGA<br>TGAAGTTGCAGATCGTGTTCGTGCACTGA<br>TTGATGAAAAAAATCTGGAAGCCGGTATG<br>AAACTGCCTGCCGAACGTCAGCTGGCAAT<br>GCAGCTGGGTGTTAGCCGTAATAGCCTGC<br>GTGAAGCACTGGCAAAACTGGTTAGCGAA<br>GGTGTTCTGCTGAGCCGTCGTGGTGGTGG<br>CACCTTTATTCGTTGGCGTCATGATACCT<br>GGTCAGAACAGAATATTGTTCAGCCGCTG<br>AAAACCCTGATGGCAGATGATCCGGATTA<br>TAGCTTTGATATTCTGGAAGCACGTTATG<br>CAATTGAAGCAAGCACCGCATGGCATGCA<br>GCAATGCGTGCAACACCGGGTGATAAAGA<br>AAAAATTCAGCTGTGTTTTGAAGCGACCC | Codon optimised sequence of the transcription factor capable of binding lactate |

TGAGCGAAGATCCGGATATTGCAAGCCAG

GCAGATGTTCGTTTTCATCTGGCAATTGC

AGAAGCCAGCCATAATATTGTGCTGCTGC

AAACCATGCGTGGTTTTTTTGATGTTCTG

CAAAGCAGCGTTAAACATAGCCGTCAGCG

TATGTATCTGGTTCCGCCTGTTTTTTCAC

AGCTGACCGAACAGCATCAGGCAGTTATT

GATGCAATTTTTGCCGGTGATGCAGATGG

TGCACGTAAAGCAATGATGGCACATCTGA

GCTTTGTTCATACCACCATGAAACGCTTT

GATGAAGATCAGGCACGTCATGCACGTAT

TACCCGTCTGCCTGGTGAACATAATGAAC

ATAGTCGCGAAAAAAACGCCTAA

Avidin- ATGGCACGTAAATGTAGCCTGACCGGTAA

Cortisol * ATGGACCAATCATGCAAATGATAACATGA

CCATTGGTGCCGTTAATAGCCGTGGTGAA

TTTACCGGCACCTATATTACCGCAGTTAC

CGCAACCAGCAACGAAATTAAAGAAAGTC

CGCTGCATGGCACCCAGAATACCATTAAC

AAACGTACCCAGCCGACCTTTGGTTTTAC

CGTTAATTGGAAACCGTATAGCATTACCA

CCGTTTTTACAGGCCAGTGCTTTATTGAT

CGCAATGGTAAAGAAGTGCTGAAAACCAT

GTGGCTGCTGCGTAGCAGCGTTAATGAT

ATTGGTGATGATTGGAAAGCAACCCGTG

TGGGCATTAACATTTTTACCCGTCTGCG

TACCCAGAAAGAATGATAA

Avidin- ATGGCACGTAAATGTAGCCTGACCGGTAA

Testosterone ATGGACCAATCGCATGAATCACAATATGA

* CCATTGGTGCAGTTAATAGCCGTGGTGAA

TTTACCGGCACCTATATTGCAACCGTTAA

TGCAACCAGCAACGAAATTAAAGAAAGTC

| | | |
|---|---|---|
| | CGCTGCATGGCACCCAGAATACCATTAAC | |
| | AAACGTACCCAGCCGACCTTTGGTTTTAC | |
| | CGTTAATTGGAAATTTAGCGAAAGCACCA | |
| | CCGTTTTTACAGGCCAGTGTTTTATTGAT | |
| | CGCAATGGTAAAGAAGTGCTGAAAACCAT | |
| | GTGGCTGCTGCGTAGCAGCGTTAATGATA | |
| | TTGGTGATGATTGGAAAGCAACCCGTGTT | |
| | GGCATTGATATCTTTACCCGTCTGCGTAC | |
| | CCAGAAAGAATAATAA | |
| AM10* | ATGGCCCTGATTATTCTGCTGGCAGCATG | Tick lipocalin which binds |
| | TCTGAGCGTTGCAACCGCACAGCAGCAGT | to histamine |
| | GTGATACCGTTAGCGCATGGCAGAGCCTG | |
| | CGTGGTCCTGGCACCGGTGGTTATTACCT | |
| | GTTTAAAACCACCGAAGGTGGTAAAACCG | |
| | ATTGCACCTATGTTAAAGGCAGCAATTTT | |
| | AACGATGCAGCACAGACCGCAACCTATAC | |
| | CTATGGTAATTTAGGTAGCGGTAATCAGC | |
| | TGACCCAGCAGACCGCCAGCGCAAGCATT | |
| | AGTGGTAATGCAATTGTTGTTGGCACCGA | |
| | TCATAGCGAAGTTCTGTATTCAGATGGTA | |
| | GCACCTGTGATGTTGTTCGTCTGAATGGT | |
| | CAGATTGAACTGTGGATTCATAGCAGCGC | |
| | AACCAGCAATACCGGTAATCTGAATAGCT | |
| | GTTGTACCGACAAATTCAACCAAGAAAAA | |
| | GGTAGCCGTCCGGAACATGTTGTTTATCG | |
| | TAGTACCTGTCCGAATCTGCCGCAGTAA | |
| GFP** | ATGCGTAAAGGAGAAGAACTTTTCACTGG | Fluorescent green |
| | AGTTGTCCCAATTCTTGTTGAATTAGATG | protein used as the |
| | GTGATGTTAATGGGCACAAATTTTCTGTC | reporter for biosensors |
| | AGTGGAGAGGGTGAAGGTGATGCAACATA | |
| | CGGAAAACTTACCCTTAAATTTATTTGCA | |
| | CTACTGGAAAACTACCTGTTCCATGGCCA | |

| | | |
|---|---|---|
| | ACACTTGTCACTACTTTCGGTTATGGTGT | |
| | TCAATGCTTTGCGAGATACCCAGATCATA | |
| | TGAAACAGCATGACTTTTTCAAGAGTGCC | |
| | ATGCCCGAAGGTTATGTACAGGAAAGAAC | |
| | TATATTTTTCAAAGATGACGGGAACTACA | |
| | AGACACGTGCTGAAGTCAAGTTTGAAGGT | |
| | GATACCCTTGTTAATAGAATCGAGTTAAA | |
| | AGGTATTGATTTTAAAGAAGATGGAAACA | |
| | TTCTTGGACACAAATTGGAATACAACTAT | |
| | AACTCACACAATGTATACATCATGGCAGA | |
| | CAAACAAAAGAATGGAATCAAAGTTAACT | |
| | TCAAAATTAGACACAACATTGAAGATGGA | |
| | AGCGTTCAACTAGCAGACCATTATCAACA | |
| | AAATACTCCAATTGGCGATGGCCCTGTCC | |
| | TTTTACCAGACAACCATTACCTGTCCACA | |
| | CAATCTGCCCTTTCGAAAGATCCCAACGA | |
| | AAAGAGAGACCACATGGTCCTTCTTGAGT | |
| | TTGTAACAGCTGCTGGGATTACACATGGC | |
| | ATGGATGAACTATACAAATAATAA | |
| sfGFP** | CGTAAAGGCGAAGAGCTGTTCACTGGTGT | Mutant version of GFP |
| | CGTCCCTATTCTGGTGGAACTGGATGGTG | with brighter |
| | ATGTCAACGGTCATAAGTTTTCCGTGCGT | fluorescence |
| | GGCGAGGGTGAAGGTGACGCAACTAATGG | |
| | TAAACTGACGCTGAAGTTCATCTGTACTA | |
| | CTGGTAAACTGCCGGTACCTTGGCCGACT | |
| | CTGGTAACGACGCTGACTTATGGTGTTCA | |
| | GTGCTTTGCTCGTTATCCGGACCATATGA | |
| | AGCAGCATGACTTCTTCAAGTCCGCCATG | |
| | CCGGAAGGCTATGTGCAGGAACGCACGAT | |
| | TTCCTTTAAGGATGACGGCACGTACAAAA | |
| | CGCGTGCGGAAGTGAAATTTGAAGGCGAT | |
| | ACCCTGGTAAACCGCATTGAGCTGAAAGG | |

| | | |
|---|---|---|
| | CATTGACTTTAAAGAAGATGGCAATATCC | |
| | TGGGCCATAAGCTGGAATACAATTTTAAC | |
| | AGCCACAATGTTTACATCACCGCCGATAA | |
| | ACAAAAAAATGGCATTAAAGCGAATTTTA | |
| | AAATTCGCCACAACGTGGAGGATGGCAGC | |
| | GTGCAGCTGGCTGATCACTACCAGCAAAA | |
| | CACTCCAATCGGTGATGGTCCTGTTCTGC | |
| | TGCCAGACAATCACTATCTGAGCACGCAA | |
| | AGCGTTCTGTCTAAAGATCCGAACGAGAA | |
| | ACGCGATCATATGGTTCTGCTGGAGTTCG | |
| | TAACCGCAGCGGGCATCACGCATGGTATG | |
| | GATGAACTGTACAAA | |
| mNeon Green (obtained from Horsfall lab University of Edinburgh) | ATGGTTTCTAAAGGTGAAGAAGATAACAT<br>GGCATCTCTGCCGGCAACCCACGAACTGC<br>ACATCTTCGGTTCTATCAACGGTGTTGAT<br>TTCGATATGGTTGGTCAGGGTACCGGTAA<br>CCCGAACGATGGTTACGAAGAACTGAACC<br>TGAAATCTACCAAAGGTGATTTACAGTTC<br>TCTCCGTGGATTCTGGTTCCGCACATCGG<br>TTACGGTTTCCACCAGTACCTGCCGTACC<br>CTGATGGTATGTCTCCGTTCCAGGCAGCA<br>ATGGTTGATGGTTCTGGTTACCAGGTTCA<br>CCGTACCATGCAGTTCGAAGATGGTGCAT<br>CTCTGACCGTTAACTACCGTTACACCTAC<br>GAAGGTTCTCACATCAAAGGTGAAGCACA<br>GGTTAAAGGTACCGGTTTCCCGGCAGATG<br>GTCCGGTTATGACCAACTCTCTGACCGCA<br>GCAGATTGGTGCCGTTCTAAAAAAACCTA<br>CCCGAACGATAAAACCATCATTTCTACCT<br>TCAAATGGTCTTACACCACCGGTAACGGT<br>AAACGTTACCGTTCTACCGCACGTACCAC<br>CTACACCTTCGCAAAACCGATGGCAGCTA | Alternative green fluorescent protein with brighter fluorescence and faster maturation |

| | | |
|---|---|---|
| | ACTACCTGAAAAACCAGCCGATGTACGTT | |
| | TTCCGTAAAACCGAACTGAAACACTCTAA | |
| | AACCGAACTGAACTTCAAAGAATGGCAGA | |
| | AAGCATTCACCGATGTTATGGGTATGGAT | |
| | GAACTGTACAAATAATAA | |
| mRFP** | ATGGCTTCCTCCGAAGACGTTATCAAAGA | Red fluorescent protein |
| | GTTCATGCGTTTCAAAGTTCGTATGGAAG | used as alternative to OD |
| | GTTCCGTTAACGGTCACGAGTTCGAAATC | for response |
| | GAAGGTGAAGGTGAAGGTCGTCCGTACGA | normalisation |
| | AGGTACCCAGACCGCTAAACTGAAAGTTA | |
| | CCAAAGGTGGTCCGCTGCCGTTCGCTTGG | |
| | GACATCCTGTCCCCGCAGTTCCAGTACGG | |
| | TTCCAAAGCTTACGTTAAACACCCGGCTG | |
| | ACATCCCGGACTACCTGAAACTGTCCTTC | |
| | CCGGAAGGTTTCAAATGGGAACGTGTTAT | |
| | GAACTTCGAAGACGGTGGTGTTGTTACCG | |
| | TTACCCAGGACTCCTCCCTGCAAGACGGT | |
| | GAGTTCATCTACAAAGTTAAACTGCGTGG | |
| | TACCAACTTCCCGTCCGACGGTCCGGTTA | |
| | TGCAGAAAAAAACCATGGGTTGGGAAGCT | |
| | TCCACCGAACGTATGTACCCGGAAGACGG | |
| | TGCTCTGAAAGGTGAAATCAAAATGCGTC | |
| | TGAAACTGAAAGACGGTGGTCACTACGAC | |
| | GCTGAAGTTAAAACCACCTACATGGCTAA | |
| | AAAACCGGTTCAGCTGCCGGGTGCTTACA | |
| | AAACCGACATCAAACTGGACATCACCTCC | |
| | CACAACGAAGACTACACCATCGTTGAACA | |
| | GTACGAACGTGCTGAAGGTCGTCACTCCA | |
| | CCGGTGCT | |
| cpGFP * | TATCCTGATCGTGTTTATATCAAGGCCGA | Circularly permuted GFP |
| | CAAGCAGAAGAACGGCATCAAGGCGAACT | for insertion into Avidin |
| | TCCAGATCCGCCACAACGTGGAGGACGGC | and AM10 proteins |

AGCGTGCAGCTCGCCGACCACTACCAGCA (Linker sequences
GAACACCCCCATCGGCGACGGCCCCGTGC underlined)
TGCTGCCCGACAACCACTACCTGAGCACC
CAGTCCGTGCTGAGCAAAGACCCCAACGA
GAAGCGCGATCACATGGTCCTGCTGGAGT
TCGTGACCGCCGCCGGGATCACTCTCGGC
ATGGACGAGCTGTACAAGGTGGACGGCGG
CACGGGTGGAAGCATGGTATCACGCGGCG
AGGAGCTGTTCACCGGGGTGGTGCCCATC
CTGGTCGAGCTGGACGGCGACGTAAACGG
CCACAAGTTCCGCGTGAGGGGCGAAGGCG
AGGGCGATGCCACCAACGGCAAGCTGACC
CTGAAGTTCATCTGCACCACCGGCAAGCT
GCCCGTGCCCTGGCCCACCCTCGTGACCA
CCTTGACCTACGGCGTGCAGTGCTTCTCC
CGCTACCCCGACCACATGAAGCAGCACGA
CTTCTTCAAGTCCGCCATGCCCGAAGGCT
ACGTCCAGGAGCGCACCATCTTCTTCAAG
GACGACGGCACCTACAAGACCCGCGCCGA
GGTGAAGTTCGAGGGCGACACCCTGGTGA
ACCGCATCGAGCTGAAGGGCATCGACTTC
AAGGAGGACGGCAACATCCTGGGGCACAA
GCTGGAGTACGAGATGGCGGGT

∗ Synthesised *de novo*

∗∗ Obtained from lab stocks

**Appendix Table 2.6: List of constructs used within this study. All constructs were built during the course of this study except those with ∗.**

| Plasmid | Description |
|---|---|
| pSB1A3 ∗ | BioBrick plasmid with pMB1 ori and AmpR |
| pSB3K3 ∗ | BioBrick plasmid with p15A ori and KanR |
| pSB4A3 ∗ | BioBrick plasmid with pSC101 ori and AmpR |
| Hyperspank lactate sensor 1A3 | pSB1A3 plasmid with Hyperspank SpoVG LldR (reverse) and PlldPRD RBS 30 GFP |
| J23114 lactate sensor 1A3 | pSB1A3 plasmid with J23114 RBS 32 LldR (reverse) and PlldPRD RBS 30 GFP |
| J23101 lactate sensor 1A3 | pSB1A3 plasmid with J23101 RBS 32 LldR (reverse) and PlldPRD RBS 30 GFP |
| J23105 lactate sensor 1A3 | pSB1A3 plasmid with J23105 RBS 32 LldR (reverse) and PlldPRD RBS 30 GFP |
| J23109 lactate sensor 1A3 | pSB1A3 plasmid with J23109 RBS 32 LldR (reverse) and PlldPRD RBS 30 GFP |
| Hyperspank lactate sensor 3K3 | pSB3K3 plasmid with Hyperspank SpoVG LldR (reverse) and PlldPRD RBS 30 GFP |
| J23114 lactate sensor 3K3 | pSB3K3 plasmid with J23114 RBS 32 LldR (reverse) and PlldPRD RBS 30 GFP |
| J23101 lactate sensor 3K3 | pSB3K3 plasmid with J23101 RBS 32 LldR (reverse) and PlldPRD RBS 30 GFP |
| J23105 lactate sensor 3K3 | pSB3K3 plasmid with J23105 RBS 32 LldR (reverse) and PlldPRD RBS 30 GFP |
| J23109 lactate sensor 3K3 | pSB3K3 plasmid with J23109 RBS 32 LldR (reverse) and PlldPRD RBS 30 GFP |
| Dual lactate sensor RBS 32 | pSB3K3 plasmid with J23101 RBS 32 mRFP J23101 RBS 32 LldR (reverse) and PlldPRD RBS 30 GFP |
| Dual lactate sensor RBS 30 | pSB3K3 plasmid with J23101 RBS 30 mRFP J23101 RBS 32 LldR (reverse) and PlldPRD RBS 30 GFP |

| | |
|---|---|
| Dual lactate sensor RBS 30 sfGFP | pSB3K3 plasmid with J23101 RBS 30 mRFP J23101 RBS 32 LldR (reverse) and PlldPRD RBS 30 sfGFP |
| Dual lactate sensor RBS 30 mNeon | pSB3K3 plasmid with J23101 RBS 30 mRFP J23101 RBS 32 LldR (reverse) and PlldPRD RBS 30 mNeonGreen |
| J23114 Trp sensor 1A3 | pSB1A3 plasmid with J23114 RBS 32 TrpR (reverse) and PTrpO RBS 30 GFP |
| J23114 Trp sensor EK49 1A3 | pSB1A3 plasmid with J23114 RBS 32 TrpR EK49 (reverse) and PTrpO RBS 30 GFP |
| J23114 Trp sensor DN46 1A3 | pSB1A3 plasmid with J23114 RBS 32 TrpR DN46 (reverse) and PTrpO RBS 30 GFP |
| J23114 Trp sensor EK13 1A3 | pSB1A3 plasmid with J23114 RBS 32 TrpR EK13 (reverse) and PTrpO RBS 30 GFP |
| J23114 Trp sensor EK49 3K3 | pSB3K3 plasmid with J23114 RBS 32 TrpR EK49 (reverse) and PTrpO RBS 30 GFP |
| J23109 Trp sensor EK49 3K3 | pSB3K3 plasmid with J23109 RBS 32 TrpR EK49 (reverse) and PTrpO RBS 30 GFP |
| J23109_31 Trp sensor EK49 3K3 | pSB3K3 plasmid with J23109 RBS 31 TrpR EK49 (reverse) and PTrpO RBS 30 GFP |
| J23109_33 Trp sensor EK49 3K3 | pSB3K3 plasmid with J23109 RBS 33 TrpR EK49 (reverse) and PTrpO RBS 30 GFP |
| J23117 Trp sensor EK49 3K3 | pSB3K3 plasmid with J23117 RBS 32 TrpR EK49 (reverse) and PTrpO RBS 30 GFP |
| Dual Trp sensor RBS 32 | pSB3K3 plasmid with J23101 RBS 32 mRFP J23109 RBS 33 TrpR EK49 (reverse) and PTrpO RBS 30 GFP |
| Dual Trp sensor RBS 30 | pSB3K3 plasmid with J23101 RBS 30 mRFP J23109 RBS 33 TrpR EK49 (reverse) and PTrpO RBS 30 GFP |

| | |
|---|---|
| Dual Trp sensor RBS 30 sfGFP | pSB3K3 plasmid with J23101 RBS 30 mRFP J23109 RBS 33 TrpR EK49 (reverse) and PTrpO RBS 30 sfGFP |
| Dual Trp sensor RBS 30 mNeon | pSB3K3 plasmid with J23101 RBS 30 mRFP J23109 RBS 33 TrpR EK49 (reverse) and PTrpO RBS 30 mNeonGreen |
| PScSA 105 ScsA | pYTK084 plasmid with J23105 RBS 30 ScsA (reverse) and PScsA RBS 30 GFP |
| PScsA 114 ScsA | pYTK084 plasmid with J23114 RBS 30 ScsA (reverse) and PScsA RBS 30 GFP |
| PScsA 105 Cpx | pYTK084 plasmid with J23105 RBS 30 CpxR and RBS 30 CpxA (reverse) and PScsA RBS 30 GFP |
| PScsA 114 Cpx | pYTK084 plasmid with J23114 RBS 30 (reverse) and PScsA RBS 30 GFP |
| PScsAext 105 ScsA | pYTK084 plasmid with J23105 RBS 30 ScsA (reverse) and PScsA extended RBS 30 GFP |
| PScsAext 114 ScsA | pYTK084 plasmid with J23114 RBS 30 ScsA (reverse) and PScsA extended RBS 30 GFP |
| PScsAext 105 Cpx | pYTK084 plasmid with J23105 RBS 30 CpxR and RBS 30 CpxA (reverse) and PScsA extended RBS 30 GFP |
| PScsAext 114 Cpx | pYTK084 plasmid with J23114 RBS 30 (reverse) and PScsA extended RBS 30 GFP |
| PTeiR 101 TeiR | pSB1A3 plasmid with J23101 RBS 32 TeiR (reverse) and PTeiR RBS 30 GFP |
| PTeiR 105 TeiR | pSB1A3 plasmid with J23105 RBS 32 TeiR (reverse) and PTeiR RBS 30 GFP |
| PTeiR 114 TeiR | pSB1A3 plasmid with J23114 RBS 32 TeiR (reverse) and PTeiR RBS 30 GFP |

| | |
|---|---|
| PTeiR114 101 TeiR | pSB1A3 plasmid with J23101 RBS 32 TeiR (reverse) and PTeiR synthetic with J23114 inserted RBS 30 GFP |
| PTeiR114 105 TeiR | pSB1A3 plasmid with J23105 RBS 32 TeiR (reverse) and PTeiR synthetic with J23114 inserted RBS 30 GFP |
| PTeiR114 114 TeiR | pSB1A3 plasmid with J23114 RBS 32 TeiR (reverse) and PTeiR synthetic with J23114 inserted RBS 30 GFP |
| PTeiR117 101 TeiR | pSB1A3 plasmid with J23101 RBS 32 TeiR (reverse) and PTeiR synthetic with J23117 inserted RBS 30 GFP |
| PTeiR117 105 TeiR | pSB1A3 plasmid with J23105 RBS 32 TeiR (reverse) and PTeiR synthetic with J23117 inserted RBS 30 GFP |
| PTeiR117 114 TeiR | pSB1A3 plasmid with J23114 RBS 32 TeiR (reverse) and PTeiR synthetic with J23117 inserted RBS 30 GFP |
| Avidin-Cortisol 55 | pSB3K3 with J23101 RBS 30 Avidin cortisol with cpGFP insertion after 55$^{th}$ amino acid |
| Avidin-Cortisol 57 | pSB3K3 with J23101 RBS 30 Avidin cortisol with cpGFP insertion after 57$^{th}$ amino acid |
| Avidin-Cortisol 88 | pSB3K3 with J23101 RBS 30 Avidin cortisol with cpGFP insertion after 88$^{th}$ amino acid |
| Avidin-Cortisol 103 | pSB3K3 with J23101 RBS 30 Avidin cortisol with cpGFP insertion after 103$^{th}$ amino acid |
| Avidin-Testosterone 55 | pSB3K3 with J23101 RBS 30 Avidin testosterone with cpGFP insertion after 55$^{th}$ amino acid |
| Avidin-Testosterone 57 | pSB3K3 with J23101 RBS 30 Avidin testosterone with cpGFP insertion after 57$^{th}$ amino acid |

| | |
|---|---|
| Avidin-Testosterone 88 | pSB3K3 with J23101 RBS 30 Avidin testosterone with cpGFP insertion after 88$^{th}$ amino acid |
| Avidin-Testosterone 103 | pSB3K3 with J23101 RBS 30 Avidin testosterone with cpGFP insertion after 103$^{th}$ amino acid |
| AM10 loop 4 | pSB4A3 with J23101 RBS 30 AM10 with cpGFP inserted in loop 4 |
| AM10 loop 5 | pSB4A3 with J23101 RBS 30 AM10 with cpGFP inserted in loop 5 |
| AM10 loop 9 | pSB4A3 with J23101 RBS 30 AM10 with cpGFP inserted in loop 9 |
| J23101 GFP | pSB3K3 with J2301 RBS 30 GFP |
| J23101 sfGFP * | pSB3K3 with J2301 RBS 30 sfGFP |
| J23101 mNeonGreen | pSB3K3 with J2301 RBS 30 mNeonGreen |
| J23101 mRFP | pSB3K3 with J2301 RBS 30 mRFP |
| J23101 32 mRFP | pSB3K3 with J2301 RBS 32 mRFP |

**Appendix Table 2.7: The table gives the concentrations of the amino acid in the 5x stock solution for making the medium for tryptophan biosensor growth and the final concentration of the amino acids in the medium.**

| Amino acid | x5 | final |
|---|---|---|
| L-Alanine | 4.0mM | 0.8mM |
| L-Arginine HCl | 26mM | 5.2mM |
| L-Asparagine | 2.0mM | 0.4mM |
| L-Aspartic Acid, Potassium Salt | 2.0mM | 0.4mM |
| L-Glutamic Acid, Potassium Salt | 3.0mM | 0.6mM |
| L-Glutamine | 3.0mM | 0.6mM |
| L-Glycine | 4.0mM | 0.8mM |
| L-Histidine HCl $H_2O$ | 1.0mM | 0.2mM |
| L-Isoleucine | 2.0mM | 0.4mM |
| L-Proline | 2.0mM | 0.4mM |
| L-Serine | 50mM | 10mM |
| L-Threonine | 2.0mM | 0.4mM |
| L-Valine | 3.0mM | 0.6mM |
| L-Leucine | 4.0mM | 0.8mM |
| L-Lysine HCl | 2.0mM | 0.4mM |
| L-Methionine | 1.0mM | 0.2mM |
| L-Phenylalanine | 2.0mM | 0.4mM |
| L-Cysteine HCl | 0.5mM | 0.1mM |
| L-Tyrosine | 1.0mM | 0.2mM |

# Appendix 2: Chapter 4 Biosensors using binding molecules

The code outline below was the code used in the bio3d program (Grant et al., 2006) to analyse protein structures to determine the change in dihedral angles between the bound and unbound protein structures

```
> library(bio3d)

> aln <-
read.fasta(file("C:/Users/maggi/Documents/fasta/avidin.fa
"))

> m <- read.fasta.pdb(aln)

pdb/seq: 1   name: http://www.rcsb.org/pdb/files/1avd.pdb

pdb/seq: 2   name: http://www.rcsb.org/pdb/files/1ave.pdb

> a <- torsion.xyz(m$xyz[1,],1)

> b <- torsion.xyz(m$xyz[2,],1)

> d <- wrap.tor(a-b)

> plot(m$resno[1,],d, typ="p", pch=19,xlab="Residue no.",
ylab="Difference Dihedral Angles (degrees)")

> abline(0,0)

> abline(0,0, lwd=2)

> print(d)
```

**Appendix Table 4.1: The table gives the change in the dihedral angle for each amino acid position in the avidin protein. The amino acid position and angles selected were underlined.**

| Amino acid position | Change in dihedral angle (°) |
|---|---|
| 1 | n/a |
| 2 | 6.800113 |
| 3 | -5.287834 |
| 4 | -8.475023 |
| 5 | 12.86421 |
| 6 | -5.67697 |
| 7 | -0.07255583 |
| 8 | -1.789161 |
| 9 | 2.398278 |
| 10 | -4.567357 |
| 11 | 3.991403 |
| 12 | -0.3352781 |
| 13 | 0.5333071 |
| 14 | 5.598927 |
| 15 | -6.624162 |
| 16 | -10.08690 |
| 17 | -11.35306 |
| 18 | -3.095838 |
| 19 | 10.89326 |
| 20 | -2.955545 |
| 21 | 2.468494 |
| 22 | 3.730486 |
| 23 | 7.405528 |
| 24 | 1.165940 |
| 25 | -14.48032 |
| 26 | 6.559291 |
| 27 | 15.33846 |
| 28 | -5.325444 |
| 29 | -10.64920 |
| 30 | 0.4812637 |
| 31 | 3.336798 |

| | |
|---|---|
| 32 | -6.165995 |
| 33 | -7.085003 |
| 34 | 6.774950 |
| 35 | -6.587248 |
| 36 | -3.376929 |
| 37 | 3.985122 |
| 38 | -2.667196 |
| 39 | 1.897966 |
| 40 | -0.5274138 |
| 41 | 2.095251 |
| 42 | 2.919628 |
| 43 | -2.764208 |
| 44 | 3.552233 |
| 45 | -1.328805 |
| 46 | 0.5683610 |
| 47 | -1.453698 |
| 48 | -17.65490 |
| 49 | 12.26411 |
| 50 | 10.39311 |
| 51 | -0.008816198 |
| 52 | -16.91925 |
| 53 | 26.91144 |
| 54 | 51.81767 |
| 55 | -163.7985 |
| 56 | 30.56925 |
| 57 | 145.7633 |
| 58 | 27.27600 |
| 59 | -8.266212 |
| 60 | 13.38214 |
| 61 | 17.78385 |
| 62 | -27.15166 |
| 63 | -14.55627 |

| | |
|---|---|
| 64 | 12.69555 |
| 65 | 3.133356 |
| 66 | -6.667568 |
| 67 | 0.7084940 |
| 68 | 8.529837 |
| 69 | -6.861002 |
| 70 | 18.12668 |
| 71 | -17.27931 |
| 72 | 21.95741 |
| 73 | -8.346875 |
| 74 | -3.468492 |
| 75 | -4.028366 |
| 76 | 3.197905 |
| 77 | 4.309918 |
| 78 | 3.817261 |
| 79 | -20.88475 |
| 80 | 4.997926 |
| 81 | 4.270534 |
| 82 | 16.60617 |
| 83 | 13.17446 |
| 84 | -21.62943 |
| 85 | -16.01792 |
| 86 | -9.517491 |
| 87 | -11.24691 |
| 88 | 27.65661 |
| 89 | 0.04087131 |
| 90 | -9.431314 |
| 91 | -3.191045 |
| 92 | -2.158094 |
| 93 | 8.602338 |
| 94 | 5.013416 |
| 95 | -11.22647 |

| | |
|---|---|
| 96 | -0.4200375 |
| 97 | 5.690363 |
| 98 | 7.369690 |
| 99 | -11.85435 |
| 100 | -2.467671 |
| 101 | 0.4580262 |
| 102 | 20.90960 |
| 103 | -21.36823 |
| 104 | -14.04450 |
| 105 | -2.465387 |
| 106 | -6.432362 |
| 107 | 2.124264 |
| 108 | 1.901681 |
| 109 | 3.878289 |
| 110 | -5.386267 |
| 111 | -3.401870 |
| 112 | 10.03267 |
| 113 | 6.775910 |
| 114 | -10.71452 |
| 115 | -5.215644 |
| 116 | 2.193280 |
| 117 | 6.702024 |
| 118 | 1.648252 |
| 119 | -4.835797 |
| 120 | -10.29826 |
| 121 | 7.486067 |
| 122 | n/a |
| 123 | n/a |

To model the behaviour of the cpGFP sensors the following equations were used

To determine the ratio of the protein which had bound to the molecule of interest the following equations was derived

$$K_D = \frac{(P_T - PL)(L_T - PL)}{PL} \quad \text{(AS1)}$$

Where $P_T$ is the total protein in the system, $PL$ is the protein ligand complex and $L_T$ is the total ligand in the system.

This simplifies to

$$0 = \frac{P_T \times L_T}{K_D} - PL\left(\frac{P_T + L_T}{K_D} + 1\right) + \frac{1}{K_D} \times PL^2 \quad \text{(AS2)}$$

From this the values for the quadratic formula can be obtained and solved taking only the negative version

$$x = \frac{-b - \sqrt{b^2 - 4ac}}{2a} \quad \text{(AS3)}$$

$$x = \frac{-\left(\frac{P_T + L_T}{K_D} + 1\right) - \sqrt{\left(\frac{P_T + L_T}{K_D} + 1\right)^2 - 4 \times \frac{1}{K_D} \times \frac{P_T \times L_T}{K_D}}}{2 \times \frac{1}{K_D}} \quad \text{(AS4)}$$

This solution would give the value for $PL$ from which the free protein ($P_F$) could be calculated knowing the total protein. Combing this with the fluorescence of the free protein and the bound protein can be used to determine the fluorescence at different concentrations of ligand.

$$TF = (F_F \times P_F) + (F_B \times PL) \quad \text{(AS5)}$$

The total fluorescence ($TF$) is found by the determining the fluorescence of the unbound cpGFP protein ($F_F \times P_F$) and the fluorescence of the bound protein ($F_B \times PL$)

# Appendix 3: Chapter 5 Building a wearable device

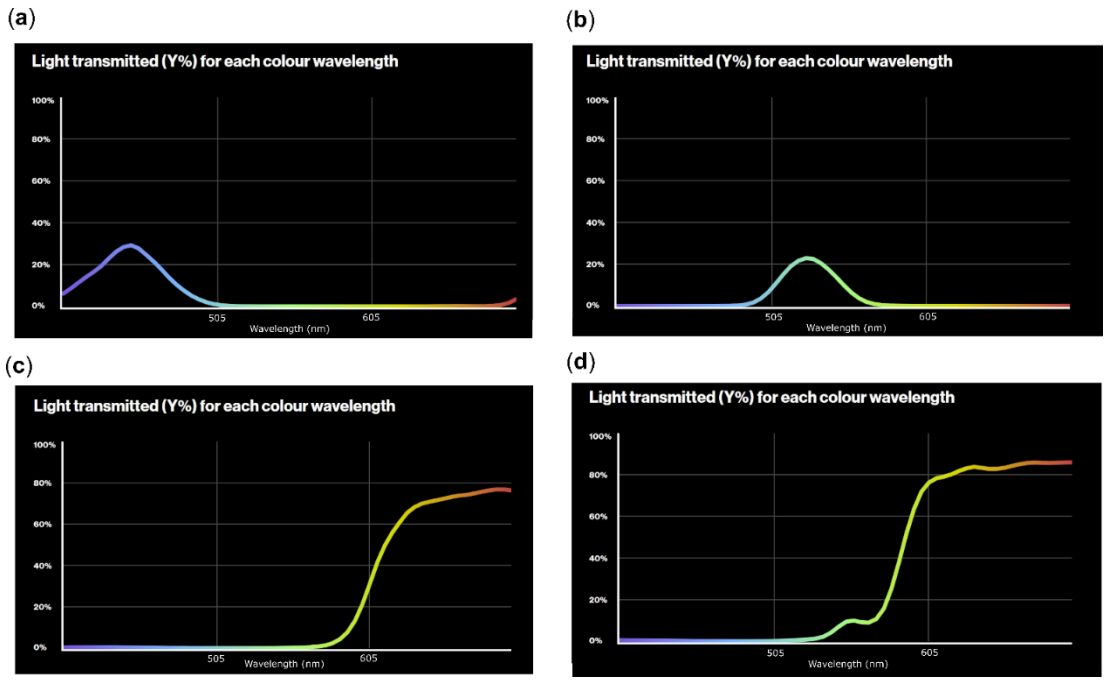


**Appendix Figure 5.1 Light spectra of the filters used in phone imaging of the wearable patch.** (**a**) shows the spectra of the Tokyo blue filter used. (**b**) shows the light spectr of the Twickenham green filter used. (**c**) shows the light spectra of the light red filter used. (**d**) shows the light spectra of the dark amber filter.

**Appendix Table 5.1: The table gives the green and red pixel value extracted from the different spot volume testing in Figure 5.9.**

| Patch | Row | Spot | | | | |
|---|---|---|---|---|---|---|
| | | 1 | 2 | 3 | 4 | 5 |
| **5 µl** | GFP | 99.296 | 108.78 | 120.145 | 129.418 | 153.558 |
| | RFP | 99.588 | 109.167 | 122.675 | 129.814 | 147.481 |
| | Blank- green | 94.863 | 94.408 | 97.388 | 109.388 | 116.189 |
| | Blank- red | 67.231 | 70.346 | 76.028 | 87.741 | 97.738 |
| **10 µl** | GFP | 112.941 | 116.467 | 122.193 | 125.652 | 130.195 |
| | RFP | 98.352 | 116.659 | 114.629 | 124.015 | 122.536 |
| | Blank- green | 94.446 | 94.755 | 105.096 | 110.726 | 117.143 |
| | Blank- red | 60.012 | 61.312 | 68.924 | 75.287 | 83.985 |

| | | | | | | |
|---|---|---|---|---|---|---|
| **15 µl** | GFP | 100.811 | 107.948 | 113.211 | 116.232 | 120.091 |
| | RFP | 119.762 | 113.427 | 123.485 | 127.044 | 131.273 |
| | Blank- green | 83.945 | 83.113 | 88.391 | 99.546 | 103.218 |
| | Blank- red | 69.42 | 72.512 | 75.183 | 75.926 | 81.923 |
| **20 µl** | GFP | 102.675 | 110.567 | 116.391 | 123.358 | n/a |
| | RFP | 89.625 | 97.703 | 105.028 | 106.498 | n/a |
| | Blank- green | 89.362 | 93.404 | 92.177 | 100.232 | n/a |
| | Blank- red | 64.812 | 70.16 | 70.112 | 74.349 | n/a |

**Appendix Table 5.2: The table gives GFP/mRFP ratio calculated from the spots in the wearable devices shown in Figure 5.11.**

| Patch | Row | Spot | | | | |
|---|---|---|---|---|---|---|
| | | 1 | 2 | 3 | 4 | 5 |
| **Uninduced** | Colony 1 | 0.962053 | 0.983227 | 1.036737 | 1.049153 | 1.022323 |
| | Colony 2 | 1.085926 | 1.089316 | 1.076036 | 1.085556 | 1.093166 |
| | Colony 3 | 1.098174 | 1.136933 | 1.202767 | 1.157279 | 1.172663 |
| **1 ml** | Colony 1 | 1.243231 | 1.156869 | 0.976814 | 0.868456 | 0.829669 |
| | Colony 2 | 1.425414 | 1.277223 | 1.100883 | 0.944515 | 0.879264 |
| | Colony 3 | 1.562806 | 1.420618 | n/a | 0.892188 | 0.8551 |
| **500 µl** | Colony 1 | 1.057533 | 1.0691 | 1.092367 | 1.107384 | 1.069962 |
| | Colony 2 | 1.123658 | 1.159178 | n/a | 1.209214 | 1.053964 |
| | Colony 3 | 1.133447 | 1.195237 | 1.264832 | 1.246202 | 1.295962 |

| | | | | | | |
|---|---|---|---|---|---|---|
| **250 µl** | Colony 1 | 1.046845 | 1.09162 | 1.095942 | 1.084667 | 1.063782 |
| | Colony 2 | 1.124831 | 1.096744 | 1.155444 | 1.111181 | 1.115663 |
| | Colony 3 | 1.139369 | 1.169801 | 1.268858 | 1.212014 | 1.206775 |
| **100 µl** | Colony 1 | 0.994165 | 1.099367 | 1.046907 | 1.036223 | 0.990116 |
| | Colony 2 | 1.023527 | 1.15162 | 1.171498 | 1.150167 | 1.049043 |
| | Colony 3 | 1.059722 | 1.145567 | 1.178842 | 1.222802 | 1.113449 |

**Appendix Table 5.3: This table gives the GFP/mRFP ratio calculated from the spots in the wearable devices shown in Figure 5.12.**

| Patch | Row | Spot | | | | |
|---|---|---|---|---|---|---|
| | | 1 | 2 | 3 | 4 | 5 |
| **Uninduced** | Colony 1 | 0.978161 | 1.028647 | 1.074962 | 1.063862 | 1.053541 |
| | Colony 2 | 1.016163 | 1.000281 | 1.051945 | 1.028713 | 1.067332 |
| | Colony 3 | 1.070762 | 1.101768 | 1.091773 | 1.019449 | 1.015 |
| **1 ml** | Colony 1 | 1.036094 | 1.095866 | 1.058206 | 1.093209 | 1.070972 |
| | Colony 2 | 1.070278 | 1.083845 | 1.121151 | 1.115595 | 1.058175 |
| | Colony 3 | 1.063463 | 1.168916 | 1.149636 | 1.142192 | 1.154944 |
| **500 µl** | Colony 1 | 2.140638 | 1.043087 | n/a | 1.111251 | 1.061231 |

| | | | | | | |
|---|---|---|---|---|---|---|
| | Colony 2 | 0.97084 | 1.069807 | 1.080737 | 1.097881 | 1.066009 |
| | Colony 3 | 1.068404 | 1.043313 | 1.242918 | 1.27064 | 1.153649 |
| | Colony 1 | 0.748188 | 0.783776 | 0.850642 | 0.78594 | 0.823846 |
| 250 µl | Colony 2 | 0.870214 | 0.929249 | 0.984406 | 0.987436 | 1.118633 |
| | Colony 3 | 0.958901 | 1.120621 | 1.087769 | 1.147795 | 1.195356 |
| | Colony 1 | 1.119194 | 1.116808 | 1.135 | 1.126006 | 1.160698 |
| 100 µl | Colony 2 | 1.139926 | 1.173636 | 1.193467 | 1.170151 | 1.174285 |
| | Colony 3 | 1.122329 | 1.177375 | 1.257203 | 1.265441 | 1.322627 |

**Appendix Table 5.4: This table gives the mNeonGreen/mRFP ratio calculated from the spots in the wearable devices shown in Figure 5.14.**

| Patch | Row | Spot | | | |
|---|---|---|---|---|---|
| | | 1 | 2 | 3 | 4 |
| Uninduced | Colony 1 | 1.140234 | 1.104822 | 1.177203 | 1.000097 |
| | Colony 2 | 1.232277 | 1.313987 | 1.185697 | 1.18512 |
| | Colony 3 | n/a | 1.245415 | 1.121624 | 1.214718 |
| 1 ml | Colony 1 | 1.060591 | 1.074554 | 1.0736 | 1.079809 |
| | Colony 2 | 1.001901 | 1.158282 | 1.194513 | 1.1972 |

| | | | | | |
|---|---|---|---|---|---|
| | Colony 3 | 1.137099 | 1.183088 | 1.055327 | 1.099478 |
| **500 µl** | Colony 1 | 0.939214 | 0.85098 | 0.894622 | 0.837257 |
| | Colony 2 | 1.028458 | 1.016766 | 1.115782 | 1.081123 |
| | Colony 3 | n/a | 0.901268 | 1.126362 | 1.14702 |
| **250 µl** | Colony 1 | 0.99209 | 0.941333 | 0.950405 | 0.920296 |
| | Colony 2 | n/a | 1.08533 | 1.00974 | 0.999648 |
| | Colony 3 | 1.100684 | 1.004317 | 0.960223 | 0.942878 |

**Appendix Table 5.5: This table gives the mNeonGreen/mRFP ratio calculated from the spots in the wearable devices shown in Figure 5.15.**

| Patch | Row | Spot | | | |
|---|---|---|---|---|---|
| | | 1 | 2 | 3 | 4 |
| **Uninduced** | Colony 1 | 1.374087 | 1.177708 | 1.083118 | n/a |
| | Colony 2 | 1.278347 | 1.172353 | 1.167077 | n/a |
| | Colony 3 | 1.0913 | 1.099832 | 1.115599 | n/a |
| **1 ml** | Colony 1 | 1.282693 | 1.21029 | 1.177248 | 1.14545 |
| | Colony 2 | n/a | 1.242771 | 1.207144 | 1.290717 |
| | Colony 3 | n/a | 1.199001 | 1.180976 | 1.142286 |

| | | | | | |
|---|---|---|---|---|---|
| **500 µl** | Colony 1 | 0.978546 | 1.109763 | 1.09976 | 0.933248 |
| | Colony 2 | 1.05626 | 1.168303 | 1.345976 | 0.980718 |
| | Colony 3 | 0.915147 | 1.039916 | 1.112972 | 1.007676 |
| **250 µl** | Colony 1 | 0.897056 | 1.014819 | 0.976528 | 0.979671 |
| | Colony 2 | 1.28205 | 1.174917 | 1.172757 | 1.108254 |
| | Colony 3 | 1.39781 | 1.056951 | 1.099989 | 1.061186 |

**Appendix Table 5.6: The table gives TAMRA/FAM ratio calculated from the spots in the wearable devices shown in Figure 5.16.**

| Patch | Filter | Row | Spot | | | | |
|---|---|---|---|---|---|---|---|
| | | | 1 | 2 | 3 | 4 | 5 |
| **Uninduced** | Light | 1 | 1.301279 | 0.959126 | 0.915495 | 0.880345 | 0.654711 |
| | Red | 2 | 0.959944 | 0.991348 | 0.950035 | 0.969363 | 0.921372 |
| | Dark | 1 | 0.588369 | 0.650679 | 0.703663 | 0.674539 | 0.46182 |
| | Amber | 2 | 0.687007 | 0.786096 | 0.702588 | 0.714854 | 0.645996 |
| **100 mM 500 µl** | Light | 1 | 0.898776 | 0.86692 | 0.820868 | 0.889101 | 0.825516 |
| | Red | 2 | 0.969087 | 0.865855 | 0.965307 | 0.875741 | 0.821316 |
| | Dark | 1 | 0.753739 | 0.846461 | 0.707479 | 0.732006 | 0.723811 |
| | Amber | 2 | 0.933709 | 0.828384 | 0.81545 | 0.700089 | 0.747078 |
| **100 mM 250 µl** | Light | 1 | 1.127659 | 1.284926 | 1.190105 | 1.117995 | 1.12054 |
| | Red | 2 | 1.27485 | 1.185483 | 1.207117 | 1.124825 | 1.139436 |
| | Dark | 1 | 0.798938 | 0.783309 | 0.760029 | 0.65415 | 0.488851 |
| | Amber | 2 | 0.848719 | 0.657067 | 0.785647 | 0.790926 | 0.725151 |
| **100 mM 100 µl** | Light | 1 | 1.211687 | 1.188509 | 1.117401 | 1.111021 | 1.13457 |
| | Red | 2 | 1.292226 | 1.151452 | 1.163873 | 1.114638 | 1.100066 |
| | | 1 | 0.978 | 0.913762 | 0.726481 | 0.65961 | 0.667944 |

| | | | | | | | |
|---|---|---|---|---|---|---|---|
| | Dark | 2 | | | | | |
| | Amber | | 0.883166 | 0.703135 | 0.726219 | 0.743425 | 0.761165 |
| | Light | 1 | 1.186814 | 1.160068 | 1.162631 | 1.102649 | 1.033304 |
| **50 mM** | Red | 2 | 1.096249 | 1.151811 | 1.115775 | 1.071948 | 1.042275 |
| **500 µl** | Dark | 1 | 0.921645 | 0.913696 | 0.973191 | 0.865349 | 0.783525 |
| | Amber | 2 | 0.863 | 1.000798 | 0.903422 | 0.81179 | 0.776762 |
| | Light | 1 | n/a | 0.953728 | 0.96219 | 1.015717 | 1.091449 |
| **50 mM** | Red | 2 | 1.026387 | 0.942616 | 1.01934 | 0.999334 | n/a |
| **250 µl** | Dark | 1 | n/a | 0.703075 | 0.742351 | 0.752249 | 0.802578 |
| | Amber | 2 | 0.725 | 0.705704 | 0.710715 | 0.734911 | n/a |
| | Light | 1 | 1.063553 | 1.034576 | 1.080847 | 1.164716 | 1.110406 |
| **50 mM** | Red | 2 | 1.117378 | 0.964649 | 1.10435 | 1.200882 | 1.022173 |
| **100 µl** | Dark | 1 | 0.821132 | 0.786181 | 0.844062 | 0.887637 | 0.813606 |
| | Amber | 2 | 0.841252 | 0.728908 | 0.870192 | 0.943653 | 0.716848 |

**Appendix Table 5.7: This table gives the mNeonGreen/mRFP ratio calculated from the spots in the wearable devices shown in Figure 5.17.**

| Patch | Row | Spot | | | |
|---|---|---|---|---|---|
| | | 1 | 2 | 3 | 4 |
| **500 µl** | MH064 | 1.356662 | 1.360199 | 1.272325 | 1.234849 |
| | MH081 | 1.173224 | 1.159734 | 1.177389 | 1.125321 |
| **250 µl** | MH064 | 1.266774 | 1.198662 | 1.213212 | 1.127419 |
| | MH081 | 1.049439 | 1.019153 | 0.972965 | 0.772142 |
| **100 µl** | MH064 | 1.35637 | 1.329495 | 1.236389 | 0.917472 |
| | MH081 | 1.174055 | 1.173699 | 1.095433 | 1.065073 |
| **Uninduced** | MH064 | 1.202102 | 1.257355 | 1.140232 | n/a |
| | MH081 | 1.089397 | 1.071226 | 0.995883 | n/a |
| **500 µl** | MH064 | 1.544412 | 1.487251 | 1.550893 | 1.463358 |
| | MH081 | 1.38539 | 1.403887 | 1.287178 | 1.29988 |
| **250 µl** | MH064 | 1.46172 | 1.456693 | 1.527613 | 1.581019 |
| | MH081 | 1.503175 | 1.444163 | 1.431274 | 1.177344 |
| **100 µl** | MH064 | 1.312085 | 1.563129 | 1.492144 | 1.343042 |

| | | | | | |
|---|---|---|---|---|---|
| **Uninduced** | MH081 | 1.323176 | 1.300666 | 1.275989 | 1.143796 |
| | MH064 | 1.379999 | 1.425957 | 1.43133 | 1.432824 |
| | MH081 | 1.233003 | 1.262185 | 1.347326 | 1.109666 |

The code given below if all of the code written to generate the first version of the App which used fixed positions for the spots within the patch.

The main activity gives the code for the homepage of the App which appears when the app is opened.

MainActivity.java

```
1    package UoE.PhDapp;
2
3    import androidx.appcompat.app.AppCompatActivity;
4
5    import android.content.Intent;
6    import android.os.Bundle;
7    import android.view.View;
8    import android.widget.Button;
9    import android.widget.ImageView;
10   import android.widget.TextView;
11
12   public class MainActivity extends AppCompatActivity
{
13
14       TextView dateLastTest;
15       ImageView lastResult;
16       Button instructions;
17       Button newAnalysis;
18       Button previousResults;
19
20       @Override
21       protected void onCreate(Bundle
savedInstanceState) {
22           super.onCreate(savedInstanceState);
23           setContentView(R.layout.activity_main);
24
25
26           instructions =
findViewById(R.id.main_activity_btn_instructions);
27           previousResults =
findViewById(R.id.main_activity_btn_previousdata);
28           dateLastTest =
findViewById(R.id.main_activity_tv_dateoflastresult);
```

```
29            lastResult =
findViewById(R.id.main_activity_iv_latestresult);
30            newAnalysis =
findViewById(R.id.main_activity_btn_takenewreading);
31
32            Intent goToInstructions = new
Intent(MainActivity.this, Instructions.class);
33            Intent goToPreviousResults = new
Intent(MainActivity.this, PreviousResults.class);
34            Intent startNewAnalysis = new
Intent(MainActivity.this, ImageCapture.class);
35
36
37                    instructions.setOnClickListener(new
View.OnClickListener() {
38
39                        @Override
40                        public void onClick(View v) {
41
42
43
startActivity(goToInstructions);
44                        }
45                    });
46
47          newAnalysis.setOnClickListener(new
View.OnClickListener() {
48
49                @Override
50                public void onClick(View v) {
51
52
53                    startActivity(startNewAnalysis);
54                }
55            });
56
57            previousResults.setOnClickListener(new
View.OnClickListener() {
58
59                @Override
60                public void onClick(View v) {
61
62
63                    startActivity(goToPreviousResults);
64                }
65            });
66
67
```

```
68          }
69
70
71
72      }
```

ImageCapture contains the code for taking the two images of the patch required for analysis, carrying out the required analysis and saving this data as well taking the used to the previous result page.

ImageCapture.java

```
1     package UoE.PhDapp;
2
3
4     import android.Manifest;
5     import android.annotation.SuppressLint;
6     import android.app.Activity;
7     import android.content.Context;
8     import android.content.DialogInterface;
9     import android.content.Intent;
10    import android.content.SharedPreferences;
11    import android.graphics.Bitmap;
12    import android.graphics.BitmapFactory;
13    import android.graphics.Color;
14    import android.net.Uri;
15    import android.os.Build;
16    import android.os.Bundle;
17    import android.os.Environment;
18    import android.util.Log;
19    import android.view.View;
20    import android.widget.Button;
21    import android.widget.ImageView;
22
23    import androidx.annotation.RequiresApi;
24    import androidx.appcompat.app.AlertDialog;
25    import androidx.appcompat.app.AppCompatActivity;
26    import androidx.core.app.ActivityCompat;
27    import androidx.core.content.FileProvider;
28
29
30    import java.io.File;
31    import java.io.FileNotFoundException;
32    import java.io.FileOutputStream;
33    import java.io.IOException;
34    import java.io.InvalidClassException;
```

```
35   import java.io.NotSerializableException;
36   import java.io.ObjectOutputStream;
37   import java.text.SimpleDateFormat;
38   import java.util.ArrayList;
39   import java.util.Arrays;
40   import java.util.Date;
41
42   import static
android.provider.MediaStore.ACTION_IMAGE_CAPTURE;
43   import static
android.provider.MediaStore.EXTRA_OUTPUT;
44
45
46   public class ImageCapture extends AppCompatActivity
{
47
48
49       static final String SHARED_PREFS_FILE = "yes";
50       static final int imageCapture = 1;
51       int requestCode;
52       Button takeImage;
53       ImageView imageTaken;
54       ImageView secondImage;
55       Uri photoURI;
56       File photoFile;
57       File resultFile;
58       String currentPhotoPath;
59       String currentResultPath;
60       int i = 0;
61       File directory =
Environment.getExternalStorageDirectory();
62       String TAG = "appNotes";
63       int fin;
64
65
66       ArrayList<String> files = new ArrayList<>();
67       ArrayList<String> filesRFP = new ArrayList<>();
68       private int[] pixelsGFP;
69       private int[] pixelsRFP;
70       int[] averageGFP= new int[25];
71       int[] averageRFP= new int[25];
72       int widthGFP;
73       int widthRFP;
74       int heightGFP;
75       int heightRFP;
76       int a=files.size();
77       int b=filesRFP.size();
78       double[] ratioPixels = new double[25];
```

```
79
80
81        public File createImageFile() throws IOException
{
82            String timeStamp = new
SimpleDateFormat("yyyyMMdd_HHmmss").format(new Date());
83            String imageFileName = "JPEG_" + timeStamp +
"_";
84            File storageDir =
getExternalFilesDir(Environment.DIRECTORY_PICTURES);
85            File image = File.createTempFile(
86                    imageFileName,  /* prefix */
87                    ".jpg",         /* suffix */
88                    storageDir      /* directory */
89            );
90
91            currentPhotoPath = image.getAbsolutePath();
92            return image;
93        }
94
95        public File createResultsFile() throws
IOException {
96            android.util.Log.i("PJW",
"ImageCapture.createResultsFile");
97            String timeStamp = new
SimpleDateFormat("yyyyMMdd_HHmmss").format(new Date());
98            String resultFileName = "RESULTS_" +
timeStamp + "_";
99            File storageDir =
getExternalFilesDir(Environment.DIRECTORY_DOCUMENTS);
100           File result = File.createTempFile(
101                   resultFileName,  /* prefix */
102                   ".result",         /* suffix */
103                   storageDir      /* directory */
104           );
105
106           currentResultPath =
result.getAbsolutePath();
107           android.util.Log.i("PJW",
"ImageCapture.createResultsFile: currentResultPath - " +
currentResultPath);
108           return result;
109       }
110
111
112
113       public Uri dispatchTakePictureIntent() {
114
```

```
115
116             Intent takePictureIntent = new
Intent(ACTION_IMAGE_CAPTURE);
117
118             try {
119                 photoFile = createImageFile();
120             } catch (IOException ignored) {
121             }
122
123             if (photoFile != null) {
124                 photoURI =
FileProvider.getUriForFile(this,
125                         "com.UoE.PhDapp.fileprovider",
126                         photoFile);
127                 takePictureIntent.putExtra(EXTRA_OUTPUT,
photoURI);
128
startActivityForResult(takePictureIntent, requestCode);
129
130
131             }
132
133             return photoURI;
134         }
135
136
137         public ArrayList<String> getGFP() {
138             SharedPreferences GFPpref =
getSharedPreferences(SHARED_PREFS_FILE, MODE_PRIVATE);
139             String GFPstring = GFPpref.getString("GFP",
"");
140
141
142             String[] split = GFPstring.split(",");
143             files = new
ArrayList<>(Arrays.asList(split));
144             return files;
145         }
146
147         public ArrayList<String> getRFP() {
148             SharedPreferences RFPpref =
getSharedPreferences(SHARED_PREFS_FILE, MODE_PRIVATE);
149             String RFPstring = RFPpref.getString("RFP",
"");
150
151
152             String[] splitRFP = RFPstring.split(",");
153
```

```
154
155             filesRFP = new
ArrayList<>(Arrays.asList(splitRFP));
156             return filesRFP;
157         }
158
159
160         @RequiresApi(api = Build.VERSION_CODES.O)
161         public void saveGFP() {
162
163             SharedPreferences prefs =
getSharedPreferences(SHARED_PREFS_FILE,
Context.MODE_PRIVATE);
164             SharedPreferences.Editor editor =
prefs.edit();
165             String listString = String.join(", ",
files);
166             editor.putString("GFP", listString);
167             editor.commit();
168         }
169
170         @RequiresApi(api = Build.VERSION_CODES.O)
171         public void saveRFP() {
172
173             SharedPreferences prefs =
getSharedPreferences(SHARED_PREFS_FILE,
Context.MODE_PRIVATE);
174             SharedPreferences.Editor editor =
prefs.edit();
175             String listString = String.join(", ",
filesRFP);
176             editor.putString("RFP", listString);
177             editor.commit();
178         }
179
180
181
182
183
184         @Override
185         protected void onCreate(Bundle
savedInstanceState) {
186             super.onCreate(savedInstanceState);
187             setContentView(R.layout.imagecapture);
188
189             takeImage =
findViewById(R.id.imagecapture_btn_takepicture);
```

```
190             secondImage =
findViewById(R.id.imageCapture_iv_RFP);
191             imageTaken =
findViewById(R.id.imageCapture_iv_GFP);
192
193
194             getGFP();
195             getRFP();
196
197
198
199
200             AlertDialog.Builder checkFilter = new
AlertDialog.Builder(ImageCapture.this);
201             checkFilter.setTitle("Check filters");
202             checkFilter.setMessage("Please check that
the filters currently set are for detecting green
fluorescence");
203             checkFilter.setPositiveButton("Ok", new
DialogInterface.OnClickListener() {
204                 @Override
205                 public void onClick(DialogInterface
dialog, int which) {
206                     checkFilter.create().cancel();
207                 }
208             });
209
210             checkFilter.create().show();
211
212
213             AlertDialog.Builder changeFilter = new
AlertDialog.Builder(ImageCapture.this);
214             changeFilter.setTitle("Change filters");
215             changeFilter.setMessage("Before taking the
second image please change the filters for detecting red
fluorescence.");
216             changeFilter.setPositiveButton("Ok", new
DialogInterface.OnClickListener() {
217                 @Override
218                 public void onClick(DialogInterface
dialog, int which) {
219                     changeFilter.create().cancel();
220                 }
221             });
222
223
224             takeImage.setOnClickListener(new
View.OnClickListener() {
```

```
225
226                 @RequiresApi(api =
Build.VERSION_CODES.O)
227                 @Override
228
229                 public void onClick(View v) {
230
ActivityCompat.requestPermissions(ImageCapture.this, new
String[]{Manifest.permission.CAMERA}, 1);
231
ActivityCompat.requestPermissions(ImageCapture.this, new
String[](DeWitte and Shakhnovich), 1);
232
ActivityCompat.requestPermissions(ImageCapture.this, new
String[](DeWitte and Shakhnovich), 1);
233
234                     if (i == 0) {
235
236                         dispatchTakePictureIntent();
237
238                         String temp = currentPhotoPath;
239                         files.add(temp);
240                         changeFilter.create().show();
241                         i = 1;
242
243                         saveGFP();
244
245
246                     } else {
247
248                         dispatchTakePictureIntent();
249                         String temp2 = currentPhotoPath;
250                         filesRFP.add(temp2);
251                         i = 0;
252                         saveRFP();
253                         fin=10;
254
255                     }
256
257                 }
258             });
259
260         }
261
262
263         @SuppressLint("NewApi")
264         @RequiresApi(api = Build.VERSION_CODES.N)
265         @Override
```

```
266      protected void onActivityResult(int requestCode,
int resultCode, Intent data) {
267          super.onActivityResult(requestCode,
resultCode, data);
268
269              if (fin==10) {
270                  BitmapFactory.Options options = new
BitmapFactory.Options();
271                  options.inMutable = true;
272
273
274                  getGFP();
275                  int n = files.size();
276                  String path = files.get((n -
1)).substring(20);
277                  String finalPath = directory + path;
278                  Bitmap GFP =
BitmapFactory.decodeFile(finalPath, options);
279                  imageTaken.setImageBitmap(GFP);
280
281
282                  getRFP();
283                  int m = filesRFP.size();
284
285                  calculationGreen(GFP);
286                  imageTaken.setImageBitmap(GFP);
287
288                  String pathRFP = filesRFP.get((m -
1)).substring(20);
289                  String finalPathRFP = directory +
pathRFP;
290                  Bitmap RFP =
BitmapFactory.decodeFile(finalPathRFP, options);
291                  secondImage.setImageBitmap(RFP);
292
293
294
295                  if ((n+m)%2==0){
296                      calculationRed(RFP);
297                      ratioCalculation();
298                    /*  AlertDialog.Builder result =
new AlertDialog.Builder(ImageCapture.this);
299                      result.setTitle("Result");
300
result.setMessage(String.valueOf(ratioPixels));
301                      result.setPositiveButton("Ok",
new DialogInterface.OnClickListener() {
302                          @Override
```

```
303                             public void
onClick(DialogInterface dialog, int which) {
304
result.create().cancel();
305                             }
306                         });
307
308                         result.create().show(); */
309                         dataSave();
310                         String temp3 =
currentResultPath;
311                         sendResult(temp3);
312                     }
313
314                      else {
315                      Log.i(TAG,"intent not started");
316                     }
317
318                 }
319             else {
320
321                 Log.i(TAG, "data is null");
322             }
323
324
325
326         }
327
328
329     public void sendResult(String path){
330
331             Intent intent = new
Intent(ImageCapture.this,PreviousResults.class);
332             int result=RESULT_OK;
333             int REQUEST_CODE=1;
334             String message = path;
335             intent.putExtra("message_key", message);
336             intent.putExtra("result",result);
337            startActivity(intent);
338         }
339
340      private void calculationGreen(Bitmap GFP) {
341
342             Log.i(TAG,"calculationGreen is called");
343
344             int[] pixelsGFPtemp = new int[10000];
345             int[] pixelsGFPtempgreen = new int[10000];
346             int z = 0;
```

```
347             int t=0;
348             int sumGFP = 0;
349 
350             widthGFP = GFP.getWidth();
351             heightGFP = GFP.getHeight();
352 
353             for (int y = 1; y < 6; y++) {
354                 for (int x = 1; x < 4; x++) {
355                     for (int d=0;d<3; d++) {
356                         for (int f=0;f<3;f++) {
357 
358 
359                             Log.i(TAG, "for loops are
run in green");
360 
361                             pixelsGFPtemp[z] =
GFP.getPixel((y * (widthGFP / 6) + d), (x * (heightGFP /
6)+f));
362                             pixelsGFPtempgreen[z] =
Color.green(pixelsGFPtemp[z]);
363 
364 
365                             GFP.setPixel((y * (widthGFP
/ 6)), (y * (heightGFP / 6)), 0xffff0000);
366 
367 
368                             sumGFP = sumGFP +
pixelsGFPtempgreen[z];
369 
370                             z = z + 1;
371                         }
372                     }
373                     averageGFP[t] = sumGFP / 9;
374                     t=t+1;
375                 }
376 
377             }
378             pixelsGFP=averageGFP;
379         }
380 
381         private void calculationRed(Bitmap RFP) {
382 
383             int[] pixelsRFPtemp = new int[10000];
384             int[] pixelsRFPtempred = new int[10000];
385             int z = 0;
386             int t=0;
387 
388             Log.i(TAG, "calculationRed is called");
```

```
389
390             widthRFP = RFP.getWidth();
391             heightRFP = RFP.getHeight();
392             int sumRFP = 0;
393
394             for (int y = 1; y < 6; y++) {
395                 for (int x = 1; x < 4; x++) {
396                     for (int d=0;d<3; d++) {
397                         for (int f = 0; f < 3; f++) {
398
399                             Log.i(TAG, "for loops are
run in red");
400
401                             pixelsRFPtemp[z] =
RFP.getPixel((y * (widthRFP / 6)+d), (x * (heightRFP /
6)+f));
402                             pixelsRFPtempred[z] =
Color.red(pixelsRFPtemp[z]);
403
404
405                             RFP.setPixel((y * (widthRFP
/ 6)), (x * (heightRFP / 6)), 0xffff0000);
406
407                             sumRFP = sumRFP +
pixelsRFPtempred[z];
408
409
410                             z = z + 1;
411                         }
412                     }
413                     averageRFP[t] = sumRFP / 9;
414                     t=t+1;
415                 }
416
417
418             }
419
420             pixelsRFP=averageRFP;
421         }
422
423         private void ratioCalculation(){
424                 for (int t=0;t<pixelsGFP.length; t++) {
425
426                     double p =
Double.valueOf(pixelsGFP[t]) /
Double.valueOf(pixelsRFP[t]);
427
428                     ratioPixels[t] = p;
```

```
429                 }
430
431         }
432
433         private void dataSave(){
434             try {
435                 resultFile = createResultsFile();
436             }catch (IOException ioe) {
437                 android.util.Log.e("IOException",
ioe.toString());
438             }
439             // Save results arrays
440             try {
441                 FileOutputStream fos = new
FileOutputStream(resultFile);
442                 ObjectOutputStream oos = new
ObjectOutputStream(fos);
443                 oos.writeObject(pixelsGFP);
444                 oos.writeObject(pixelsRFP);
445                 oos.writeObject(ratioPixels);
446                 oos.flush();
447                 oos.close();
448             }catch(FileNotFoundException fnfe){
449                 android.util.Log.e("PJW", "Caught an
FileNotFoundException - " + fnfe.toString());
450             }
451             catch(InvalidClassException ice){
452                 android.util.Log.e("PJW", "Caught an
InvalidClassException - " + ice.toString());
453             }
454             catch(NotSerializableException nse){
455                 android.util.Log.e("PJW", "Caught an
NotSerializableException - " + nse.toString());
456             }
457             catch(IOException ioe) {
458                 android.util.Log.e("PJW", "Caught an
IOException - " + ioe.toString());
459             }
460         }
461
462     }
463
464
```

Instructions gives the code for the instruction page of the App which could be accessed from the homepage

Instructions.java

```
1    package UoE.PhDapp;
2
3    import android.content.Intent;
4    import android.os.Bundle;
5    import android.view.View;
6    import android.widget.Button;
7    import android.widget.ImageView;
8    import android.widget.TextView;
9
10   import androidx.appcompat.app.AppCompatActivity;
11
12   public class Instructions extends AppCompatActivity
{
13
14       Button back;
15       ImageView stepOneIV;
16       TextView stepOneTV;
17       ImageView stepTwoIV;
18       TextView stepTwoTv;
19       ImageView stepThreeIV;
20       TextView stepThreeTV;
21       ImageView stepFourIV;
22       TextView stepFourTV;
23       ImageView stepFiveIV;
24       TextView stepFiveTV;
25       ImageView stepSixIV;
26       TextView stepSixTV;
27       ImageView stepSevenIV;
28       TextView stepSevenTV;
29       ImageView stepEightIV;
30       TextView stepEightTV;
31       ImageView stepNineIV;
32       TextView stepNineTV;
33       ImageView stepTenIV;
34       TextView stepTenTV;
35
36
37
38
39       String instructionOne= "To start a new analysis
click on the button on the homepage labelled Start a new
analysis";
```

```
40        String instructionTwo= "Once you have clicked to
start a new analysis you should see the following page
and message";
41        String instructionThree= "Check that the filters
over the flash and camera in the attachment are the
correct filters for GFP and then click OK to close this
pop-up" +
42                "\nWhen changing the filters ensure that
you do not directly touch the filter but carefully hold
on the edge as finger marks will affect the accuracy";
43        String instructionFour= "You are now ready to
start your analysis position the wearable device under
the camera and then click the purple button to start";
44        String instructionFive= "On clicking the button
the app will open up the phone camera, double check the
device is positioned in the centre of the image and click
to take the image";
45        String instructionSix= "You will then need to
confirm that you are happy with the picture by clicking
the tick, if not press the cross to retake the picture";
46        String instructionSeven= "After confirming the
picture you will be returned to the app and a new pop-up
will have appeared";
47        String instructionEight= "Change the filters to
the second pair required as stated on the pop-up and
click OK" +
48                "\nWhen changing the filters ensure that
you do not directly touch the filter but carefully hold
on the edge as finger marks will affect the accuracy";
49        String instructionNine= "Click the purple button
again to return to the camer and take the picture in the
same way as in steps 4, 5 and 6";
50        String instructionTen= "You have now completed
carrying out the analysis the app will then use these two
images to determine the levels of biomarkers in your
sweat, the results will be displayed on the home page and
in the previous results page when the results of all
analyses can be found";
51
52
53
54        @Override
55        protected void onCreate(Bundle
savedInstanceState) {
56            super.onCreate(savedInstanceState);
57            setContentView(R.layout.instructions);
58
```

```
59            back =
findViewById(R.id.instructions_btn_home);
60            stepOneTV =
findViewById(R.id.instructions_tv_stepOne);
61            stepTwoTv =
findViewById(R.id.instructions_tv_stepTwo);
62            stepThreeTV =
findViewById(R.id.instructions_tv_stepThree);
63            stepFourTV =
findViewById(R.id.instructions_tv_stepFour);
64            stepFiveTV =
findViewById(R.id.instructions_tv_stepFive);
65            stepSixTV =
findViewById(R.id.instruction_tv_stepSix);
66            stepSevenTV =
findViewById(R.id.instructions_tv_stepSeven);
67            stepEightTV =
findViewById(R.id.instructions_tv_stepEight);
68            stepNineTV =
findViewById(R.id.instructions_tv_stepNine);
69            stepTenTV =
findViewById(R.id.instructions_tv_stepTen);
70
71            stepOneIV =
findViewById(R.id.instructions_iv_stepOne);
72            stepTwoIV =
findViewById(R.id.instructions_iv_stepTwo);
73            stepThreeIV =
findViewById(R.id.instructions_iv_stepThree);
74            stepFourIV =
findViewById(R.id.instructions_iv_stepFour);
75            stepFiveIV =
findViewById(R.id.instructions_iv_stepFive);
76            stepSixIV =
findViewById(R.id.instructions_iv_stepSix);
77            stepSevenIV =
findViewById(R.id.instructions_iv_stepSeven);
78            stepEightIV =
findViewById(R.id.instructions_iv_stepEight);
79            stepNineIV =
findViewById(R.id.instruction_iv_stepNine);
80            stepTenIV =
findViewById(R.id.instructions_iv_stepTen);
81
82
83            stepOneTV.setText(instructionOne);
84            stepTwoTv.setText(instructionTwo);
85            stepThreeTV.setText(instructionThree);
```

```
86            stepFourTV.setText(instructionFour);
87            stepFiveTV.setText(instructionFive);
88            stepSixTV.setText(instructionSix);
89            stepSevenTV.setText(instructionSeven);
90            stepEightTV.setText(instructionEight);
91            stepNineTV.setText(instructionNine);
92            stepTenTV.setText(instructionTen);
93
94
stepOneIV.setImageResource(R.mipmap.home_page_cropped);
95
stepTwoIV.setImageResource(R.mipmap.check_filters_gfp_cro
pped);
96
stepSevenIV.setImageResource(R.mipmap.check_filters_rfp_c
ropped);
97
98
99
100           Intent goBack = new
Intent(Instructions.this, MainActivity.class);
101
102           back.setOnClickListener(new
View.OnClickListener() {
103               @Override
104               public void onClick(View v) {
105                   startActivity(goBack);
106               }
107
108
109           });
110
111       }
112   }
113
```

PreviousResults gives the code for the page which would store all of the date from previous tests. In the version of the App constructed this page is opened at the end of the analysis to display the result of that test.

PreviousResults.java

```
1    package UoE.PhDapp;
2
3    import android.content.DialogInterface;
4    import android.content.Intent;
5    import android.os.Bundle;
6    import android.util.Log;
7    import android.view.View;
8    import android.widget.Button;
9    import android.widget.TextView;
10
11   import androidx.appcompat.app.AlertDialog;
12   import androidx.appcompat.app.AppCompatActivity;
13
14   import java.io.FileInputStream;
15   import java.io.IOException;
16   import java.io.InvalidClassException;
17   import java.io.NotSerializableException;
18   import java.io.ObjectInputStream;
19   import java.util.ArrayList;
20   import java.util.Arrays;
21
22   import static android.content.ContentValues.TAG;
23
24
25   public class PreviousResults extends
AppCompatActivity {
26
27       Button back;
28       TextView resultOne;
29       double[] inputRatio;
30
31
32
33
34       @Override
35       protected void onCreate(Bundle
savedInstanceState) {
36           super.onCreate(savedInstanceState);
37           setContentView(R.layout.results);
38
39           back = findViewById(R.id.results_btn_home);
```

```
40            resultOne = findViewById(R.id.textView5);
41            Intent goBack = new
Intent(PreviousResults.this, MainActivity.class);
42
43
44            back.setOnClickListener(new
View.OnClickListener() {
45                @Override
46                public void onClick(View v) {
47                    startActivity(goBack);
48                }
49
50
51            });
52
53
54
55
56
57                String message =
getIntent().getStringExtra("message_key");
58
59            if (message!=null){
60                openFiles(message);
61
62
resultOne.setText(String.valueOf(inputRatio));
63
64                Log.i(TAG, "onActivityResult: if loop
run");
65
66            }
67            else {
68                Log.i(TAG, "onActivityResult: loop not
run");
69            }
70
71
72        }
73
74
75        public double[] openFiles(String path) {
76            try {
77
78                FileInputStream fis = new
FileInputStream(path);
79                ObjectInputStream ois = new
ObjectInputStream(fis);
```

```
80                int[] inputGFP = (int[])
ois.readObject();
81                int[] inputRFP = (int[])
ois.readObject();
82                inputRatio = (double[])
ois.readObject();
83                ois.close();
84
85
86                android.util.Log.i("PJW",
"ImageCapture.ratioCalculation Stored Green Pixels - " +
Arrays.toString(inputGFP));
87                android.util.Log.i("PJW",
"ImageCapture.ratioCalculation Stored Red Pixels - " +
Arrays.toString(inputRFP));
88                android.util.Log.i("PJW",
"ImageCapture.ratioCalculation Stored Ratios - " +
Arrays.toString(inputRatio));
89
90            } catch (ClassNotFoundException cnfe) {
91                android.util.Log.e("PJW", "Caught a
ClassNotFoundException - " + cnfe.toString());
92            } catch (InvalidClassException ice) {
93                android.util.Log.e("PJW", "Caught an
InvalidClassException - " + ice.toString());
94            } catch (NotSerializableException nse) {
95                android.util.Log.e("PJW", "Caught an
NotSerializableException - " + nse.toString());
96            } catch (IOException ioe) {
97                android.util.Log.e("PJW", "Caught an
IOException - " + ioe.toString());
98            }
99            return inputRatio;
100       }
101
102
103   }
```

The xml files give the layouts of each page of the App

Activity_main gives the layout for the homepage

activity_main.xml

```
1    <?xml version="1.0" encoding="utf-8"?>
2    <androidx.constraintlayout.widget.ConstraintLayout
xmlns:android="http://schemas.android.com/apk/res/android
"
3        xmlns:app="http://schemas.android.com/apk/res-
auto"
4        xmlns:tools="http://schemas.android.com/tools"
5        android:layout_width="match_parent"
6        android:layout_height="match_parent"
7        android:background="#BFC5E3"
8        android:foregroundTint="#3F51B5"
9        tools:context=".MainActivity">
10
11       <ImageView
12
android:id="@+id/main_activity_iv_latestresult"
13           android:layout_width="wrap_content"
14           android:layout_height="wrap_content"
15           android:adjustViewBounds="true"
16
android:contentDescription="@string/graph_of_results_from
_last_analysis_carried_out"
17           app:layout_constraintEnd_toEndOf="parent"
18
app:layout_constraintStart_toStartOf="parent"
19           app:layout_constraintTop_toTopOf="parent"
20
tools:srcCompat="@tools:sample/backgrounds/scenic" />
21
22       <TextView
23
android:id="@+id/main_activity_tv_dateoflastresult"
24           android:layout_width="wrap_content"
25           android:layout_height="wrap_content"
26           android:layout_marginTop="15dp"
27           android:text="@string/date"
28           app:layout_constraintEnd_toEndOf="parent"
29           app:layout_constraintHorizontal_bias="0.1"
30
app:layout_constraintStart_toStartOf="parent"
```

```
31
app:layout_constraintTop_toBottomOf="@+id/main_activity_i
v_latestresult" />
32
33        <Button
34
android:id="@+id/main_activity_btn_instructions"
35
style="@style/Widget.AppCompat.Button.Borderless"
36            android:layout_width="240dp"
37            android:layout_height="wrap_content"
38            android:layout_marginTop="32dp"
39            android:background="#673AB7"
40            android:fontFamily="sans-serif-thin"
41
android:text="@string/how_to_analyse_your_wearable_device
"
42            android:textAllCaps="false"
43            android:textStyle="bold"
44            app:layout_constraintEnd_toEndOf="parent"
45
app:layout_constraintStart_toStartOf="parent"
46
app:layout_constraintTop_toBottomOf="@+id/main_activity_t
v_dateoflastresult" />
47
48        <LinearLayout
49            android:layout_width="0dp"
50            android:layout_height="wrap_content"
51            android:layout_margin="16dp"
52            android:layout_marginStart="16dp"
53            android:layout_marginTop="32dp"
54            android:layout_marginEnd="16dp"
55            android:layout_marginBottom="16dp"
56            android:orientation="horizontal"
57
app:layout_constraintBottom_toBottomOf="parent"
58            app:layout_constraintEnd_toEndOf="parent"
59
app:layout_constraintStart_toStartOf="parent"
60
app:layout_constraintTop_toBottomOf="@+id/main_activity_b
tn_instructions"
61            app:layout_marginBaseline="16dp">
62
63            <Button
64
android:id="@+id/main_activity_btn_takenewreading"
```

```
65                style="@style/Widget.AppCompat.Button"
66                android:layout_width="wrap_content"
67                android:layout_height="wrap_content"
68                android:layout_weight="1"
69                android:background="#673AB7"
70                android:backgroundTint="#FFFFFF"
71                android:fontFamily="sans-serif-thin"
72                android:insetRight="12dp"
73
android:text="@string/start_new_analysis"
74                android:textAllCaps="false"
75                android:textSize="18sp"
76                android:textStyle="bold" />
77
78            <Button
79
android:id="@+id/main_activity_btn_previousdata"
80                style="@style/Widget.AppCompat.Button"
81                android:layout_width="wrap_content"
82                android:layout_height="wrap_content"
83                android:layout_weight="1"
84                android:background="#673AB7"
85                android:fontFamily="sans-serif-thin"
86                android:insetLeft="12dp"
87                android:text="@string/previous_results"
88                android:textAllCaps="false"
89                android:textSize="18sp"
90                android:textStyle="bold" />
91        </LinearLayout>
92
93    </androidx.constraintlayout.widget.ConstraintLayout>
```

Imagecapture gives the layout for the image analysis page of the App

Imagecapture.xml

```
1     <?xml version="1.0" encoding="utf-8"?>
2     <androidx.constraintlayout.widget.ConstraintLayout
3
xmlns:android="http://schemas.android.com/apk/res/android
"
4         xmlns:app="http://schemas.android.com/apk/res-
auto"
5         xmlns:tools="http://schemas.android.com/tools"
6         android:layout_width="match_parent"
7         android:layout_height="match_parent">
8
9         <Button
```

```
10
android:id="@+id/imagecapture_btn_takepicture"
11          style="@style/Widget.AppCompat.Button.Small"
12          android:layout_width="wrap_content"
13          android:layout_height="wrap_content"
14
app:layout_constraintBottom_toBottomOf="parent"
15          app:layout_constraintEnd_toEndOf="parent"
16          app:layout_constraintHorizontal_bias="0.50"
17
app:layout_constraintStart_toStartOf="parent"
18          app:layout_constraintTop_toTopOf="parent"
19          app:layout_constraintVertical_bias="0.95"
20          />
21
22      <LinearLayout
23          android:id="@+id/linearLayout"
24          android:layout_width="wrap_content"
25          android:layout_height="wrap_content"
26          android:orientation="vertical"
27
app:layout_constraintBottom_toBottomOf="parent"
28          app:layout_constraintEnd_toEndOf="parent"
29
app:layout_constraintStart_toStartOf="parent"
30          app:layout_constraintTop_toTopOf="parent">
31
32          <ImageView
33              android:id="@+id/imageCapture_iv_GFP"
34              android:layout_width="wrap_content"
35              android:layout_height="wrap_content"
36              android:layout_marginTop="16dp"
37              android:layout_marginBottom="16dp"
38              android:layout_weight="1"
39
android:contentDescription="@string/gfp_fluoresence_image
"
40              android:visibility="invisible"
41
tools:srcCompat="@drawable/ic_launcher_background" />
42
43          <ImageView
44              android:id="@+id/imageCapture_iv_RFP"
45              android:layout_width="wrap_content"
46              android:layout_height="wrap_content"
47              android:layout_marginBottom="16dp"
48              android:layout_weight="1"
```

```
49
android:contentDescription="@string/rfp_flourescence_imag
e"
50                android:visibility="invisible"
51
tools:srcCompat="@drawable/ic_launcher_background" />
52        </LinearLayout>
53
54
55    </androidx.constraintlayout.widget.ConstraintLayout>
```

Instructions gives the layout for the instruction page of the App

Instructions.xml

```
1     <?xml version="1.0" encoding="utf-8"?>
2     <androidx.constraintlayout.widget.ConstraintLayout
3
xmlns:android="http://schemas.android.com/apk/res/android
"
4         xmlns:app="http://schemas.android.com/apk/res-
auto"
5         xmlns:tools="http://schemas.android.com/tools"
6         android:layout_width="match_parent"
7         android:layout_height="match_parent">
8
9         <Button
10            android:id="@+id/instructions_btn_home"
11            android:layout_width="wrap_content"
12            android:layout_height="wrap_content"
13            android:layout_marginTop="8dp"
14            android:layout_marginEnd="8dp"
15            android:fontFamily="sans-serif-thin"
16            android:text="@string/home"
17            android:textAllCaps="false"
18
android:textAppearance="@style/TextAppearance.AppCompat.B
ody1"
19            android:textSize="18sp"
20            android:textStyle="bold"
21            app:layout_constraintEnd_toEndOf="parent"
22            app:layout_constraintTop_toTopOf="parent" />
23
24        <ScrollView
25            android:layout_width="match_parent"
26            android:layout_height="match_parent"
27            tools:layout_editor_absoluteX="202dp"
```

```
28          tools:layout_editor_absoluteY="167dp">
29
30          <LinearLayout
31              android:layout_width="match_parent"
32              android:layout_height="wrap_content"
33              android:orientation="vertical" >
34
35              <ImageView
36
android:id="@+id/instructions_iv_stepOne"
37                  android:layout_width="wrap_content"
38                  android:layout_height="wrap_content"
39
android:contentDescription="@string/image_highlighting_st
art_new_analysis_button_on_homepages"
40
tools:srcCompat="@tools:sample/backgrounds/scenic" />
41
42              <TextView
43
android:id="@+id/instructions_tv_stepOne"
44                  android:layout_width="match_parent"
45                  android:layout_height="wrap_content"
46                  android:text="@string/step_one" />
47
48              <ImageView
49
android:id="@+id/instructions_iv_stepTwo"
50                  android:layout_width="wrap_content"
51                  android:layout_height="wrap_content"
52
android:contentDescription="@string/image_of_pop_up_remdi
ning_to_check_correct_filters"
53
tools:srcCompat="@tools:sample/backgrounds/scenic" />
54
55              <TextView
56
android:id="@+id/instructions_tv_stepTwo"
57                  android:layout_width="match_parent"
58                  android:layout_height="wrap_content"
59                  android:text="@string/step_two" />
60
61              <ImageView
62
android:id="@+id/instructions_iv_stepThree"
63                  android:layout_width="wrap_content"
64                  android:layout_height="wrap_content"
```

```
65
tools:srcCompat="@tools:sample/backgrounds/scenic" />
66
67                <TextView
68
android:id="@+id/instructions_tv_stepThree"
69                    android:layout_width="match_parent"
70                    android:layout_height="wrap_content"
71                    android:text="@string/step_three" />
72
73                <ImageView
74
android:id="@+id/instructions_iv_stepFour"
75                    android:layout_width="wrap_content"
76                    android:layout_height="wrap_content"
77
tools:srcCompat="@tools:sample/backgrounds/scenic" />
78
79                <TextView
80
android:id="@+id/instructions_tv_stepFour"
81                    android:layout_width="match_parent"
82                    android:layout_height="wrap_content"
83                    android:text="@string/step_four" />
84
85                <ImageView
86
android:id="@+id/instructions_iv_stepFive"
87                    android:layout_width="wrap_content"
88                    android:layout_height="wrap_content"
89
tools:srcCompat="@tools:sample/backgrounds/scenic" />
90
91                <TextView
92
android:id="@+id/instructions_tv_stepFive"
93                    android:layout_width="match_parent"
94                    android:layout_height="wrap_content"
95                    android:text="@string/step_five" />
96
97                <ImageView
98
android:id="@+id/instructions_iv_stepSix"
99                    android:layout_width="wrap_content"
100                    android:layout_height="wrap_content"
101
tools:srcCompat="@tools:sample/backgrounds/scenic" />
102
```

```
103             <TextView
104
android:id="@+id/instruction_tv_stepSix"
105                 android:layout_width="match_parent"
106                 android:layout_height="wrap_content"
107                 android:text="@string/step_six" />
108
109             <ImageView
110
android:id="@+id/instructions_iv_stepSeven"
111                 android:layout_width="wrap_content"
112                 android:layout_height="wrap_content"
113
android:contentDescription="@string/image_of_second_pop_r
eminding_to_change_filters"
114
tools:srcCompat="@tools:sample/backgrounds/scenic" />
115
116             <TextView
117
android:id="@+id/instructions_tv_stepSeven"
118                 android:layout_width="match_parent"
119                 android:layout_height="wrap_content"
120                 android:text="@string/step_seven" />
121
122             <ImageView
123
android:id="@+id/instructions_iv_stepEight"
124                 android:layout_width="wrap_content"
125                 android:layout_height="wrap_content"
126
tools:srcCompat="@tools:sample/backgrounds/scenic" />
127
128             <TextView
129
android:id="@+id/instructions_tv_stepEight"
130                 android:layout_width="match_parent"
131                 android:layout_height="wrap_content"
132                 android:text="@string/step_eight" />
133
134             <ImageView
135
android:id="@+id/instruction_iv_stepNine"
136                 android:layout_width="wrap_content"
137                 android:layout_height="wrap_content"
138
tools:srcCompat="@tools:sample/backgrounds/scenic" />
139
```

```
140             <TextView
141
android:id="@+id/instructions_tv_stepNine"
142                 android:layout_width="match_parent"
143                 android:layout_height="wrap_content"
144                 android:text="@string/step_nine" />
145
146             <ImageView
147
android:id="@+id/instructions_iv_stepTen"
148                 android:layout_width="wrap_content"
149                 android:layout_height="wrap_content"
150
tools:srcCompat="@tools:sample/backgrounds/scenic" />
151
152             <TextView
153
android:id="@+id/instructions_tv_stepTen"
154                 android:layout_width="match_parent"
155                 android:layout_height="wrap_content"
156                 android:text="@string/step_ten" />
157
158         </LinearLayout>
159     </ScrollView>
160 </androidx.constraintlayout.widget.ConstraintLayout>
```

Results gives the layout for the result page of the App

Results.xml

```
1    <?xml version="1.0" encoding="utf-8"?>
2    <androidx.constraintlayout.widget.ConstraintLayout
3
xmlns:android="http://schemas.android.com/apk/res/android
"
4        xmlns:app="http://schemas.android.com/apk/res-
auto"
5        xmlns:tools="http://schemas.android.com/tools"
6        android:layout_width="match_parent"
7        android:layout_height="match_parent">
8
9        <Button
10           android:id="@+id/results_btn_home"
11           android:layout_width="wrap_content"
12           android:layout_height="wrap_content"
13           android:layout_marginTop="8dp"
14           android:layout_marginEnd="8dp"
```

```
15          android:fontFamily="sans-serif-thin"
16          android:text="@string/home"
17          android:textAllCaps="false"
18
android:textAppearance="@style/TextAppearance.AppCompat.B
ody1"
19          android:textSize="18sp"
20          android:textStyle="bold"
21
app:layout_constraintBottom_toBottomOf="@+id/scrollView2"
22
app:layout_constraintEnd_toStartOf="@+id/searchView"
23          app:layout_constraintHorizontal_bias="1.0"
24
app:layout_constraintStart_toStartOf="parent"
25
app:layout_constraintTop_toTopOf="@+id/scrollView2"
26          app:layout_constraintVertical_bias="0.0" />
27
28      <SearchView
29          android:id="@+id/searchView"
30          android:layout_width="wrap_content"
31          android:layout_height="wrap_content"
32          android:layout_marginTop="8dp"
33          android:layout_marginEnd="8dp"
34
app:layout_constraintEnd_toEndOf="@+id/scrollView2"
35
app:layout_constraintTop_toTopOf="@+id/scrollView2">
36
37      </SearchView>
38
39      <ScrollView
40          android:id="@+id/scrollView2"
41          android:layout_width="match_parent"
42          android:layout_height="match_parent"
43          tools:layout_editor_absoluteX="175dp"
44          tools:layout_editor_absoluteY="200dp">
45
46          <LinearLayout
47              android:layout_width="match_parent"
48              android:layout_height="wrap_content"
49              android:orientation="vertical">
50
51              <ImageView
52                  android:id="@+id/imageView5"
53                  android:layout_width="wrap_content"
54                  android:layout_height="wrap_content"
```

```
                    android:layout_weight="1"

tools:srcCompat="@tools:sample/backgrounds/scenic" />

                <TextView
                    android:id="@+id/textView5"
                    android:layout_width="wrap_content"
                    android:layout_height="wrap_content"
                    android:layout_weight="1"
                    android:text="TextView" />

                <ImageView
                    android:id="@+id/imageView6"
                    android:layout_width="match_parent"
                    android:layout_height="wrap_content"
                    android:layout_weight="1"

tools:srcCompat="@tools:sample/backgrounds/scenic" />

                <TextView
                    android:id="@+id/textView6"
                    android:layout_width="match_parent"
                    android:layout_height="wrap_content"
                    android:layout_weight="1"
                    android:text="TextView" />

            </LinearLayout>
        </ScrollView>

    </androidx.constraintlayout.widget.ConstraintLayout>
```

# Appendix 4: Publications

Parts of Chapter 1 have been written and adapted from ‘Synthetic Biology Enables Programmable Cell-Based Biosensors’ *ChemPhysChem* 2020

# References


AGUILERA, L., CAMPOS, E., GIMÉNEZ, R., BADÍA, J., AGUILAR, J. & BALDOMA, L. 2008. Dual role of LldR in regulation of the lldPRD operon, involved in L-lactate metabolism in *Escherichia coli*. *Journal of Bacteriology,* 190**,** 2997.

AL-TAMER, Y. Y. & HADI, E. A. 1994. Age dependent reference intervals of glucose, urea, protein, lactate and electrolytes in thermally induced sweat. *European Journal of Clinical Chemistry and Clinical Biochemistry,* 32**,** 71-77.

ALCANTAR, N. A., AYDIL, E. S. & ISRAELACHVILI, J. N. 2000. Polyethylene glycol-coated biocompatible surfaces. *J Biomed Mater Res,* 51**,** 343-51.

AMES, B. N., LEE, F. D. & DURSTON, W. E. 1973. An Improved Bacterial Test System for the Detection and Classification of Mutagens and Carcinogens. *Proceedings of the National Academy of Sciences,* 70**,** 782-786.

ANASTASOVA, S., CREWTHER, B., BEMBNOWICZ, P., CURTO, V., IP, H. M. D., ROSA, B. & YANG, G.-Z. 2017. A wearable multisensing patch for continuous sweat monitoring. *Biosensors and Bioelectronics,* 93**,** 139-145.

ANG, J., HARRIS, E., HUSSEY, B. J., KIL, R. & MCMILLEN, D. R. 2013. Tuning Response Curves for Synthetic Biology. *ACS Synthetic Biology,* 2**,** 547-567.

ARAKAWA, T., KUROKI, Y., NITTA, H., CHOUHAN, P., TOMA, K., SAWADA, S.-I., TAKEUCHI, S., SEKITA, T., AKIYOSHI, K., MINAKUCHI, S. & MITSUBAYASHI, K. 2016. Mouthguard biosensor with telemetry system for monitoring of saliva glucose: A novel cavitas sensor. *Biosensors and Bioelectronics,* 84**,** 106-111.

BAKER, L. B. 2017. Sweating Rate and Sweat Sodium Concentration in Athletes: A Review of Methodology and Intra/Interindividual Variability. *Sports Medicine,* 47**,** 111-128.

BAKER, L. B. 2019a. Physiology of sweat gland function: The roles of sweating and sweat composition in human health. *Temperature* 6**,** 211-259.

BAKER, L. B. 2019b. Physiology of sweat gland function: The roles of sweating and sweat composition in human health. *Temperature,* 6**,** 211-259.

BAKER, M. 2015. Reproducibility crisis: Blame it on the antibodies. *Nature,* 521**,** 274-276.

BANKS, A. M., WHITFIELD, C. J., BROWN, S. R., FULTON, D. A., GOODCHILD, S. A., GRANT, C., LOVE, J., LENDREM, D. W., FIELDSEND, J. E. & HOWARD, T. P. 2022a. Key reaction components affect the kinetics and performance robustness of cell-free protein synthesis reactions. *Comput Struct Biotechnol J,* 20**,** 218-229.

BANKS, A. M., WHITFIELD, C. J., BROWN, S. R., FULTON, D. A., GOODCHILD, S. A., GRANT, C., LOVE, J., LENDREM, D. W., FIELDSEND, J. E. & HOWARD, T. P. 2022b. Key reaction components affect the kinetics and performance robustness of cell-free protein synthesis reactions. *Computational and Structural Biotechnology Journal,* 20**,** 218-229.

BATES, G. P. & MILLER, V. S. 2008. Sweat rate and sodium loss during work in the heat. *Journal of Occupational Medicine and Toxicology,* 3**,** 4-9.

BAUMGARTNER, J. W., KIM, C., BRISSETTE, R. E., INOUYE, M., PARK, C. & HAZELBAUER, G. L. 1994. Transmembrane signalling by a hybrid protein: communication from the domain of chemoreceptor Trg that recognizes sugar-binding proteins to the kinase/phosphatase domain of osmosensor EnvZ. *Journal of Bacteriology,* 176**,** 1157-1163.

BECSKEI, A. & SERRANO, L. 2000. Engineering stability in gene networks by autoregulation. *Nature,* 405**,** 590-593.
BEGGAH, S., VOGNE, C., ZENARO, E. & VAN DER MEER, J. R. 2008. Mutant HbpR transcription activator isolation for 2-chlorobiphenyl via green fluorescent protein-based flow cytometry and cell sorting. *Microbial Biotechnology,* 1**,** 68-78.
BEREPIKI, A., KENT, R., MACHADO, L. F. M. & DIXON, N. 2020. Development of High-Performance Whole Cell Biosensors Aided by Statistical Modeling. *ACS Synth Biol,* 9**,** 576-589.
BIOTECHNOLOGY ACTIVITIES, O. O. 2019. NIH Guidelines for Research Involving Recombinant or Synthetic Nucleic Acid Molecules. *In:* ACTIVITIES, O. O. B. (ed.). National Institute of Health.
BONAWITZ, R. E., DUNCAN, J., HAMMOND, E., HAMOMBA, L., NAMBULE, J., SAMBAMBI, K., MUSONDA, V., CALISE, A., KNAPP, A., MWALE, J., MCCAULEY, J., THEA, D. & HERLIHY, J. M. 2015. Assessment of the impact of rapid syphilis tests on syphilis screening and treatment of pregnant women in Zambia. *International Journal of Gynecology & Obstetrics,* 130**,** S58-S62.
BORKOWSKI, O., CERONI, F., STAN, G.-B. & ELLIS, T. 2016. Overloaded and stressed: whole-cell considerations for bacterial synthetic biology. *Current Opinion in Microbiology,* 33**,** 123-130.
BOUSSE, L. 1996. Whole cell biosensors. *Sensors and Actuators B: Chemical,* 34**,** 270-275.
BOYD, M. A. & KAMAT, N. P. 2021. Designing Artificial Cells towards a New Generation of Biosensors. *Trends in Biotechnology,* 39**,** 927-939.
BOYD, M. A., THAVARAJAH, W., LUCKS, J. B. & KAMAT, N. P. 2023. Robust and tunable performance of a cell-free biosensor encapsulated in lipid vesicles. *Science Advances,* 9**,** eadd6605.
BOYSEN, T. C., YANAGAWA, S., SATO, F. & SATO, K. 1984. A modified anaerobic method of sweat collection. *Journal of Applied Physiology,* 56**,** 1302-1307.
BRADLEY, R. W., BUCK, M. & WANG, B. 2016. Recognizing and engineering digital-like logic gates and switches in gene regulatory networks. *Current Opinion in Microbiology,* 33**,** 74-82.
BROPHY, J. A. N. & VOIGT, C. A. 2016. Antisense transcription as a tool to tune gene expression. *Molecular Systems Biology,* 12**,** 854.
BRUEN, D., DELANEY, C., FLOREA, L. & DIAMOND, D. 2017. Glucose Sensing for Diabetes Monitoring: Recent Developments. *Sensors (Basel),* 17**,** 1-21.
BUFFI, N., BEGGAH, S., TRUFFER, F., GEISER, M., VAN LINTEL, H., RENAUD, P. & VAN DER MEER, J. R. 2016. An automated microreactor for semi-continuous biosensor measurements. *Lab on a Chip,* 16**,** 1383-1392.
BULICH, A. A. & ISENBERG, D. L. 1981. Use of the luminescent bacterial system for the rapid assessment of aquatic toxicity. *ISA Trans,* 20**,** 29-33.
BUONO, M. J., LEE, N. V. L. & MILLER, P. W. 2010. The relationship between exercise intensity and the sweat lactate excretion rate. *The Journal of Physiological Sciences,* 60**,** 103-107.
CAMERON, D. E. & COLLINS, J. J. 2014. Tunable protein degradation in bacteria. *Nature Biotechnology,* 32**,** 1276-1281.
CAMPBELL, R. E., TOUR, O., PALMER, A. E., STEINBACH, P. A., BAIRD, G. S., ZACHARIAS, D. A. & TSIEN, R. Y. 2002. A monomeric red fluorescent protein. *Proceedings of the National Academy of Sciences,* 99**,** 7877-7882.
CATHERINE, A. T., SHISHIDO, S. N., ROBBINS-WELTY, G. A. & DIEGELMAN-PARENTE, A. 2014. Rational design of a structure-switching DNA aptamer for potassium ions. *FEBS Open Bio,* 4**,** 788-795.

CAYRON, J., PRUDENT, E., ESCOFFIER, C., GUEGUEN, E., MANDRAND-BERTHELOT, M.-A., PIGNOL, D., GARCIA, D. & RODRIGUE, A. 2017. Pushing the limits of nickel detection to nanomolar range using a set of engineered bioluminescent Escherichia coli. *Environmental Science and Pollution Research,* 24**,** 4-14.

CELLESI, F., TIRELLI, N. & HUBBELL, J. A. 2002. Materials for cell encapsulation via a new tandem approach combining reverse thermal gelation and covalent crosslinking. *Macromolecular Chemistry and Physics,* 203**,** 1466-1472.

CHAN, C. T. Y., LEE, J. W., CAMERON, D. E., BASHOR, C. J. & COLLINS, J. J. 2015. 'Deadman' and 'Passcode' microbial kill switches for bacterial containment. *Nature Chemical Biology,* 12**,** 82.

CHANDRA, A., SHARMA, A., DEHZANGI, A., RANGANATHAN, S., JOKHAN, A., CHOU, K.-C. & TSUNODA, T. 2018. PhoglyStruct: Prediction of phosphoglycerylated lysine residues using structural properties of amino acids. *Scientific Reports,* 8**,** 17923.

CHEN, S.-Y., WEI, W., YIN, B.-C., TONG, Y., LU, J. & YE, B.-C. 2019. Development of a Highly Sensitive Whole-Cell Biosensor for Arsenite Detection through Engineered Promoter Modifications. *ACS Synthetic Biology,* 8**,** 2295-2302.

CHEN, X. J., WANG, B., THOMPSON, I. P. & HUANG, W. E. 2021. Rational Design and Characterization of Nitric Oxide Biosensors in E. coli Nissle 1917 and Mini SimCells. *ACS Synthetic Biology,* 10**,** 2566-2578.

CHEN, Y., HO, J. M. L., SHIS, D. L., GUPTA, C., LONG, J., WAGNER, D. S., OTT, W., JOSIĆ, K. & BENNETT, M. R. 2018. Tuning the dynamic range of bacterial promoters regulated by ligand-inducible transcription factors. *Nature Communications,* 9**,** 64.

CHIEN, T., HARIMOTO, T., KEPECS, B., GRAY, K., COKER, C., HOU, N., PU, K., AZAD, T., NOLASCO, A., PAVLICOVA, M. & DANINO, T. 2022. Enhancing the tropism of bacteria via genetically programmed biosensors. *Nat Biomed Eng,* 6**,** 94-104.

COX, R. S., SURETTE, M. G. & ELOWITZ, M. B. 2007. Programming gene expression with combinatorial promoters. *Molecular Systems Biology,* 3**,** 145.

DACQUAY, L. C. & MCMILLEN, D. R. 2021. Improving the design of an oxidative stress sensing biosensor in yeast. *FEMS Yeast Research,* 21**,** foab025.

DAEFFLER, K. N. M., GALLEY, J. D., SHETH, R. U., ORTIZ-VELEZ, L. C., BIBB, C. O., SHROYER, N. F., BRITTON, R. A. & TABOR, J. J. 2017. Engineering bacterial thiosulfate and tetrathionate sensors for detecting gut inflammation. *Molecular Systems Biology,* 13**,** 923.

DANA, G. V., KUIKEN, T., REJESKI, D. & SNOW, A. A. 2012. Four steps to avoid a synthetic-biology disaster. *Nature,* 483**,** 29-29.

DE AVILA E SILVA, S., ECHEVERRIGARAY, S. & GERHARDT, G. J. L. 2011. BacPP: Bacterial promoter prediction—A tool for accurate sigma-factor specific assignment in enterobacteria. *Journal of Theoretical Biology,* 287**,** 92-99.

DELGADO-POVEDANO, M. M., CALDERÓN-SANTIAGO, M., PRIEGO-CAPOTE, F. & LUQUE DE CASTRO, M. D. 2016. Study of sample preparation for quantitative analysis of amino acids in human sweat by liquid chromatography–tandem mass spectrometry. *Talanta,* 146**,** 310-317.

DERBYSHIRE, P. J., BARR, H., DAVIS, F. & HIGSON, S. P. J. 2012. Lactate in human sweat: a critical review of research to the present day. *The Journal of Physiological Sciences,* 62**,** 429-440.

DEWITTE, R. S. & SHAKHNOVICH, E. I. 1994a. Pseudodihedrals: simplified protein backbone representation with knowledge-based energy. *Protein Sci,* 3**,** 1570-81.

DEWITTE, R. S. & SHAKHNOVICH, E. I. 1994b. Pseudodihedrals: simplified protein backbone representation with knowledge-based energy. *Protein Science,* 3**,** 1570-81.
DON, R. H., COX, P. T., WAINWRIGHT, B. J., BAKER, K. & MATTICK, J. S. 1991. 'Touchdown' PCR to circumvent spurious priming during gene amplification. *Nucleic Acids Res,* 19**,** 4008.
DOPP, J. L., JO, Y. R. & REUEL, N. F. 2019a. Methods to reduce variability in E. Coli-based cell-free protein expression experiments. *Synthetic and Systems Biotechnology,* 4**,** 204-211.
DOPP, J. L., JO, Y. R. & REUEL, N. F. 2019b. Methods to reduce variability in E. Coli-based cell-free protein expression experiments. *Synth Syst Biotechnol,* 4**,** 204-211.
DUNSTAN, R. H., SPARKES, D. L., DASCOMBE, B. J., MACDONALD, M. M., EVANS, C. A., STEVENS, C. J., CROMPTON, M. J., GOTTFRIES, J., FRANKS, J., MURPHY, G., WOOD, R. & ROBERTS, T. K. 2016. Sweat Facilitated Amino Acid Losses in Male Athletes during Exercise at 32-34°C. *PLOS ONE,* 11**,** e0167844.
DURDAGI, S., ROUX, B. & NOSKOV, S. Y. 2013. Potassium-Binding Site Types in Proteins. *In:* KRETSINGER, R. H., UVERSKY, V. N. & PERMYAKOV, E. A. (eds.) *Encyclopedia of Metalloproteins.* New York, NY: Springer New York.
DWIDAR, M., SEIKE, Y., KOBORI, S., WHITAKER, C., MATSUURA, T. & YOKOBAYASHI, Y. 2019. Programmable Artificial Cells Using Histamine-Responsive Synthetic Riboswitch. *Journal of the American Chemical Society,* 141**,** 11103-11114.
DWIDAR, M. & YOKOBAYASHI, Y. 2019. Development of a histamine aptasensor for food safety monitoring. *Scientific Reports,* 9**,** 16659.
EL-OSTA, A., WORINGER, M., PIZZO, E., VERHOEF, T., DICKIE, C., NI, M. Z., HUDDY, J. R., SOLJAK, M., HANNA, G. B. & MAJEED, A. 2017. Does use of point-of-care testing improve cost-effectiveness of the NHS Health Check programme in the primary care setting? A cost-minimisation analysis. *BMJ Open,* 7**,** e015494.
ESPAH BORUJENI, A., CHANNARASAPPA, A. S. & SALIS, H. M. 2014. Translation rate is controlled by coupled trade-offs between site accessibility, selective RNA unfolding and sliding at upstream standby sites. *Nucleic Acids Research,* 42**,** 2646-2659.
FAN, C., DAVISON, P. A., HABGOOD, R., ZENG, H., DECKER, C. M., GESELL SALAZAR, M., LUEANGWATTANAPONG, K., TOWNLEY, H. E., YANG, A., THOMPSON, I. P., YE, H., CUI, Z., SCHMIDT, F., HUNTER, C. N. & HUANG, W. E. 2020. Chromosome-free bacterial cells are safe and programmable platforms for synthetic biology. *Proc Natl Acad Sci U S A,* 117**,** 6752-6761.
FAN, H. & GONG, J. P. 2020. Fabrication of Bioinspired Hydrogels: Challenges and Opportunities. *Macromolecules,* 53**,** 2769-2782.
FAN, J. Y., CUI, Z. Q., WEI, H. P., ZHANG, Z. P., ZHOU, Y. F., WANG, Y. P. & ZHANG, X. E. 2008. Split mCherry as a new red bimolecular fluorescence complementation system for visualizing protein-protein interactions in living cells. *Biochem Biophys Res Commun,* 367**,** 47-53.
FETTER, L., RICHARDS, J., DANIEL, J., ROON, L., ROWLAND, T. J. & BONHAM, A. J. 2015. Electrochemical aptamer scaffold biosensors for detection of botulism and ricin toxins. *Chemical Communications,* 51**,** 15137-15140.
GADORE, V. & AHMARUZZAMAN, M. 2021. Smart materials for remediation of aqueous environmental contaminants. *Journal of Environmental Chemical Engineering,* 9**,** 106486.

GALLAGHER, R. R., PATEL, J. R., INTERIANO, A. L., ROVNER, A. J. & ISAACS, F. J. 2015. Multilayered genetic safeguards limit growth of microorganisms to defined environments. *Nucleic Acids Research,* 43**,** 1945-1954.

GAO, R. & STOCK, A. M. 2009. Biological insights from structures of two-component proteins. *Annual Review of Microbiology,* 63**,** 133-154.

GAO, W., EMAMINEJAD, S., NYEIN, H. Y. Y., CHALLA, S., CHEN, K., PECK, A., FAHAD, H. M., OTA, H., SHIRAKI, H., KIRIYA, D., LIEN, D.-H., BROOKS, G. A., DAVIS, R. W. & JAVEY, A. 2016. Fully integrated wearable sensor arrays for multiplexed in situ perspiration analysis. *Nature,* 529**,** 509-514.

GARDEN, J. W. 1966. Plasma and sweat histamine concentrations after heat exposure and physical exercise. *Journal of Applied Physiology,* 21**,** 631-5.

GE, L. & RUDOLPH, P. 1997. Simultaneous Introduction of Multiple Mutations Using Overlap Extension PCR. *BioTechniques,* 22**,** 28-30.

GEORGI, C., BUERGER, J., HILLEN, W. & BERENS, C. 2012. Promoter strength driving TetR determines the regulatory properties of Tet-controlled expression systems. *PLoS One,* 7**,** e41620.

GIBSON, D. G., YOUNG, L., CHUANG, R.-Y., VENTER, J. C., HUTCHISON, C. A. & SMITH, H. O. 2009. Enzymatic assembly of DNA molecules up to several hundred kilobases. *Nature Methods,* 6**,** 343-345.

GISIN, V., CHAN, A. & WELSH, J. B. 2017. Manufacturing Process Changes and Reduced Skin Irritations of an Adhesive Patch Used for Continuous Glucose Monitoring Devices. *Journal of Diabetes Science and Technology,* 12**,** 725-726.

GOERS, L., AINSWORTH, C., GOEY, C. H., KONTORAVDI, C., FREEMONT, P. S. & POLIZZI, K. M. 2017. Whole-cell Escherichia coli lactate biosensor for monitoring mammalian cell cultures during biopharmaceutical production. *Biotechnology and Bioengineering,* 114**,** 1290-1300.

GOLDSTEIN, L. N., WELLS, M. & VINCENT-LAMBERT, C. 2019. The cost-effectiveness of upfront point-of-care testing in the emergency department: a secondary analysis of a randomised, controlled trial. *Scandinavian Journal of Trauma, Resuscitation and Emergency Medicine,* 27**,** 110.

GOOTENBERG, J. S., ABUDAYYEH, O. O., LEE, J. W., ESSLETZBICHLER, P., DY, A. J., JOUNG, J., VERDINE, V., DONGHIA, N., DARINGER, N. M., FREIJE, C. A., MYHRVOLD, C., BHATTACHARYYA, R. P., LIVNY, J., REGEV, A., KOONIN, E. V., HUNG, D. T., SABETI, P. C., COLLINS, J. J. & ZHANG, F. 2017. Nucleic acid detection with CRISPR-Cas13a/C2c2. *Science,* 356**,** 438.

GOSSET, G., ZHANG, Z., NAYYAR, S., CUEVAS, W. A. & SAIER, M. H., JR. 2004. Transcriptome analysis of Crp-dependent catabolite control of gene expression in Escherichia coli. *J Bacteriol,* 186**,** 3516-24.

GRACIE, K., SMITH, W. E., YIP, P., SUTTER, J. U., BIRCH, D. J., GRAHAM, D. & FAULDS, K. 2014. Interaction of fluorescent dyes with DNA and spermine using fluorescence spectroscopy. *Analyst,* 139**,** 3735-43.

GRANT, B. J., RODRIGUES, A. P., ELSAWY, K. M., MCCAMMON, J. A. & CAVES, L. S. 2006. Bio3d: an R package for the comparative analysis of protein structures. *Bioinformatics,* 22**,** 2695-6.

GREEN, J. M., BISHOP, P. A., MUIR, I. H., MCLESTER, J. R., JR. & HEATH, H. E. 2000. Effects of high and low blood lactate concentrations on sweat lactate response. *Int J Sports Med,* 21**,** 556-60.

GUO, Z., MURPHY, L., STEIN, V., JOHNSTON, W. A., ALCALA-PEREZ, S. & ALEXANDROV, K. 2016. Engineered PQQ-glucose dehydrogenase as a universal biosensor platform. *Journal of the American Chemical Society,* 138**,** 10108-10111.

GUPTA, S. D., WU, H. C. & RICK, P. D. 1997. A Salmonella typhimurium genetic locus which confers copper tolerance on copper-sensitive mutants of Escherichia coli. *J Bacteriol,* 179**,** 4977-84.

GÖHLER, A., XIONG, G., PAULSEN, S., TRENTMANN, G. & MASER, E. 2008. Testosterone-inducible Regulator Is a Kinase That Drives Steroid Sensing and Metabolism in Comamonas testosteroni*. *Journal of Biological Chemistry,* 283**,** 17380-17390.

HAN, W. T., JANG, T., CHEN, S., CHONG, L. S. H., JUNG, H.-D. & SONG, J. 2020. Improved cell viability for large-scale biofabrication with photo-crosslinkable hydrogel systems through a dual-photoinitiator approach. *Biomaterials Science,* 8**,** 450-461.

HAO, N., KRISHNA, S., AHLGREN-BERG, A., CUTTS, E. E., SHEARWIN, K. E. & DODD, I. B. 2014. Road rules for traffic on DNA-systematic analysis of transcriptional roadblocking in vivo. *Nucleic Acids Research,* 42**,** 8861-8872.

HEIKENFELD, J. 2016. Non-invasive Analyte Access and Sensing through Eccrine Sweat: Challenges and Outlook circa 2016. *Electroanalysis,* 28**,** 1242-1249.

HEIKENFELD, J., JAJACK, A., FELDMAN, B., GRANGER, S. W., GAITONDE, S., BEGTRUP, G. & KATCHMAN, B. A. 2019. Accessing analytes in biofluids for peripheral biochemical monitoring. *Nature Biotechnology,* 37**,** 407-419.

HETTIARATCHI, M. H., SCHUDEL, A., ROUSE, T., GARCÍA, A. J., THOMAS, S. N., GULDBERG, R. E. & MCDEVITT, T. C. 2018. A rapid method for determining protein diffusion through hydrogels for regenerative medicine applications. *APL Bioengineering,* 2**,** 026110.

HLADEK, M. D., SZANTON, S. L., CHO, Y.-E., LAI, C., SACKO, C., ROBERTS, L. & GILL, J. 2018. Using sweat to measure cytokines in older adults compared to younger adults: A pilot study. *Journal of Immunological Methods,* 454**,** 1-5.

HOEKSTRA, R., BLONDEAU, P. & ANDRADE, F. J. 2018. Distributed electrochemical sensors: recent advances and barriers to market adoption. *Analytical and Bioanalytical Chemistry,* 410**,** 4077-4089.

HOOSHANGI, S., THIBERGE, S. & WEISS, R. 2005. Ultrasensitivity and noise propagation in a synthetic transcriptional cascade. *Proceedings of the National Academy of Sciences of the United States of America,* 102**,** 3581.

HURLBURT, B. K. & YANOFSKY, C. 1990. Enhanced operator binding by trp superrepressors of Escherichia coli. *Journal of Biological Chemistry,* 265**,** 7853-7858.

JADOON, S., KARIM, S., AKRAM, M. R., KALSOOM KHAN, A., ZIA, M. A., SIDDIQI, A. R. & MURTAZA, G. 2015. Recent developments in sweat analysis and its applications. *International journal of analytical chemistry,* 2015**,** 164974-164974.

JIA, M., CHEW, W. M., FEINSTEIN, Y., SKEATH, P. & STERNBERG, E. M. 2016. Quantification of cortisol in human eccrine sweat by liquid chromatography – tandem mass spectrometry. *Analyst,* 141**,** 2053-2060.

JIA, W., BANDODKAR, A. J., VALDÉS-RAMÍREZ, G., WINDMILLER, J. R., YANG, Z., RAMÍREZ, J., CHAN, G. & WANG, J. 2013. Electrochemical Tattoo Biosensors for Real-Time Noninvasive Lactate Monitoring in Human Perspiration. *Analytical Chemistry,* 85**,** 6553-6560.

JOHNS, N. I., GOMES, A. L. C., YIM, S. S., YANG, A., BLAZEJEWSKI, T., SMILLIE, C. S., SMITH, M. B., ALM, E. J., KOSURI, S. & WANG, H. H. 2018. Metagenomic mining of regulatory elements enables programmable species-selective gene expression. *Nature Methods,* 15**,** 323–329.

JUNG, J. K., ALAM, K. K. & LUCKS, J. B. 2022. ROSALIND: Rapid detection of chemical contaminants with *In Vitro* transcription factor-based biosensors. *Methods in Molecular Biology,* 2433**,** 325-342.

JUNG, J. K., ALAM, K. K., VEROSLOFF, M. S., CAPDEVILA, D. A., DESMAU, M., CLAUER, P. R., LEE, J. W., NGUYEN, P. Q., PASTÉN, P. A., MATIASEK, S. J., GAILLARD, J.-F., GIEDROC, D. P., COLLINS, J. J. & LUCKS, J. B. 2020. Cell-free biosensors for rapid detection of water contaminants. *Nature Biotechnology,* 38**,** 1451-1459.

KANG, C., KIM, S., LEE, E., RYU, J., LEE, M. & KWON, Y. 2021. Genetically Encoded Sensor Cells for the Screening of Glucocorticoid Receptor (GR) Effectors in Herbal Extracts. *Biosensors (Basel),* 11.

KARPOVA, E. V., LAPTEV, A. I., ANDREEV, E. A., KARYAKINA, E. E. & KARYAKIN, A. A. 2020. Relationship Between Sweat and Blood Lactate Levels During Exhaustive Physical Exercise. *ChemElectroChem,* 7**,** 191-194.

KAWAI, Y., SATO, M. & UMEZAWA, Y. 2004. Single color fluorescent indicators of protein phosphorylation for multicolor imaging of intracellular signal flow dynamics. *Anal Chem,* 76**,** 6144-9.

KILLION, J. A., GEEVER, L. M., DEVINE, D. M., KENNEDY, J. E. & HIGGINBOTHAM, C. L. 2011. Mechanical properties and thermal behaviour of PEGDMA hydrogels for potential bone regeneration application. *Journal of the Mechanical Behavior of Biomedical Materials,* 4**,** 1219-1227.

KIM, J., CAMPBELL, A. S., DE AVILA, B. E. & WANG, J. 2019. Wearable biosensors for healthcare monitoring. *Nature Biotechnology,* 37**,** 389-406.

KIM, J., VALDÉS-RAMÍREZ, G., BANDODKAR, A. J., JIA, W., MARTINEZ, A. G., RAMÍREZ, J., MERCIER, P. & WANG, J. 2014. Non-invasive mouthguard biosensor for continuous salivary monitoring of metabolites. *Analyst,* 139**,** 1632-1636.

KIMME, F., BRICK, P., CHATTERJEE, S. & KHANH, T. Q. 2013. Optimized flash light-emitting diode spectra for mobile phone cameras. *Applied Optics,* 52**,** 8779-8788.

KING, J. M. H., DIGRAZIA, P. M., APPLEGATE, B., BURLAGE, R., SANSEVERINO, J., DUNBAR, P., LARIMER, F. & SAYLER, G. S. 1990. Rapid, Sensitive Bioluminescent Reporter Technology for Naphthalene Exposure and Biodegradation. *Science,* 249**,** 778-781.

KITSERA, N., KHOBTA, A. & EPE, B. 2007. Destabilized green fluorescent protein detects rapid removal of transcription blocks after genotoxic exposure. *BioTechniques,* 43**,** 222-227.

KNIGHT, T. F. Idempotent Vector Design for Standard Assembly of Biobricks. 2003.

KOH, A., KANG, D., XUE, Y., LEE, S., PIELAK, R. M., KIM, J., HWANG, T., MIN, S., BANKS, A., BASTIEN, P., MANCO, M. C., WANG, L., AMMANN, K. R., JANG, K.-I., WON, P., HAN, S., GHAFFARI, R., PAIK, U., SLEPIAN, M. J., BALOOCH, G., HUANG, Y. & ROGERS, J. A. 2016. A soft, wearable microfluidic device for the capture, storage, and colorimetric sensing of sweat. *Science Translational Medicine,* 8**,** 366ra165.

KOLEWE, K. W., PEYTON, S. R. & SCHIFFMAN, J. D. 2015. Fewer Bacteria Adhere to Softer Hydrogels. *ACS applied materials & interfaces,* 7**,** 19562-19569.

KOSTYUK, A. I., DEMIDOVICH, A. D., KOTOVA, D. A., BELOUSOV, V. V. & BILAN, D. S. 2019. Circularly Permuted Fluorescent Protein-Based Indicators: History, Principles, and Classification. *International Journal of Molecular Sciences* [Online], 20.

KRONING, K. E., LI, M., PETRESCU, D. I. & WANG, W. 2021. A genetically encoded sensor with improved fluorescence intensity for opioid detection at cellular resolution. *Chem Commun (Camb),* 57**,** 10560-10563.

KYLILIS, N., RIANGRUNGROJ, P., LAI, H.-E., SALEMA, V., FERNÁNDEZ, L. Á., STAN, G.-B. V., FREEMONT, P. S. & POLIZZI, K. M. 2019. Whole-cell biosensor with tunable limit of detection enables low-cost agglutination assays for medical diagnostic applications. *ACS Sensors,* 4**,** 370-378.

LA COUNT, T. D., JAJACK, A., HEIKENFELD, J. & KASTING, G. B. 2019. Modeling Glucose Transport From Systemic Circulation to Sweat. *J Pharm Sci,* 108**,** 364-371.

LAJOIE, M. J., ROVNER, A. J., GOODMAN, D. B., AERNI, H.-R., HAIMOVICH, A. D., KUZNETSOV, G., MERCER, J. A., WANG, H. H., CARR, P. A., MOSBERG, J. A., ROHLAND, N., SCHULTZ, P. G., JACOBSON, J. M., RINEHART, J., CHURCH, G. M. & ISAACS, F. J. 2013. Genomically Recoded Organisms Expand Biological Functions. *Science,* 342**,** 357.

LAOHAKUNAKORN, N. 2020a. Cell-free 3PGA energy solution. *protocols.io*.

LAOHAKUNAKORN, N. 2020b. Cell-free lysate (*E. coli*) preparation with sonication. *protocols.io*.

LARA, B., GALLO-SALAZAR, C., PUENTE, C., ARECES, F., SALINERO, J. J. & DEL COSO, J. 2016. Interindividual variability in sweat electrolyte concentration in marathoners. *Journal of the International Society of Sports Nutrition,* 13**,** 31 1-8.

LEE, E. C., FRAGALA, M. S., KAVOURAS, S. A., QUEEN, R. M., PRYOR, J. L. & CASA, D. J. 2017a. Biomarkers in Sports and Exercise: Tracking Health, Performance, and Recovery in Athletes. *Journal of Strength and Conditioning Research,* 31**,** 2920-2937.

LEE, H., SONG, C., HONG, Y. S., KIM, M. S., CHO, H. R., KANG, T., SHIN, K., CHOI, S. H., HYEON, T. & KIM, D.-H. 2017b. Wearable/disposable sweat-based glucose monitoring device with multistage transdermal drug delivery module. *Science Advances,* 3.

LEE, T. H. & MAHESHRI, N. 2012. A regulatory role for repeated decoy transcription factor binding sites in target gene expression. *Molecular Systems Biology,* 8**,** 576.

LEHTONEN, S. I., TULLILA, A., AGRAWAL, N., KUKKURAINEN, S., KÄHKÖNEN, N., KOSKINEN, M., NEVANEN, T. K., JOHNSON, M. S., AIRENNE, T. T., KULOMAA, M. S., RIIHIMÄKI, T. A. & HYTÖNEN, V. P. 2016. Artificial Avidin-Based Receptors for a Panel of Small Molecules. *ACS Chemical Biology,* 11**,** 211-221.

LEI, H., DONG, L., LI, Y., ZHANG, J., CHEN, H., WU, J., ZHANG, Y., FAN, Q., XUE, B., QIN, M., CHEN, B., CAO, Y. & WANG, W. 2020. Stretchable hydrogels with low hysteresis and anti-fatigue fracture based on polyprotein cross-linkers. *Nature Communications,* 11**,** 4032.

LEVSKAYA, A., CHEVALIER, A. A., TABOR, J. J., SIMPSON, Z. B., LAVERY, L. A., LEVY, M., DAVIDSON, E. A., SCOURAS, A., ELLINGTON, A. D., MARCOTTE, E. M. & VOIGT, C. A. 2005. Engineering Escherichia coli to see light. *Nature,* 438**,** 441-442.

LI, P., MÜLLER, M., CHANG, M. W., FRETTLÖH, M. & SCHÖNHERR, H. 2017a. Encapsulation of Autoinducer Sensing Reporter Bacteria in Reinforced Alginate-Based Microbeads. *ACS Appl Mater Interfaces,* 9**,** 22321-22331.

LI, P., MÜLLER, M., CHANG, M. W., FRETTLÖH, M. & SCHÖNHERR, H. 2017b. Encapsulation of autoinducer sensing reporter bacteria in reinforced alginate-based microbeads. *ACS Applied Materials & Interfaces,* 9**,** 22321-22331.

LI, X., YANG, Y., ZHANG, B., LIN, X., FU, X., AN, Y., ZOU, Y., WANG, J.-X., WANG, Z. & YU, T. 2022. Lactate metabolism in human health and disease. *Signal Transduction and Targeted Therapy,* 7**,** 305.

LIU, Q., SCHUMACHER, J., WAN, X., LOU, C. & WANG, B. 2018a. Orthogonality and burdens of heterologous AND gate gene circuits in E. coli. *ACS Synthetic Biology,* 7**,** 553-564.

LIU, X., TANG, T.-C., THAM, E., YUK, H., LIN, S., LU, T. K. & ZHAO, X. 2017. Stretchable living materials and devices with hydrogel–elastomer hybrids hosting programmed cells. *Proceedings of the National Academy of Sciences,* 114**,** 2200-2205.

LIU, X., YUK, H., LIN, S., PARADA, G. A., TANG, T. C., THAM, E., DE LA FUENTE-NUNEZ, C., LU, T. K. & ZHAO, X. 2018b. 3D Printing of Living Responsive Materials and Devices. *Advanced Materials,* 30**,** 1-9.

LOPEZ, G. & ANDERSON, J. C. 2015. Synthetic Auxotrophs with Ligand-Dependent Essential Genes for a BL21(DE3) Biosafety Strain. *ACS Synthetic Biology,* 4**,** 1279-1286.

LOPRESIDE, A., WAN, X., MICHELINI, E., RODA, A. & WANG, B. 2019. Comprehensive Profiling of Diverse Genetic Reporters with Application to Whole-Cell and Cell-Free Biosensors. *Analytical Chemistry,* 91**,** 15284-15292.

LÖNNEBORG, R., VARGA, E. & BRZEZINSKI, P. 2012. Directed evolution of the transcriptional regulator DntR: isolation of mutants with improved DNT-response. *PLoS One,* 7**,** e29994.

MA, D., SHEN, L., WU, K., DIEHNELT, C. W. & GREEN, A. A. 2018a. Low-cost detection of norovirus using paper-based cell-free systems and synbody-based viral enrichment. *Synthetic biology (Oxf),* 3**,** ysy018.

MA, L., HU, L., FENG, X. & WANG, S. 2018b. Nitrate and Nitrite in Health and Disease. *Aging and Disease,* 9**,** 938-945.

MAGRO, L., JACQUELIN, B., ESCADAFAL, C., GARNERET, P., KWASIBORSKI, A., MANUGUERRA, J.-C., MONTI, F., SAKUNTABHAI, A., VANHOMWEGEN, J., LAFAYE, P. & TABELING, P. 2017. Paper-based RNA detection and multiplexed analysis for Ebola virus diagnostics. *Scientific Reports,* 7**,** 1347.

MANDELL, D. J., LAJOIE, M. J., MEE, M. T., TAKEUCHI, R., KUZNETSOV, G., NORVILLE, J. E., GREGG, C. J., STODDARD, B. L. & CHURCH, G. M. 2015. Biocontainment of genetically modified organisms by synthetic protein design. *Nature,* 518**,** 55.

MANNAN, A. A., LIU, D., ZHANG, F. & OYARZÚN, D. A. 2017. Fundamental design principles for transcription-factor-based metabolite biosensors. *ACS Synthetic Biology,* 6**,** 1851-1859.

MAO, N., CUBILLOS-RUIZ, A., CAMERON, D. E. & COLLINS, J. J. 2018. Probiotic strains detect and suppress cholera in mice. *Science Translational Medicine,* 10**,** eaao2586.

MARCHAND, A. & GABELICA, V. 2016. Folding and misfolding pathways of G-quadruplex DNA. *Nucleic Acids Res,* 44**,** 10999-11012.

MARK, H. & HARDING, C. R. 2013. Amino acid composition, including key derivatives of eccrine sweat: potential biomarkers of certain atopic skin conditions. *International Journal of Cosmetic Science,* 35**,** 163-168.

MARVIN, J. S., SCHREITER, E. R., ECHEVARRÍA, I. M. & LOOGER, L. L. 2011. A genetically encoded, high-signal-to-noise maltose sensor. *Proteins,* 79**,** 3025-36.

MAZIDI, Z., JAVANMARDI, S., NAGHIB, S. M. & MOHAMMADPOUR, Z. 2022. Smart stimuli-responsive implantable drug delivery systems for programmed and on-

demand cancer treatment: An overview on the emerging materials. *Chemical Engineering Journal,* 433**,** 134569.
MEHENNAOUI, S., POORAHONG, S., JIMENEZ, G. C. & SIAJ, M. 2019. Selection of high affinity aptamer-ligand for dexamethasone and its electrochemical biosensor. *Scientific Reports,* 9**,** 6600.
MEHTA, A. R. 2008. Why does the plasma urea concentration increase in acute dehydration? *Advances in Physiology Education,* 32**,** 336-336.
MEHTA, S., ZHANG, Y., ROTH, R. H., ZHANG, J. F., MO, A., TENNER, B., HUGANIR, R. L. & ZHANG, J. 2018. Single-fluorophore biosensors for sensitive and multiplexed detection of signalling activities. *Nat Cell Biol,* 20**,** 1215-1225.
MILLACURA, F. A., LI, M., VALENZUELA-ORTEGA, M. & FRENCH, C. E. 2019. TXO: Transcription-Only genetic circuits as a novel cell-free approach for Synthetic Biology. *bioRxiv***,** 826230.
MIMEE, M., NADEAU, P., HAYWARD, A., CARIM, S., FLANAGAN, S., JERGER, L., COLLINS, J., MCDONNELL, S., SWARTWOUT, R., CITORIK, R. J., BULOVIĆ, V., LANGER, R., TRAVERSO, G., CHANDRAKASAN, A. P. & LU, T. K. 2018. An ingestible bacterial-electronic system to monitor gastrointestinal health. *Science,* 360**,** 915-918.
MORASKIE, M., ROSHID, M. H. O., O'CONNOR, G., DIKICI, E., ZINGG, J.-M., DEO, S. & DAUNERT, S. 2021. Microbial whole-cell biosensors: Current applications, challenges, and future perspectives. *Biosensors and Bioelectronics,* 191**,** 113359.
NADLER, D. C., MORGAN, S.-A., FLAMHOLZ, A., KORTRIGHT, K. E. & SAVAGE, D. F. 2016. Rapid construction of metabolite biosensors using domain-insertion profiling. *Nature Communications,* 7**,** 12266.
NAGAI, T., YAMADA, S., TOMINAGA, T., ICHIKAWA, M. & MIYAWAKI, A. 2004. Expanded dynamic range of fluorescent indicators for Ca2+ by circularly permuted yellow fluorescent proteins. *Proceedings of the National Academy of Sciences,* 101**,** 10554-10559.
NARDONE, E., ROSANO, C., SANTAMBROGIO, P., CURNIS, F., CORTI, A., MAGNI, F., SICCARDI, A. G., PAGANELLI, G., LOSSO, R., APREDA, B., BOLOGNESI, M., SIDOLI, A. & AROSIO, P. 1998. Biochemical characterization and crystal structure of a recombinant hen avidin and its acidic mutant expressed in Escherichia coli. *European Journal of Biochemistry,* 256**,** 453-460.
NEILLY, I. J., COPLAND, M., HAJ, M., ADEY, G., BENJAMIN, N. & BENNETT, B. 1995. Plasma nitrate concentrations in neutropenic and non-neutropenic patients with suspected septicaemia. *British Journal of Haematology,* 89**,** 199-202.
NGUYEN, T. U., WATKINS, K. E. & KISHORE, V. 2019. Photochemically crosslinked cell-laden methacrylated collagen hydrogels with high cell viability and functionality. *J Biomed Mater Res A,* 107**,** 1541-1550.
NIELSEN, A. A. K., DER, B. S., SHIN, J., VAIDYANATHAN, P., PARALANOV, V., STRYCHALSKI, E. A., ROSS, D., DENSMORE, D. & VOIGT, C. A. 2016. Genetic circuit design automation. *Science,* 352**,** aac7341.
NISTALA, G. J., WU, K., RAO, C. V. & BHALERAO, K. D. 2010. A modular positive feedback-based gene amplifier. *Journal of Biological Engineering,* 4**,** 4.
OHKUWA, T., TSUKAMOTO, K., YAMAI, K., ITOH, H., YAMAZAKI, Y. & TSUDA, T. 2009. The Relationship between Exercise Intensity and Lactate Concentration on the Skin Surface. *International journal of biomedical science : IJBS,* 5**,** 23-27.

PANDI, A., GRIGORAS, I., BORKOWSKI, O. & FAULON, J.-L. 2019. Optimizing Cell-Free Biosensors to Monitor Enzymatic Production. *ACS Synthetic Biology,* 8**,** 1952-1957.

PARDEE, K., GREEN, A. A., TAKAHASHI, M. K., BRAFF, D., LAMBERT, G., LEE, J. W., FERRANTE, T., MA, D., DONGHIA, N., FAN, M., DARINGER, N. M., BOSCH, I., DUDLEY, D. M., O'CONNOR, D. H., GEHRKE, L. & COLLINS, J. J. 2016. Rapid, low-cost detection of Zika virus using programmable biomolecular components. *Cell,* 165**,** 1255-1266.

PLÉSIAT, P. & NIKAIDO, H. 1992. Outer membranes of Gram-negative bacteria are permeable to steroid probes. *Molecular Microbiology,* 6**,** 1323-1333.

PORCHETTA, A., VALLÉE-BÉLISLE, A., PLAXCO, K. W. & RICCI, F. 2012. Using Distal-Site Mutations and Allosteric Inhibition To Tune, Extend, and Narrow the Useful Dynamic Range of Aptamer-Based Sensors. *Journal of the American Chemical Society,* 134**,** 20601-20604.

POWER, B., LIU, X., GERMAINE, K. J., RYAN, D., BRAZIL, D. & DOWLING, D. N. 2011. Alginate beads as a storage, delivery and containment system for genetically modified PCB degrader and PCB biosensor derivatives of Pseudomonas fluorescens F113. *Journal of Applied Microbiology,* 110**,** 1351-1358.

PRUNEDA-PAZ, J. L., LINARES, M., CABRERA, J. E. & GENTI-RAIMONDI, S. 2004. TeiR, a LuxR-Type Transcription Factor Required for Testosterone Degradation in *Comamonas testosteroni*. *Journal of Bacteriology,* 186**,** 1430.

PU, J., ZINKUS-BOLTZ, J. & DICKINSON, B. C. 2017. Evolution of a split RNA polymerase as a versatile biosensor platform. *Nature Chemical Biology,* 13**,** 432.

PUBLIC GENERAL ACTS, U. 1990. Environmental Protection Act 1990.

PUGLIESE, L., CODA, A., MALCOVATI, M. & BOLOGNESI, M. 1993. Three-dimensional Structure of the Tetragonal Crystal Form of Egg-white Avidin in its functional Complex with Biotin at 2·7 Å Resolution. *Journal of Molecular Biology,* 231**,** 698-710.

QIAN, Y., HUANG, H.-H., JIMÉNEZ, J. I. & DEL VECCHIO, D. 2017. Resource Competition Shapes the Response of Genetic Circuits. *ACS Synthetic Biology,* 6**,** 1263-1272.

RAMAN, S., ROGERS, J. K., TAYLOR, N. D. & CHURCH, G. M. 2014. Evolution-guided optimization of biosynthetic pathways. *Proceedings of the National Academy of Sciences,* 111**,** 17803.

RHEA, K. A., MCDONALD, N. D., COLE, S. D., NOIREAUX, V., LUX, M. W. & BUCKLEY, P. E. 2022. Variability in cell-free expression reactions can impact qualitative genetic circuit characterization. *Synthetic Biology,* 7**,** ysac011.

RICHARD, D. M., DAWES, M. A., MATHIAS, C. W., ACHESON, A., HILL-KAPTURCZAK, N. & DOUGHERTY, D. M. 2009. L-Tryptophan: Basic Metabolic Functions, Behavioral Research and Therapeutic Indications. *Int J Tryptophan Res,* 2**,** 45-60.

ROGERS, J. K., TAYLOR, N. D. & CHURCH, G. M. 2016. Biosensor-based engineering of biosynthetic pathways. *Current Opinion in Biotechnology,* 42**,** 84-91.

ROSANO, G. L. & CECCARELLI, E. A. 2014. Recombinant protein expression in Escherichia coli: advances and challenges. *Frontiers in Microbiology,* 5.

ROVNER, A. J., HAIMOVICH, A. D., KATZ, S. R., LI, Z., GROME, M. W., GASSAWAY, B. M., AMIRAM, M., PATEL, J. R., GALLAGHER, R. R., RINEHART, J. & ISAACS, F. J. 2015. Recoded organisms engineered to depend on synthetic amino acids. *Nature,* 518**,** 89-93.

RUTZ, A. L., HYLAND, K. E., JAKUS, A. E., BURGHARDT, W. R. & SHAH, R. N. 2015. A Multimaterial Bioink Method for 3D Printing Tunable, Cell-Compatible Hydrogels. *Advanced Materials,* 27**,** 1607-1614.

RYU, J., LEE, E., KANG, C., LEE, M., KIM, S., PARK, S., LEE, D. Y. & KWON, Y. 2021. Rapid Screening of Glucocorticoid Receptor (GR) Effectors Using Cortisol-Detecting Sensor Cells. *Int J Mol Sci,* 22.

SAKHAROV, D. A., SHKURNIKOV, M. U., VAGIN, M. Y., YASHINA, E. I., KARYAKIN, A. A. & TONEVITSKY, A. G. 2010. Relationship between Lactate Concentrations in Active Muscle Sweat and Whole Blood. *Bulletin of Experimental Biology and Medicine,* 150**,** 83-85.

SALIS, H. M., MIRSKY, E. A. & VOIGT, C. A. 2009. Automated design of synthetic ribosome binding sites to control protein expression. *Nature Biotechnology,* 27**,** 946-950.

SANGAL, A., PASINI, P. & DAUNERT, S. 2011. Stability of spore-based biosensing systems under extreme conditions. *Sensors and Actuators B: Chemical,* 158**,** 377-382.

SCHMIDL, S. R., EKNESS, F., SOFJAN, K., DAEFFLER, K. N. M., BRINK, K. R., LANDRY, B. P., GERHARDT, K. P., DYULGYAROV, N., SHETH, R. U. & TABOR, J. J. 2019. Rewiring bacterial two-component systems by modular DNA-binding domain swapping. *Nature Chemical Biology***,** 690–698.

SCHMIDT, M. 2010. Xenobiology: A new form of life as the ultimate biosafety tool. *BioEssays,* 32**,** 322-331.

SCHULZ-SCHÖNHAGEN, K., LOBSIGER, N. & STARK, W. J. 2019. Continuous production of a shelf-stable living material as a biosensor platform. *Advanced Materials Technologies,* 0**,** 1900266.

SEKAR, K., GENTILE, A. M., BOSTICK, J. W. & TYO, K. E. J. 2016. N-terminal-based targeted, inducible protein degradation in Escherichia coli. *PLOS ONE,* 11**,** e0149746.

SEMPIONATTO, J. R., NAKAGAWA, T., PAVINATTO, A., MENSAH, S. T., IMANI, S., MERCIER, P. & WANG, J. 2017. Eyeglasses based wireless electrolyte and metabolite sensor platform. *Lab on a chip,* 17**,** 1834-1842.

SHANER, N. C., LAMBERT, G. G., CHAMMAS, A., NI, Y., CRANFILL, P. J., BAIRD, M. A., SELL, B. R., ALLEN, J. R., DAY, R. N., ISRAELSSON, M., DAVIDSON, M. W. & WANG, J. 2013. A bright monomeric green fluorescent protein derived from Branchiostoma lanceolatum. *Nat Methods,* 10**,** 407-9.

SHEMER, B., PALEVSKY, N., YAGUR-KROLL, S. & BELKIN, S. 2015. Genetically engineered microorganisms for the detection of explosives' residues. *Frontiers in Microbiology,* 6**,** 1175.

SHETTY, R. S., DEO, S. K., LIU, Y. & DAUNERT, S. 2004. Fluorescence-based sensing system for copper using genetically engineered living yeast cells. *Biotechnol Bioeng,* 88**,** 664-70.

SIEGFRIED, K., ENDES, C., BHUIYAN, A. F. M. K., KUPPARDT, A., MATTUSCH, J., VAN DER MEER, J. R., CHATZINOTAS, A. & HARMS, H. 2012. Field testing of arsenic in groundwater samples of Bangladesh using a test kit based on lyophilized bioreporter bacteria. *Environmental Science & Technology,* 46**,** 3281-3287.

SILVERMAN, A. D., AKOVA, U., ALAM, K. K., JEWETT, M. C. & LUCKS, J. B. 2020. Design and Optimization of a Cell-Free Atrazine Biosensor. *ACS Synth Biol,* 9**,** 671-677.

SILVERMAN, A. D., KELLEY-LOUGHNANE, N., LUCKS, J. B. & JEWETT, M. C. 2019. Deconstructing Cell-Free Extract Preparation for in Vitro Activation of Transcriptional Genetic Circuitry. *ACS Synth Biol,* 8**,** 403-414.

SINGLETON, C. K., ROEDER, W. D., BOGOSIAN, G., SOMERVILLE, R. L. & WEITH, H. L. 1980. DNA sequence of the *E. coli* trpR gene and prediction of the amino acid sequence of Trp repressor. *Nucleic Acids Res,* 8**,** 1551-60.

SONNER, Z., WILDER, E., HEIKENFELD, J., KASTING, G., BEYETTE, F., SWAILE, D., SHERMAN, F., JOYCE, J., HAGEN, J., KELLEY-LOUGHNANE, N. & NAIK, R. 2015. The microfluidics of the eccrine sweat gland, including biomarker partitioning, transport, and biosensing implications. *Biomicrofluidics,* 9**,** 031301-031301.

STATUTORY INSTRUMENTS, S. 2002. The Genetically Modified Organisms (Deliberate Release) (Scotland) Regulations 2002. Environmental Protection.

STATUTORY INSTRUMENTS, U. 2014. The Genetically Modified Organsisms (Contained Use) Regulations 2014. *In:* SAFETY, H. A. (ed.).

STIRLING, F., BITZAN, L., O'KEEFE, S., REDFIELD, E., OLIVER, J. W. K., WAY, J. & SILVER, P. A. 2017. Rational Design of Evolutionarily Stable Microbial Kill Switches. *Molecular Cell,* 68**,** 686-697.e3.

STRUSS, A., PASINI, P., ENSOR, C. M., RAUT, N. & DAUNERT, S. 2010. Paper strip whole cell biosensors: a portable test for the semiquantitative detection of bacterial quorum signaling molecules. *Analytical Chemistry,* 82**,** 4457-4463.

SU, J., HU, B.-H., LOWE, W. L., KAUFMAN, D. B. & MESSERSMITH, P. B. 2010. Anti-inflammatory peptide-functionalized hydrogels for insulin-secreting cell encapsulation. *Biomaterials,* 31**,** 308-314.

TAMADA, J. A., BOHANNON, N. J. V. & POTTS, R. O. 1995. Measurement of glucose in diabetic subjects using noninvasive transdermal extraction. *Nature Medicine,* 1**,** 1198-1201.

TAURIAINEN, S., KARP, M., CHANG, W. & VIRTA, M. 1997. Recombinant luminescent bacteria for measuring bioavailable arsenite and antimonite. *Appl Environ Microbiol,* 63**,** 4456-61.

THOMASON, M. K. & STORZ, G. 2010. Bacterial Antisense RNAs: How Many Are There, and What Are They Doing? *Annual Review of Genetics,* 44**,** 167-188.

TINAFAR, A., JAENES, K. & PARDEE, K. 2019. Synthetic Biology Goes Cell-Free. *BMC Biology,* 17**,** 64.

TORABI, S.-F., WU, P., MCGHEE, C. E., CHEN, L., HWANG, K., ZHENG, N., CHENG, J. & LU, Y. 2015. In vitro selection of a sodium-specific DNAzyme and its application in intracellular sensing. *Proceedings of the National Academy of Sciences,* 112**,** 5903.

TORRENTE-RODRÍGUEZ, R. M., TU, J., YANG, Y., MIN, J., WANG, M., SONG, Y., YU, Y., XU, C., YE, C., ISHAK, W. W. & GAO, W. 2020. Investigation of Cortisol Dynamics in Human Sweat Using a Graphene-Based Wireless mHealth System. *Matter,* 2**,** 921-937.

TRANTIDOU, T., DEKKER, L., POLIZZI, K., CES, O. & ELANI, Y. 2018. Functionalizing cell-mimetic giant vesicles with encapsulated bacterial biosensors. *Interface Focus,* 8**,** 1-7.

TSENG, S.-C., WU, T.-Y., CHOU, J.-C., LIAO, Y.-H., LAI, C.-H., YAN, S.-J. & TSENG, T.-W. 2018. Investigation of Sensitivities and Drift Effects of the Arrayed Flexible Chloride Sensor Based on $RuO_2$/GO at Different Temperatures. *Sensors (Basel, Switzerland),* 18**,** 632.

TYRRELL, R. M. & PEAK, M. J. 1978. Interactions between uv radiation of different energies in the inactivation of bacteria. *Journal of Bacteriology,* 136**,** 437.

UEYAMA, H., TAKAGI, M. & TAKENAKA, S. 2002. A Novel Potassium Sensing in Aqueous Media with a Synthetic Oligonucleotide Derivative. Fluorescence Resonance Energy Transfer Associated with Guanine Quartet−Potassium Ion

Complex Formation. *Journal of the American Chemical Society,* 124**,** 14286-14287.
UTSUMI, R., BRISSETTE, R. E., RAMPERSAUD, A., FORST, S. A., OOSAWA, K. & INOUYE, M. 1989. Activation of Bacterial Porin Gene Expression by a Chimeric Signal Transducer in Response to Aspartate. *Science,* 245**,** 1246-1249.
VAIRO, D., BRUZZESE, L., MARLINGE, M., FUSTER, L., ADJRIOU, N., KIPSON, N., BRUNET, P., CAUTELA, J., JAMMES, Y., MOTTOLA, G., BURTEY, S., RUF, J., GUIEU, R. & FENOUILLET, E. 2017. Towards Addressing the Body Electrolyte Environment via Sweat Analysis:Pilocarpine Iontophoresis Supports Assessment of Plasma Potassium Concentration. *Scientific Reports,* 7**,** 11801 1-7.
VERBRUGGHE, E., DHAENENS, M., LEYMAN, B., BOYEN, F., SHEARER, N., VAN PARYS, A., HAESENDONCK, R., BERT, W., FAVOREEL, H., DEFORCE, D., THOMPSON, A., HAESEBROUCK, F. & PASMANS, F. 2016. Host Stress Drives Salmonella Recrudescence. *Scientific Reports,* 6**,** 20849.
VERDE, T., SHEPHARD, R. J., COREY, P. & MOORE, R. 1982. Sweat composition in exercise and in heat. *Journal of Applied Physiology,* 53**,** 1540-1545.
VERMEULEN, N., KEELER, W. J., NANDAKUMAR, K. & LEUNG, K. T. 2008. The bactericidal effect of ultraviolet and visible light on Escherichia coli. *Biotechnol Bioeng,* 99**,** 550-6.
VOYVODIC, P. L., PANDI, A., KOCH, M., CONEJERO, I., VALJENT, E., COURTET, P., RENARD, E., FAULON, J.-L. & BONNET, J. 2019. Plug-and-play metabolic transducers expand the chemical detection space of cell-free biosensors. *Nature Communications,* 10**,** 1697.
WACKWITZ, A., HARMS, H., CHATZINOTAS, A., BREUER, U., VOGNE, C. & VAN DER MEER, J. R. 2008. Internal arsenite bioassay calibration using multiple bioreporter cell lines. *Microb Biotechnol,* 1**,** 149-57.
WAN, L., YOSHIKAWA, A., EISENSTEIN, M. & SOH, H. T. 2022. A high-throughput strategy for enhancing aptamer performance across different environmental conditions. *bioRxiv***,** 2022.09.13.507853.
WAN, X. 2019. *Synthetic biology enabled cellular and cell-free biosensors for environmental contaminants.* University of Edinburgh.
WAN, X., VOLPETTI, F., PETROVA, E., FRENCH, C., MAERKL, S. J. & WANG, B. 2019a. Cascaded amplifying circuits enable ultrasensitive cellular sensors for toxic metals. *Nature chemical biology,* 15**,** 540-548.
WAN, X., VOLPETTI, F., PETROVA, E., FRENCH, C., MAERKL, S. J. & WANG, B. 2019b. Cascaded amplifying circuits enable ultrasensitive cellular sensors for toxic metals. *Nat Chem Biol,* 15**,** 540-548.
WANG, B., BARAHONA, M. & BUCK, M. 2013a. A modular cell-based biosensor using engineered genetic logic circuits to detect and integrate multiple environmental signals. *Biosensors and Bioelectronics,* 40**,** 368-376.
WANG, B., BARAHONA, M. & BUCK, M. 2014. Engineering modular and tunable genetic amplifiers for scaling transcriptional signals in cascaded gene networks. *Nucleic Acids Research,* 42**,** 9484-92.
WANG, B., BARAHONA, M. & BUCK, M. 2015a. Amplification of small molecule-inducible gene expression via tuning of intracellular receptor densities. *Nucleic Acids Research,* 43**,** 1955-1964.
WANG, B., BARAHONA, M. & BUCK, M. 2015b. Amplification of small molecule-inducible gene expression via tuning of intracellular receptor densities. *Nucleic Acids Res,* 43**,** 1955-64.

WANG, B., BARAHONA, M., BUCK, M. & SCHUMACHER, J. 2013b. Rewiring cell signalling through chimaeric regulatory protein engineering. *Biochemical Society Transactions,* 41**,** 1195–1200.
WANG, B. & BUCK, M. 2012. Customizing cell signaling using engineered genetic logic circuits. *Trends in Microbiology,* 20**,** 376-384.
WANG, B. & BUCK, M. 2014. Rapid engineering of versatile molecular logic gates using heterologous genetic transcriptional modules. *Chemical Communications,* 50**,** 11642-11644.
WANG, B., KITNEY, R. I., JOLY, N. & BUCK, M. 2011. Engineering modular and orthogonal genetic logic gates for robust digital-like synthetic biology. *Nat Commun,* 2**,** 508.
WATSTEIN, D. M. & STYCZYNSKI, M. P. 2018. Development of a pigment-based whole-cell zinc biosensor for human serum. *ACS Synthetic Biology,* 7**,** 267-275.
WELLER, R., PATTULLO, S., SMITH, L., GOLDEN, M., ORMEROD, A. & BENJAMIN, N. 1996. Nitric Oxide Is Generated on the Skin Surface by Reduction of Sweat Nitrate. *Journal of Investigative Dermatology,* 107**,** 327-331.
WEN, K. Y., RUTTER, J. W., BARNES, C. P. & DEKKER, L. 2019. Fundamental Building Blocks of Whole-Cell Biosensor Design. *In:* THOUAND, G. (ed.) *Handbook of Cell Biosensors.* Cham: Springer International Publishing.
WILLIAMS, C. G., MALIK, A. N., KIM, T. K., MANSON, P. N. & ELISSEEFF, J. H. 2005. Variable cytocompatibility of six cell lines with photoinitiators used for polymerizing hydrogels and cell encapsulation. *Biomaterials,* 26**,** 1211-1218.
WRIGHT, O., DELMANS, M., STAN, G.-B. & ELLIS, T. 2015. GeneGuard: a modular plasmid system designed for biosafety. *ACS Synthetic Biology,* 4**,** 307-316.
WU, T., ZHANG, C., WANG, Z., REN, H., KANG, Y. & DU, Y. 2016. Tuning the sensing range of potassium ions by changing the loop size of G-quadruplex sensors. *New Journal of Chemistry,* 40**,** 9285-9290.
XIONG, Y., ZHANG, J., YANG, Z., MOU, Q., MA, Y., XIONG, Y. & LU, Y. 2020. Functional DNA Regulated CRISPR-Cas12a Sensors for Point-of-Care Diagnostics of Non-Nucleic-Acid Targets. *Journal of the American Chemical Society,* 142**,** 207-213.
XUE, H., SHI, H., YU, Z., HE, S., LIU, S., HOU, Y., PAN, X., WANG, H., ZHENG, P., CUI, C., VIETS, H., LIANG, J., ZHANG, Y., CHEN, S., ZHANG, H. M. & OUYANG, Q. 2014. Design, construction, and characterization of a set of biosensors for aromatic compounds. *ACS Synthetic Biology,* 3**,** 1011-1014.
YAGUR-KROLL, S., AMIEL, E., ROSEN, R. & BELKIN, S. 2015a. Detection of 2,4-dinitrotoluene and 2,4,6-trinitrotoluene by an Escherichia coli bioreporter: performance enhancement by directed evolution. *Applied Microbiology and Biotechnology,* 99**,** 7177-88.
YAGUR-KROLL, S., SCHREUDER, E., INGHAM, C. J., HEIDEMAN, R., ROSEN, R. & BELKIN, S. 2015b. A miniature porous aluminum oxide-based flow-cell for online water quality monitoring using bacterial sensor cells. *Biosensors & Bioelectronics,* 64**,** 625-632.
YANG, C. H., WANG, M. X., HAIDER, H., YANG, J. H., SUN, J.-Y., CHEN, Y. M., ZHOU, J. & SUO, Z. 2013. Strengthening Alginate/Polyacrylamide Hydrogels Using Various Multivalent Cations. *ACS Applied Materials & Interfaces,* 5**,** 10418-10422.
YANOFSKY, C. 2004. The different roles of tryptophan transfer RNA in regulating trp operon expression in E. coli versus B. subtilis. *Trends Genet,* 20**,** 367-74.
YOO, H., JO, H. & OH, S. S. 2020. Detection and beyond: challenges and advances in aptamer-based biosensors. *Materials Advances,* 1**,** 2663-2687.

YOUSEFI, H., ALI, M. M., SU, H.-M., FILIPE, C. D. M. & DIDAR, T. F. 2018. Sentinel Wraps: Real-Time Monitoring of Food Contamination by Printing DNAzyme Probes on Food Packaging. *ACS Nano,* 12**,** 3287-3294.

YUK, H., ZHANG, T., PARADA, G. A., LIU, X. & ZHAO, X. 2016. Skin-inspired hydrogel–elastomer hybrids with robust interfaces and functional microstructures. *Nature Communications,* 7**,** 12028.

ZHANG, G., HU, S. & JIA, X. 2021a. Highly Sensitive Whole-Cell Biosensor for Cadmium Detection Based on a Negative Feedback Circuit. *Frontiers in Bioengineering and Biotechnology,* 9.

ZHANG, M., OLDENHOF, H., SYDYKOV, B., BIGALK, J., SIEME, H. & WOLKERS, W. F. 2017a. Freeze-drying of mammalian cells using trehalose: preservation of DNA integrity. *Scientific Reports,* 7**,** 6198.

ZHANG, S., LI, X., ZHAO, S., DROBIZHEV, M. & AI, H.-W. 2021b. A fast, high-affinity fluorescent serotonin biosensor engineered from a tick lipocalin. *Nature Methods*.

ZHANG, Y., QIAN, L., WEI, W., WANG, Y., WANG, B., LIN, P., LIU, W., XU, L., LI, X., LIU, D., CHENG, S., LI, J., YE, Y., LI, H., ZHANG, X., DONG, Y., ZHAO, X., LIU, C., ZHANG, H. M., OUYANG, Q. & LOU, C. 2017b. Paired Design of dCas9 as a Systematic Platform for the Detection of Featured Nucleic Acid Sequences in Pathogenic Strains. *ACS Synthetic Biology,* 6**,** 211-216.

ZHAO, S., WU, D., WU, P., WANG, Z. & HUANG, J. 2015. Serum IL-10 Predicts Worse Outcome in Cancer Patients: A Meta-Analysis. *PLOS ONE,* 10**,** e0139598 1-15.

ZHAO, Y., ZHAI, Q., DONG, D., AN, T., GONG, S., SHI, Q. & CHENG, W. 2019. Highly Stretchable and Strain-Insensitive Fiber-Based Wearable Electrochemical Biosensor to Monitor Glucose in the Sweat. *Analytical Chemistry,* 91**,** 6569-6576.

ZHOU, W., DING, J. & LIU, J. 2016. A highly specific sodium aptamer probed by 2-aminopurine for robust Na+ sensing. *Nucleic Acids Research,* 44**,** 10377-10385.

ZHOU, W., DING, J. & LIU, J. 2017. Splitting a DNAzyme enables a $Na^+$ dependent FRET signal from the embedded aptamer. *Organic & Biomolecular Chemistry,* 15**,** 6959-6966.

ZHU, H., YAGLIDERE, O., SU, T.-W., TSENG, D. & OZCAN, A. 2011. Cost-effective and compact wide-field fluorescent imaging on a cell-phone. *Lab on a Chip,* 11**,** 315-322.

ZHU, Z., GUO, S.-Z., HIRDLER, T., EIDE, C., FAN, X., TOLAR, J. & MCALPINE, M. C. 2018. 3D Printed Functional and Biological Materials on Moving Freeform Surfaces. *Advanced Materials,* 30**,** 1707495.

ZÚÑIGA, A., CAMACHO, M., CHANG, H. J., FRISTOT, E., MAYONOVE, P., HANI, E. H. & BONNET, J. 2021. Engineered l-Lactate Responding Promoter System Operating in Glucose-Rich and Anoxic Environments. *ACS Synth Biol,* 10**,** 3527-3536.